MULTIVARIABLE CONTROL LAW DESIGN FOR THE X-29 AIRCRAFT

THESIS

AFIT/GE/ENG/84D-21 Terry L. Courtheyn
Major USAF

DEPARTMENT OF THE AIR FORCE
AIR UNIVERSITY
AIR FORCE INSTITUTE OF TECHNOLOGY

Wright-Patterson Air Force Base, Ohio

AFIT/GE/ENG/84D-21

MULTIVARIABLE CONTROL LAW DESIGN

FOR THE X-29 AIRCRAFT

THESIS

AFIT/GE/ENG/84D-21 Terry L. Courtheyn
Major USAF

Approved for public release; distribution unlimited

AFIT/GE/ENG-84D-21

MULTIVARIABLE CONTROL LAW DESIGN FOR THE X-29 AIRCRAFT

THESIS

Presented to the Faculty of the School of Engineering
of the Air Force Institute of Technology
Air University
in Partial Fulfillment of the
Requirements for the Degree of
Master of Science

Terry L. Courtheyn, B.S.
Major USAF
Graduate Electrical Engineering
December 1984

Preface

This research effort concentrates on the development of flight control laws for the X-29 forward swept wing demonstrator aircraft by applying recent advances in multivariable control law theory. Such an approach is of great importance to the Air Force because past design techniques are very tedious, time consuming, complex, and expensive when applied to the design of the intercoupled multiple input, multiple output flight control systems now required on new advanced technology aircraft.

The author wishes to express his gratitude to Captain David Potts and others at the Flight Dynamics Laboratory for sponsoring this thesis.

The technical expertise, assistance, suggestions, and stimulating technical discussions provided by my thesis advisor Professor John J. D'Azzo had a profound effect on the work. Also appreciation is expressed to Professor D'Azzo and my reader, Professor Constantine H. Houpis, for carefully and thoroughly reviewing the manuscript. A very special thanks to Captain John West at NASA Dryden, Edwards AFB, California for his timely and important contributions in obtaining appropriate models of the aircraft. Most importantly, I am deeply grateful to my wife, Patricia, whose assistance, patience, understanding, and constant supportiveness made the success of this effort possible.

Major Terry L. Courtheyn

Contents

List of Figures

List of Tables

List of Symbols

$\underline{A}$	Plant state matrix
a	Acceleration
A	Longitudinal acceleration
α	Angle of attack, perturbation angle of attack in perturbation equations
$\underline{B}$, $\underline{b}$	Control input matrix
β	Sideslip angle
$\underline{C}$	Plant output matrix
C	Circumference of a circle
cg	Center of gravity
com	Command
cos	Cosine
deg	Degree
δ_C	Canard deflection
δ_F	Flaperon deflection
δ_R	Rudder deflection
δ_S	Strake flap deflection
δ_T	Differential throttle angle position
$\underline{e}(t)$, $\underline{e}$	Error vector
$\underline{e}(KT)$	Discrete error vector
e_C	Signal input to canard actuator
e_S	Signal input to strake flap actuator
e_T	Signal input to engine throttle actuator

ε	Epsilon scalar multiplier
ft	Feet
f	Sampling frequency
g	Gravity, gain constant
$\underline{G}(s)$	Transfer function matrix
$\underline{G}(0)$	Steady state transfer function matrix
$\underline{I}$	Identity matrix
K	Kilo (1000)
$\underline{K}_0$	Proportional control law feedback matrix
$\underline{K}_1$	Integral control law feedback matrix
lbs	Pounds
λ	Eigen value
$\underline{M}$	Measurement matrix
m	Mass, number of inputs
$\underline{M}_C$	Controllability matrix
$\underline{M}_O$	Observability matrix
n	Number of states
N_{cg}	Normal acceleration at aircraft's center of gravity
N_y	Lateral acceleration
N_{ZP}	Normal acceleration at pilot's station
p	Number of outputs, roll rate
ϕ	Roll angle
q	Pitch rate
Q	Pitch rate
r	Yaw rate
R	Radius

rad	Radians
s	Laplace operator
sec	Seconds
sin	Sine
ss	Steady state
$\underline{\Sigma}$	Sigma gain weighting matrix
$\underline{\Gamma}$	Discrete output matrix
T	Sampling period
θ	Pitch angle
U	Velocity along x-axis
u	Perturbation velocity
$\underline{u}$	Input vector
V	Velocity along y-axis
v	Perturbation velocity along y-axis, tangential velocity
$\underline{v}$	Command input vector
W	Aircraft weight
w	Perturbation velocity along z-axis
$\underline{x}$	State vector
$\underline{y}$	Output vector
$z(t), \underline{z}$	Integral of error vector
$z(kT)$	Discrete Integral of error vector
z_t	Transmission zeros
ψ	Yaw angle

Abstract

Flight control laws are designed for the X-29 forward swept wing demonstrator aircraft using a design technique based on multivariable control law theory developed by Professor Brian Porter of the University of Salford, England. The computer-aided design program called MULTI is used to develop and refine the control laws. MULTI also simulates the complete closed-loop control system and generates appropriate time response plots for analysis.

Aircraft dynamics for several points in the flight envelope are represented by linearized state space equations obtained from NASA Dryden, an agency responsible for the development and testing of the X-29. Decoupled longitudinal and lateral equations are used to design separate longitudinal and lateral controllers.

Control laws are developed to stabilize the aircraft and perform longitudinal maneuvers (direct climb, vertical translation, and beta pointing) at three different flight conditions, with and without first order-actuator dynamics and computational time delay added to the simulation. The responses are compared. Although some degradation of performance is observed when the actuator dynamics and time delay are added, the results show fast and well-behaved

control of the aircraft motion parameters with quick and smooth tracking of pilot input commands. Similarly, lateral control laws are developed for the coordinated turn and beta pointing maneuvers at five different flight conditions with comparable results.

Finally, future areas of research are recommended which also include proposed modifications and additions to MULTI.

MULTIVARIABLE CONTROL LAW DESIGN FOR THE X-29

1. Introduction

1-1 Background

Fighter pilots will not be able to accomplish their missions unless future tactical aircraft incorporate the latest in technological advances to counter the ever-increasing lethal capability of the enemy's air defense systems. Adversaries are dramatically improving their surface to air missiles, radar guided anti-aircraft artillery, fighter-interceptor aircraft, air to air missiles, and other air defense weapons.

In order to neutralize these deadly threats, tactical aircraft of the future need the capability to fly higher, farther, faster, and to fly with greater maneuverability and survivability at all altitudes and airspeeds. To accomplish these goals, future vehicles must be smaller, lighter, more fuel efficient, and have better aeronautical designs.

New airplanes like the X-29 advanced technology fighter are expected to meet these challenges with innovative features such as forward swept wings, static instability, and multiple function control surfaces.

However, the aerodynamic designs which provide this enhanced capability cause two serious problems. Because of the statically unstable airframe, it is impossible for a pilot to fly the aircraft without automatic stability augmentation provided by a flight control computer. In addition, it is not feasible for a pilot to independently control all of the added flight control surfaces. But a properly designed flight control system can accomplish this difficult task by optimally deflecting the appropriate control surfaces when the pilot commands a specific maneuver. Thus, the performance requirements for future fighter aircraft dictate the need for sophisticated flight control systems.

Digital flight control systems will be standard equipment on most future high performance aircraft. Rapidly advancing technology in digital electronics and computational proficiency of microprocessors make them ideal for solving the complicated algorithms required in state-of-the-art flight control systems.

The question arises as to the best method for designing the control laws and algorithms for the flight control digital computer. Classical control theory techniques are best suited for the simple single input, single output (SISO) flight control systems currently used on conventional aircraft. These older methods are very tedious and time consuming for designing complex intercoupled

multiple input, multiple output (MIMO) systems. In response to this problem, experts in flight control theory have developed several new MIMO design methods such as linear quadratic regulator (LQR) and quantitative feedback theory (QFT). This thesis uses another technique recently developed by Professor Brian Porter of the University of Salford, England (10).

1-2 Problem

The static instability of the X-29 plus the added number of flight control surfaces dictate the necessity for a full authority digital flight control system.

Engineers are having difficulty designing optimum control laws for the X-29 digital flight controller because of the highly relaxed static stability and the complexity of the aircraft's aerodynamic design.

Using the Porter technique and the computer-aided design package called MULTI, this thesis designs improved control laws for the longitudinal and lateral flight controllers for the maneuvers and flight conditions listed below:

Longitudinal Maneuvers

1. Direct climb
2. Vertical translation
3. Pitch pointing

Flight Conditions

1. 0.4 Mach at sea level
2. 0.7 Mach at 15,000 feet
3. 1.2 Mach at 15,000 feet

Lateral Maneuvers

1. Coordinated turn
2. Beta pointing

Flight Conditions

1. 0.4 Mach at sea level
2. 0.9 Mach at sea level
3. 0.7 Mach at 15,000 feet
4. 1.2 Mach at 15,000 feet
5. 0.9 Mach at 50,000 feet

1-3 Scope

This project expands on the work completed by Lieutenant Scott Feldman on a digital flight controller for the X-29 (5). Those designs did not include actuator dynamics and computational time delay which reduce the phase margin and make it a harder task to assure stabilization of the system. Specifically, this research effort accomplishes the following goals:

1. Redesign the flight control system with actuator dynamics included in the closed-loop simulation but external to the plant state equations.

2. Evaluate the aircraft responses with and without computational time delay and actuator dynamics included in the closed loop simulation.

3. Enhance the capability of the computer program MULTI by developing additional FORTRAN source code to:

a. calculate the steady-state G(0) and $G(0)^{-1}$ matrices for use in calculating steady state aircraft control deflections; and

b. convert output simulation data from dimensions of radians to degrees prior to plotting the time responses.

1-4 Standards

This research effort evaluates the final digital control system design using computer simulations. The controller should meet the following standards:

1. Provide stability augmentation.

2. Show fast and well-behaved control of aircraft angles, rates, and velocity.

3. Quickly and smoothly track the pilot's input commands.

4. Feedback motion parameters that are measured with currently available sensors.

1-5 Approach

This research work applies the design technique of Professor Brian Porter to develop the appropriate

control laws for the X-29 digital flight controller. His method uses the state space time domain approach of multivariable control theory. Specifically, integral plus proportional control is applied to all forward loops. In addition, his procedure employs output feedback which has a great practical advantage because the outputs to be controlled are accessible and easily measured with sensors. More information is presented in Appendix A where the theory of Professor Porter's method is discussed in greater detail.

1-6 Materials and Equipment

This research effort uses the Control Data Corporation "Cyber" main frame computer located at Aeronautical Systems Division, Wright-Patterson AFB, Ohio to run the software programs called TOTAL, ZERO, and MULTI. The computer-aided design package called MULTI is needed to apply Porter's control law theories. The program also allows on-line design changes and generates output response plots. A comprehensive user's manual with illustrative examples, describes the available options and capabilities of the program (8).

1-7 Overview

Chapter 2 begins with a general description of the X-29 aircraft and continues with a discussion of its unique design features. Then, Chapter 3 presents the origin, assumptions, limitations, and dimensions for the

linearized state space equations of motion for the X-29. Next, Chapter 4 describes the detailed procedure developed in this research effort to design a proportional plus integral multivariable discrete time tracking controller for the X-29 in the longitudinal mode. Detailed results for the longitudinal control system designs are presented in Chapter 5 for three maneuvers from a sample of flight conditions. Chapter 6 highlights significant steps related to the lateral design procedure. This is followed by a presentation and analysis of the results of the lateral controller designs for two maneuvers at one flight condition. Conclusions are given in Chapter 7 with recommendations for future research. Appendix A provides a description of multivariable control theory as it applies to the Porter technique. Then, Appendices B and C document improvements made to the computer program MULTI. Next, Appendices D, E, and F present additional data not included in the discussions of Chapter 5. This additional data includes state space matrices, design parameters, controller matrices, figures of merit, and response plots for the longitudinal controllers. Similarly, Appendices G and H present the remainder of the lateral information not provided in Chapter 6. Finally, Appendix I overviews some unsuccessful design attempts.

2. The X-29 Aircraft

2-1 General Description

The X-29, illustrated in Fig. 2-1, is an experimental advanced technology demonstrator aircraft built to evaluate the feasibility and capability of several new aeronautical design concepts. Specifically, the vehicle is designed to exercise the full spectrum of forward swept wing (FSW) technologies in a cost effective and timely manner. For example, 56 percent of the aircraft weight includes components common to existing aircraft (14:11). However, the remainder of the vehicle incorporates many new and unique design features as outlined below:

1. statically unstable airframe
2. forward swept wings
3. thin supercritical airfoils
4. close coupled canards
5. strake flaps
6. variable camber control surfaces
7. control configured design

The remainder of this chapter describes these new innovations in more detail.

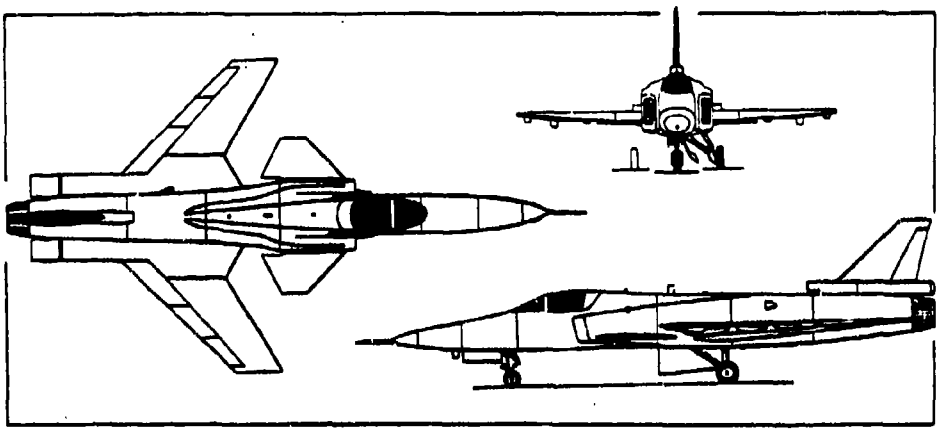

Figure 2-1. Grumman X-29 Aircraft (16)

Dimensions, External:

Wing span	27 ft	2 in
Wing chord: at root	9 ft	8 in
at tip	3 ft	11 in
Wing aspect ratio		4
Length of fuselage	48 ft	1 in
Height	14 ft	3 in
Wheel base	18 ft	0 in

Weights

Weight empty	13,326 lb
Max fuel weight	3,978 lb
Max takeoff weight	17,303 lb

2-2 Airframe

Grumman designed the small single engine aircraft with an overall shape developed by blending an optimized forward swept wing and canard arrangement to an exsiting F-5A forward fuselage module with modified engine ducts and a new mid and aft fuselage (14:3).

Engineers purposely designed the airframe with high static instability to maximize the vehicle's maneuverability and to minimize trim drag. As a result, the short period roots are unstable at subsonic speed flight conditions. The time to double amplitude is less than 0.5 seconds. This rate of divergence of the unstable mode illustrates the need for a highly reliable stability augmentation system (14:24).

2-3 Forward Swept Wings

Background. Aeronautical engineers invented both forward and aft swept wings during World War II in a concentrated effort to increase the maximum and cruise speeds of aircraft. Both aft and forward swept configurations delay Mach drag divergence and produce weaker oblique wing shock waves at transonic velocities. Initial designs had wings swept in both directions and, in fact, the Germans flew the first swept wing aircraft (the Jungers JU 287 bomber) during World War II. It had forward swept wings (6:147). Unfortunately, continued development of the FSW was short lived. After World War II, engineers attempted additional

forward swept wing designs, but no aircraft prototypes were ever built due to an inherent malady--aeroelastic divergence. The existence of the problem was known from the beginning but the severity was not fully appreciated until the late 1940s when Diederick demonstrated a drastic drop in the divergence speed with increased forward sweep angle (6:147). The divergence phenomenon increased the FSW weight penalty to impractical values. Thus, FSW technology was abandoned and designs concentrated solely on aft swept wings. Thirty years later, the invention of advanced lightweight composite materials suddenly provided a solution to the divergence problem.

Aeroelastic divergence occurs when the wing tip twists upwards as dynamic pressure under the wing increases. This upwards twisting increases angle of attack and generates additional torque which is greater than the structural elastic restoring forces. As a result, the deformation continues until the structure fails (6:147).

Aeroelastic Tailoring. Grumman material engineers overcame aeroelastic deformation by using a new process called aeroelastic tailoring. Boron fiber, graphite, plastic adhesives, and other composite materials produce non-metallic wings 30 percent lighter than metal wings of similar strength. By varying the fiber direction and thickness, the designer tailors the wing stiffness characteristics to suit a particular loading condition, distributing

the twisting load (greatest at the wing tips) over the entire wing.

Wave Drag. An aircraft flying through the atmosphere produces a "pressure wave" as the fuselage, wings, and other parts of the vehicle push the air out of the way. Pressure waves cannot travel faster than the speed of sound. When an aircraft flying at a supersonic velocity overtakes the pressure wave, the vehicle experiences a phenomenon called "wave drag." The magnitude of the wave drag is reduced by using a minimum and uniform aircraft cross-sectional area perpendicular to the airstream. Therefore, a correctly designed fuselage is "pinched in" where the wing attaches to the fuselage to account for the added cross-sectional area of the wing. Aft swept wings, by necessity, attach to a "pinched in" fuselage near the center of gravity. Unfortunately, the payload also is concentrated near the aircraft's center of gravity to minimize the pitching moment. This lowers the available cargo space in the vehicle. Advantageously, forward swept wings connect to the fuselage farther aft of the center of gravity outside the area of payload concentration (6:148).

Stall Progression. The forward swept wing provides the X-29 with the capability of flying at low airspeeds and at angles of attack as high as 70 degrees. This is possible because stalls progress opposite to the direction of airflow from the trailing edge to the leading edge and from

the most aft to the most forward part of the wing. Therefore, aft swept wings stall first at the wing tips near the ailerons. As a result, the ailerons become ineffective and lateral control is lost at approximately 30 degrees angle of attack. Moving the ailerons away from the wing tips is not practical because it lessens the roll moment due to a shorter lever arm. In contrast, for the forward swept wing, the stall begins at the root of the wing away from the ailerons and progresses toward the wing tips. This phenomenon allows greater maneuverability at low airspeed--a valuable aerial combat advantage.

Super Critical Airfoil. The X-29 wings are not only swept forward, but also "supercritical," which decreases drag and minimizes loss of lift at supersonic airspeeds. Geometrically, the leading edge of the wing has a greater radius of curvature and a flatter top surface than the conventional airfoil. The curvature causes air flowing over the supercritical wing to quickly reach supersonic speed. The flat top surface sustains the supersonic velocity of the air so the shock wave forms at the trailing edge of the wing, where drag is lower and loss of lift is less (5:26).

2-4 Canard

The canard, located just behind the cockpit, increases the capability of the forward swept wing and is the primary airfoil for generating the control moments and

stabilizing the aircraft's longitudinal axis (see Fig. 2-2). The canard and wing interact to minimize trim drag at all mach numbers. Also the canard directs additional air to the root of the wing to further resist stall at high angles of attack.

Since the X-29 is statically unstable, the center of gravity of the aircraft is aft of the center of pressure. Therefore, the canards must generate a negative lift during one "g" trimmed steady level flight to cancel the positive moment produced by the wing. Fortunately, during high "g" maneuvers, the canard creates a positive pitching moment with a positive aerodynamic force that adds to the total lift on the vehicle. Additionally, this arrangement allows greater movement of the center of gravity and enhances flexibility in payload distribution.

The range of canard surface deflection is -60 degrees to +30 degrees with a rate limit of 105 degrees per second (14:18).

2-5 Strake Flaps

The strakes in Fig. 2-2 are horizontal airfoils connected to the fuselage from the wings to the tail. Primarily, the strakes function to produce a nose down pitching moment at high angles of attack. The flaps at the end of the strakes provide the control power.

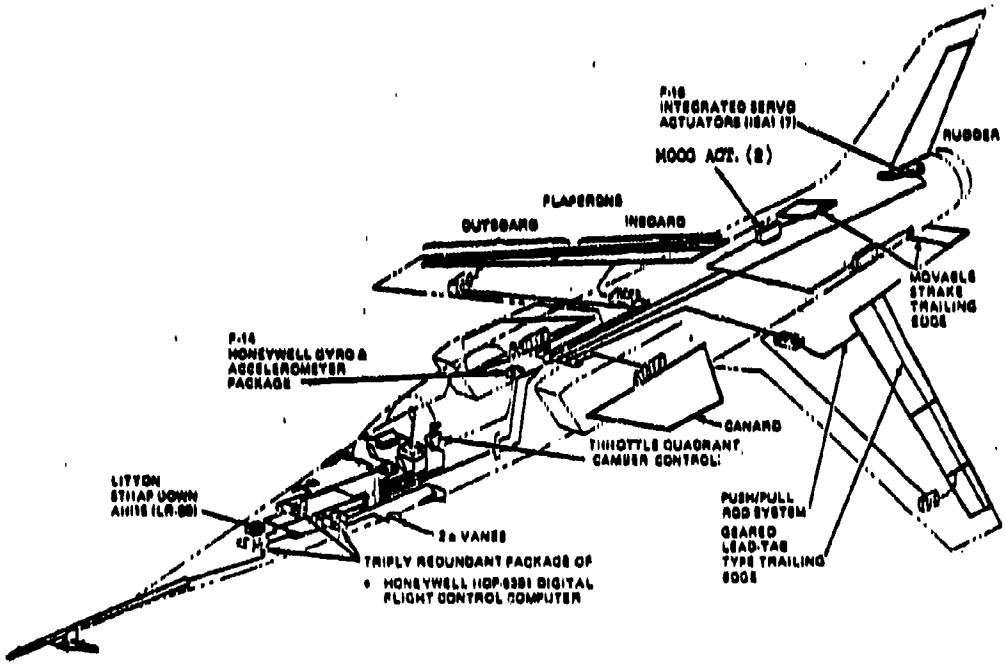

Figure 2-2. X-29 Control Surface Configuration (15)

The deflection limits for the strake flaps are -30 degrees to +30 degrees. The rate limit is a slow 27 degrees per second (15:3-47).

2-6 Variable Camber Control Surfaces

Dual hinged flaperons, attached to the trailing edge of the forward swept wing, provide high lift flaps, lateral control, and discrete variable camber to maximize lift/drag ratio over all flight conditions (see Fig. 2-2).

Dividing the flaperons into three separate sections along the wing combats aerodynamic flutter. The inboard flaperon, consisting of two parts, generates additional lift similar to a standard flap. The outboard section operates differentially like ailerons to provide roll control. All three sections move together as symmetrical flaperons for variable camber.

Variable camber allows a flight control computer to automatically optimize the wing shape for maximum efficiency during steady level cruise flight. In the "normal mode" of operation, a full authority digital flight control computer trims not only the variable camber flaperons, but also the canard and strake flap positions for optimal airflow over all airfoils to minimize drag for the desired flight condition. In the "reversion mode" an analog backup system sets the canard and strake flaps to zero position and adjusts only the forward swept wing camber to trim the aircraft for a particular flight condition.

The flaperons deflect in the range of -19.5 degrees to +13 degrees with a rate limit of 68 degrees per second (15:3-44).

2-7 Summary

The X-29 advanced technology demonstrator with forward swept wings and high negative static margin aerodynamics provides a significant advantage in performance and overall flexibility as follows:

1. improved area rule configurations
2. higher volumetric efficiencies
3. more versatile weight and balance arrangements
4. improved pilot visibility
5. smaller aircraft size--reduced radar profile
6. simpler and lighter installations for hydraulics
7. more compatible wing pylon store carriage
8. superb maneuvering over a wide range of airspeeds and angles of attack
9. enhanced fuel efficiency at transonic and supersonic velocities

The added features of this aircraft are expected to revolutionize air combat tactics and provide a superior fighting capability.

3. Mathematical Model of X-29 Aerodynamics

3-1 Introduction

The development of control laws using the Porter design method requires an accurate state space matrix representation of the equations of motion of the aircraft. The equations of motion are a mathematical model of the physical system (plant) that relate external forces and moments to the linear and angular accelerations of the vehicle in accordance with Newton's laws of motion. To derive the equations, certain assumptions must be made and an appropriate axis system defined.

This chapter describes the origin, axis system, assumptions, limitations, and dimensions of the aircraft equations. Also included in the chapter are the mathematical equations that model the engine thrust and control surface actuator dynamics. Understanding these details is critical to the successful design of a control system.

3-2 Origin of Data

Grumman Aerospace Corporation, manufacturer of the X-29, calculates all aerodynamic data including stability derivatives for the aircraft using wind tunnel tests and other techniques. As with any development project, they continually update and upgrade the data as new information

and aircraft modifications occur. In late 1983, Grumman supplied aerodynamic data set number four to NASA Ames Research Center at Edwards AFB, California. On 24 May 1984, NASA used their own computer program (2) and Grumman's aerodynamic data set four to derive the six degree of freedom state space matrix equations used in this thesis.

3-3 Assumptions

The complexity of formulating and solving problems in flight dynamics necessitates the need to make commonly accepted approximations involving the equations of motion. Judiciously selected assumptions reduce the design effort with minimum loss of accuracy.

The equations of motion in this research effort include the following assumptions:

1. The earth is an inertial reference. This is a commonly accepted approximation because aircraft maneuvers have short durations compared to earth rate. Also the flight control system's sensors are too insensitive to detect the earth's rotational rate and corriolis acceleration.

2. The atmosphere is assumed fixed with respect to the earth. This assumption limits the scope for a preliminary design. Final designs should include the effects of random gusts, wind shears, and steady winds.

3. The aircraft is a rigid body. Initial designs generally incorporate this assumption. A bending mode

analysis may be necessary in the final design depending on the type and size of the aircraft and the maneuver performed. However, limiting the flight control system bandwidth reduces interaction with bending and vibration modes which generally occur at higher frequencies.

4. The aircraft mass is constant. This is a good approximation during a 10 to 15 second maneuver.

5. The airstream surrounding the airplane changes instantaneously when the vehicle is disturbed from equilibrium. At transonic and supersonic speeds the compressibility drag reduces the validity of this assumption, but it is a good first approximation.

6. Aerodynamics of the vehicle are fixed at the trim point for a particular Mach number and altitude. Although perturbations in velocity and altitude occur during the maneuvers, the stability derivatives change slowly (except in the transonic region). Therefore, the approximation is valid for small variations from the reference point.

7. The equations of motion can be decoupled into longitudinal and lateral sets of equations. The only cross coupling term in the equations of motion for the X-29 is a slight influence by beta (side slip angle) in the pitch rate equation. This is safely ignored for the preliminary design attempt of this thesis.

8. Linear perturbation equations about an operating point (flight condition) can be derived from the nonlinear aircraft dynamic equations.

3-4 Limitations

Knowledge of the limitations of the aircraft model ensure that commanded aircraft maneuvers remain within the accuracy boundaries of the equations. Limitations are as follows:

1. The equations of motion are written in the body fixed reference frame because sensors providing feedback signals measure body accelerations. Also, the pilot prefers to control quantities that his senses can easily detect such as body accelerations and rates. Figure 3-1 illustrates the geometry of the reference frame. The origin of the body axes is at the mass center of the vehicle. The axes are mutually perpendicular. The x and z axes lie in the longitudinal plane and the y axis is in the lateral plane.

2. The linear perturbation equations are derived from the nonlinear equations of motion of an aircraft which is in steady level trimmed flight at a particular flight condition (operating point). Therefore, solutions to the linear equations represent deviations from the trimmed operating point.

3. This thesis uses the "normal mode" equations. The "normal mode" equations of motion for the X-29 represent

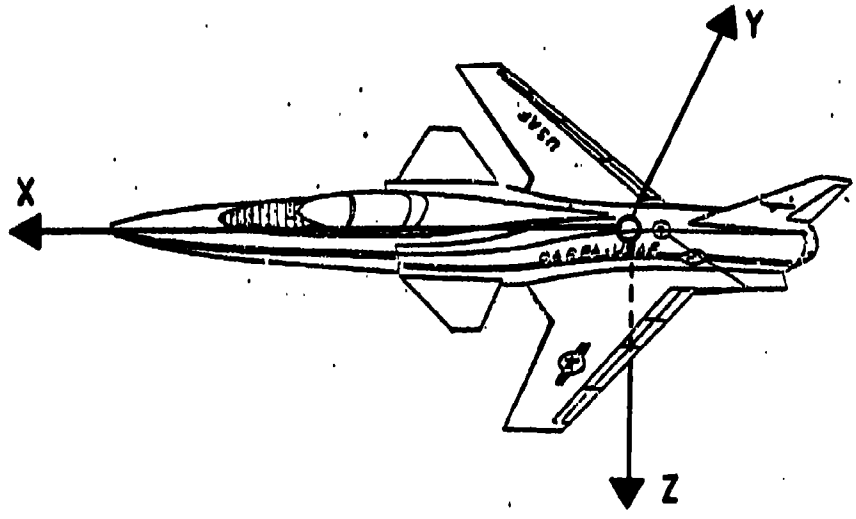

Figure 3-1. Body Axis Definition

an optimum steady level trimmed condition at each flight condition which minimizes drag on the aircraft using the canards, symmetrical variable camber wing flaps, and the strake flaps. The "reversion mode" equations of motion represent a trimmed condition using only the symmetrical variable camber wing flaps with the canard and strake flaps set to zero deflection. See Chapter 2 for additional details on the function and operation of all the control surfaces.

4. The linear equations of motion are valid for bank angles of 30 degrees or less and yaw, pitch, and angle of attack angles of 15 degrees or less.

3-5 Dimensions

The linear perturbation equations of motion furnished by NASA (2) have the following variables and associated dimensions:

1. Pitch angle (θ)--radians
2. Angle of attack (α)--radians
3. Pitch rate (q)--radians per second
4. Change in forward velocity (u)--feet per second
5. Normal acceleration at the pilot station (N_{ZP})--g's
6. Normal acceleration, aircraft center of gravity (N_{CG})--g's
7. Side slip angle (β)--radians
8. Roll angle (ϕ)--radians

9. Yaw rate (r)--radians per second

10. Roll rate (p)--radians per second

11. Lateral acceleration (N_Y)--g's

12. Canard surface deflection (δ_C)--minus 60 degrees to positive 30 degrees (positive deflection produces pitch up moment, negative deflection produces pitch down moment)

13. Canard surface deflection rate ($\dot{\delta}_C$)--maximum of 105 degrees per second

14. Strake flap surface deflection (δ_S)--minus 30 degrees to positive 30 degrees (positive deflection produces pitch down moment, negative deflection produces pitch up moment)

15. Strake flaps deflection rate ($\dot{\delta}_S$)--maximum 27 degrees per second

16. Thrust (δ_T)--differential throttle angle position setting, values from 0.04 to 0.791 represent idle to military thrust, values from 0.792 to 1.0 represent afterburner thrust. Actual values of engine thrust in pounds of force are not defined.

17. Differential wing flap (flaperon) surface deflection (δ_F)--minus 19.5 degrees to plus 13 degrees

18. Flaperon surface deflection rate ($\dot{\delta}_F$)--maximum of 68 degrees per second

19. Rudder surface deflection (δ_R)--minus 31 degrees to plus 31 degrees

20. Rudder surface deflection rate ($\dot{\delta}_R$)--maximum of 141 degrees per second

21. All the equations in the thesis use an aircraft weight of 15000 pounds

22. Numbers in the aircraft equation of motion matrices are accurate to four significant figures

3-6 Actuator Dynamics

The equations of motion for the X-29 aircraft, furnished by NASA, do not include actuator dynamics. However, an objective of the thesis is the design and evaluation of a flight control system for the aircraft with engine thrust and control surface actuator dynamics included in the complete closed-loop system.

To approximate the dynamics of the canard actuator and engine thrust response, this research effort uses first order differential equations with a time constant of 0.05 seconds. It is the same time constant utilized by Grumman engineers in their Forward Swept Wing Demonstrator Technology Integration and Evaluation Study (14:18).

The strake flap actuator time constant is set at 0.20 seconds, which is four times longer than the time constant of the canard actuator. This simulates the rate limit of 27 degrees per second for the strake flap which is approximately four times slower than the maximum deflection rate of 105 degrees per second for the canard.

Using the above time constants results in Laplace transfer functions as follows:

$$\delta_C/e_C = 20/(s+20) \qquad (3\text{-}1)$$

$$\delta_S/e_S = 5/(s+5) \qquad (3\text{-}2)$$

$$\delta_T/e_T = 20/(s+20) \qquad (3\text{-}3)$$

where

δ_C = canard deflection

δ_S = strake flap deflection

δ_T = thrust

e_C = signal input to canard actuator

e_S = signal input to strake flap actuator

e_T = signal input to engine throttle actuator

The computer-aided design program MULTI (11) requires the above equations in state space representation where

$$\dot{\underline{x}} = \underline{A}\,\underline{x} + \underline{b}\,\underline{u} \qquad (3\text{-}4)$$

$$\dot{\underline{\delta}}_C = -20\,\underline{\delta}_C + 20\,\underline{e}_C \qquad (3\text{-}5)$$

$$\dot{\underline{\delta}}_S = -5\,\underline{\delta}_S + 5\,\underline{e}_C \qquad (3\text{-}6)$$

$$\dot{\underline{\delta}}_T = -20\,\underline{\delta}_T + 20\,\underline{e}_T \qquad (3\text{-}7)$$

and

$$\underline{y} = \underline{C}\,\underline{x} \qquad (3\text{-}8)$$

3-7 Summary

The assumptions and limitations associated with the linear perturbation equations of motion for the X-29 aircraft are numerous but still provide an adequate model of the vehicle for the initial design of an aircraft control system.

The next chapter describes in detail the design of the longitudinal axis flight control system which includes the aircraft model equations and control laws.

4. Longitudinal Controller Design Procedure

4-1 Introduction

This chapter describes in detail the procedure developed in this research effort and subsequently followed to design a proportional plus integral multivariable discrete-time tracking system for the X-29 aircraft, implemented with and without computer time delay and actuator dynamics. The comprehensive design procedure applies the Porter design method and includes the following major steps:

1. Validate the aircraft model
2. Analyze the aircraft open-loop transfer functions
3. Select the required output variables and feedback signals
4. Check controllability and observability
5. Calculate the transmission zeros
6. Determine measurement matrix if required
7. Estimate maximum maneuvers using the G(0) matrix
8. Determine appropriate control input magnitudes and rates
9. Specify sigma weighting matrix elements
10. Choose the epsilon and alpha proportional plus integral gain factors

11. Use MULTI to:

a. calculate the $\underline{K}_0$ and $\underline{K}_1$ matrices

b. form the closed-loop control system to check for stable roots in the characteristic polynomial

c. run a discrete simulation of the entire control system and display the time responses

d. optimize the design with actuators and computational time delay

Throughout the remainder of this chapter, sample calculations for the flight condition of 0.7 mach at 15,000 feet illustrate specific details in each step of the design procedure outlined above. Chapter 5 and Appendices D through F present the data and results for the other flight conditions.

4-2 Validation of Aircraft Model

Chapter 3 describes in detail the origin, assumptions, limitations, and dimensions associated with the state space representation of the linear perturbation equations of motion of the aircraft.

This research effort does not derive the equations of motion for the X-29 aircraft. The equations are a product of NASA Ames Research Center's computer program "X-29 Trim and Linearized Data Routine, Forward Swept Wing Linear Six Degree of Freedom Simulation" (2). The data represents the fourth update and refinement and includes Grumman's aerodynamic data set number four.

A typical example of the information provided by NASA is the A and B matrix longitudinal axis equations for 0.7 mach at 15,000 feet as shown below:

$$\underline{\dot{x}} = \underline{A}\,\underline{x} + \underline{B}\,\underline{u} \qquad (4\text{-}1)$$

$$\begin{bmatrix} \dot{\theta} \\ \dot{u} \\ \dot{\alpha} \\ \dot{q} \end{bmatrix} = \begin{bmatrix} 0 & 0 & 0 & 1 \\ -32.13 & -0.01199 & -1.718 & -0.3504 \\ -0.3246E\text{-}06 & -0.1298E\text{-}03 & -1.138 & 0.9917 \\ 0 & 0.2986E\text{-}03 & 18.92 & -0.4928 \end{bmatrix} \begin{bmatrix} \theta \\ u \\ \alpha \\ q \end{bmatrix} + \begin{bmatrix} 0 & 0 & 0 \\ -0.05895 & 0.02621 & 27.24 \\ -0.001161 & -0.7808E\text{-}03 & -0,002099 \\ 0.1720 & -0.05630 & -0.1929 \end{bmatrix} \begin{bmatrix} \delta_C \\ \delta_S \\ \delta_T \end{bmatrix}$$

This thesis assumes the numerical values in the matrices are correct. Obviously, the equations relating kinematic relationships are accurate. In addition, a check of all the signs on the open-loop transfer functions for the unaugmented aircraft indicate the correct direction of movement of the vehicle for a given control deflection.

4-3 Analysis of Aircraft Model

An analysis of the open-loop transfer functions of the unaugmented aircraft provide insight into the possible difficulty in designing a satisfactory control system. As

described in Chapter 2-2 "Airframe," the X-29 aircraft is statically unstable at subsonic mach numbers. The following open-loop transfer functions for 0.7 mach at 15000 feet clearly illustrate this phenomena:

Characteristic Polynomial (C.P.)
$= (s + 5.16)(s - 3.529)(s + 0.005907 \pm j\ 0.06082)$ (4-2)

$q/\delta_C = 0.172\ s\ (s + 1.01)(s + 0.0125)/C.P.$ (4-3)

$q/\delta_S = -0.0563\ s\ (s + 1.4)(s + 0.01254)/C.P.$ (4-4)

$q/\delta_T = -0.1929\ s\ (s + 0.9985)(s + 0.3152)/C.P.$ (4-5)

$u/\delta_C = -0.05895\ (s + 0.7165 \pm j\ 8.906)(s + 1.186)/C.P.$ (4-6)

$u/\delta_S = -0.02621\ (s + 0.3287 \pm j\ 7.367)(s + 1.777)/C.P.$ (4-7)

$u/\delta_T = 27.24\ (s + 5.139)(s - 3.489)(s - 0.01705)/C.P.$ (4-8)

$\alpha/\delta_C = -0.001161\ (s - 146.4)(s + 0.005991 \pm j\ 0.06417/C.P.$ (4-9)

$\alpha/\delta_S = -0.0007808\ (s + 72.0)(s + 0.005934 \pm j\ 0.065380)/C.P.$ (4-10)

$\alpha/\delta_T = -0.02099\ (s + 93.35)(s - 0.01025 \pm j\ 0.06406)/C.P.$ (4-11)

There is an unstable root at 3.529 in the characteristic polynomial. Also, several of the transfer functions have zeros in the right half plane. As an illustration, examine the transfer function for α/δ_C. From a single-input-single-output (SISO) classical root locus point of

view, the zero at 146.4 and the pole at 3.529 depict a system that is highly unstable for all positive values of feedback gain. Without compensation, the closed-loop system characteristic polynomial has a root between 3.529 and 146.4 depending on the value of the feedback gain. This degree of instability in an aircraft is very unusual. The plant is a non-minimum phase system. Therefore, the successful design of a control system is difficult. This is especially true when actuator/sensor dynamics and computational time delay are added to the basic equations. These additions may reduce the phase margin and make it a harder task to assure stabilization of the system.

4-4 Controlled Variables

The output vector "$\underline{y}$" represents the controlled variables. The outputs can be states of the aircraft plant or linear combinations of states. The inputs to the control system, represented by the vector "$\underline{y}$", are the commands to be tracked by the output vector $\underline{y}$ (see Fig. A-1). Examples include pitch rate and angle of attack. Inputs to the aerodynamic model (plant), represented by the vector "$\underline{u}$", are the controllable mechanisms on the vehicle that can modify its motion. For the X-29 longitudinal axis, the inputs include the canards, strake flaps, thrust, and symmetrical flaperons. For the lateral axes, the inputs are the rudder and flaperons.

The Porter design technique requires an equal number of input and output (controlled) variables. Additionally, the Porter method incorporates output feedback and all outputs are fed back to the input of the control system. See Appendix A for more theory and block diagrams of the high-gain error-actuated closed-loop control system configuration.

Each independently controlled variable requires a separate control input for a decoupled and completely controllable vehicle response. This is a basic requirement which is independent of the design method. For example, controlling pitch angle, velocity, and angle of attack requires three control mechanisms in the longitudinal axis of the aircraft (canards, strake flaps, and engine thrust for the X-29).

Selecting the correct control output variables is very important and depends on several conditions outlined below:

1. the available aircraft control inputs
2. practicality and reliability of measuring the controlled variables
3. the desired maneuvers
4. restraints of the design method

Aircraft Controls. Canards, symmetrical flaperons, strake flaps, and thrust are the longitudinal axis aircraft control inputs on the X-29. These four control inputs

ovide the capability to command four independent longitudinal outputs. It is difficult to command four separate outputs that do not conflict with each other. Therefore, the designs in this thesis control three longitudinal variables using the canards, strakes flaps, and thrust as the three control inputs. The symmetrical flaperons are not used as a control input because their primary function is trimming the aircraft to minimize drag at each cruise flight condition by optimizing the air flow over the canards, wings, and strakes. Since this research effort uses the "normal mode" equations of motion, the symmetrical flaperons are already set to the optimum position for minimum drag. Also, the maneuvers are small perturbations about the trimmed operating point, thereby minimizing the need to move the symmetrical flaperons.

Measurement of Output Variables. The pilot feels angular rates and accelerations and, in actuality, he controls those quantities when flying conventional aircraft. In addition, it is more reliable to measure rates and accelerations using rate gyros and accelerometers than to measure pitch and bank angles. The pitch and bank angle measurements are generally obtained from an inertial navigation system with significantly lower hardware reliability than the flight control system. Angle of attack measurements are reasonably reliable but are subject to wind gusts and turbulence.

This thesis is successful in performing several important longitudinal maneuvers using pitch rate, velocity, and angle of attack as the output variables. An attempt to control normal acceleration was unsuccessful due to current limitations with the design method.

Desired Longitudinal Maneuvers. The multiple control surfaces in the longitudinal axis allow the X-29 to generate "direct forces," i.e., aircraft movements uncoupled or not related to aircraft rotation. "Direct force" in the longitudinal axis makes possible three new maneuvers called "direct lift," "pitch pointing," and "vertical translation."

The "direct lift" mode produces a longitudinal acceleration while holding angle of attack constant. The aircraft flight path angle changes due to additional lift generated without changing angle of attack. To accomplish this maneuver the flight control system commands pitch rate and velocity to a desired value and angle of attack to zero. A variation to the "direct lift" mode is the "direct climb" whereby pitch rate is commanded as a pulse of length sufficient to generate a desired pitch angle. The flight path angle equals the new pitch angle since alpha is commanded to zero.

The "pitch pointing" mode provides the pilot the ability to command changes in angle of attack while maintaining a constant aircraft flight path angle and velocity.

Commanding a pitch rate pulse that creates a pitch angle equal to angle of attack accomplishes the maneuver.

"Vertical translation" allows the aircraft to change altitude, i.e., translate vertically, without rotating the aircraft or changing its forward velocity. This maneuver requires pitch rate commanded to zero, no change in forward velocity, and a negative angle of attack to translate the aircraft upwards and positive angle of attack to translate the aircraft downwards.

The ability of the aircraft to perform any of the "direct force" maneuvers depends on the force generating capability of the control surfaces and their deflection limits.

Design Method Restraints. Selecting the proper output variables depends not only on the desired aircraft maneuvers but also the restraints of the design method. For example, the design method requires the number of outputs to equal the number of inputs. Furthermore, the technique mandates that all input variables be commanded to a specific value, including zero. Consequently, some maneuvers require precomputations to determine the correct input commands. For example, a constant "g" normal acceleration maneuver requires a precomputed pitch rate and angle of attack command. Still other maneuvers are difficult to command. As an example, if pitch rate, velocity, and angle of attack are the output variables and the desired maneuver

is a constant thrust climb; the Porter control system needs a velocity input command. Precomputing the change in velocity is difficult. In this case, changing the output matrix to remove velocity is more efficient and eliminates the need for precomputations. However, modifying the output matrix does introduce additional problems with implementation of the system.

Careful selection of output variables is necessary to design an efficient flight control system.

4-5 Controllability and Observability

Properties of the state space representation of the system determine controllability and observability. A completely controllable system implies the numerical value of each state variable $x(t)$ at any initial time, t_0, can be changed to any other numerical value in a finite time by means of an unconstrained control input vector $\underline{u}(t)$ (3:442). For a time variant linear system, complete controllability requires the controllability matrix $\underline{M}_C$ to have full rank where

$$\text{Rank } \underline{M}_C = \text{Rank } [\underline{B}\ \underline{AB}\ \ldots\ \underline{A}^{n-1}\underline{B}] = n \qquad (4\text{-}12)$$

A system is completely observable if every state affects the output $y(t)$. This implies that the numerical value of every state $x(t)$ can be determined from the measurements of the output vector $\underline{y}(t)$ (3:442). For a time invariant system, the observability matrix $\underline{M}_0$ must have

full rank where

$$\text{rank } \underline{M}_0 = \text{Rank } [\underline{C}^T \ \underline{A}^T\underline{C}^T \ \ldots \ \underline{A}^{T(n-1)}\underline{C}^T] = n \qquad (4\text{-}13)$$

Also a system is completely controllable and observable if there are no input and no output decoupling zeros. In lieu of directly determining the rank of the $\underline{M}_C$ and $\underline{M}_0$ matrices, this thesis uses an alternative computer program called "Zero" to calculate the transmission, input decoupling, and output decoupling zeros of the state and output aircraft plant equations (7).

In this research effort, the X-29 aircraft open-loop plant is completely controllable and observable, i.e., there are no input or output decoupling zeros, for all the flight conditions and output variable configurations (C matrices).

Likewise, a check of the controllability and observability of the closed-loop tracking system augmented with integrators is very important. A sampled data system augmented with a "Porter configured" proportional plus integral digital controller is completely controllable and observable when the open-loop plant is controllable and observable and

$$\text{rank} \begin{bmatrix} \phi(T)-I & \psi(T) \\ -T\Gamma & 0 \end{bmatrix} = \begin{array}{l}\text{number of states} \\ \quad + \text{number of outputs}\end{array} \qquad (4\text{-}14)$$

Multiplying this matrix by the frequency "f" does not change the rank of the matrix. For the case when "f" approaches infinity, this becomes

$$\text{rank } f \begin{bmatrix} \phi(T)-I & \psi(T) \\ -T\Gamma & 0 \end{bmatrix} = \text{rank} \begin{bmatrix} A & B \\ -C & 0 \end{bmatrix} \qquad (4\text{-}15)$$

as shown by Bradshaw and Porter (10:822).

This satisfies the definition of total controllability whereby every bounded input yields bounded outputs and states.

However, when pitch rate is an output variable, the above matrix is rank deficient and the closed-loop tracking system does not satisfy the strict definition of controllability. But the system is still "conditionally" controllable. The circumstance often occurs when rates and accelerations are the output variables. The cause is a transmission zero at the origin that makes pitch angle unbounded with a constant pitch rate input. This is desirable for fighter aircraft as explained in more detail in the next topic.

4-6 Transmission Zeros

By definition, a transmission zero of a transfer function G(s) blocks the transmission of an exponential signal from the input to the state variable X(s). For example if

$$u(t) = e^{\lambda t} \tag{4-16}$$

then

$$x(t) \neq e^{\lambda t} \tag{4-17}$$

As discussed in Appendix A, Multivariable Control Law Theory, the transmission zeros of a system are regions to which certain finite (slow) roots of the closed loop characteristic equation migrate with increasing gain. As the system's closed loop gains approach infinity or sampling time approaches zero for discrete systems, the affected roots asymptotically approach the transmission zero locations. Output feedback does not alter the number or location of transmission zeros.

Multivariable control theory requires transmission zeros in the left half Laplace s-plane to insure stability at high gains. However, this does not guarantee stability for gains less than infinity because the locus of roots may travel into and out of the unstable region before approaching the locality of the transmission zeros. Therefore, systems with stable transmission zeros are theoretically guaranteed stable only for infinite gains. However, for most systems, especially minimum phase plants, gains much lower than infinity result in stable systems with excellent performance. Thus, control is achieved with gains of reasonable magnitude.

A successful controller design for a non-minimum phase plant with unstable transmission zeros may be possible with the Porter method. In such cases gain boundaries must be established where the locus of roots are in the stable region. Unfortunately, there is no theoretical method to determine the gain boundaries and the system may not be stable for any value of gain. Currently, trial and error is the only technique available. Although there may be a range of gains for stable operation, finding the gain values can be very difficult and time consuming.

The X-29 is a non-minimum phase plant with open-loop zeros and poles in the right half s plane as detailed earlier in this chapter. For example, the unaugmented open-loop aircraft plant without control surface actuators for 0.7 mach at 15000 feet has a transmission zero at the origin. Therefore, unstable roots in the closed-loop characteristic equation are easily possible depending on the values of the gains.

Theoretically, a transmission zero at the origin is undesirable if the control system requires "bounded input-bounded output" controllability. The structure of the X-29 aircraft state equations and the desire to control pitch and roll rates cause transmission zeros to occur at the origin. This means that a bounded input may result in an unbound output. For example, in this investigation, the output variables are pitch rate, velocity, and angle of

attack; and the state variables are pitch angle, velocity, angle of attack, and pitch rate. A pitch rate step command results in the pitch angle ramping to infinity. This is predictable and normal since the pitch angle is simply the integral of the pitch rate. Hence, in fighter aircraft with "rates" as inputs and outputs, the pilot achieves the desired pitch angle by simply commanding a pitch rate pulse.

4-7 Measurement Matrix

If the CB does not have full rank, the plant is "irregular" and the control system requires a measurement matrix. See Appendix A for an explanation of irregular designs. The measurement matrix introduces additional transmission zeros, which can be changed by altering the numerical values of the measurement matrix elements. Furthermore, a sparse measurement matrix generates transmission zeros in the s-plane which are the inverse of the measurement matrix elements. As an example, a 0.2 element in the measurement matrix results in a transmission zero at -5.0. But the relationship is true only for a sparse measurement matrix.

The control engineer should make an effort to eliminate the need for a measurement matrix by reordering the equations or selecting different outputs, if possible. A measurement matrix is always necessary if control surface actuator equations are incorporated as part of the A matrix because of the structure of the equations.

The longitudinal designs in this research effort require no measurement matrix because the outputs are pitch rate, velocity, and angle of attack. The first Markov parameter is satisfied since the matrix $\underline{CB}$ has full rank. In preliminary designs, not presented in this report, the output variables include pitch angle. This results in a rank deficiency of one for $\underline{CB}$ and a need for a measurement matrix with a minimum of one non-zero element.

4-8 Steady-State Transfer Function $\underline{G}(0)$

The maximum magnitude of any steady-state maneuver is dependent on the aircraft plant and is independent of the control system. The largest possible maneuver depends on the aircraft dynamics, structural limitations, and control surface deflection limits. The $\underline{G}(0)$ matrix for the open-loop aircraft plant is useful for evaluating maximum commanded inputs based on the control surface deflections limits. The derivation of the $\underline{G}(0)$ matrix begins with the state space matrix representation of the aircraft open loop plant where

$$\dot{\underline{x}} = \underline{A}\underline{x} + \underline{B}\underline{u} \tag{4-18}$$

$$\underline{y} = \underline{C}\underline{x} \tag{4-19}$$

Solving for $\underline{Y}(s)$ gives

$$\underline{Y}(s) = (\underline{C}[s\underline{I} - \underline{A}]^{-1}\underline{B})\ \underline{U}(s) \tag{4-20}$$

where

$$\underline{G}(s) = (\underline{C}[s\underline{I} - \underline{A}]^{-1}\underline{B}) \tag{4-21}$$

Solving for $\underline{U}(s)$ results in

$$\underline{U}(s) = \underline{G}(s)^{-1}\underline{Y}(s) \tag{4-22}$$

Using the Laplace final value theorem

$$\underline{u}(t)_{ss} = \lim_{s\to 0} [s\ \underline{U}(s)] - \lim_{s\to 0} [s\ \underline{G}(s)^{-1}\underline{Y}(s)] \tag{4-23}$$

When $\underline{y}(t)$ is a constant vector

$$\underline{Y}(s) = K/s \tag{4-24}$$

and the free s in the numerator and denominator cancel, thus the final result is

$$\underline{u}(t)_{ss} = \underline{G}(0)^{-1}K \tag{4-25}$$

For the X-29 at 0.7 mach and 15000 feet with the pitch angle, velocity, and angle of attack as the output variables; the steady state transfer function is:

$$\underline{G}(0)^{-1} = \begin{bmatrix} 0.1915 & -0.03771 & -395.0 \\ -3.469 & -0.1150 & -870.7 \\ 1.183 & -0.0004662 & -0.0496 \end{bmatrix} \tag{4-26}$$

Calculations using the above relationship show that the maximum angle of attack command is two degrees for vertical translation without exceeding control deflection limits.

For the pitch pointing maneuver the maximum pitch angle and angle of attack command is also two degrees. Furthermore, the $\underline{G}(0)^{-1}$ matrix for this aircraft demonstrates that a very small change in steady-state angle of attack commands very large changes in the control surface deflections. This is easily seen by observing the relatively large numbers in the third column of the $\underline{G}(0)^{-1}$ matrix. The relationship is valuable in the design phase when selecting the sigma element that controls the angle of attack. The element value must be small to prevent excessive control surface deflections.

Another use of the $\underline{G}(0)^{-1}$ matrix allows the designer to cross-check the validity of the steady state closed-loop control system time plots. After the completion of the transients, the final values of the control surface positions and the thrust magnitude on the response plots should agree with those calculated with the $\underline{G}(0)^{-1}$ matrix in equation (4-25).

Appendix B documents an improvement to MULTI that provides the capability to calculate the $\underline{G}(0)$ and $\underline{G}(0)^{-1}$ matrices directly from the $\underline{A}$, $\underline{B}$, and $\underline{C}$ matrices of the plant. Also, the user is given the option to enter the plant output vector "$\underline{y}$" and have MULTI automatically calculate the input vector "$\underline{u}$" using the relationship

$$\underline{u}(t)_{ss} = \underline{G}(0)^{-1}\, \underline{y}(t)_{ss} \qquad (4\text{-}27)$$

where

$$\underline{y}(t)_{ss} = \text{a constant vector} \qquad (4\text{-}28)$$

The user may also enter the plant input vector "$\underline{u}$" and have MULTI automatically calculate the plant output vector "$\underline{y}$" using the equation

$$\underline{y}(t)_{ss} = \underline{G}(0)\ \underline{u}(t)_{ss}$$

where

$$\underline{u}(t)_{ss} = \text{a constant vector}$$

For example, the direct climb maneuver for 0.7 mach at 15000 feet has command inputs which generate 7.5 degree pitch and flight path angles with zero change in velocity and angle of attack. For these conditions, the $\underline{G}(0)^{-1}$ matrix calculates steady state values of

canard deflection = 0.02 degrees
strake flaps deflection = -0.44 degrees
thrust = 0.15 throttle angle ratio

These values agree with the time response plots of the closed-loop tracking system.

Often the $\underline{G}(0)^{-1}$ matrix is singular when rates and accelerations are output variables. As an example, when pitch rate is an output variable the $\underline{G}(0)$ matrix is singular (no inverse is possible) because pitch rate is the derivative of pitch angle. An extra "free" s occurs in the

numerator of the corresponding row of the $\underline{G}(s)$ matrix. That s does not cancel when applying the Laplace final value theorem and the outcome is an all zero row. As a consequence of the structure of the state equations, the aircraft control surfaces do not in this case directly control pitch rate because it is kinematically related to pitch angle, i.e.,

$$\dot{\underline{\theta}} = \underline{q} + 0 * \underline{\delta}_C + 0 * \underline{\delta}_S + 0 * \underline{\delta}_T \qquad (4\text{-}29)$$

4-9 Control Input Magnitudes and Rates

The Porter design method creates a controller which tracks the input commands. For step inputs, the controller rapidly drives the control surfaces to maximum deflection at very high rates. Actuators may reduce the surface rates, but not to magnitudes below the specification limits. However, ramping the input command to the desired value slows down the rate of control surface deflection to acceptable limits. The MULTI computer-aided design program provides the capability to represent command inputs as ramp-to-hold signals. For many of the maneuvers in this research effort the input command ramp time durations are calculated by dividing the maximum surface deflection position by the minimum surface rate. For example, most of the X-29 input signals are ramped over a 1.1 second interval as established by the strake flaps position and rate limits.

In addition to the rate limit restrictions, the maximum magnitude and duration of the input commands must keep the aircraft motion within the linear region of the aircraft equations of motion. For example, in this investigation, pitch rate is an input command and its magnitude and the pulse duration determine the final pitch angle for the direct climb maneuver.

Furthermore, the pitch rate pulse rotates the nose of the aircraft and produces normal acceleration of the vehicle during the pull up. The relationship

$$q = (1845/U) * A_n \qquad (4-30)$$

where

q = pitch rate in degrees per second

U = forward velocity in feet per second

A_n = normal acceleration in "g's"

calculates the correct pitch rate for a desired "g" level (1:107). For the direct climb maneuvers in this thesis, the peak magnitude of the pitch rate pulse generates a change of one "g" for the flight condition of 0.7 Mach at 15000 feet as follows:

$$q = (1845 \text{ / } 740 \text{ ft per sec}) * 1 \text{ g} = 2.5 \text{ deg per sec} \qquad (4-31)$$

Since the aircraft is already at one "g" in steady level flight, an increase of one "g" creates the equivalent of a

two "g" normal pull up acceleration during the rotation phase of the direct climb maneuver. The two "g" pull up is sufficient to evaluate the controller's stability augmentation capability in the longitudinal mode. For comparison purposes, the same input command is used for the other flight conditions.

For the vertical translation and pitch pointing maneuvers the limiting factor is not the linear range of the aircraft equations of motion, but the control surface deflection limits. The $\underline{G}(0)^{-1}$ matrix is used to calculate the maximum possible control inputs for the maneuvers at steady state without exceeding the control surface position limits. These input magnitudes need adjustment only if the control surface deflections overshoot their maximum steady state values during the transient response.

4-10 Sigma Weighting Matrix

The elements of the sigma weighting matrix assign the first-order roots which approach infinity with increasing gain. In addition, as the gain nears infinity, the slow modes vanish because they become asymptotically uncontrollable and unobservable. This leaves only the fast modes (infinite roots). In addition, if the sigma weighting matrix is also diagonal, the system exhibits increasingly tight and non-interacting behavior as the gain of the closed-loop system approaches infinity. See Appendix A for more details.

From a practical implementation point of view, the values of the sigma weighting matrix elements ultimately determine the time responses of the outputs. Each diagonal element affects the time response of the corresponding output. As an example, the X-29 longitudinal mode controller has the following outputs:

y_1 = pitch rate (q)

y_2 = forward velocity (u)

y_3 = angle of attack (α)

Therefore, the sigma matrix has a 3 x 3 dimension. Specifically, the diagonal element in row one of the sigma matrix affects the time response of the pitch rate, the diagonal element in row two modifies the forward velocity response, and the third row diagonal element influences the angle of attack response. In general, increasing the value of a sigma element causes a faster time response for the corresponding output. However, for the aircraft to respond more rapidly, the controller commands greater control surface deflection positions and faster rates which may exceed the design specifications.

For a minimum phase plant which is statically stable, the initial selection of the weighting matrix elements for a preliminary design is easy and most designers begin by assigning the value of one for all the elements. After completing the computer simulation, the engineer

analyzes the transient responses and iterates the appropriate sigma element magnitudes to improve undesirable results.

Unfortunately, the X-29 aircraft is a non-minimum plase plant with static instability. In fact, starting with a value of one for all the sigma weighting matrix elements gives an unstable response for all flight conditions. Thus a lengthy trial and error process begins to locate sigma values which produce stability. An analysis of the steady state $\underline{G}(0)^{-1}$ matrix provides some insight on the relative magnitude of the elements that may produce a stable system. As discussed earlier in this chapter, the X-29 control surface deflections are very large for small angle of attack changes. Therefore, the sigma element controlling the angle of attack must be small to achieve a stable system with acceptable control surface deflections. For illustration, the following sigma weighting matrix provides the best direct climb time response for the X-29 at 0.7 Mach, 15000 feet without control surface actuators or computer time delay:

$$\underline{\Sigma} = \begin{bmatrix} 1.7 & 0 & 0 \\ 0 & 1.2 & 0 \\ 0 & 0 & 0.01 \end{bmatrix}$$

4-11 Proportional Plus Integral Gains

The most efficient technique to determine the best proportional and integral gains begins by setting the α

and ε gain multipliers to magnitudes of one. Next, iterate the individual weighting matrix elements to optimize the transient response for each output. In effect, this sets the best proportional gain, which primarily affects the transient response of the system. Finally, adjust only the integral gain to improve steady state performance.

However, in MULTI, the alpha factor varies the proportional gain instead of the desired integral gain as shown below:

$$\underline{K}_0 = \alpha\varepsilon[\underline{CB}]^{-1}\underline{\Sigma} \tag{4-32}$$

$$\underline{K}_1 = \varepsilon[\underline{CB}]^{-1}\underline{\Sigma} \tag{4-33}$$

where

$\underline{K}_0$ = proportional gain matrix

$\underline{K}_1$ = integral gain matrix

To efficiently solve this problem, first set the ε parameter to the desired integral gain. Next, enter an α parameter equal to the reciprocal of ε. This adjusts the proportional gain back to its original value. The result is ε multiplying the $\underline{K}_1$ matrix by the appropriate integral gain.

4-12 MULTI

The successful design of a digital controller for a realistic aircraft plant using the techniques developed

by Professor Porter requires an interactive computer program to perform the arithmetic operations necessary to calculate the control matrices, run the simulations, and then iterate the process many times to achieve the optimum design. The interactive computer program called "MULTI" provides that capability (8).

$\underline{K_0}$ and $\underline{K_1}$ Matrices. After entering the aircraft plant, the desired sigma weighting matrix, epsilon, alpha, and measurement matrix for irregular designs, MULTI calculates the $\underline{K_0}$ and $\underline{K_1}$ control matrices using Porter's control law. As an illustration with the X-29 aircraft, 0.7 Mach at 15000 feet, no actuators, and no time delay; the optimum design parameters and the resulting control matrices calculated using MULTI are as follows:

$$\alpha = 0.71429$$

$$\varepsilon = 1.4$$

$$\sum = \begin{bmatrix} 1.7 & 0 & 0 \\ 0 & 1.2 & 0 \\ 0 & 0 & 0.01 \end{bmatrix}$$

$$\underline{K_0} = \begin{bmatrix} 6.652 & 0.007181 & -2.819 \\ -9.955 & -0.1295 & -8.621 \\ 0.02397 & 0.04419 & -0.002194 \end{bmatrix}$$

$$\underline{K}_1 = \begin{bmatrix} 9.313 & 0.01005 & -3.947 \\ -13.94 & -0.1813 & -12.07 \\ -0.03356 & 0.6187 & 0.003071 \end{bmatrix}$$

Simulation. In addition to the above items, MULTI requires the sampling time, computational delay time, total simulation time, calculation step size, command input vector, and actuator/sensor state space equations before running the simulation.

This thesis uses a sample period of 0.025 seconds which is easily within the capability of current flight control microprocessors.

Final designs in this research effort employ a computational time delay of one sample period to allow the digital controller time to calculate the control signal.

The total simulation time must be long enough to ensure the transient response is completed and the steady state response remains stable. This report uses a simulation time of 16 seconds.

The calculation step size is set equal to the sampling period unless there is a special need to observe the response between sampling times.

Each maneuver is entered into MULTI via a command vector. MULTI has the capability to pulse and ramp-to-hold all input variables.

MULTI has the versatility to add actuator and sensor dynamics external to the aircraft plant. With this implementation, the actuators and sensors are not used in the computation of $\underline{K}_0$ and $\underline{K}_1$ control matrices. However, the actuator and sensor dynamics are included in the complete closed-loop system simulation.

In this paper, the system is first designed without actuators. Then, using the same design parameters as a starting point, the simulation is rerun with actuator dynamics added. Based on an analysis of the time response plots, the parameters are modified and the simulation is run again. The process is repeated several times until the best possible design is achieved. The same iterative procedure is employed when computer time delay is added to the system.

Appendix C documents an improvement to MULTI that provides the capability to easily convert the simulation output from units of radians to degrees prior to plotting the data and calculating the figures of merit. At the prompt, the user enters the vectors and states requiring conversion.

4-13 Summary

This chapter details the 11 major steps necessary to successfully design a digital controller with actuators and time delay for the X-29 aircraft. For clarity,

numerical examples illustrate many of the steps in the procedure. The next chapter presents the design data and evaluates the results.

5. Results for Longitudinal Control System Designs

5-1 Introduction

This chapter details the design data and presents time history response plots for the X-29 aircraft, implemented with a "Porter configured" error actuated flight control system. This thesis includes results for the direct climb, pitch pointing, and vertical translation maneuvers at 0.4 Mach, sea level; 0.7 Mach, 15000 feet; and 1.2 Mach, 15000 feet. For illustration and analysis, responses are presented for the three longitudinal maneuvers with samples selected from the three flight conditions. Design data and plots for the maneuvers at flight conditions not detailed in this chapter are included in the appendices.

This research effort investigates the effects of adding actuator dynamics and computational time delay to the simulation. For each maneuver and flight condition, a series of longitudinal controllers are designed with the following system configurations:

1. basic aircraft equations (plant) only
2. actuator dynamics added as an input to the plant

3. basic plant with one sample period computational time delay

4. plant with both actuator dynamics and computational time delay

5-2 Direct Climb Maneuver for 0.7 Mach at 15000 Feet

The longitudinal state space matrices are tabulated in Table 5-1. The command vector $\underline{y}$, design parameters, and controller matrices for this maneuver are presented in Table 5-2. Table 5-3 lists the figures of merit. The aircraft time response plots are provided in Figs. 5-1 through 5-24. Note that all angles are converted from radians to degrees before plotting.

In this maneuver a pitch rate pulse command generates a steady state climb angle of $\theta = 7.5$ degrees with a one g change in normal acceleration during the rotation phase of the maneuver. This is within the linear range of the aircraft equations of motion. The change in velocity and angle of attack are commanded to zero.

An analysis of the time histories for all configurations including actuators and computational time delay shows very good aircraft responses.

As expected, the time plots with no actuators and no computational time delay are the best. For example, the aircraft closely and smoothly follows the commanded pitch rate pulse with only a slight overshoot (see Fig. 5-1).

TABLE 5-1

LONGITUDINAL STATE SPACE MATRICES

FLIGHT CONDITION: 0.7 Mach at 15000 Feet

A (Plant Matrix)

.0000E+00	.0000E+00	.0000E+00	.1000E+01
-.3213E+02	-.1199E-01	-.1718E+01	-.3504E+00
-.3243E-06	-.1298E-03	-.1138E+01	.9917E+00
.0000E+00	.2986E-03	.1892E+02	-.4928E+00

B (Control Input Matrix)

.0000E+00	.0000E+00	.0000E+00
-.5895E-01	.2621E-01	.2724E+02
-.1161E-02	-.7808E-03	-.2099E-02
.1720E+00	-.5630E-01	-.1929E+00

C (Output Matrix)

.0000E+00	.0000E+00	.0000E+00	.1000E+01
.0000E+00	.1000E+01	.0000E+00	.0000E+00
.0000E+00	.0000E+00	.1000E+01	.0000E+00

Notes

1. States (listed in order) are pitch angle, change in forward velocity, angle-of-attack, and pitch rate.

2. Control inputs (listed in order) are canards, strake flaps, and thrust.

3. Outputs (listed in order) are pitch rate, change in forward velocity, and angle of attack.

TABLE 5-2

DESIGN PARAMETERS AND CONTROLLER MATRICES
FOR LONGITUDINAL CONTROLLERS

FLIGHT CONDITION: 0.7 Mach at 15000 Feet
MANEUVER: Direct Climb
COMMAND VECTOR $\underline{v}$*: 1.1, 0.0436, 3, 4.1
0, 0, 0, 0
0, 0, 0, 0

Plant Only

Alpha	Epsilon	Sigma**	$\underline{K}_0$***		
		1.7	-.6652E+01	.7181E-02	-.2819E+01
0.7143	1.4	1.2	-.9956E+01	-.1295E+00	-.8621E+01
		0.01	.2397E-01	.4419E-01	.2194E-02

Plant and Computational Time Delay

Alpha	Epsilon	Sigma**	$\underline{K}_0$***		
		1.9	.7435E+01	.7181E-02	-.5639E+01
0.7143	1.4	1.2	-.1113E+02	-.1295E+00	-.1724E+02
		0.02	.2680E-01	.4419E-01	.4387E-02

Plant with Actuator Dynamics

Alpha	Epsilon	Sigma**	$\underline{K}_0$***		
		1.9	.7435E+01	.7181E-02	-.2819E+01
0.7143	1.4	1.2	-.1113E+02	-.1295E+00	-.8621E+01
		0.01	.2680E-01	.4419E-01	.2194E-02

Plant with Actuator Dynamics and Computational Time Delay

Alpha	Epsilon	Sigma**	$\underline{K}_0$***		
		2.3	.9000E+01	.7181E-02	-.4229E+01
0.7143	1.4	1.2	-.1347E+02	-.1295E+00	-.1293E+02
		0.015	.3244E-01	.4419E-01	.3290E-02

Notes

*Each pulse entry in $\underline{v}$ has four parts:
1. The time in seconds the input reaches steady-state;
2. Steady-state value (angles in radians);
3. Time the input leaves steady-state; and
4. Time the input reaches zero.

**Diagonal element values of the matrix.

***$\underline{K}_0$ = alpha * $\underline{K}_1$.

TABLE 5-3

LONGITUDINAL FIGURES OF MERIT

FLIGHT CONDITION: 0.7 Mach at 15000 Feet

MANEUVER: Direct Climb

COMMAND VECTOR $\underline{y}$:* 1.1, 0.0436, 3, 4.1
0, 0, 0, 0
0, 0, 0, 0

Plant Only

Output	Peak Value**	Peak Time	Settling Time
Pitch Rate	2.66	1.4	***
Forward Velocity	-0.02	2.8	***
Angle of Attack	1.22	1.925	***
Pitch Angle	7.7	3.95	4.0
Flight Path Angle	8.1	5.0	8.0

Plant and Computational Time Delay

Output	Peak Value**	Peak Time	Settling Time
Pitch Rate	2.78	1.525	***
Forward Velocity	-0.0414	2.625	***
Angle of Attack	1.28	1.925	***
Pitch Angle	7.7	3.9	4.0
Flight Path Angle	8.2	4.5	8.0

TABLE 5-3 --Continued

Plant with Actuator Dynamics

Output	Peak Value**	Peak Time	Settling Time
Pitch Rate	2.71	1.4	***
Forward Velocity	- .0199	2.45	***
Angle of Attack	1.29	1.925	***
Pitch Angle	7.6	3.8	7.6
Flight Path Angle	8.2	5.0	8.1

Plant with Actuator Dynamics and Computational Time Delay

Output	Peak Value**	Peak Time	Settling Time
Pitch Rate	2.85	1.525	***
Forward Velocity	-0.033	2.0	***
Angle of Attack	1.4	1.925	***
Pitch Angle	7.7	4.0	8.0
Flight Path Angle	8.2	5.0	8.1

Notes

1. Figures of merit for the pitch angle and the flight path angle are estimated from the response plots.

2. Pitch rate, forward velocity, and angle of attack are components of the output vector $\underline{y}$.

3. Pitch rate and angle of attack are commanded to achieve desired responses in the pitch angle and the flight path angle for each maneuver.

*Commanded inputs in order:
(1) pitch rate in radians per second;
(2) forward velocity in feet per second; and
(3) angle of attack in radians.

**Angles are converted from radians to degrees prior to calculating the figures of merit.

***Final value of the output is zero. Settling time undefined using definition of 2 percent of final value.

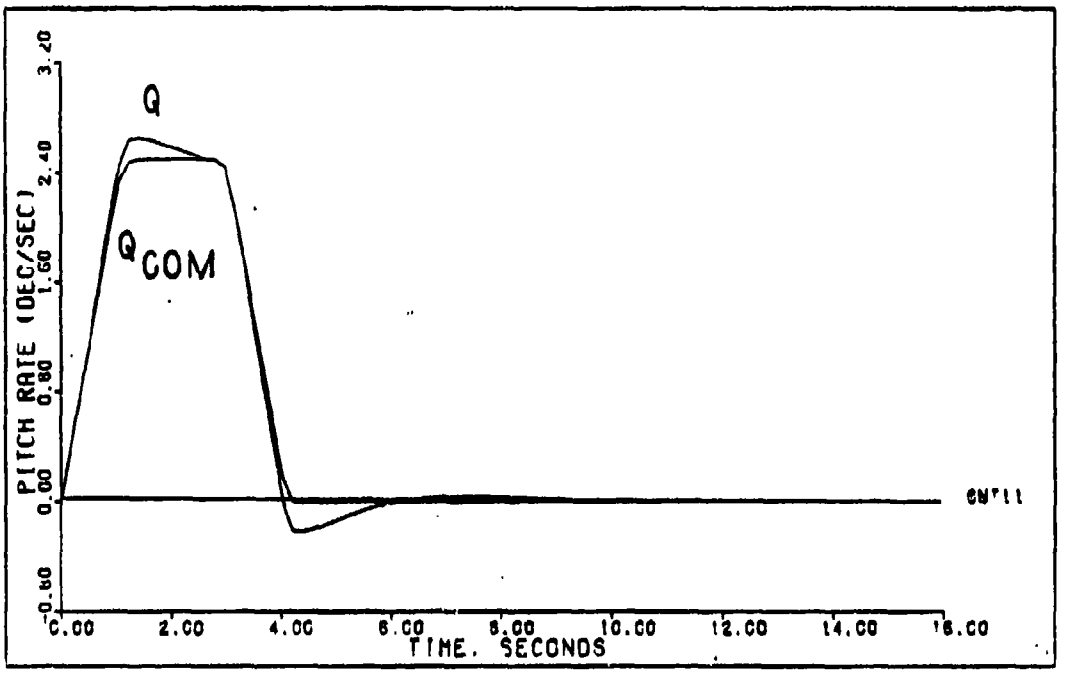

DIRECT CLIMB (0.7M 15K FT)

Figure 5-1

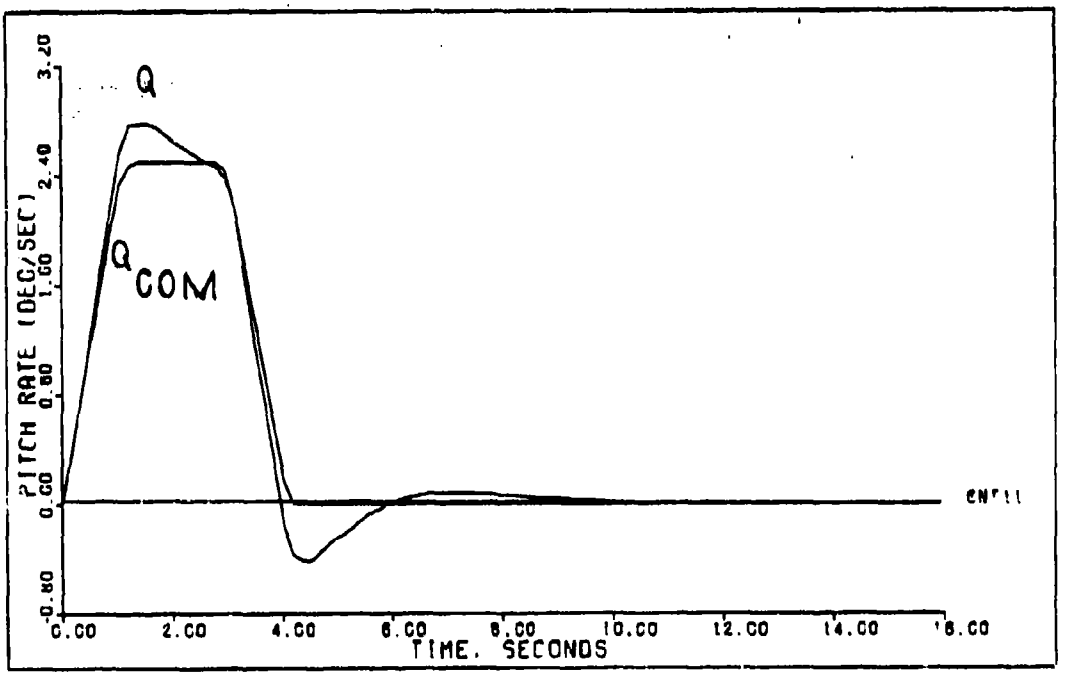

DIRECT CLIMB (0.7M 15K FT) DELAY=0.025 SEC

Figure 5-2

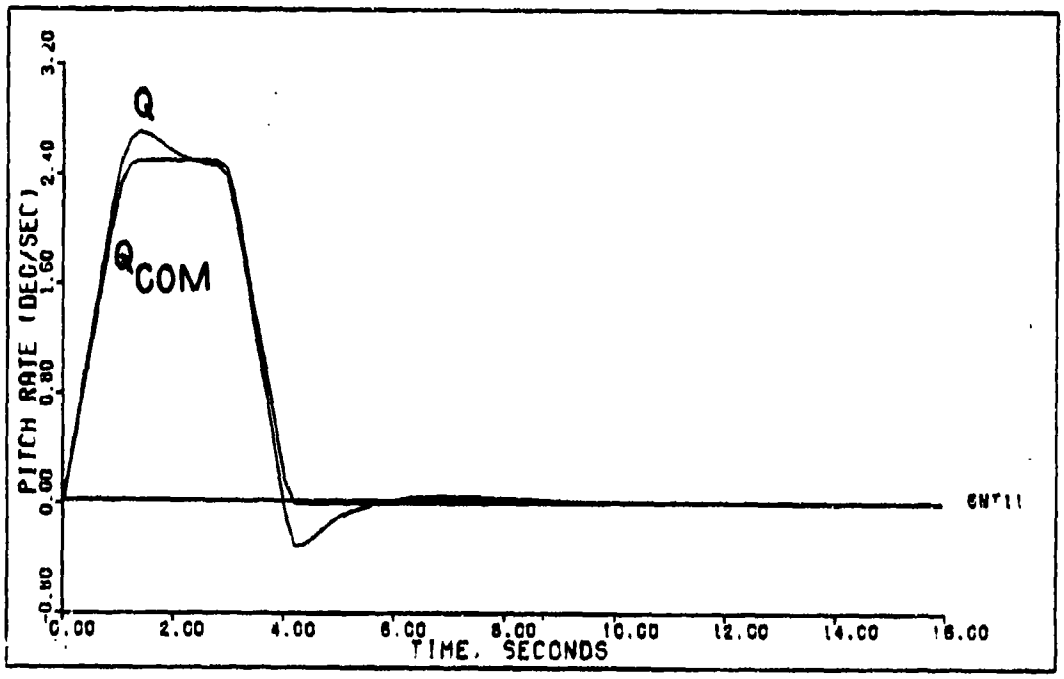

Figure 5-3

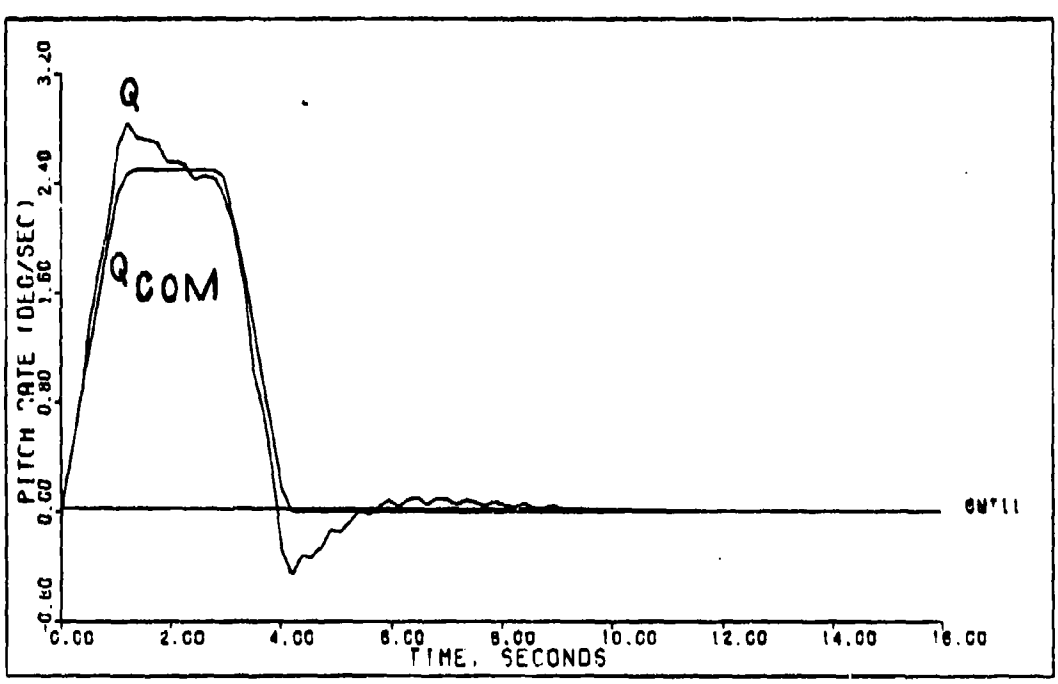

Figure 5-4

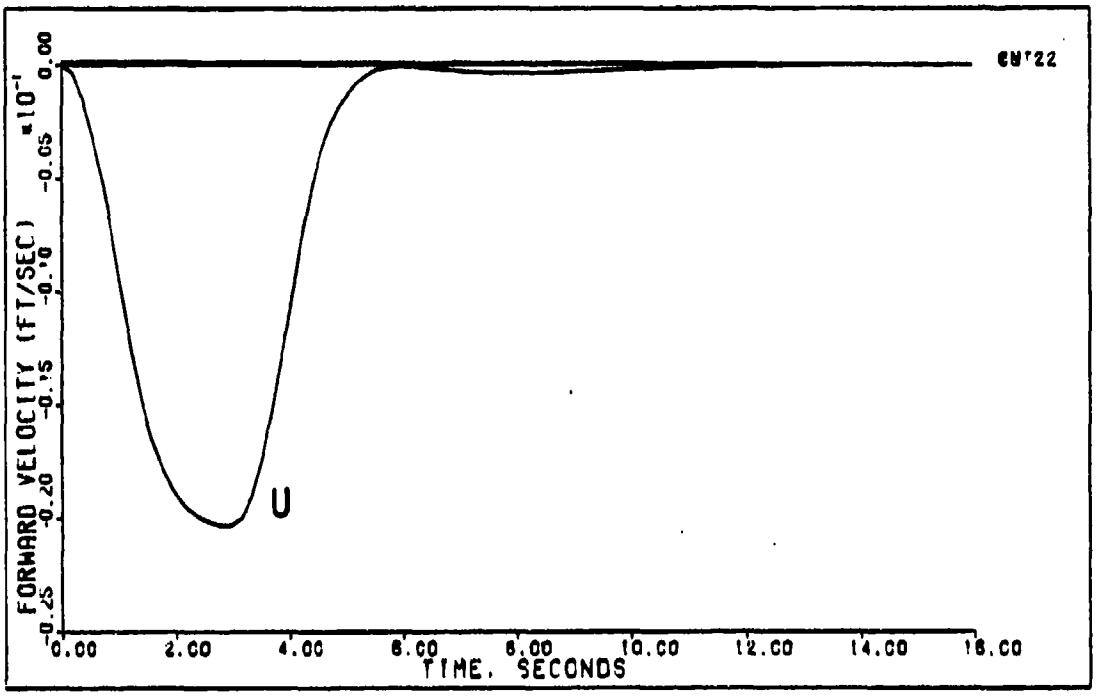

DIRECT CLIMB (0.7M 15K FT)

Figure 5-5

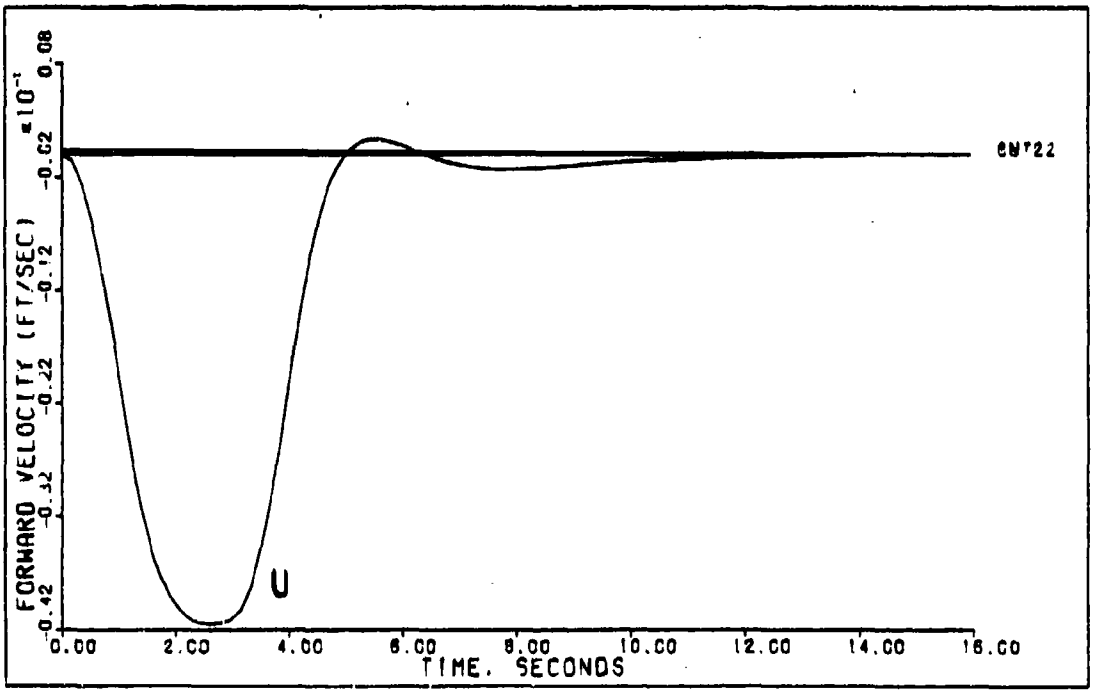

DIRECT CLIMB (0.7M 15K FT) DELAY=0.025 SEC

Figure 5-6

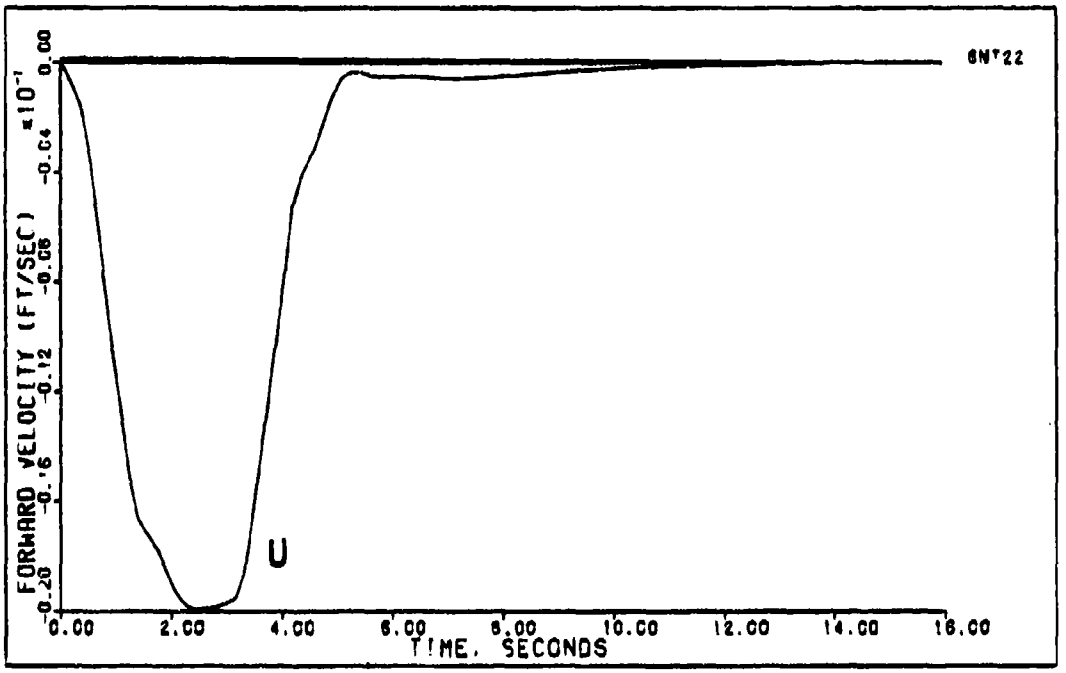

DIRECT CLIMB (0.7M 15K FT) ACTUATORS

Figure 5-7

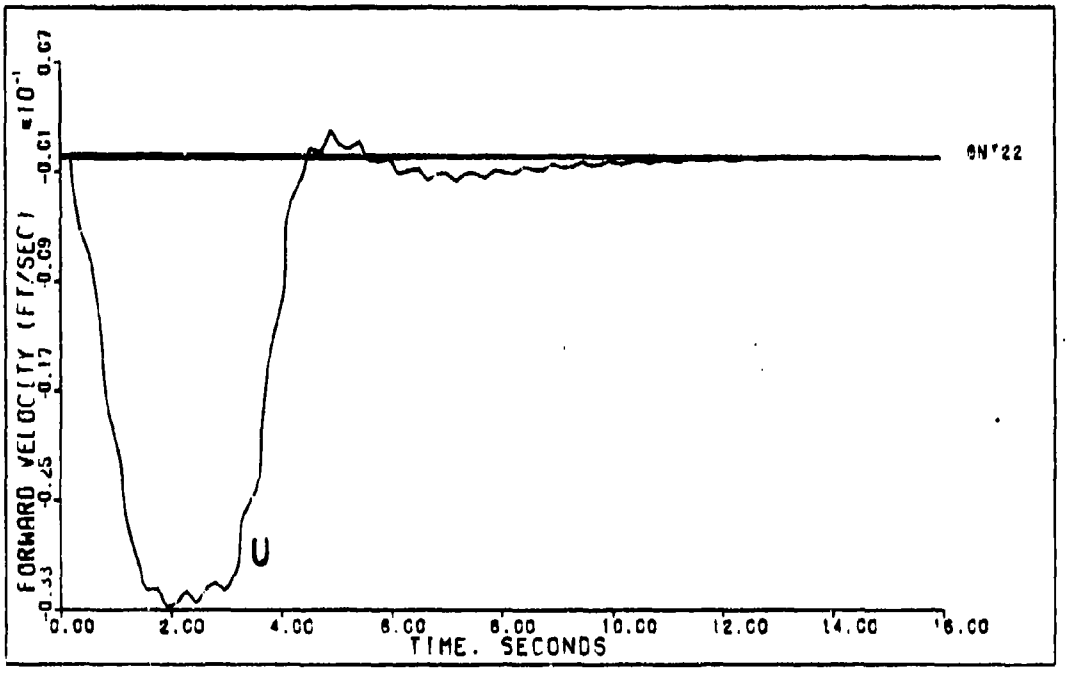

DIRECT CLIMB (0.7M 15K FT) DELAY=0.025 SEC ACTUATORS

Figure 5-8

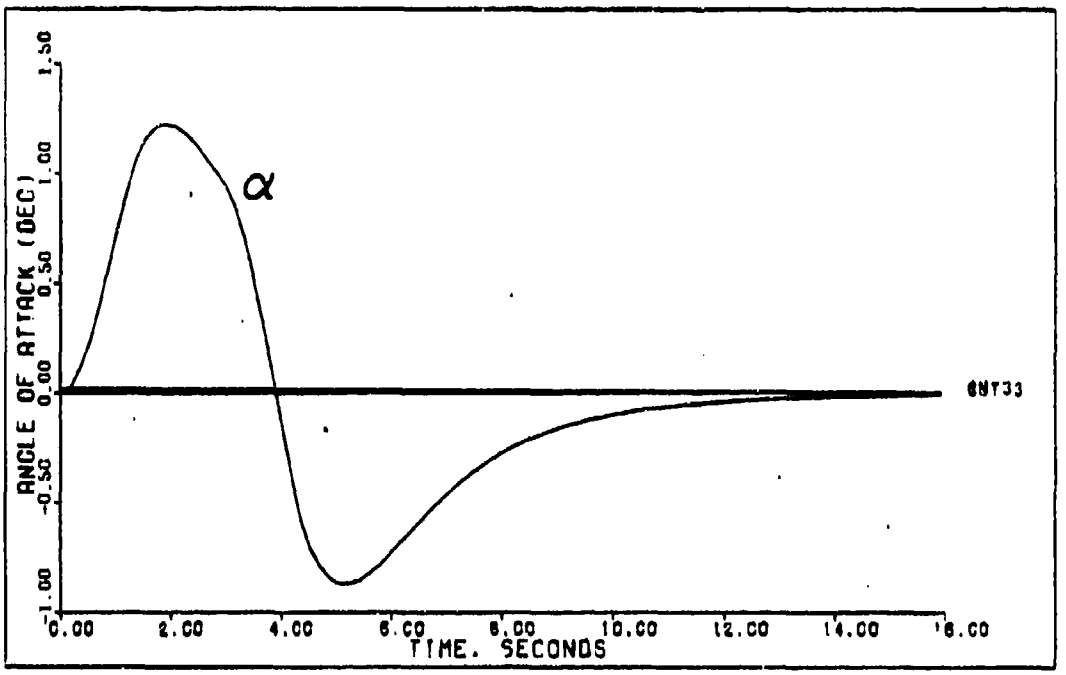

DIRECT CLIMB (0.7M 15K FT)

Figure 5-9

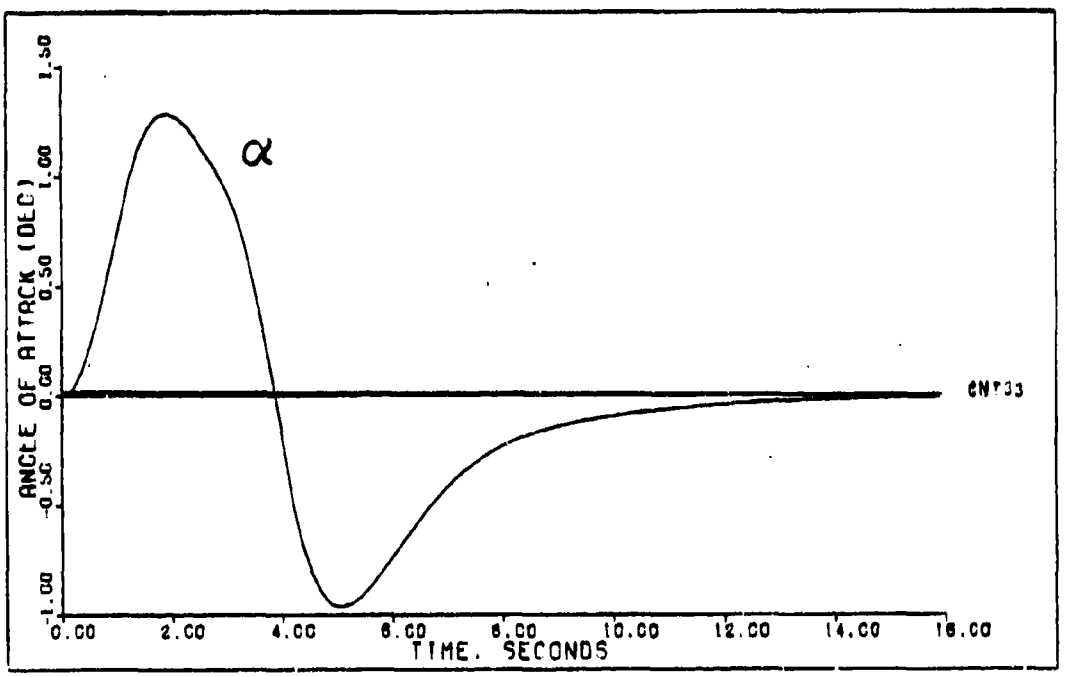

DIRECT CLIMB (0.7M 15K FT) DELAY=0.025 SEC

Figure 5-10

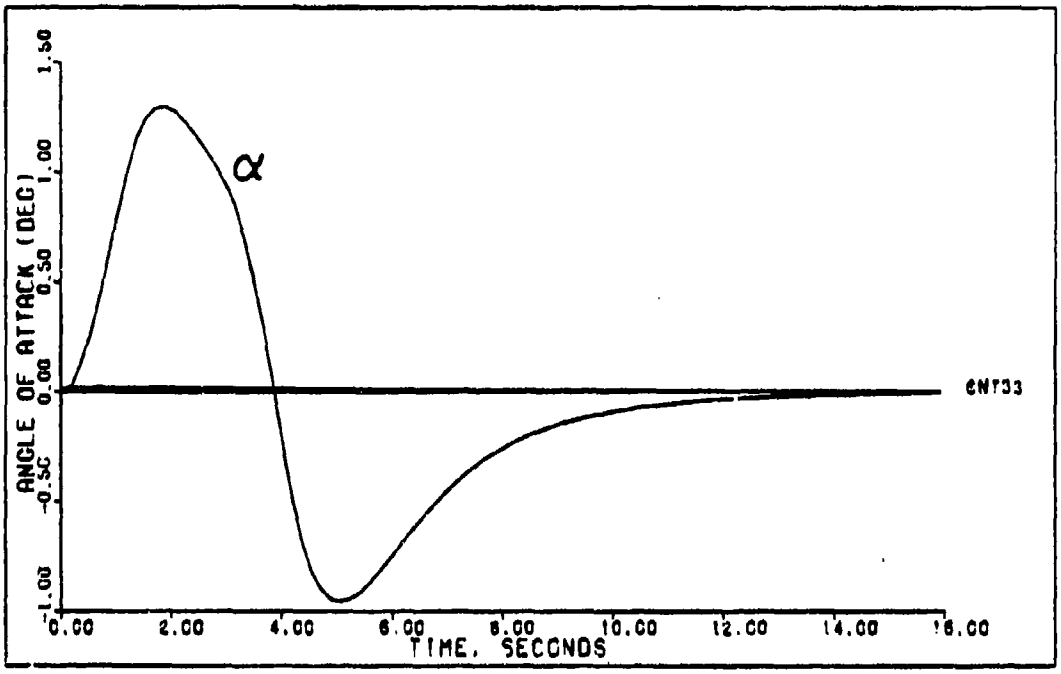

DIRECT CLIMB (0.7M 15K FT) ACTUATORS

Figure 5-11

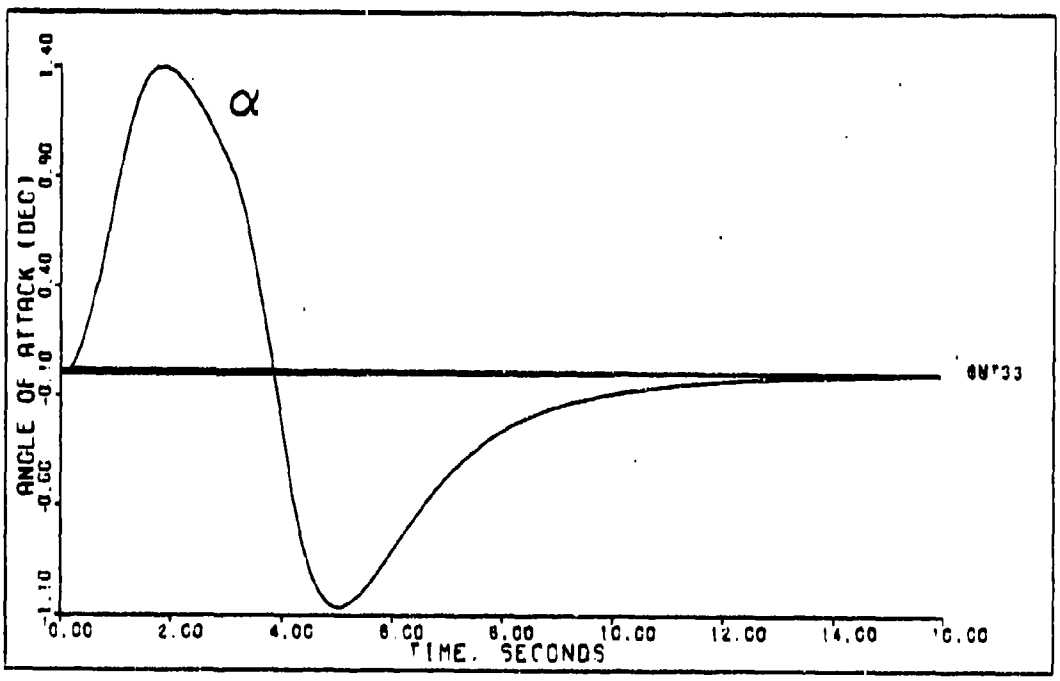

DIRECT CLIMB (0.7M 15K FT) DELAY=0.025 SEC ACTUATORS

Figure 5-12

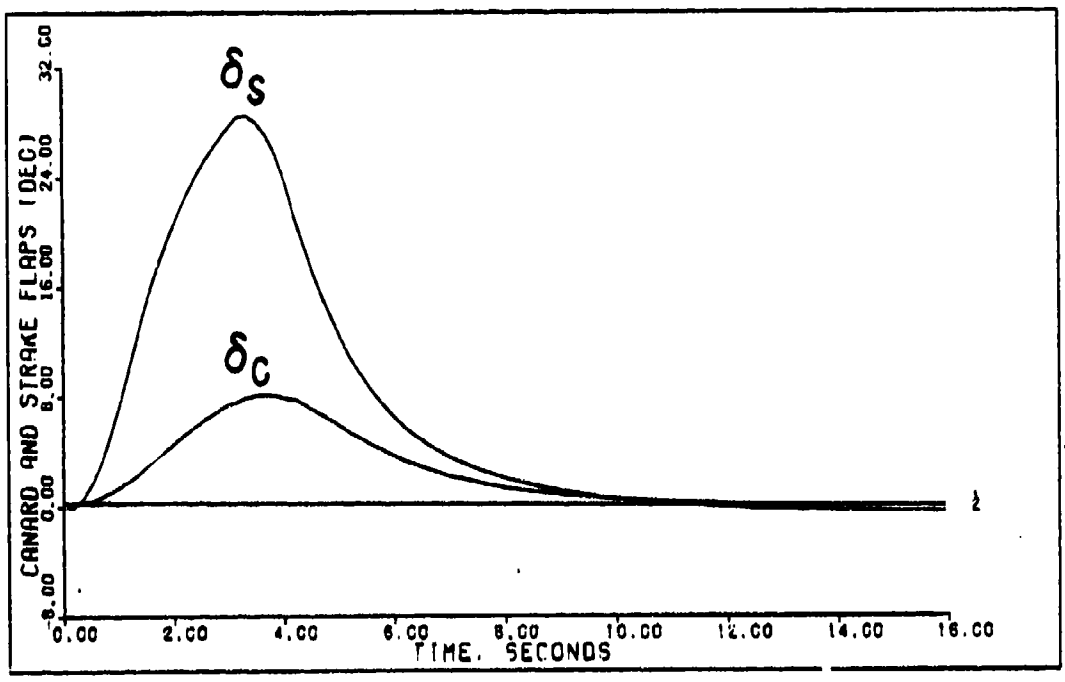

DIRECT CLIMB (0.7M 15K FT)

Figure 5-13

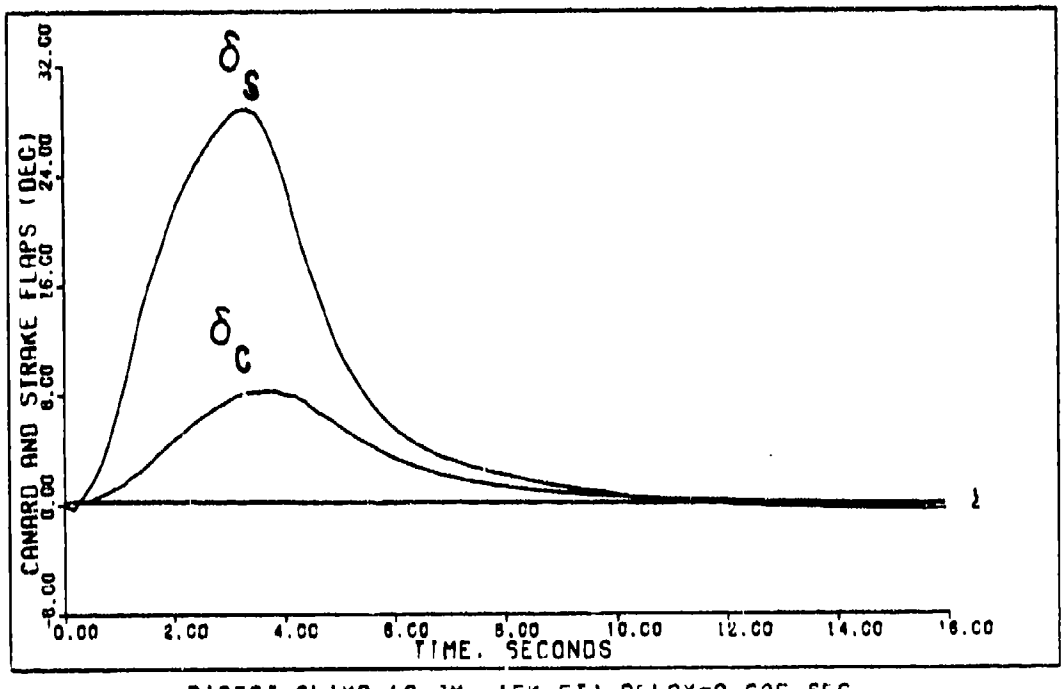

DIRECT CLIMB (0.7M 15K FT) DELAY=0.026 SEC

Figure 5-14

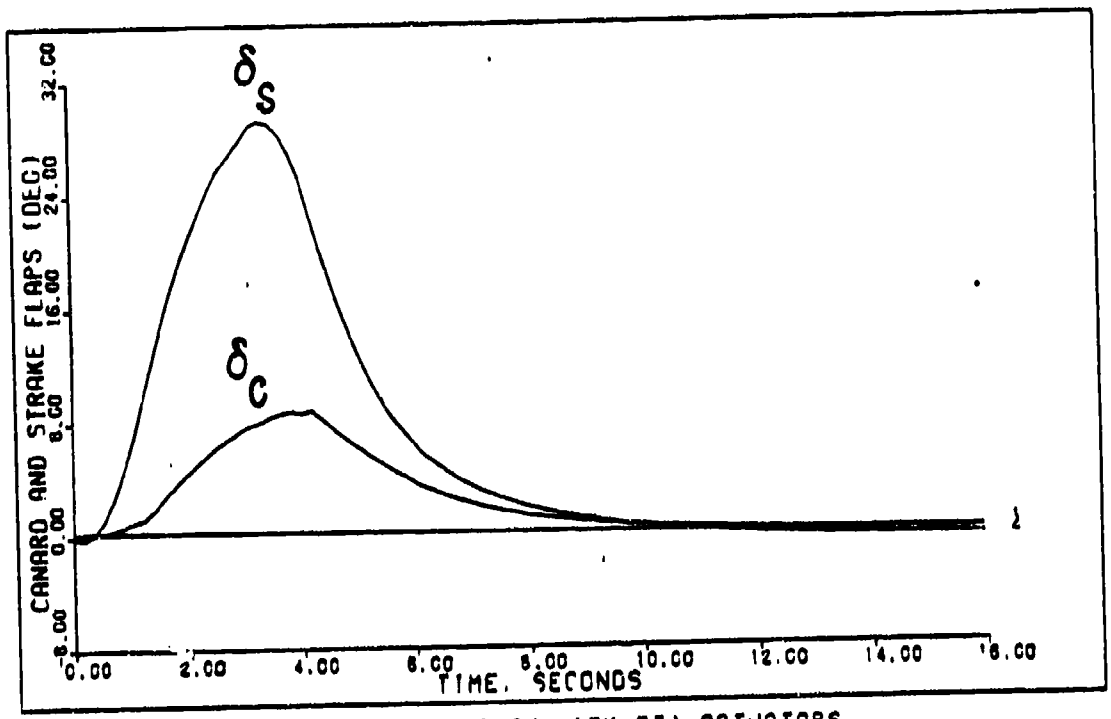

DIRECT CLIMB (0.7M 15K FT) ACTUATORS

Figure 5-15

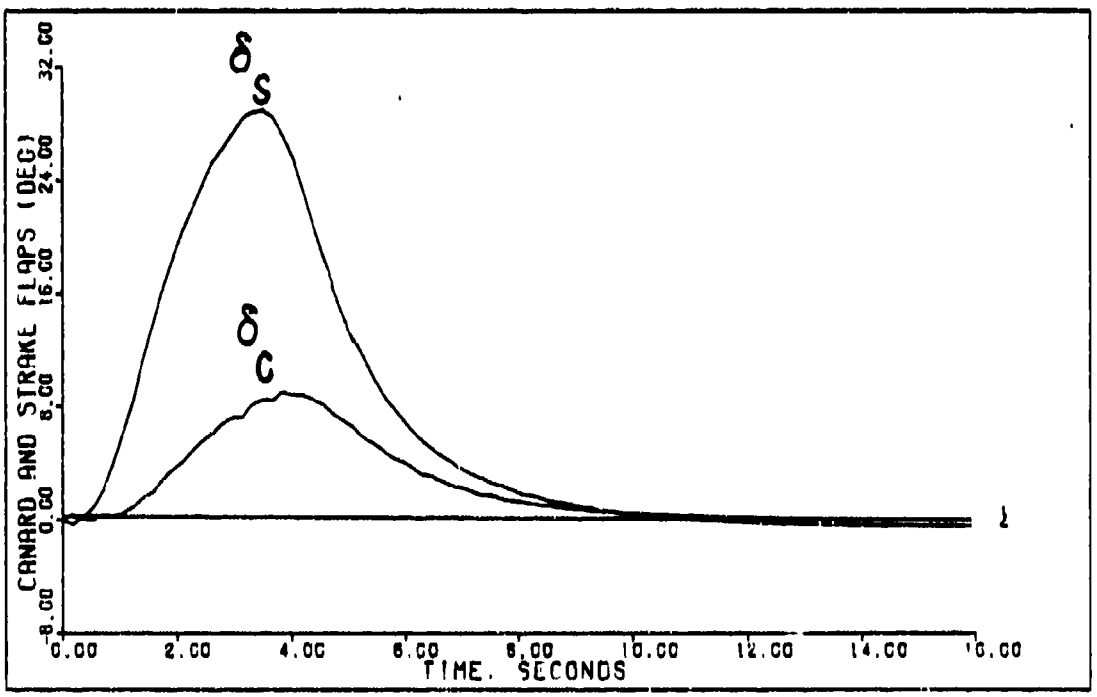

DIRECT CLIMB (0.7M 15K FT) DELAY=0.025 SEC ACTUATORS

Figure 5-16

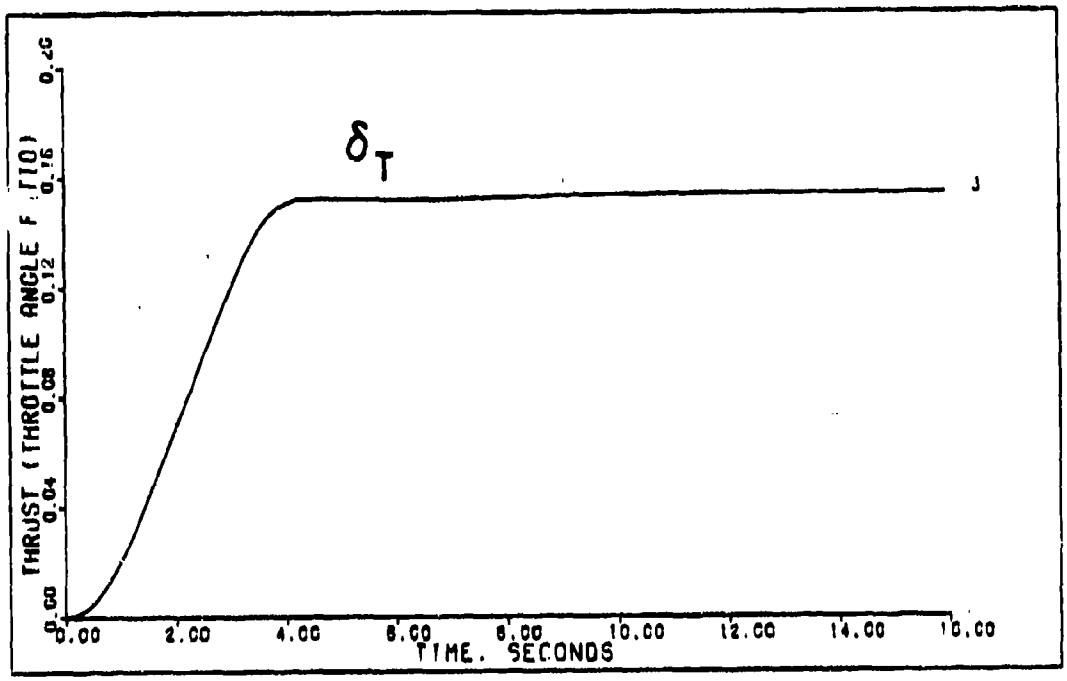

DIRECT CLIMB (0.7M 15K FT)

Figure 5-17

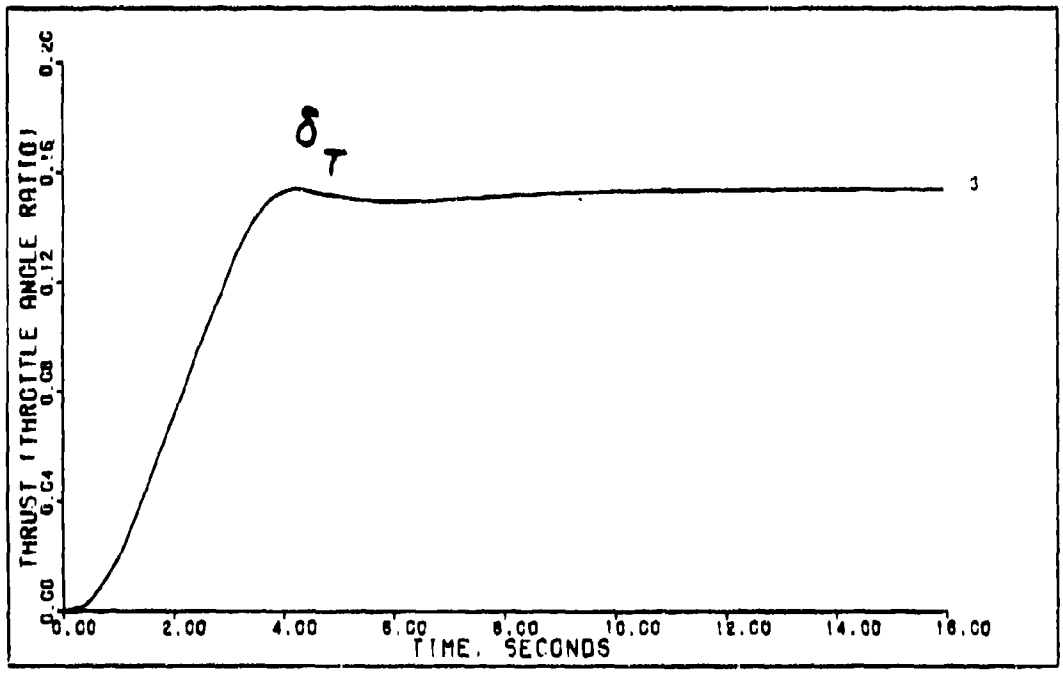

DIRECT CLIMB (0.7M 15K FT) DELAY=0.025 SEC

Figure 5-18

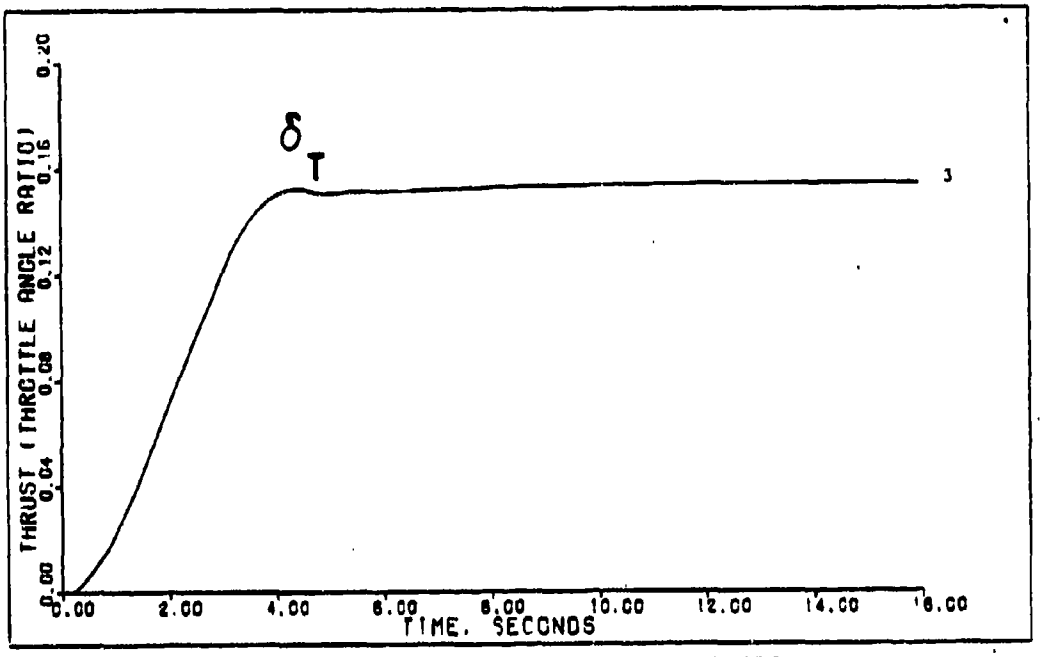

DIRECT CLIMB (0.7M 15K FT) ACTUATORS

Figure 5-19

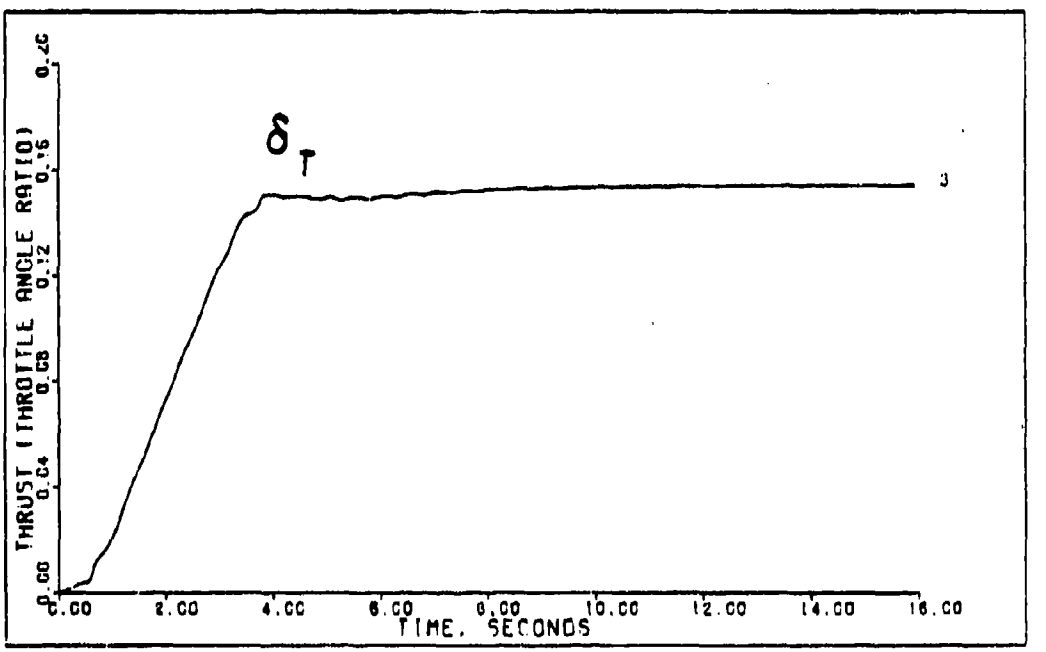

DIRECT CLIMB (0.7M 15K FT) DELAY=0.025 SEC ACTUATORS

Figure 5-20

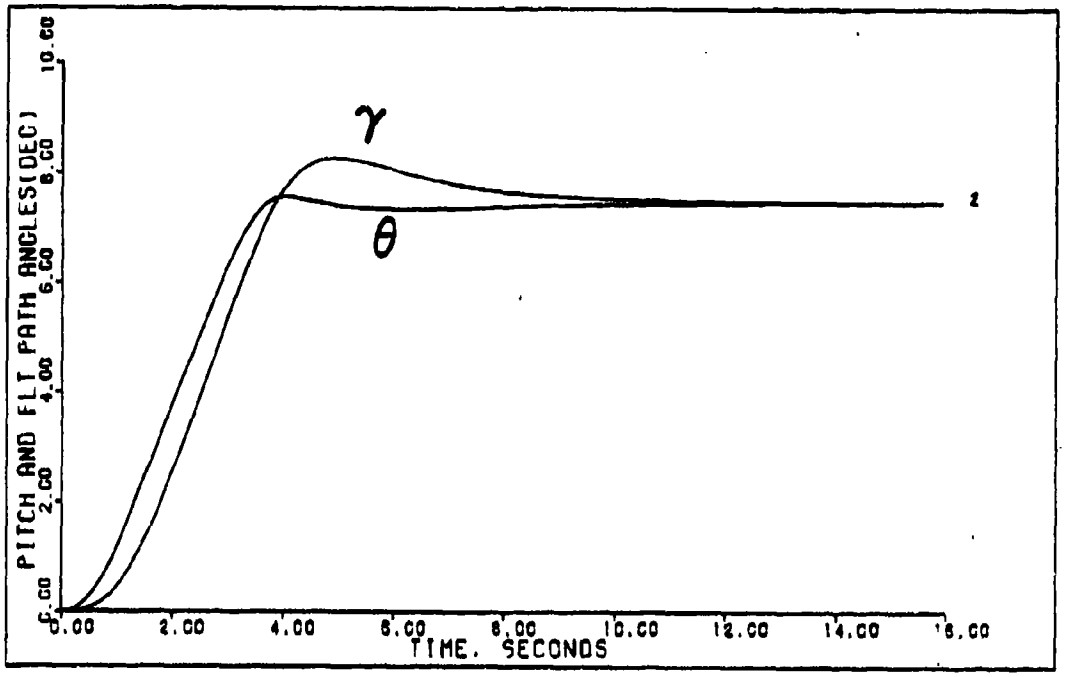

DIRECT CLIMB (0.7M 15K FT)

Figure 5-21

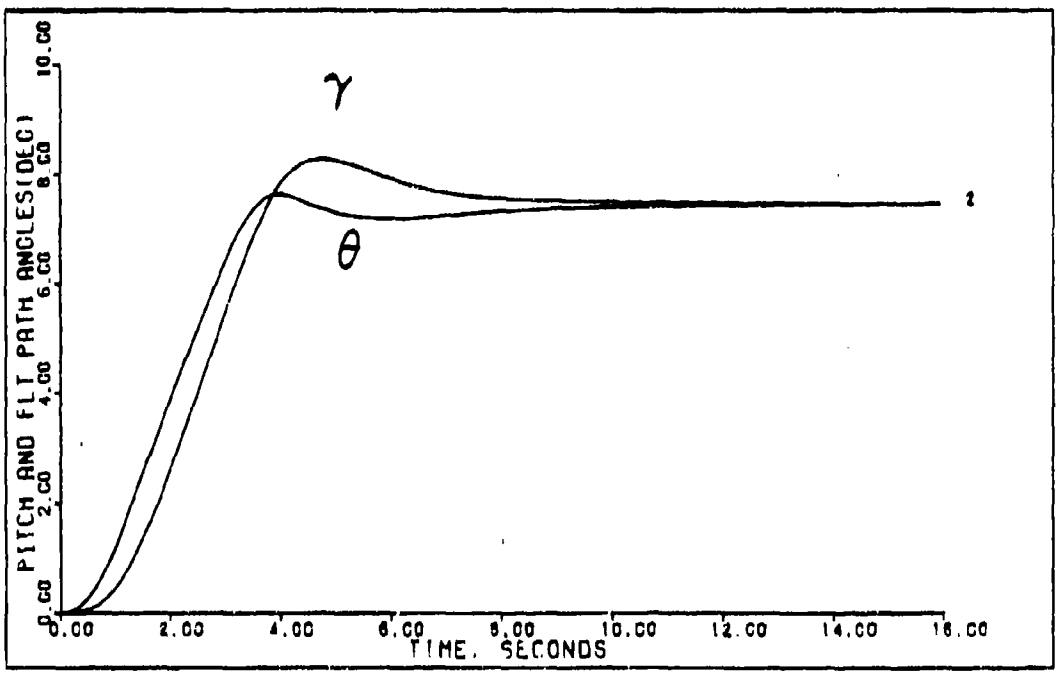

DIRECT CLIMB (0.7M 15K FT) DELAY=0.025 SEC

Figure 5-22

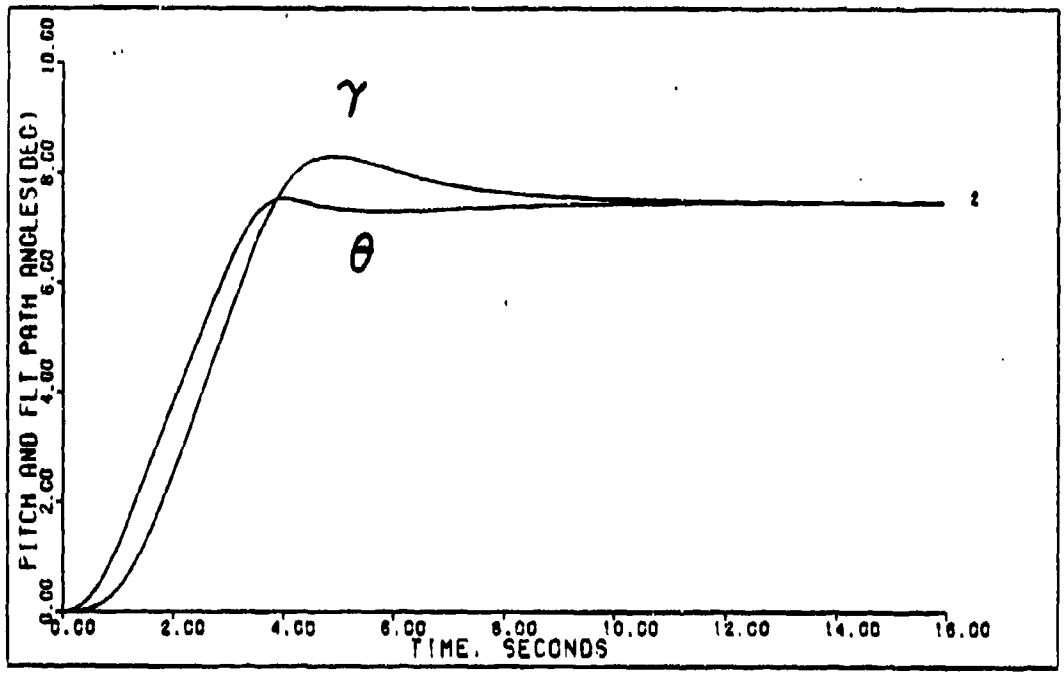

DIRECT CLIMB (0.7M 15K FT) ACTUATORS

Figure 5-23

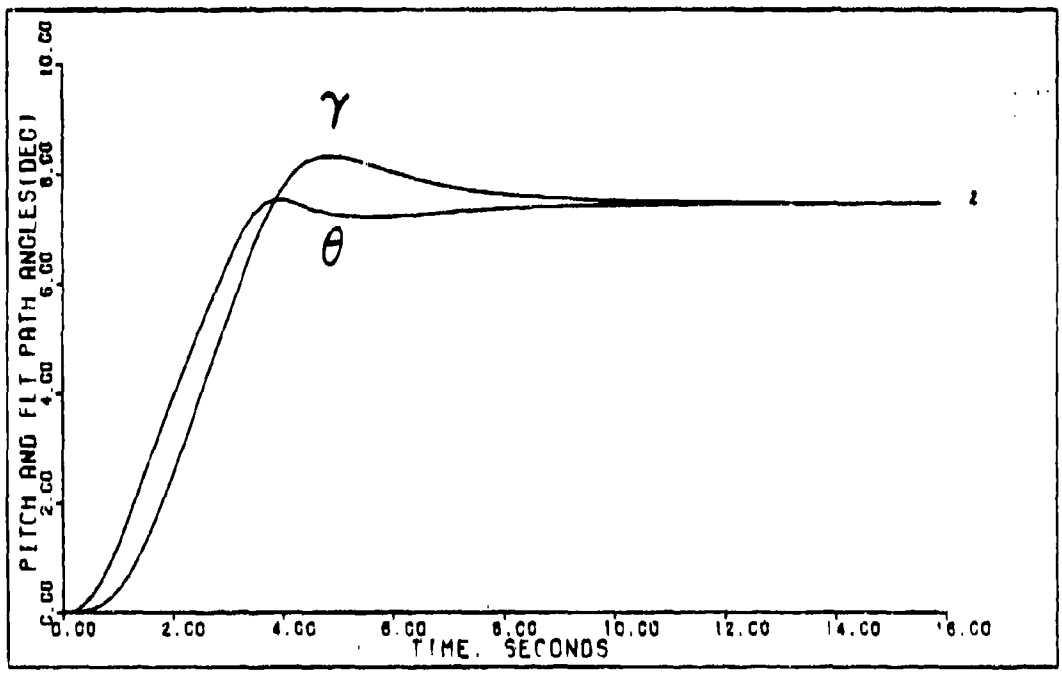

DIRECT CLIMB (0.7M 15K FT) DELAY=0.025 SEC ACTUATORS

Figure 5-24

The change in velocity in Fig. 5-5 is very slight. The angle of attack momentarily peaks at 1.25 degrees, then decreases to -0.9 degrees during the transient before returning to zero degrees in the steady state (see Fig. 5-9). The maximum strake flap deflection of 30 degrees in Fig. 5-13 occurs at approximately 3.5 seconds. The strake flap deflection rate peaks at 16 degrees per second which is well within the rate limit of 27 degrees per second. Because the deflection and rate limits of the strake flap are the governing factors in all the maneuvers, the canard deflection position and rate always remain within limits (see Figs. 5-13 through 5-16). An analysis of the time history of the control surface movements shows the canard initially deflects in a positive direction to rotate the nose of the aircraft upwards. Because the aircraft is statically unstable, the aircraft tends to continue rotating. The strake flap offsets the rotation by producing a negative moment. This is observed by the positive deflection and resulting positive lift generated by the strake flap which is located aft of the center of gravity. The maneuver is efficiently accomplished since the lift created by both the canard and strake flap during the maneuver remains positive at all times. In contrast, a pitch up maneuver in a conventional aircraft requires the stabilator or elevator to produce a negative lift, thereby reducing the total lift on the vehicle.

the design parameters completely eliminate the oscillations.

Responses for the direct climb maneuver are also very good for the other flight conditions. The design parameters and plots are presented in Appendices D through F.

5-3 Vertical Translation Maneuver for 0.4 Mach at Sea Level

The aircraft longitudinal state space matrices are tabulated in Table 5-4. The command vector $\underline{y}$, design parameters, and controller matrices for this maneuver are presented in Table 5-5. The figures of merit are listed in Table 5-6. The aircraft time plots are provided in Figs. 5-25 through 5-48. Note that the angles in all plots are in degrees.

The objective of this maneuver is to change the aircraft's altitude without rotating the vehicle while maintaining a constant forward velocity. The maneuver requires that pitch rate and forward velocity be commanded to zero. A commanded negative angle of attack increases the aircraft's altitude and a positive angle of attack decreases the vehicle's altitude. Thus, the aircraft translates upwards only when the canard and strake generate a change ir positive lift that is greater than the lift lost on the main wings.

TABLE 5-4

LONGITUDINAL STATE SPACE MATRICES

FLIGHT CONDITION: 0.4 Mach at Sea Level

A (Plant Matrix)

.0000E+00	.0000E+00	.0000E+00	.1000E+01
-.3217E+02	-.1660E-01	.4880E-01	-.4273E+00
.0000E+00	-.3172E-03	-.1001E+01	.9880E+00
.0000E+00	.2823E-03	.1012E+02	-.4340E+00

B (Control Input Matrix)

.0000E+00	.0000E+00	.0000E+00
-.4891E-01	.2592E-01	.3779E+02
-.9426E-03	-.8021E-03	-.6761E-02
.9328E-01	-.3603E-01	-.2679E+00

C (Output Matrix)

.0000E+00	.0000E+00	.0000E+00	.1000E+01
.0000E+00	.1000E+01	.0000E+00	.0000E+00
.0000E+00	.0000E+00	.1000E+01	.0000E+00

Notes

1. States (listed in order) are pitch angle, change in forward velocity, angle-of-attack, and pitch rate.

2. Control inputs (listed in order) are canards, strake flaps, and thrust.

3. Outputs (listed in order) are pitch rate, change in forward velocity, and angle of attack.

TABLE 5-5

DESIGN PARAMETERS AND CONTROLLER MATRICES
FOR LONGITUDINAL CONTROLLERS

FLIGHT CONDITION: 0.4 Mach at Sea Level
MANEUVER: Vertical Translation
COMMAND VECTOR $\underline{v}$*: 0, 0, 0, 0
0, 0, 0, 0
1.1, -0.0349, 50, 50

Plant Only

Alpha	Epsilon	Sigma**	$\underline{K}_0$***		
		1.5	.1105E+02	-.7022E-02	-.3313E+01
0.4545	2.2	1.0	-.1319E+02	-.2160E+00	-.8588E+01
		0.01	.2335E-01	.2660E-01	.1603E-02

Plant and Computational Time Delay

Alpha	Epsilon	Sigma**	$\underline{K}_0$***		
		1.5	.1105E+02	-.7022E-02	-.8281E+01
0.4545	2.2	1.0	-.1319E+02	-.2160E+00	-.2147E+02
		0.025	.2335E-01	.2660E-01	.4008E-02

Plant with Actuator Dynamics

Alpha	Epsilon	Sigma**	$\underline{K}_0$***		
		1.5	.1105E+02	-.7022E-02	-.2484E+01
0.4545	2.2	1.0	-.1319E+02	-.2160E+00	-.6441E+01
		0.0075	.2335E-01	.2660E-01	.1202E-02

Plant with Actuator Dynamics and Computational Time Delay

Alpha	Epsilon	Sigma**	$\underline{K}_0$***		
		1.5	.1105E+02	-.1053E-01	-.6625E+01
0.4545	2.2	1.5	-.1319E+02	-.3240E+00	-.1718E+02
		0.02	.2335E-01	.3990E-01	.3206E-02

Notes

*Each pulse entry in $\underline{v}$ has four parts:
1. The time in seconds the input reaches steady-state;
2. Steady-state value (angles in radians);
3. Time the input leaves steady-state; and
4. Time the input reaches zero.

**Diagonal element values of the matrix.

***$\underline{K}_0$ = alpha * $\underline{K}_1$.

TABLE 5-6

LONGITUDINAL FIGURES OF MERIT

FLIGHT CONDITION: 0.4 Mach at Sea Level

MANEUVER: Vertical Translation

COMMAND VECTOR $\underline{v}$:* 0, 0, 0, 0
0, 0, 0, 0
0, 1.1, -0.0349, 50, 50

Plant Only

Output	Peak Value**	Peak Time	Settling Time
Pitch Rate	-0.062	1.75	***
Forward Velocity	0.0003	2.275	***
Angle of Attack	-2.04	4.9	5.1
Pitch Angle	-0.15	4.1	4.1
Flight Path Angle	1.9	5.0	5.0

Plant and Computational Time Delay

Output	Peak Value**	Peak Time	Settling Time
Pitch Rate	-0.146	1.75	***
Forward Velocity	0.0016	2.1	***
Angle of Attack	-2.06	4.025	4.9
Pitch Angle	0.3	3.9	3.9
Flight Path Angle	1.8	3.9	3.9

TABLE 5-6 --Continued

Plant with Actuator Dynamics

Output	Peak Value**	Peak Time	Settling Time
Pitch Rate	-0.0772	1.925	***
Forward Velocity	-0.0009	0.7	***
Angle of Attack	-2.03	5.95	4.375
Pitch Angle	-0.17	4.1	4.1
Flight Path Angle	1.85	5.0	5.0

Plant with Actuator Dynamics and Computational Time Delay

Output	Peak Value**	Peak Time	Settling Time
Pitch Rate	-0.22	1.75	***
Forward Velocity	-0.0019	0.525	***
Angle of Attack	-2.05	4.2	5.25
Pitch Angle	-0.3	4.0	4.1
Flight Path Angle	1.8	3.9	4.5

Notes

1. Figures of merit for the pitch angle and the flight path angle are estimated from the response plots.

2. Pitch rate, forward velocity, and angle of attack are components of the output vector $\underline{y}$.

3. Pitch rate and angle of attack are commanded to achieve desired responses in the pitch angle and the flight path angle for each maneuver.

*Commanded inputs in order:
(1) pitch rate in radians per second;
(2) forward velocity in feet per second; and
(3) angle of attack in radians.

**Angles are converted from radians to degrees prior to calculating the figures of merit.

***Final value of the output is zero. Settling time undefined using definition of 2 percent of final value.

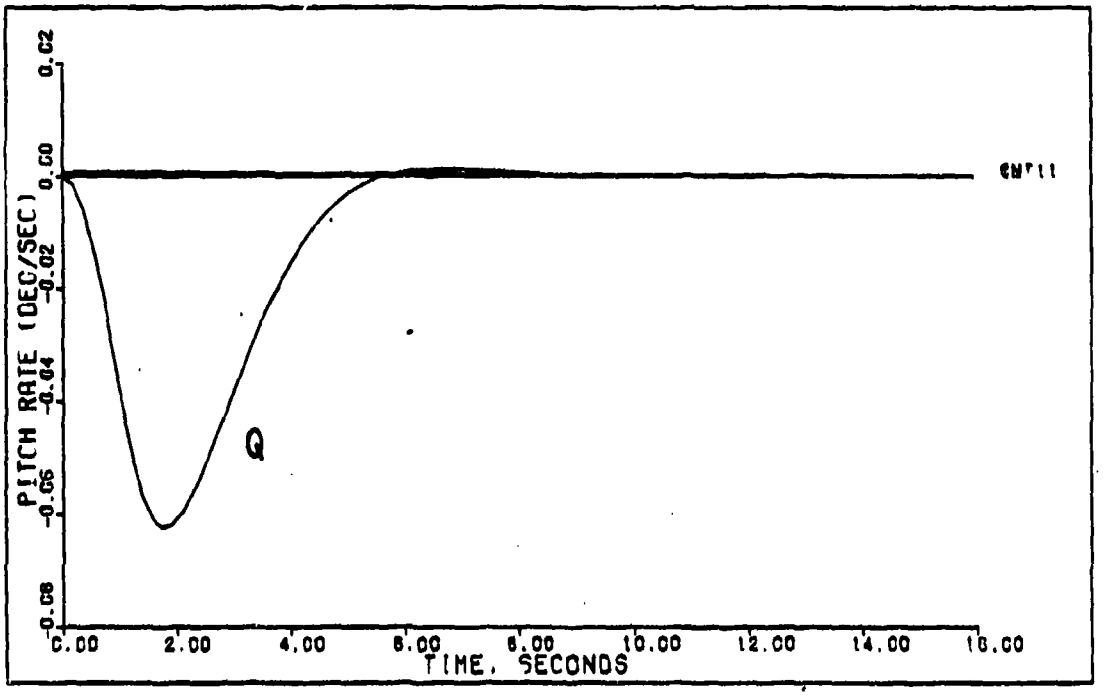

VERTICAL TRANSLATION (0.4M OK FT)

Figure 5-25

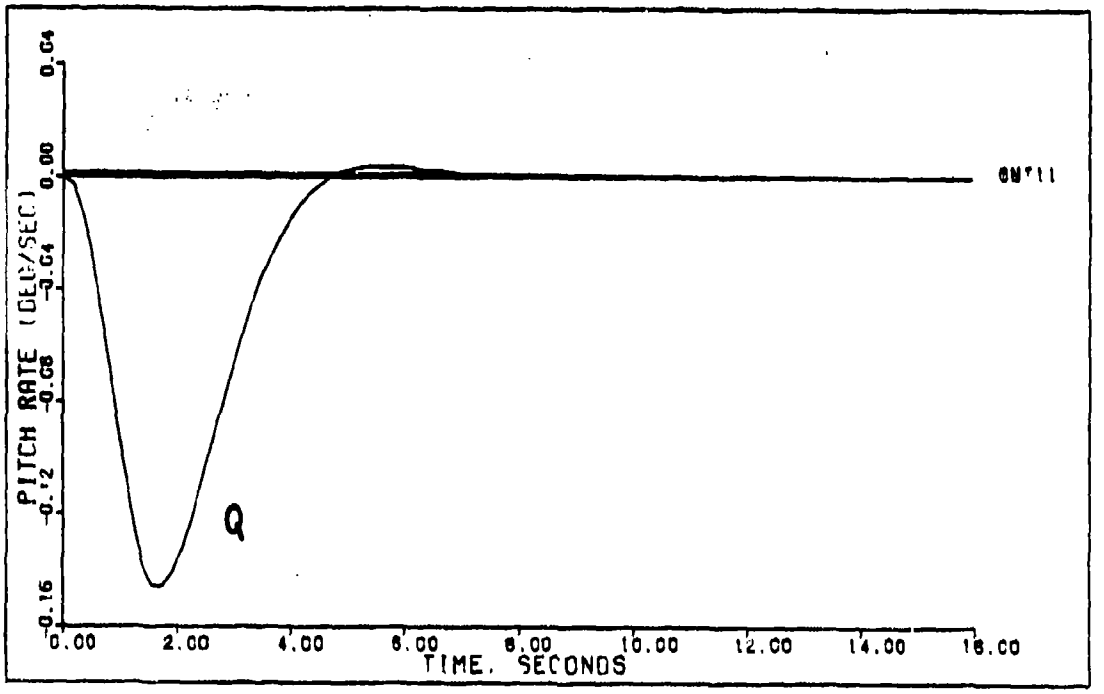

VERTICAL TRANSLATION (0.4M OK FT) DELAY=0.025 SEC

Figure 5-26

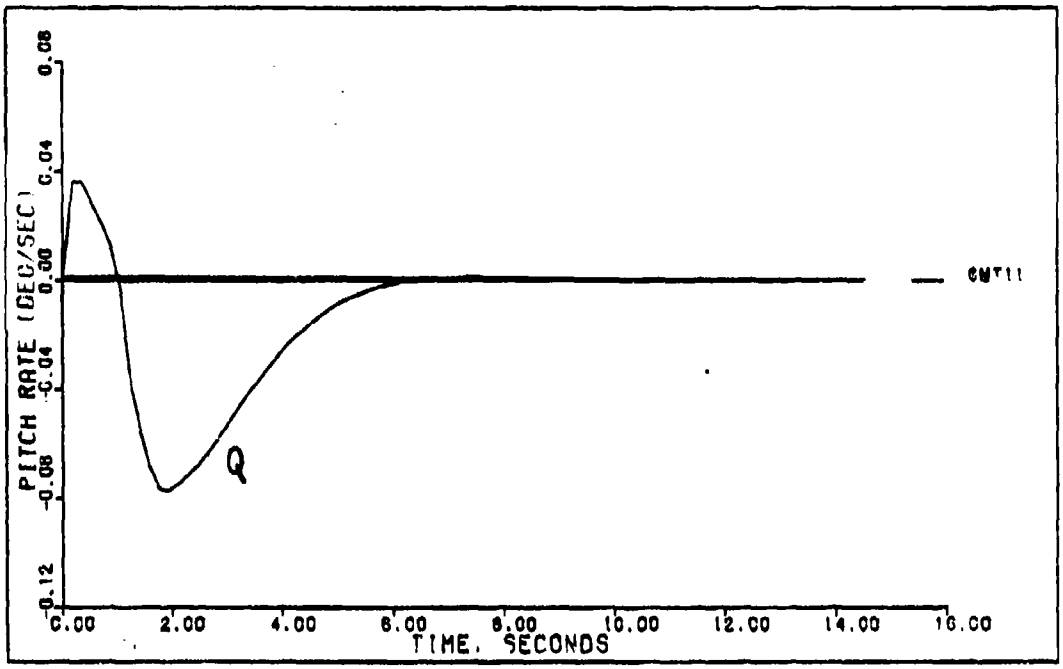

VERTICAL TRANSLATION (0.4M OK FT) ACTUATORS

Figure 5-27

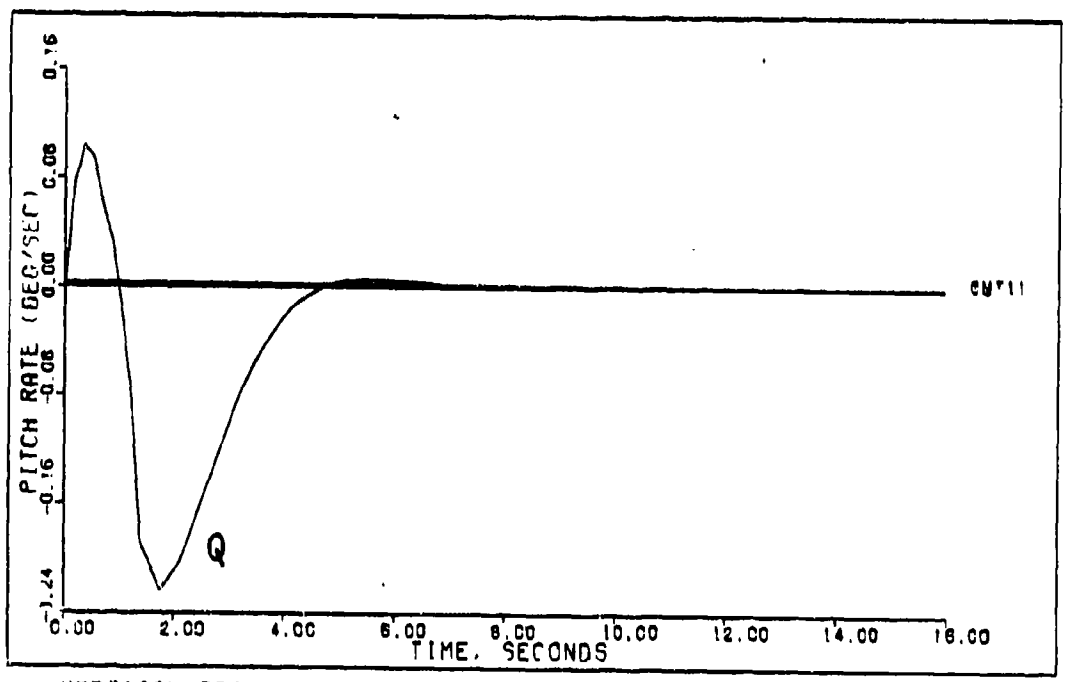

VERTICAL TRANSLATION (0.4M OK FT) DELAY=0.025 SEC ACTUATORS

Figure 5-28

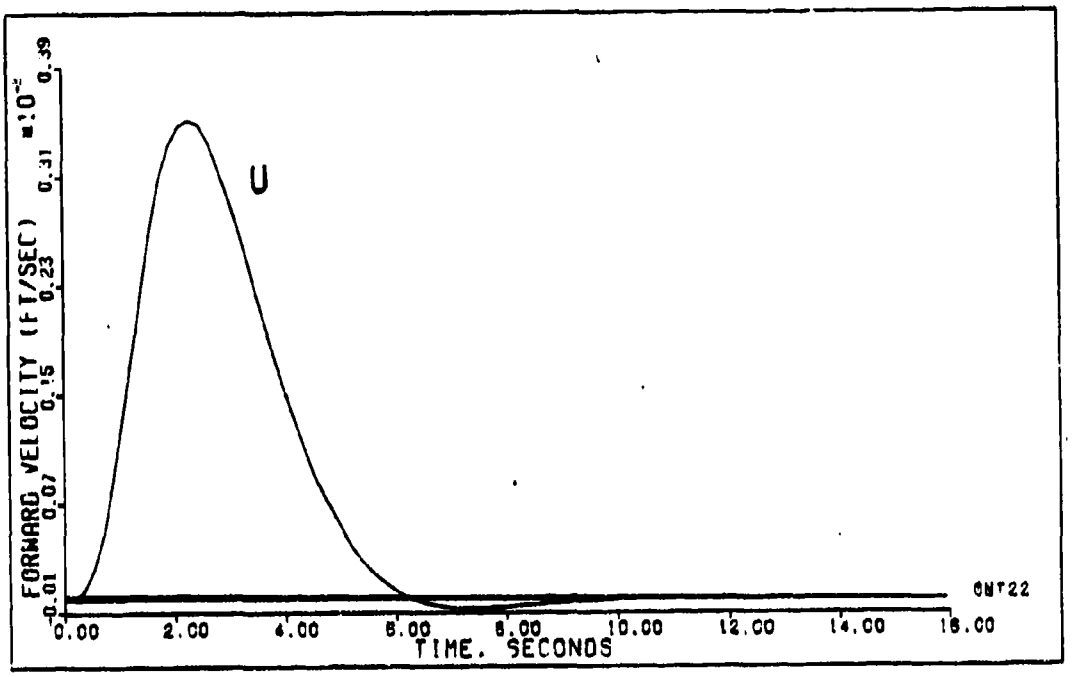

VERTICAL TRANSLATION (0.4M OK FT)

Figure 5-29

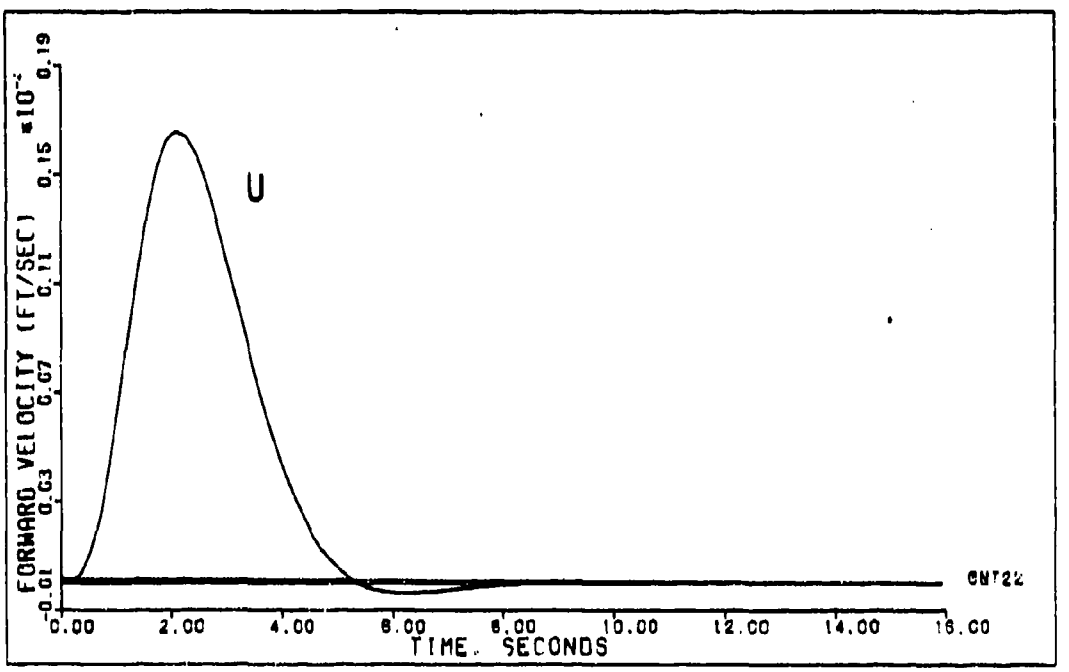

VERTICAL TRANSLATION (0.4M OK FT) DELAY=0.025 SEC

Figure 5-30

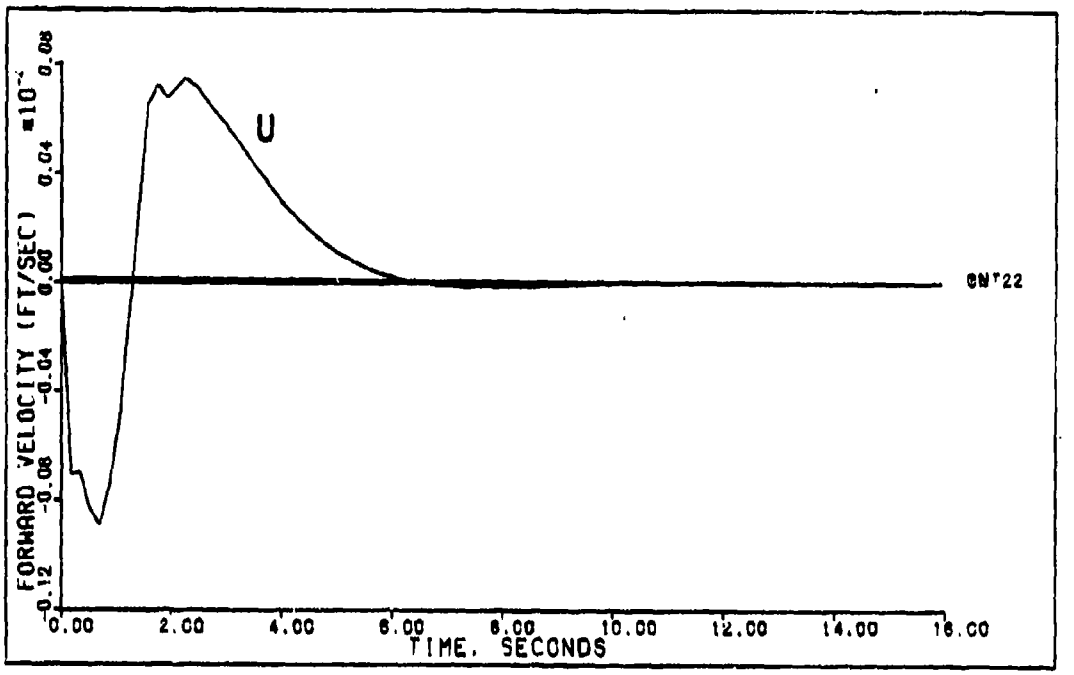

VERTICAL TRANSLATION (0.4M OK FT) ACTUATORS

Figure 5-31

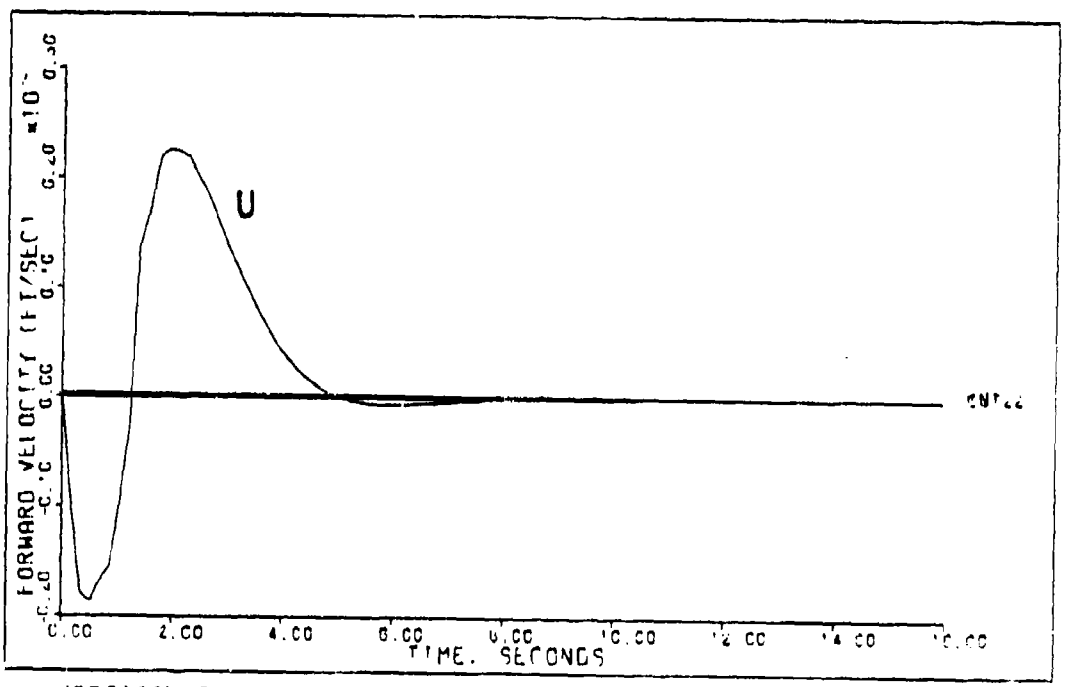

VERTICAL TRANSLATION (0.4M OK FT) DELAY=0.025 SEC ACTUATORS

Figure 5-32

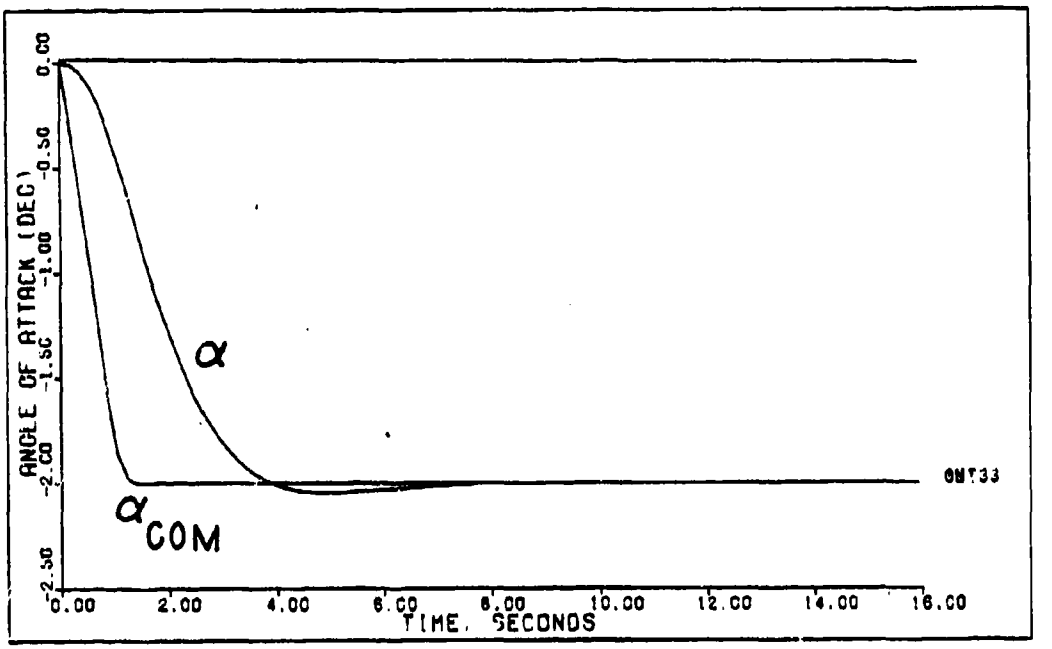

VERTICAL TRANSLATION (0.4M OK FT)

Figure 5-33

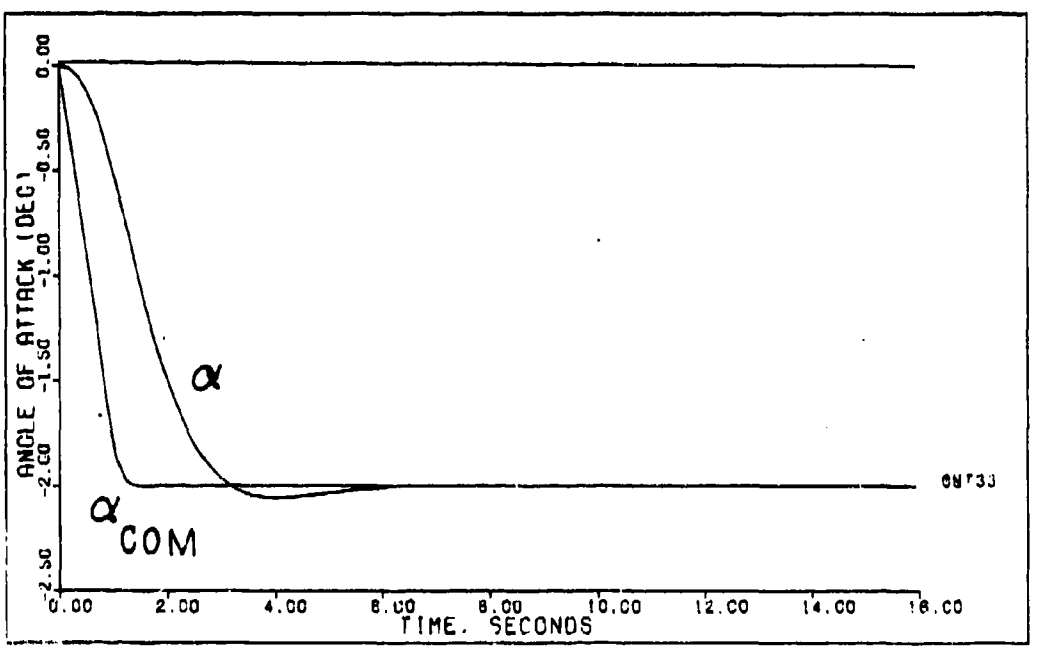

VERTICAL TRANSLATION (0.4M OK FT) DELAY=0.025 SEC

Figure 5-34

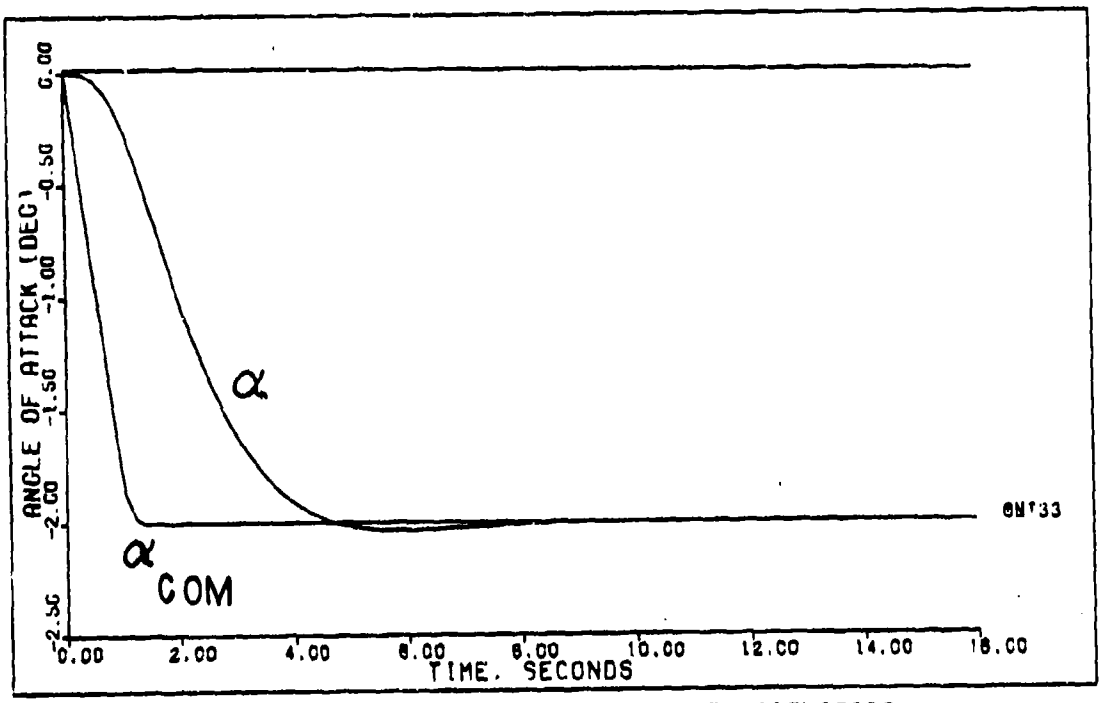

VERTICAL TRANSLATION (0.4M OK FT) ACTUATORS

Figure 5-35

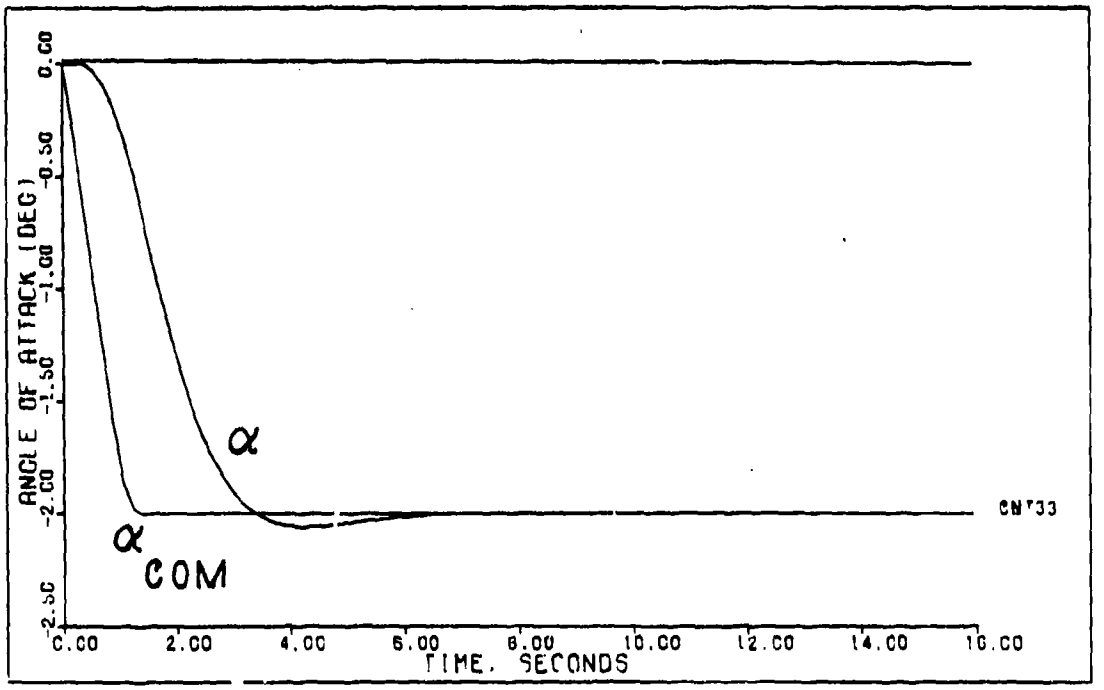

VERTICAL TRANSLATION (0.4M OK FT) DELAY=0.025 SEC ACTUATORS

Figure 5-36

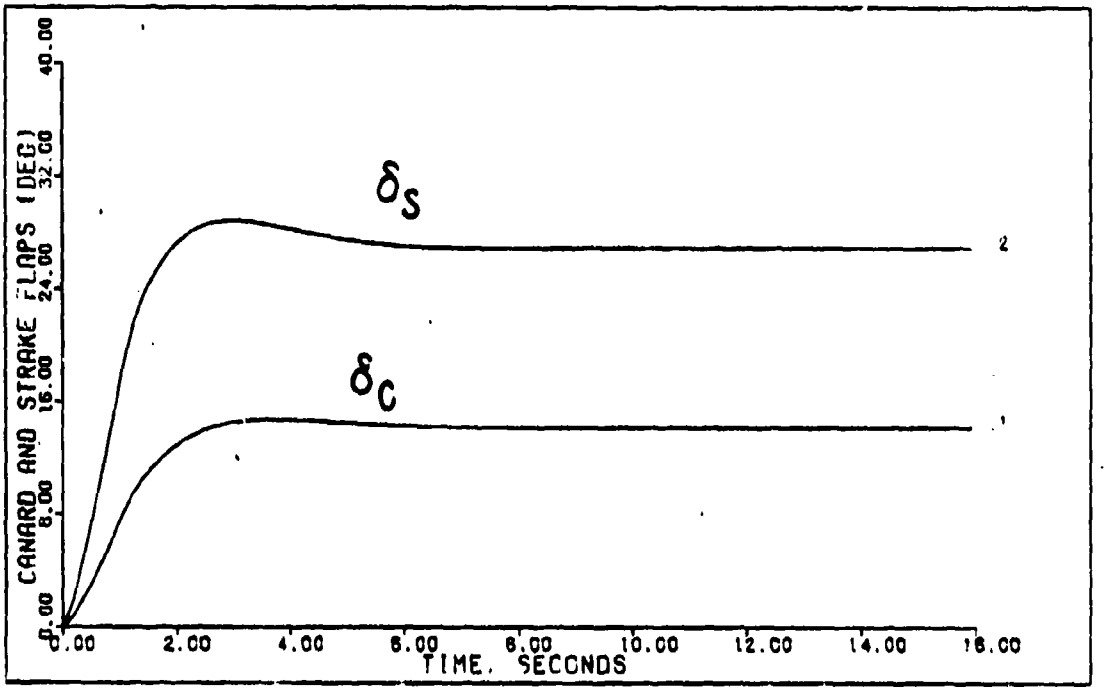

VERTICAL TRANSLATION (0.4M OK FT)

Figure 5-37

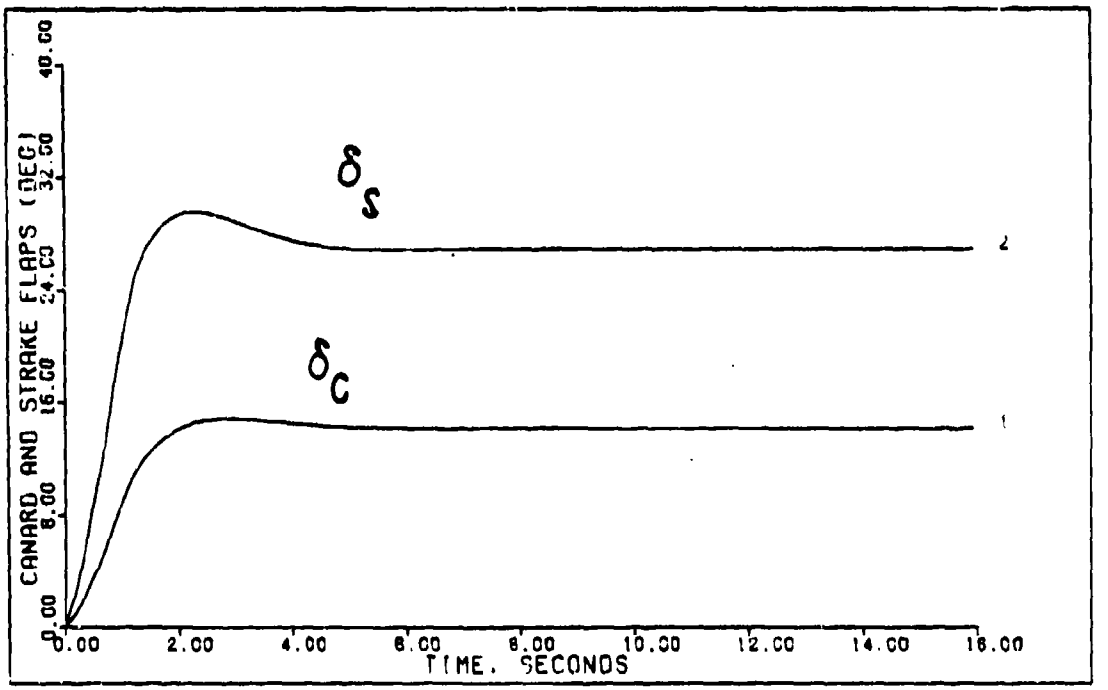

VERTICAL TRANSLATION (0.4M OK FT) DELAY=0.025 SEC

Figure 5-38

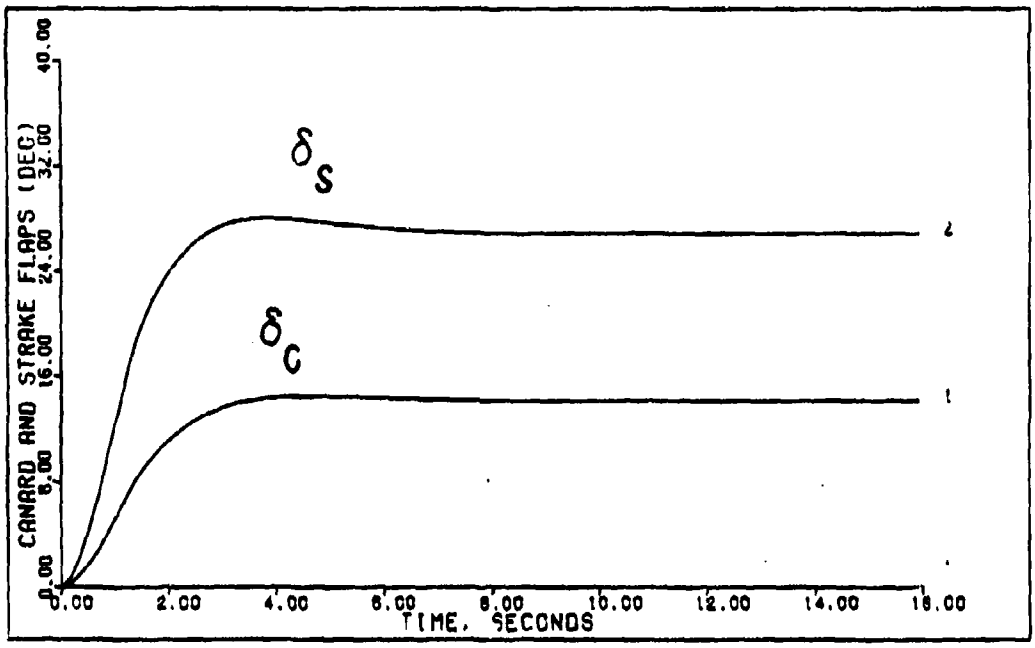

VERTICAL TRANSLATION (0.4M OK FT) ACTUATORS

Figure 5-39

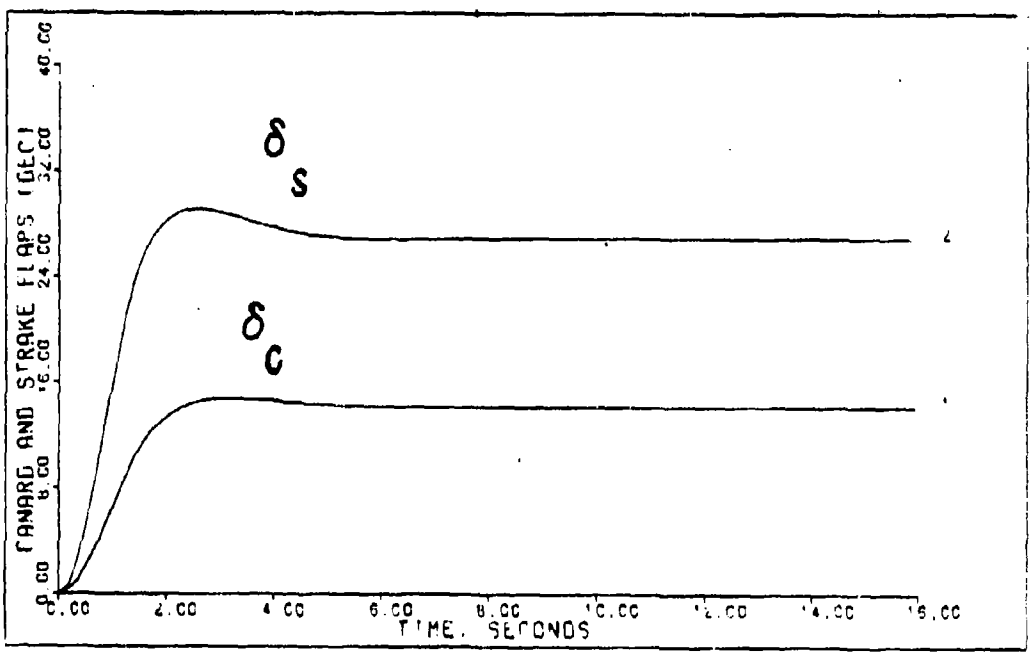

VERTICAL TRANSLATION (0.4M OK FT) DELAY=0.025 SEC ACTUATORS

Figure 5-40

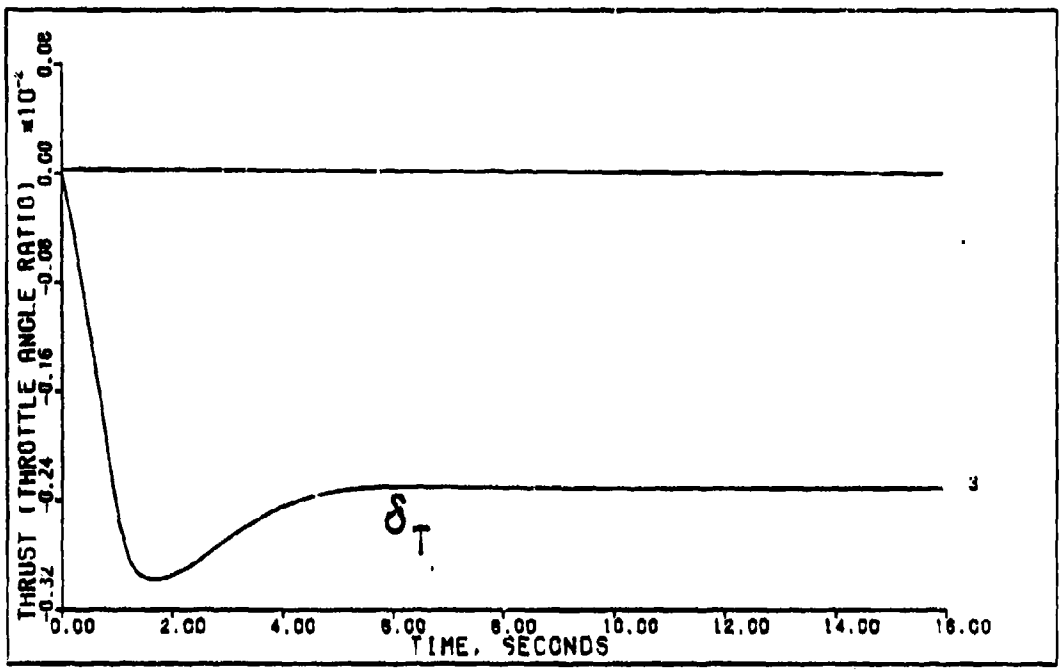

VERTICAL TRANSLATION (0.4M OK FT)

Figure 5-41

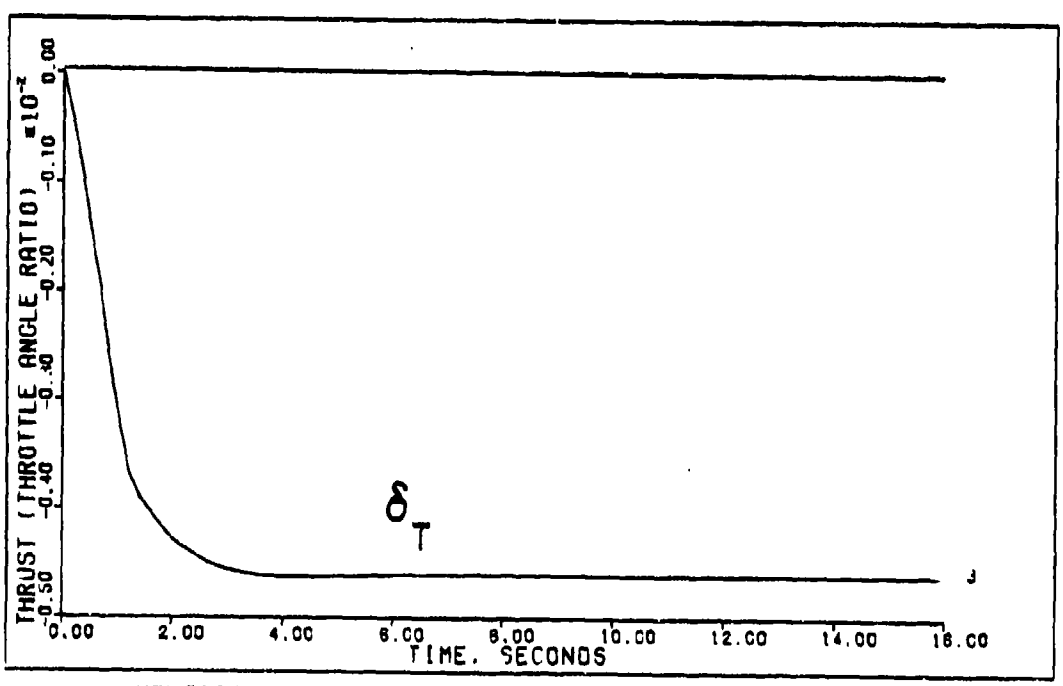

VERTICAL TRANSLATION (0.4M OK FT) DELAY=0.025 SEC

Figure 5-42

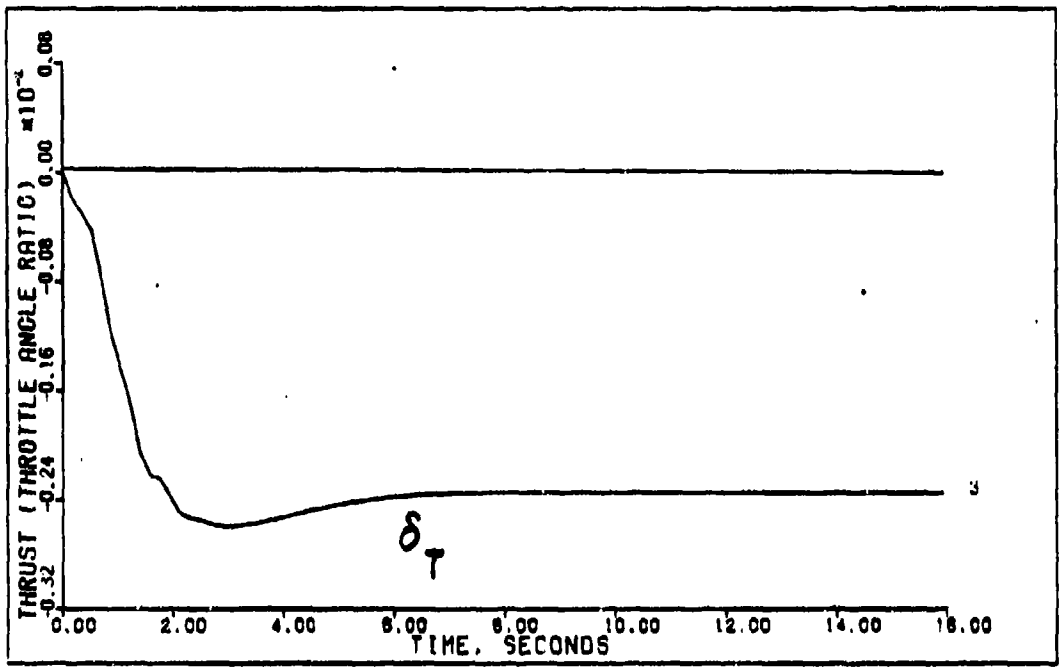

VERTICAL TRANSLATION (0.4M OK FT) ACTUATORS

Figure 5-43

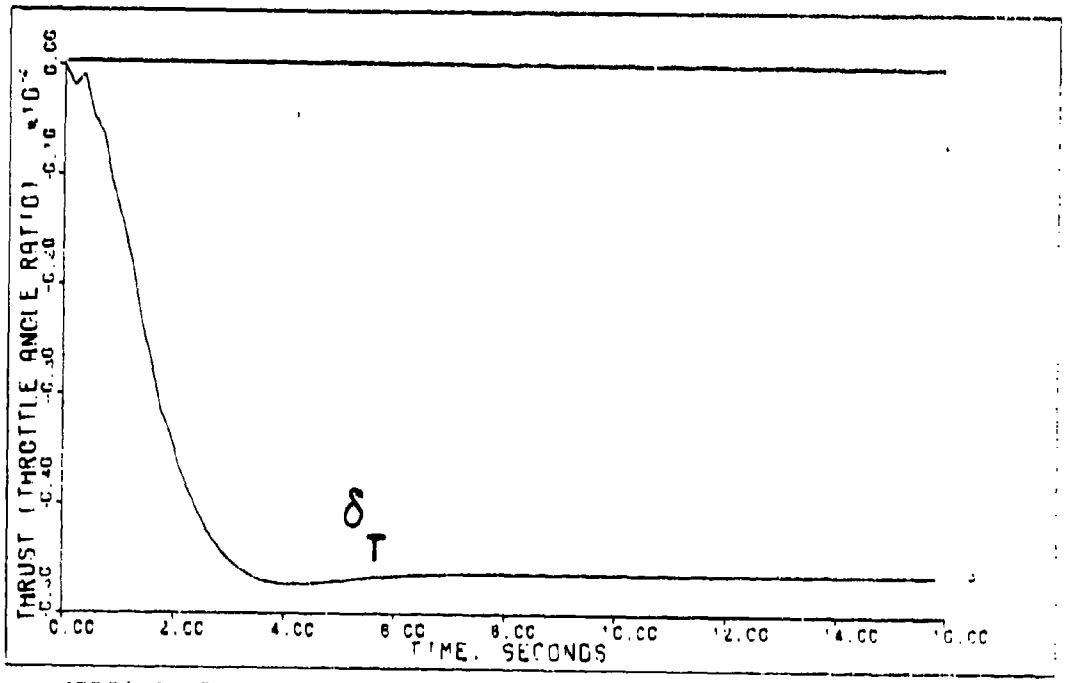

VERTICAL TRANSLATION (0.4M OK FT) DELAY=0.025 SEC ACTUATORS

Figure 5-44

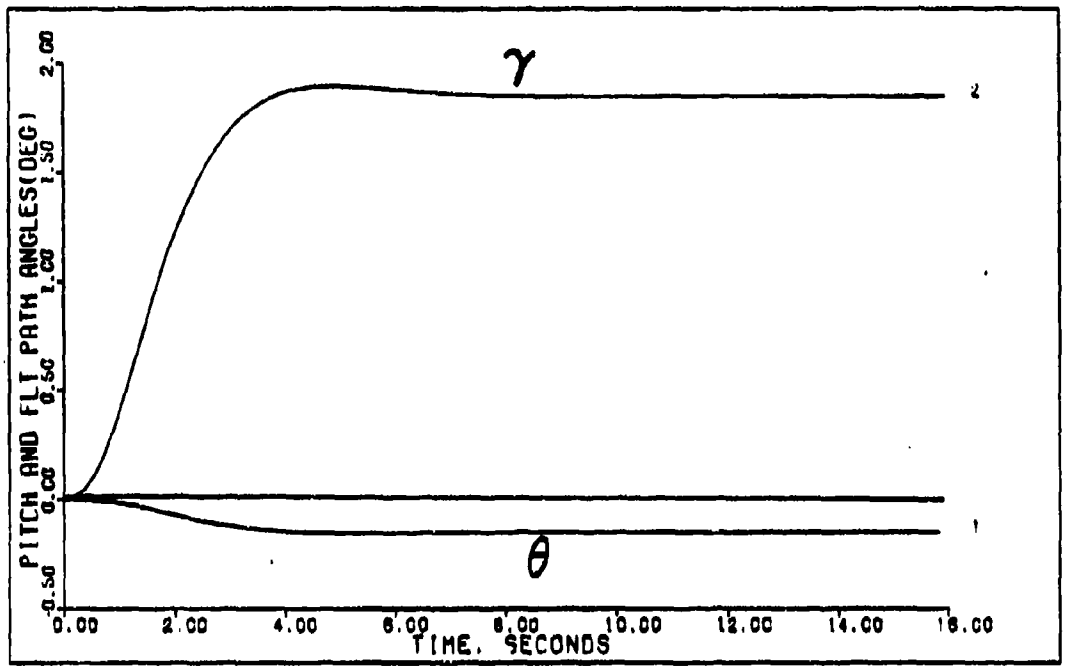

VERTICAL TRANSLATION (0.4M OK FT)

Figure 5-45

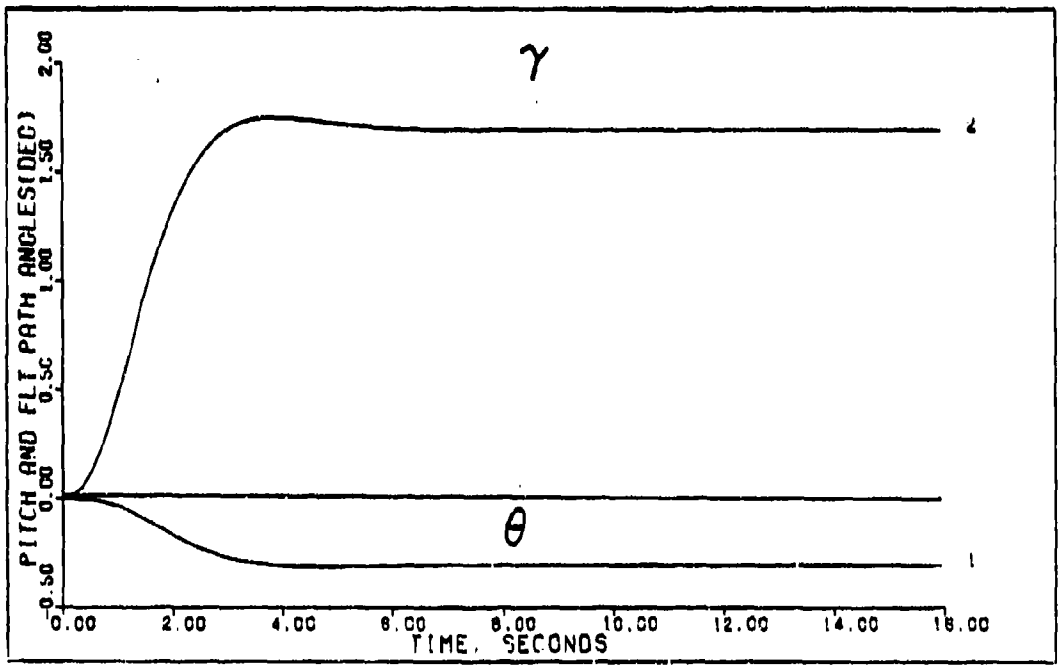

VERTICAL TRANSLATION (0.4M OK FT) DELAY=0.025 SEC

Figure 5-46

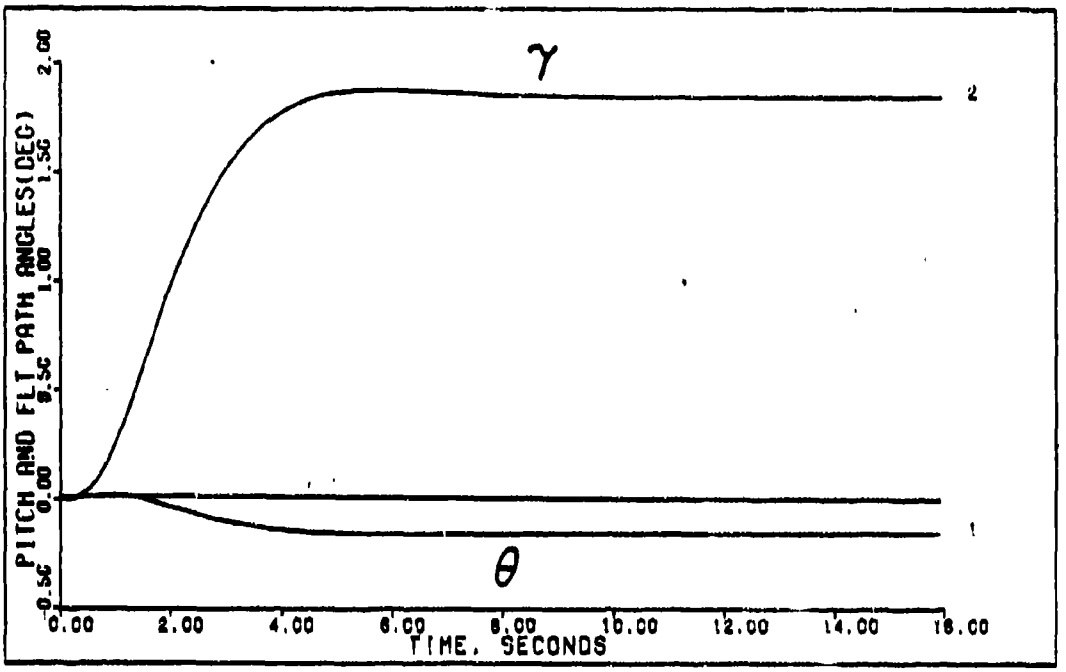

VERTICAL TRANSLATION (0.4M OK FT) ACTUATORS

Figure 5-47

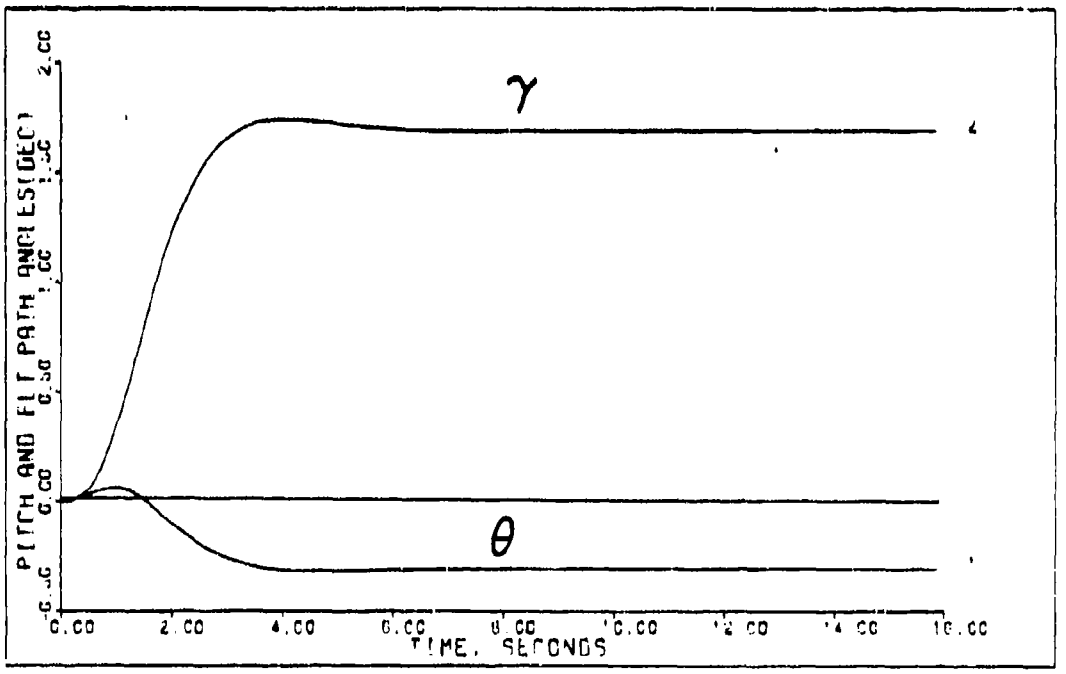

VERTICAL TRANSLATION (0.4M OK FT) DELAY=0.025 SEC ACTUATORS

Figure 5-48

In this maneuver, a ramp-to-hold input signal commands the angle of attack to negative two degrees. In addition, the pitch rate and velocity are commanded to zero. The result is an upward translation of the aircraft.

All the time plots show smooth and well behaved aircraft responses with and without actuators and computational time delay.

For the configuration without actuators and computational time delay, the aircraft smoothly follows the commanded angle of attack with just a slight overshoot as shown in Fig. 5-33. The velocity changes only a fraction of a foot per second during the maneuver (see Fig. 5-29). The aircraft rotates slightly during the transient response and correspondingly, the pitch rate of Fig. 5-25 momentarily peaks at minus 0.06 degrees per second before returning to zero. Because it is unrealistic to expect the pitch rate to remain at exactly zero during the maneuver, a small pitch angle error results from the integral of the pitch rate response and the resulting pitch angle is about minus 0.2 degrees (see Fig. 5-45). Therefore, the flight path angle is slightly less than the commanded angle of attack (see Figs. 5-45 through 5-48). This occurs because the flight path angle is the difference between the pitch angle and the angle of attack.

When rates are the input variables, then angles are indirectly controlled. Therefore, a slight error always

occurs in the steady state response. This error is completely eliminated only if angles are the input variables.

The canard and strake deflections are both positive and within the deflection limits. The waveshapes are smooth with a slight overshoot (Fig. 5-37).

Adding computational time delay requires an increase in the angle of attack weighting element in the sigma matrix. With the additional gain, the results are very similar to the responses for the basic aircraft configuration.

When actuator dynamics are incorporated as an input to the aircraft plant, the sigma weighting matrix element controlling the angle of attack is reduced slightly to minimize the overshoot. As a result, it takes the aircraft approximately 0.5 seconds longer to reach the commanded angle of attack (see Fig. 5-35). The pitch rate goes momentarily positive, then negative, making the area under the pitch rate curve small (see Fig. 5-27). The resulting pitch angle error of 0.15 degrees in Fig. 5-47 is less than for the basic aircraft. The canard and strake deflections in Fig. 5-39 are within limits and have a smooth response.

The design of the controller with both actuator and dynamics and computational time delay has very good time responses which are very similar to those of the basic aircraft. To achieve the best design, the weighting matrix element corresponding to the angle of attack is increased

to a value lower than for the configuration with only time delay, but higher than for the design with just actuators.

Responses for the vertical translation maneuver are also very good for the other flight conditions. The design parameters and plots are presented in Appendices D through F.

5-4 Pitch Pointing Maneuver for 0.4 Mach at Sea Level

The longitudinal state space matrices are listed in Table 5-4. The command vector $\underline{v}$, design parameters, and controller matrices for this maneuver are tabulated in Table 5-7. Table 5-8 presents the figures of merit. The aircraft time response plots are provided in Figs. 5-49 through 5-72. Note that all angles are converted from radians to degrees before plotting.

The purpose of this maneuver is to change the aircraft pitch attitude, i.e., point the nose of the aircraft longitudinally, without changing the vehicle's flight path angle or velocity. To accomplish this maneuver, the pitch rate command is pulsed to generate a desired pitch angle and the change of velocity is commanded to zero. In addition, the angle of attack is commanded to equal the new pitch angle so the resulting flight path angle remains unchanged.

TABLE 5-7

DESIGN PARAMETERS AND CONTROLLER MATRICES
FOR LONGITUDINAL CONTROLLERS

FLIGHT CONDITION: 0.4 Mach at Sea Level
MANEUVER: Pitch Pointing
COMMAND VECTOR $\underline{v}$*: 0.8, 0.0349, 1.0, 1.8
0, 0, 0, 0
0.8, 0.0349, 50, 50

Plant Only

Alpha	Epsilon	Sigma**	$\underline{K}_0$***		
		1.9	.1400E+02	-.7019E-02	-.4967E+01
0.357	2.8	1.0	-.1670E+02	-.2159E+00	-.1288E+00
		0.015	.2957E-01	.2659E-01	.2404E-02

Plant and Computational Time Delay

Alpha	Epsilon	Sigma**	$\underline{K}_0$***		
		1.9	.1400E+02	-.7019E-02	-.4967E+01
0.357	2.8	1.0	-.1670E+02	-.2159E+00	-.1288E+02
		0.015	.2957E-01	.2659E-01	.2404E-02

Plant with Actuator Dynamics

Alpha	Epsilon	Sigma**	$\underline{K}_0$***		
		1.9	.1400E+02	-.7019E-02	-.4967E+01
0.357	2.8	1.0	-.1670E+02	-.2159E+00	-.1266E+02
		0.105	.2957E-01	.2659E-01	.2404E-02

Plant with Actuator Dynamics and Computational Time Delay

Alpha	Epsilon	Sigma**	$\underline{K}_0$***		
		1.6	.1179E+02	-.3510E-02	-.4967E+01
0.357	2.8	0.5	-.1406E+02	-.1079E+00	-.1288E+02
		0.015	.2490E-01	.1330E-01	.2404E-02

Notes

*Each pulse entry in $\underline{v}$ has four parts:
1. The time in seconds the input reaches steady-state;
2. Steady-state value (angles in radians);
3. Time the input leaves steady-state; and
4. Time the input reaches zero.

**Diagonal element values of the matrix.

***$\underline{K}_0$ = alpha * $\underline{K}_1$.

TABLE 5-8

LONGITUDINAL FIGURES OF MERIT

FLIGHT CONDITION: 0.4 Mach at Sea Level

MANEUVER: Pitch Pointing

COMMAND VECTOR $\underline{v}$:* 0.8, 0.0349, 1.0, 1.8
0, 0, 0, 0
0.8, 0.0349, 50, 50

Plant Only

Output	Peak Value**	Peak Time	Settling Time
Pitch Rate	2.08	0.875	***
Forward Velocity	-0.008	1.225	***
Angle of Attack	2.02	5.425	4.2
Pitch Angle	2.05	1.8	1.8
Flight Path Angle	0.3	2.5	4.5

Plant and Computational Time Delay

Output	Peak Value**	Peak Time	Settling Time
Pitch Rate	2.19	1.05	***
Forward Velocity	-0.018	1.225	***
Angle of Attack	2.01	7.175	5.6
Pitch Angle	2.05	1.8	1.9
Flight Path Angle	0.7	2.5	6.0

TABLE 5-8 --Continued

Plant with Actuator Dynamics

Output	Peak Value**	Peak Time	Settling Time
Pitch Rate	2.16	1.05	***
Forward Velocity	-0.0102	1.05	***
Angle of Attack	2.036	5.25	4.2
Pitch Angle	2.1	1.6	1.6
Flight Path Angle	0.3	2.4	5.6

Plant with Actuator Dynamics and Computational Time Delay

Output	Peak Value**	Peak Time	Settling Time
Pitch Rate	2.26	0.875	***
Forward Velocity	-0.045	1.225	***
Angle of Attack	2.02	6.65	5.25
Pitch Angle	2.01	1.8	2.5
Flight Path Angle	0.75	2.3	5.2

Notes

1. Figures of merit for the pitch angle and the flight path angle are estimated from the response plots.

2. Pitch rate, forward velocity, and angle of attack are components of the output vector y.

3. Pitch rate and angle of attack are commanded to achieve desired responses in the pitch angle and the flight path angle for each maneuver.

*Commanded inputs in order:
(1) pitch rate in radians per second;
(2) forward velocity in feet per second; and
(3) angle of attack in radians.

**Angles are converted from radians to degrees prior to calculating the figures of merit.

***Final value of the output is zero. Settling time undefined using definition of 2 percent of final value.

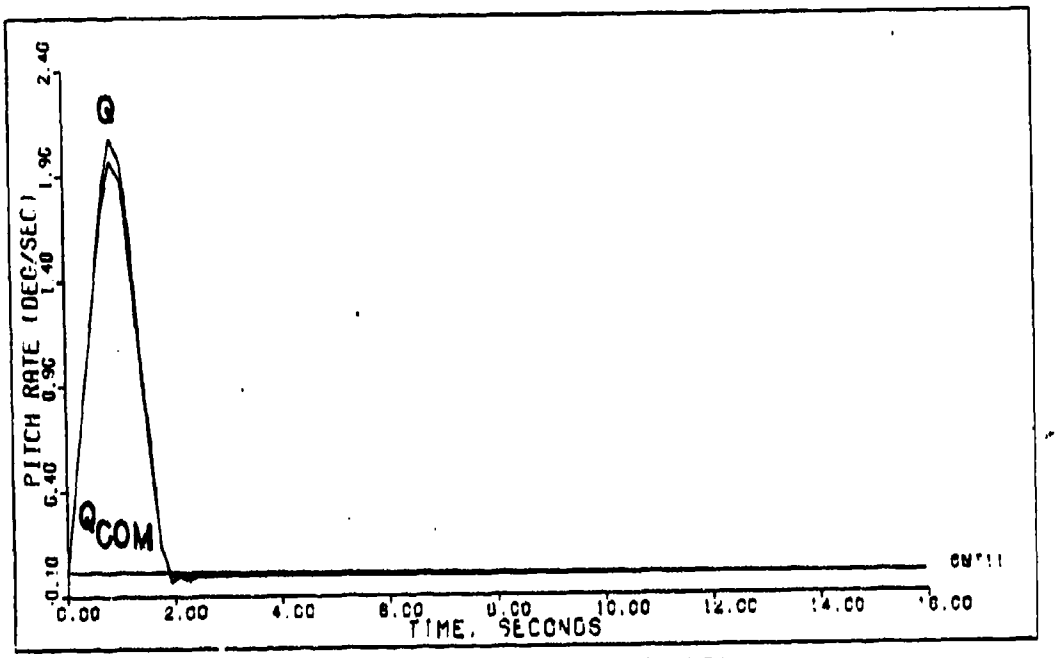

PITCH POINTING (0.4M OK FT)

Figure 5-49

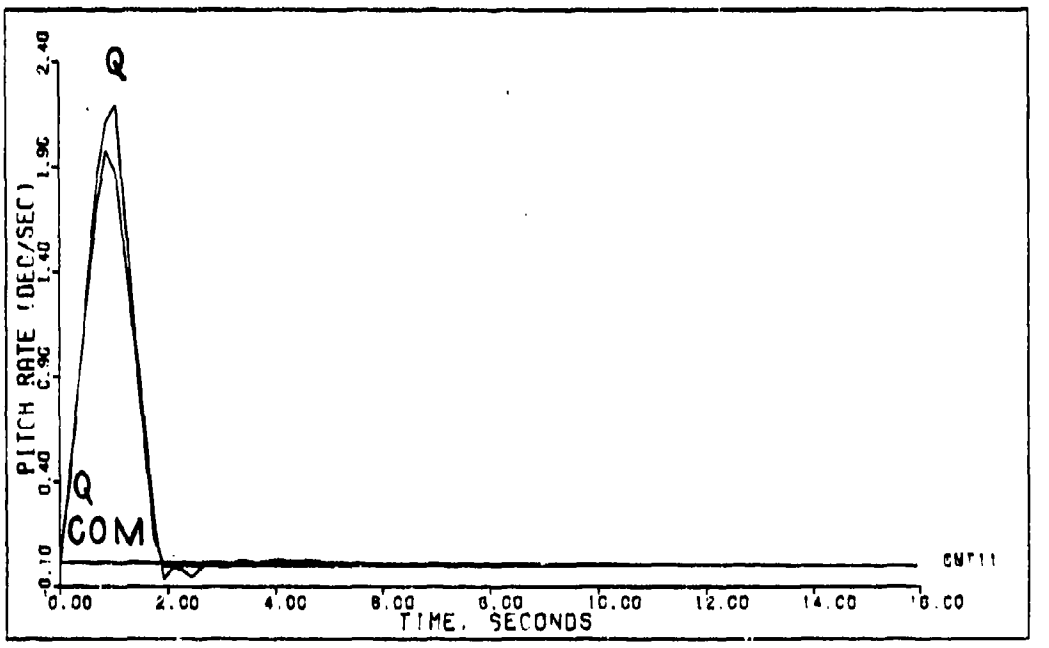

PITCH POINTING (0.4M OK FT) DELAY=0.025 SEC

Figure 5-50

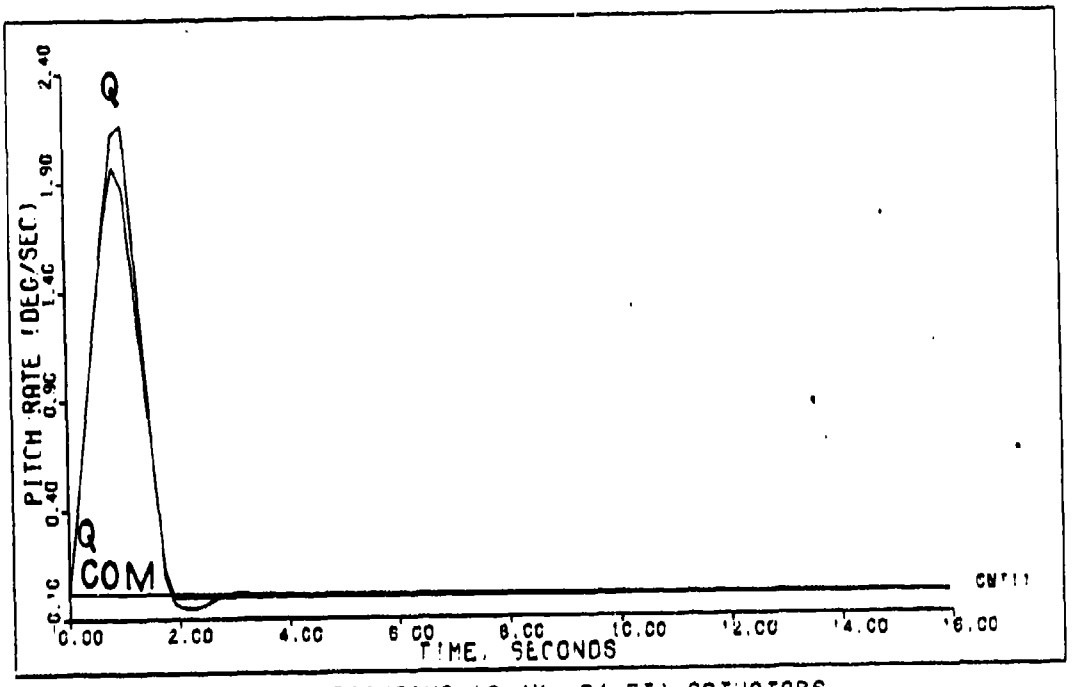

PITCH POINTING (0.4M OK FT) ACTUATORS

Figure 5-51

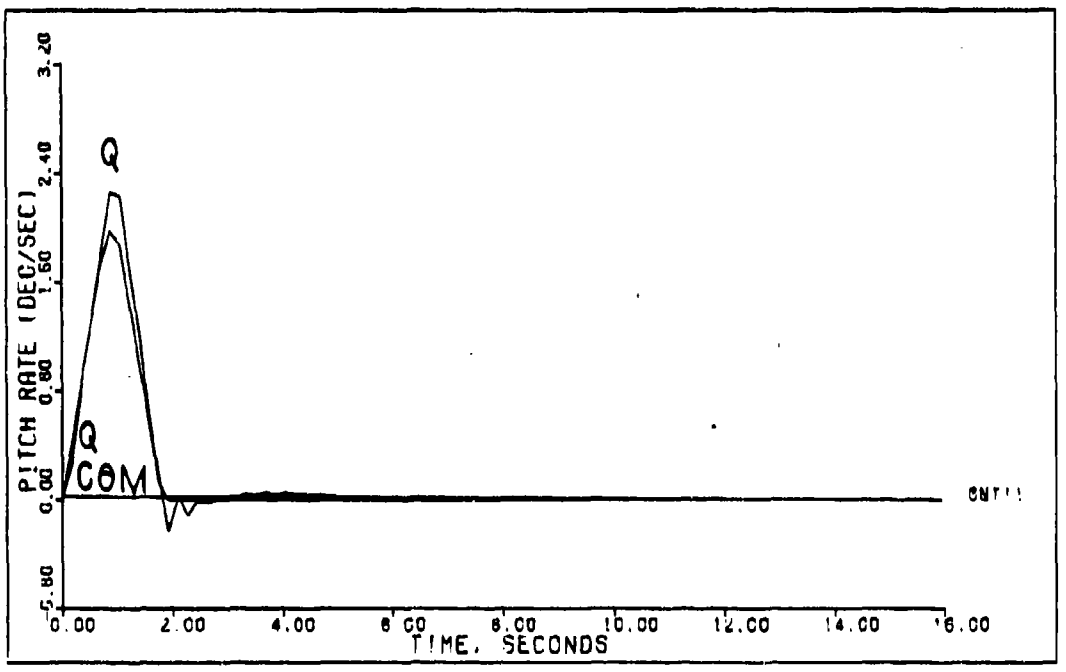

PITCH POINTING (0.4M OK FT) DELAY=0.025 SEC ACTUATORS

Figure 5-52

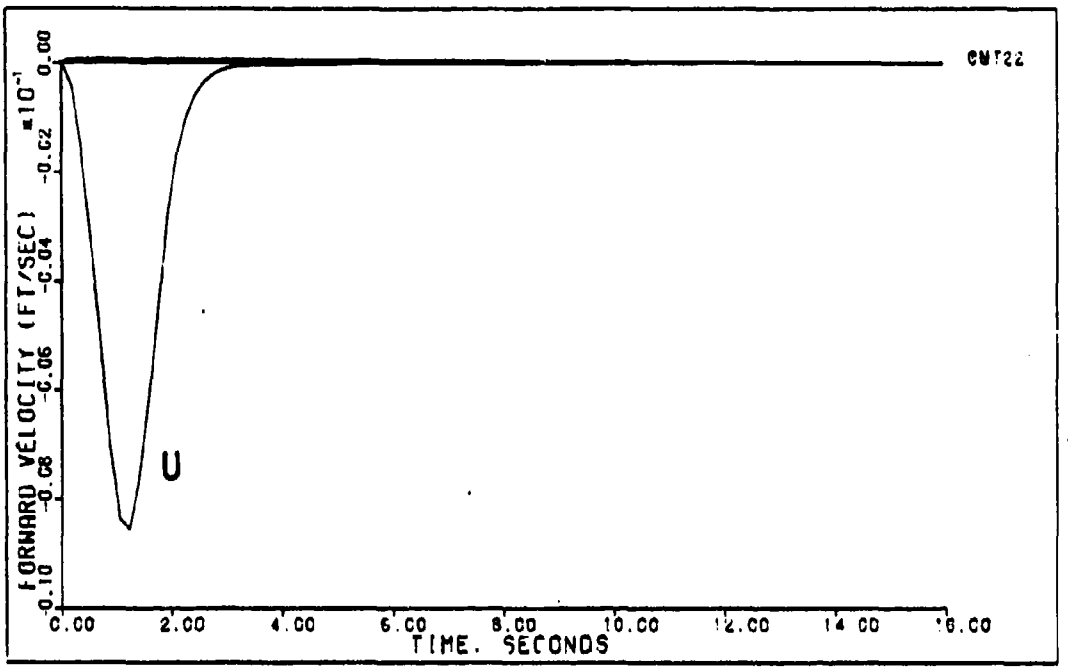

PITCH POINTING (0.4M OK FT)

Figure 5-53

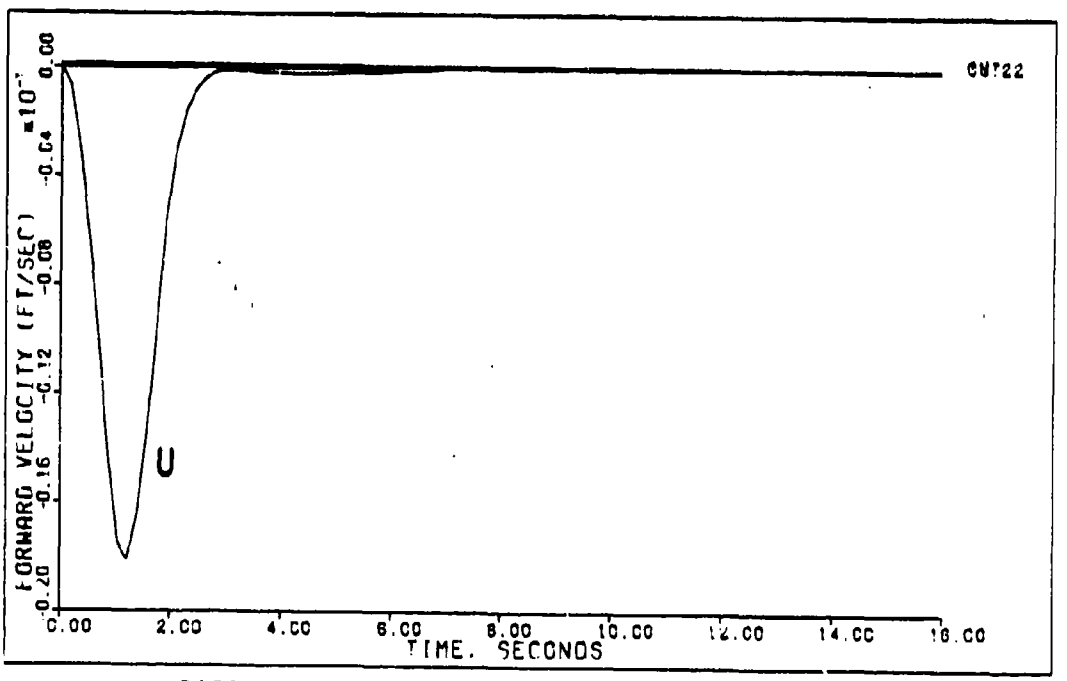

PITCH POINTING (0.4M OK FT) DELAY=0.025 SEC

Figure 5-54

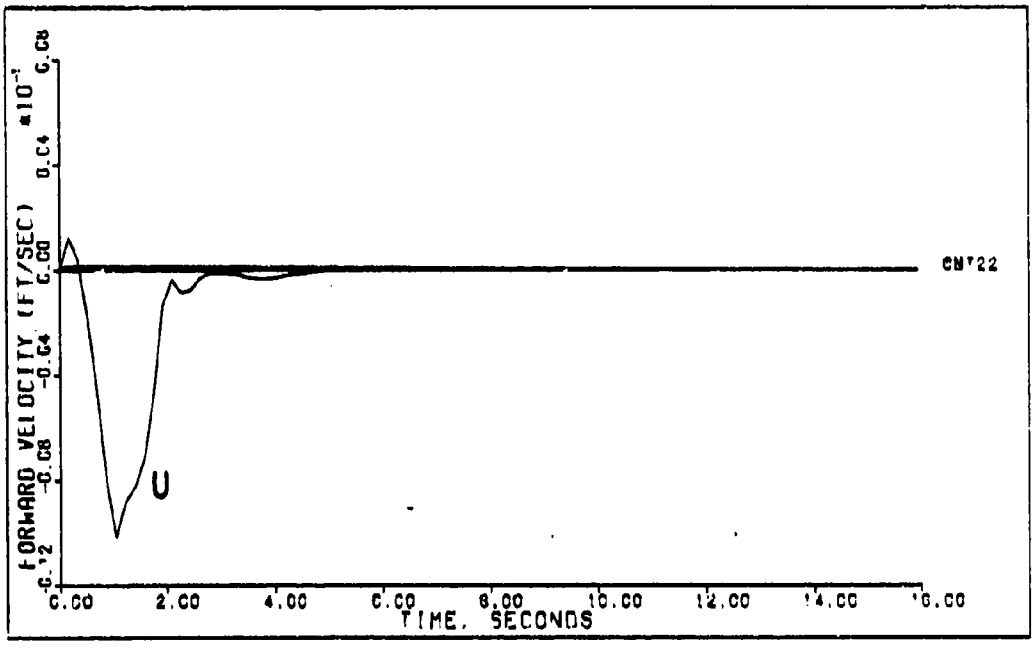

PITCH POINTING (0.4M OK FT) ACTUATORS

Figure 5-55

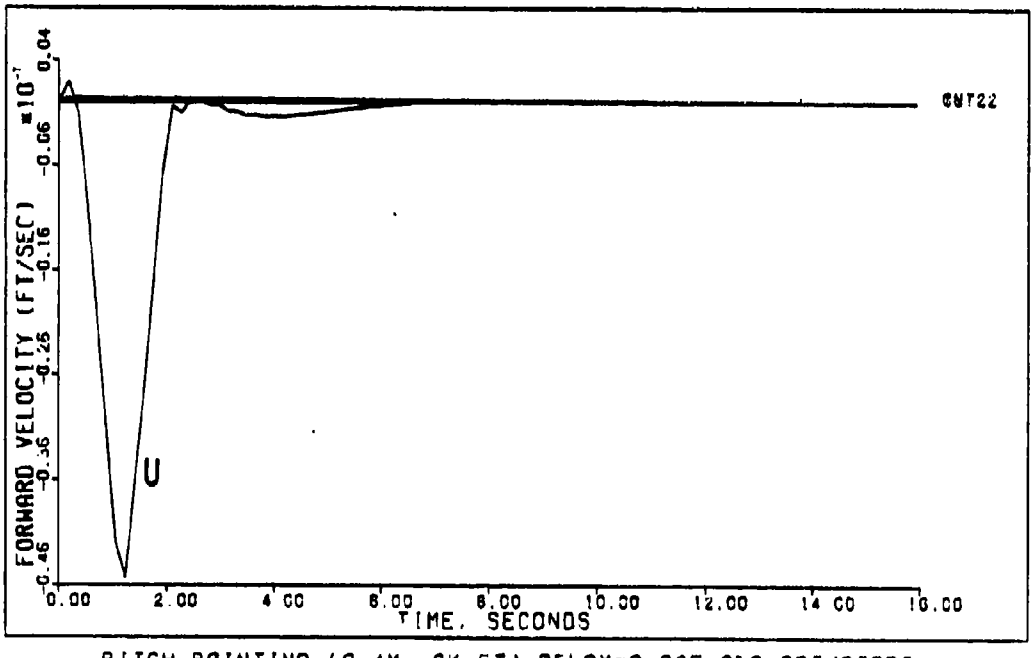

PITCH POINTING (0.4M OK FT) DELAY=0.025 SEC ACTUATORS

Figure 5-56

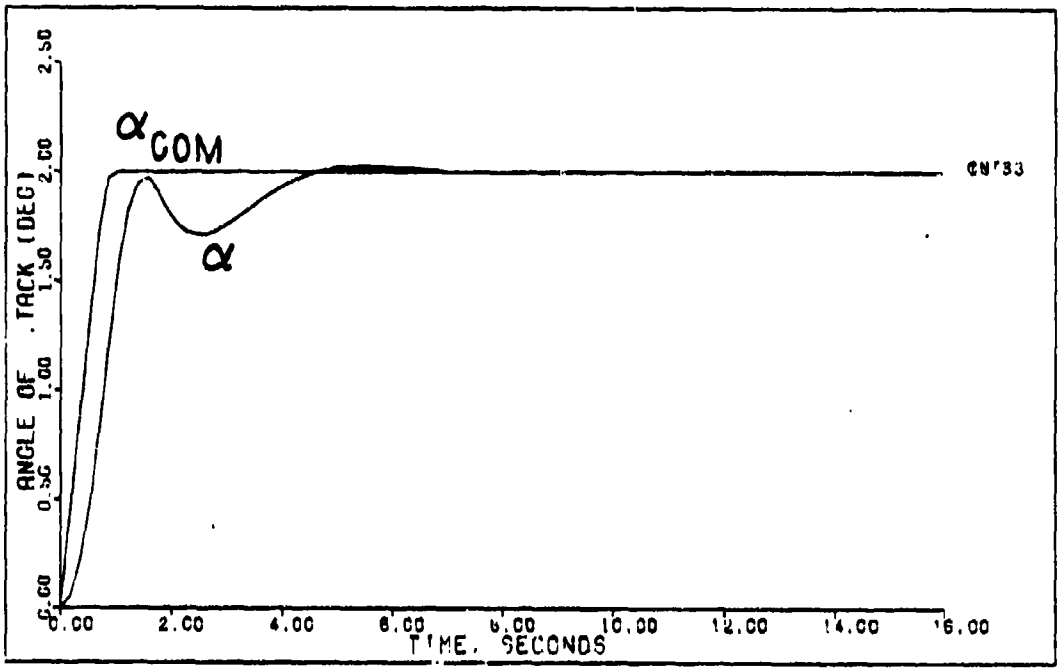

PITCH POINTING (0.4M OK FT)

Figure 5-57

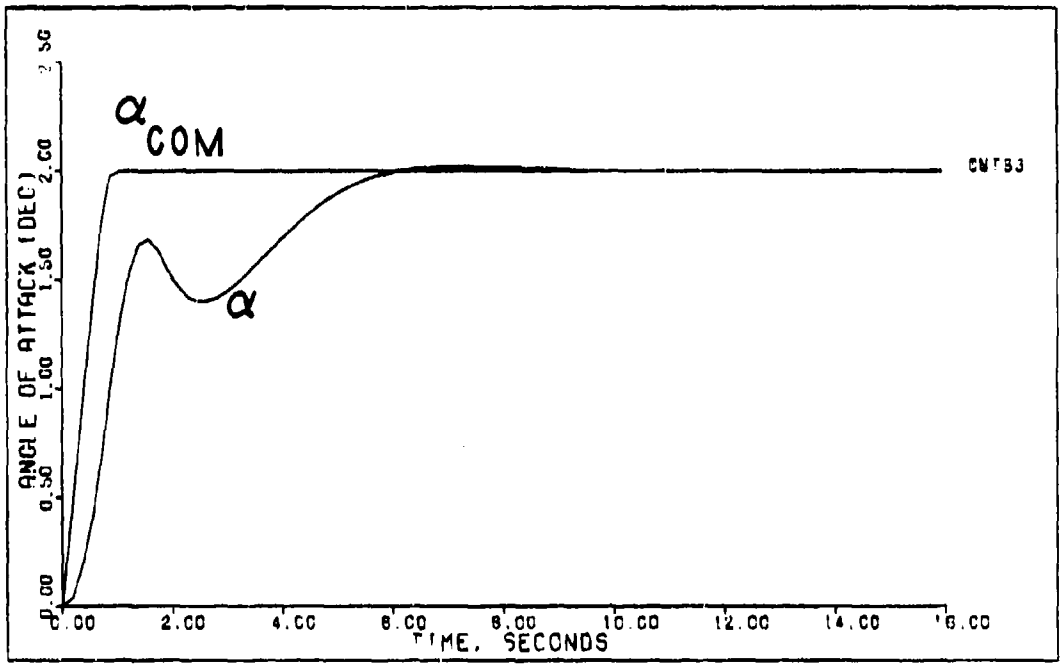

PITCH POINTING (0.4M OK FT) DELAY=0.025 SEC

Figure 5-58

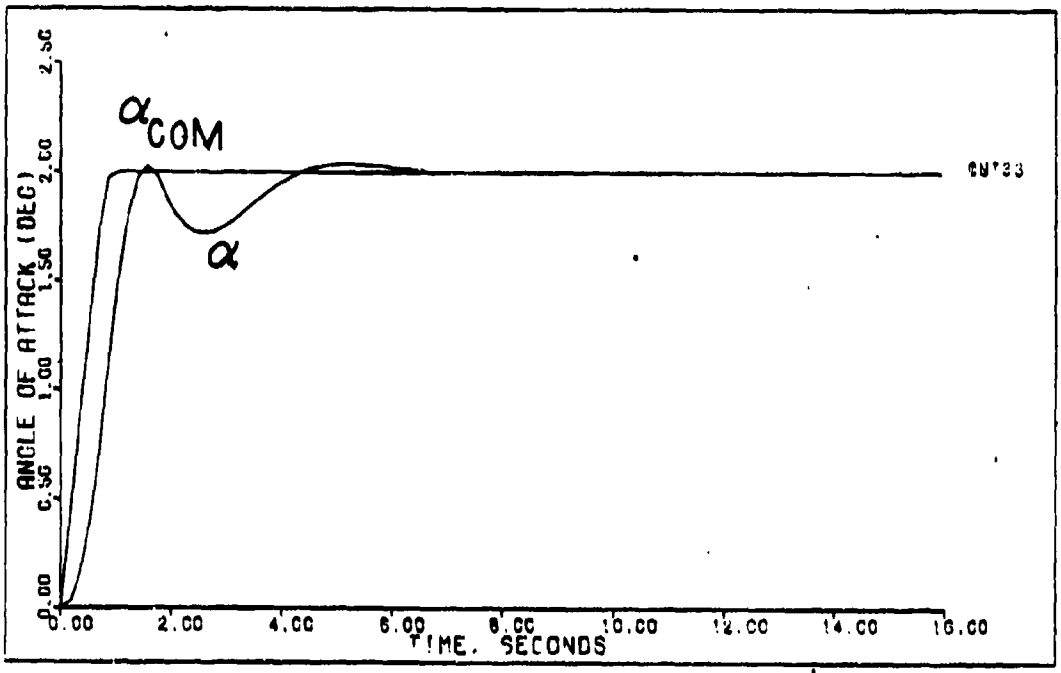

PITCH POINTING (0.4M OK FT) ACTUATORS

Figure 5-59

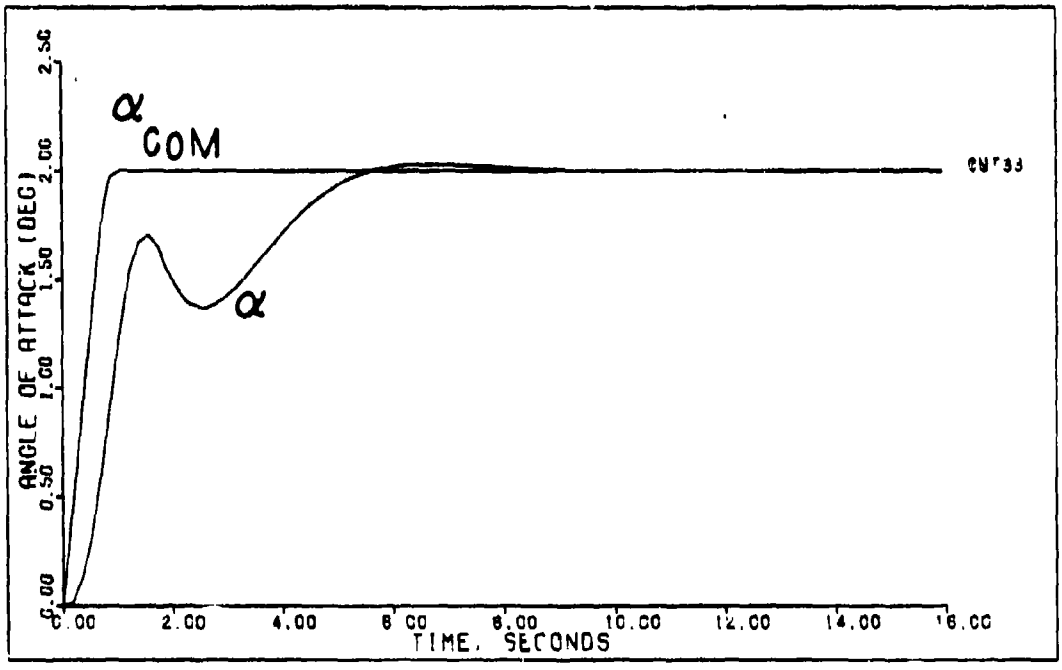

PITCH POINTING (0.4M OK FT) DELAY=0.025 SEC ACTUATORS

Figure 5-60

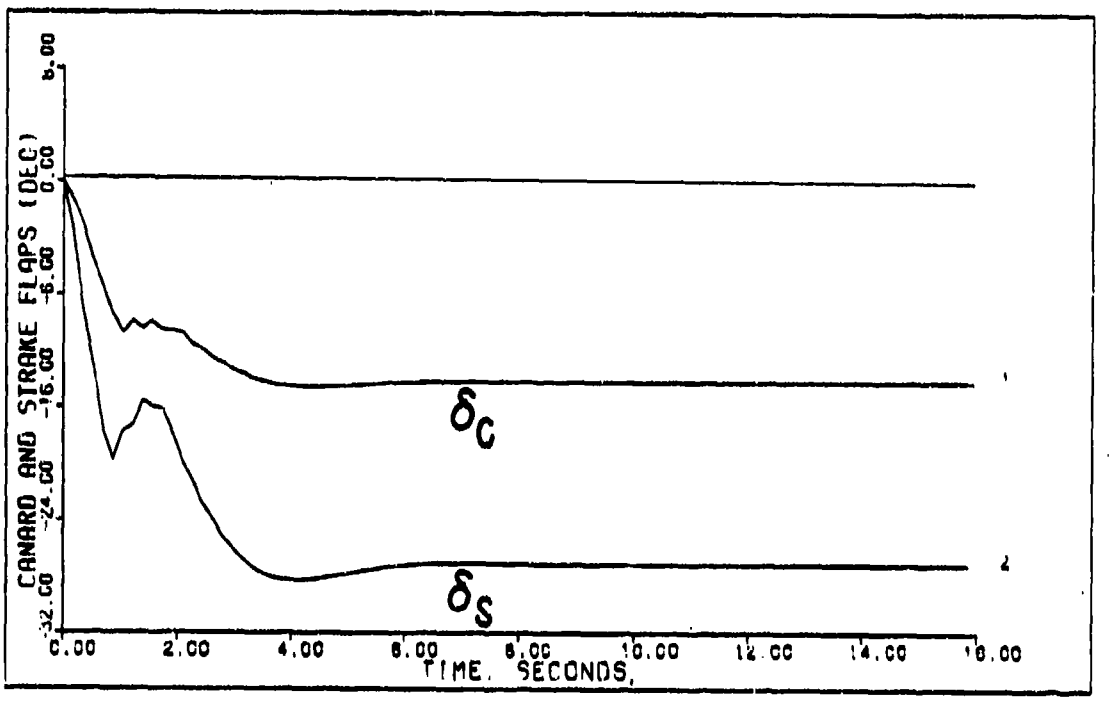

PITCH POINTING (0.4M OK FT)

Figure 5-61

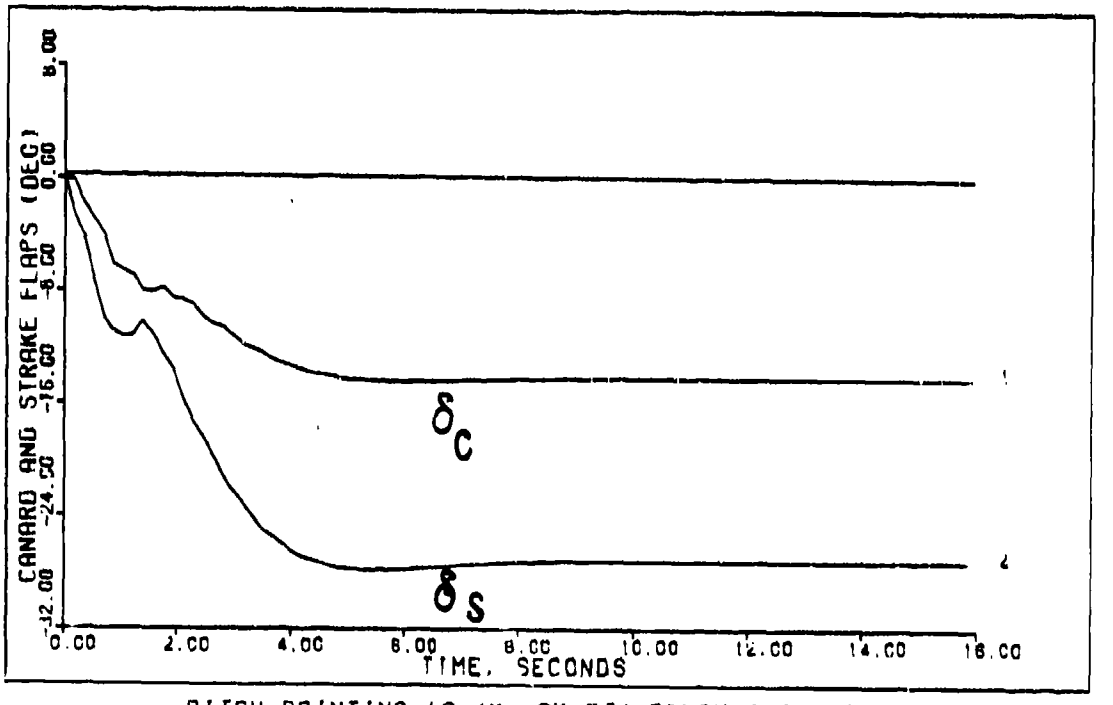

PITCH POINTING (0.4M OK FT) DELAY=0.025 SEC

Figure 5-62

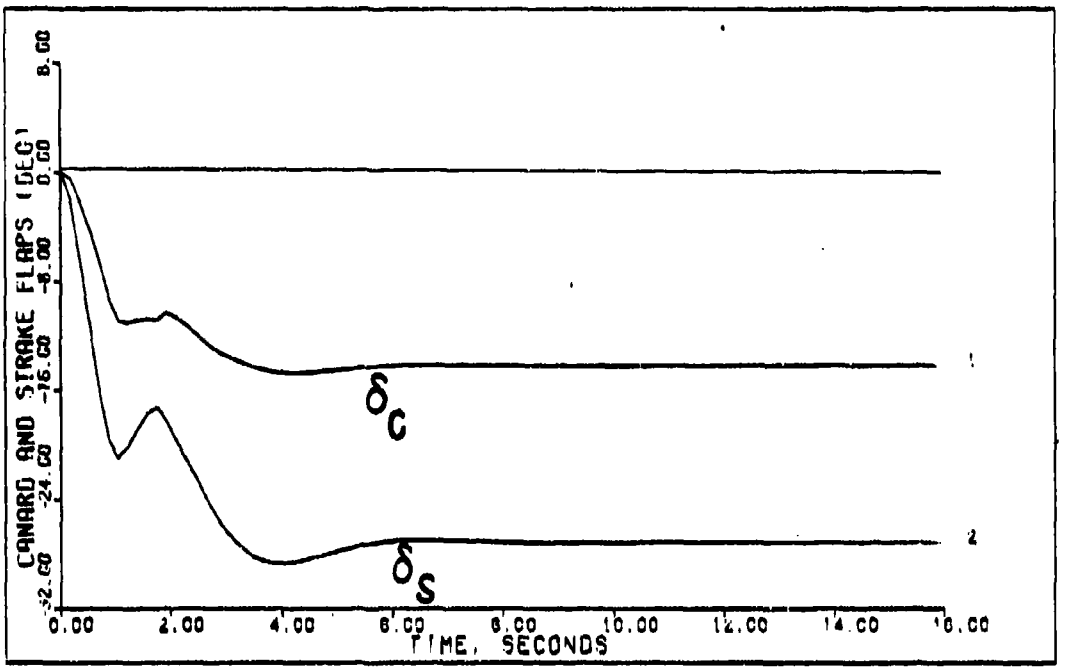

PITCH POINTING (0.4M OK FT) ACTUATORS

Figure 5-63

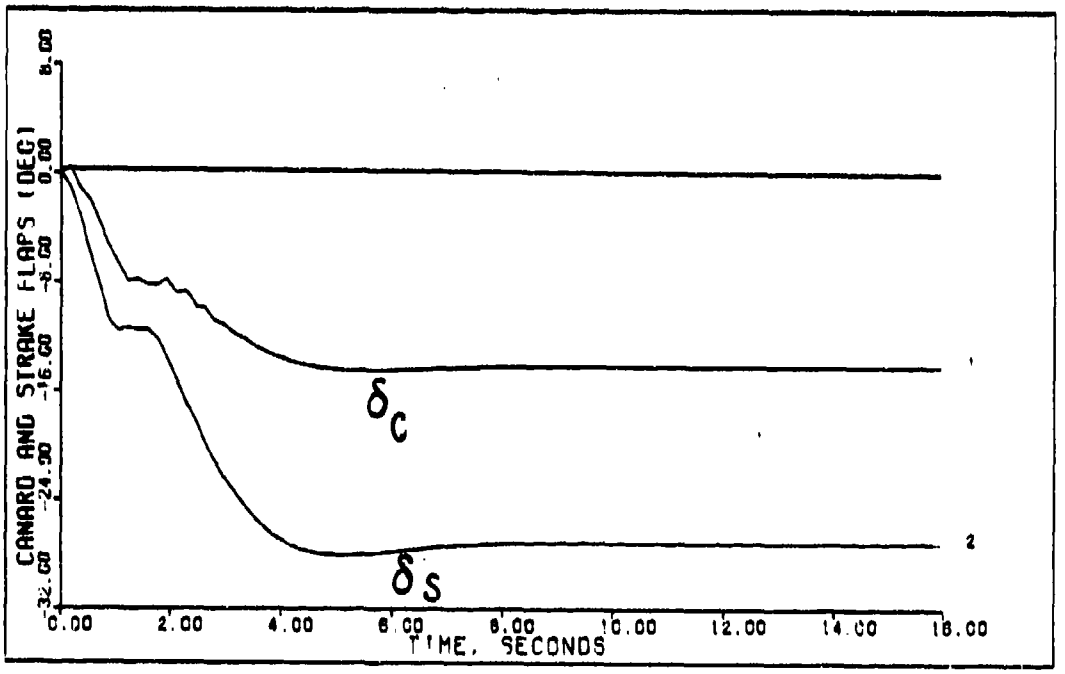

PITCH POINTING (0.4M OK FT) DELAY=0.025 SEC ACTUATORS

Figure 5-64

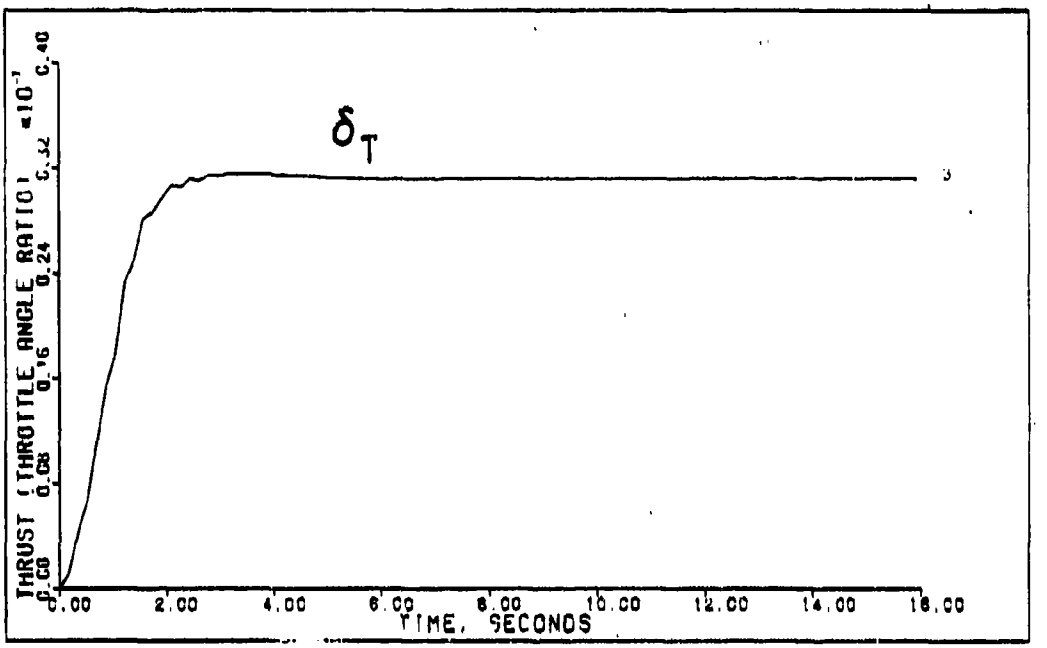

PITCH POINTING (0.4M OK FT)

Figure 5-65

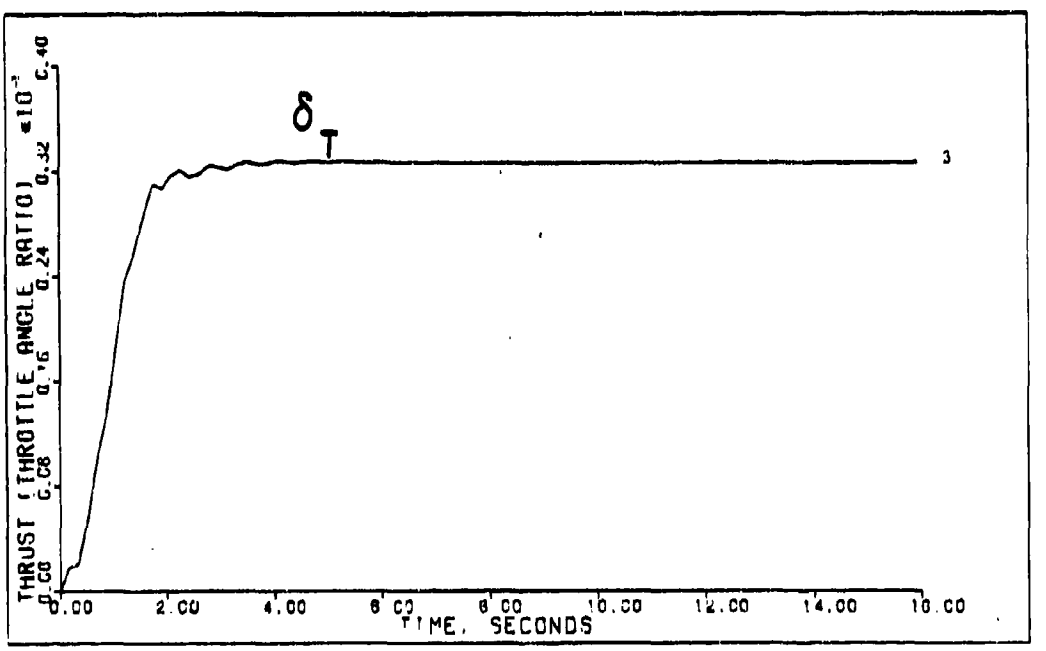

PITCH POINTING (0.4M OK FT) DELAY=0.025 SEC

Figure 5-66

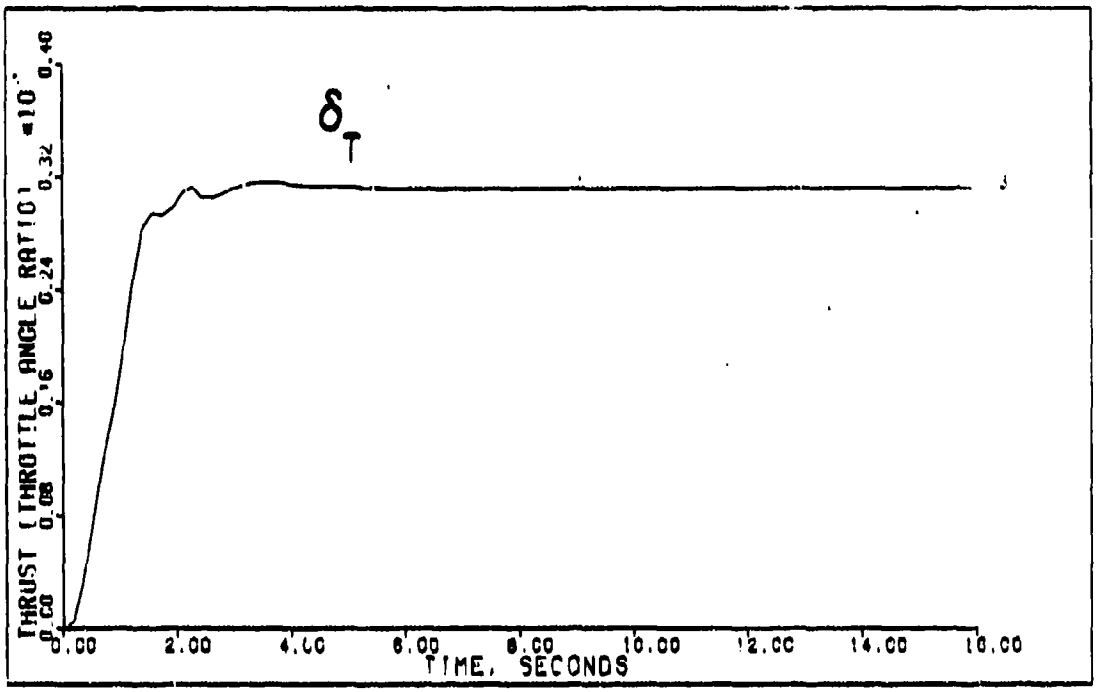

PITCH POINTING (0.4M OK FT) ACTUATORS

Figure 5-67

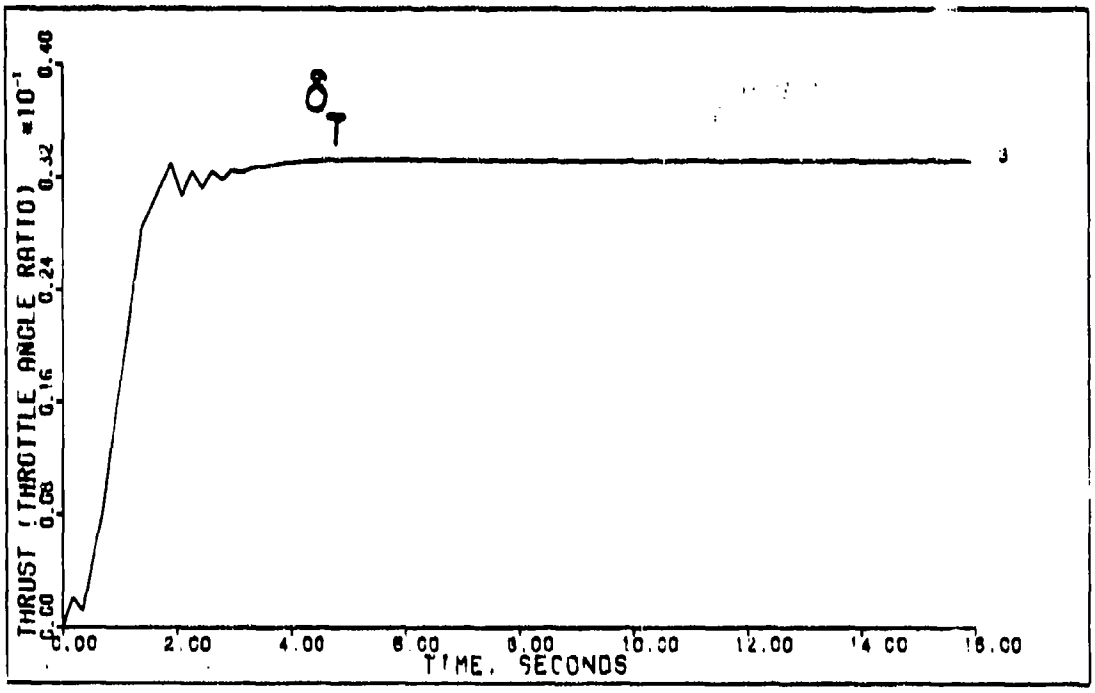

PITCH POINTING (0.4M OK FT) DELAY=0.025 SEC ACTUATORS

Figure 5-68

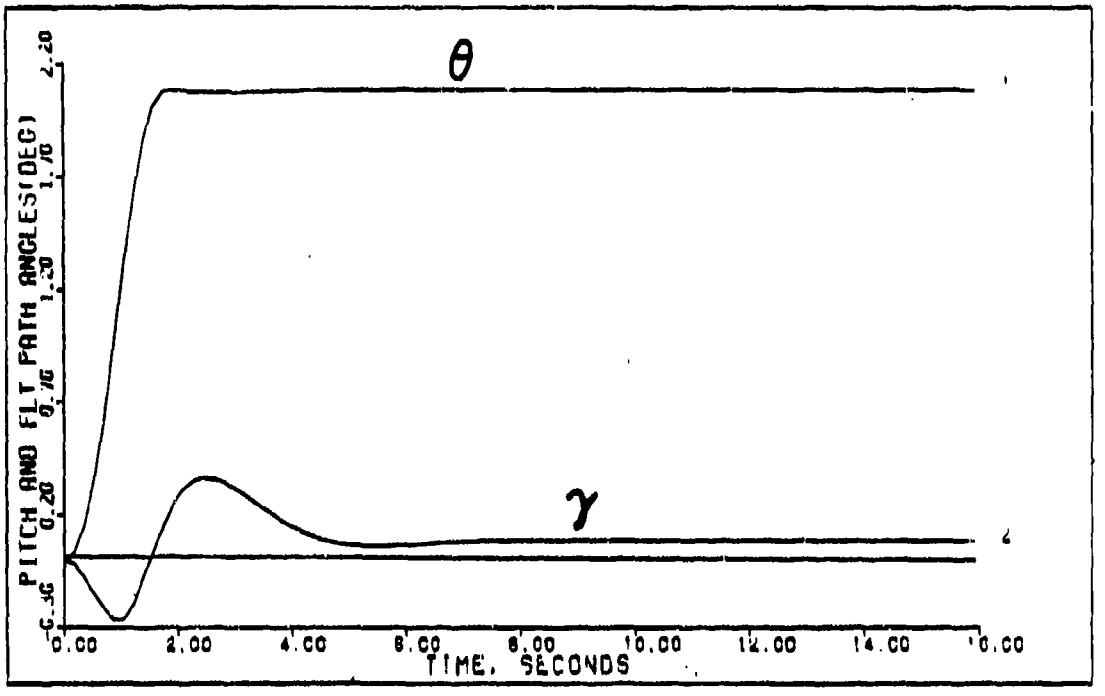

PITCH POINTING (0.4M OK FT)

Figure 5-69

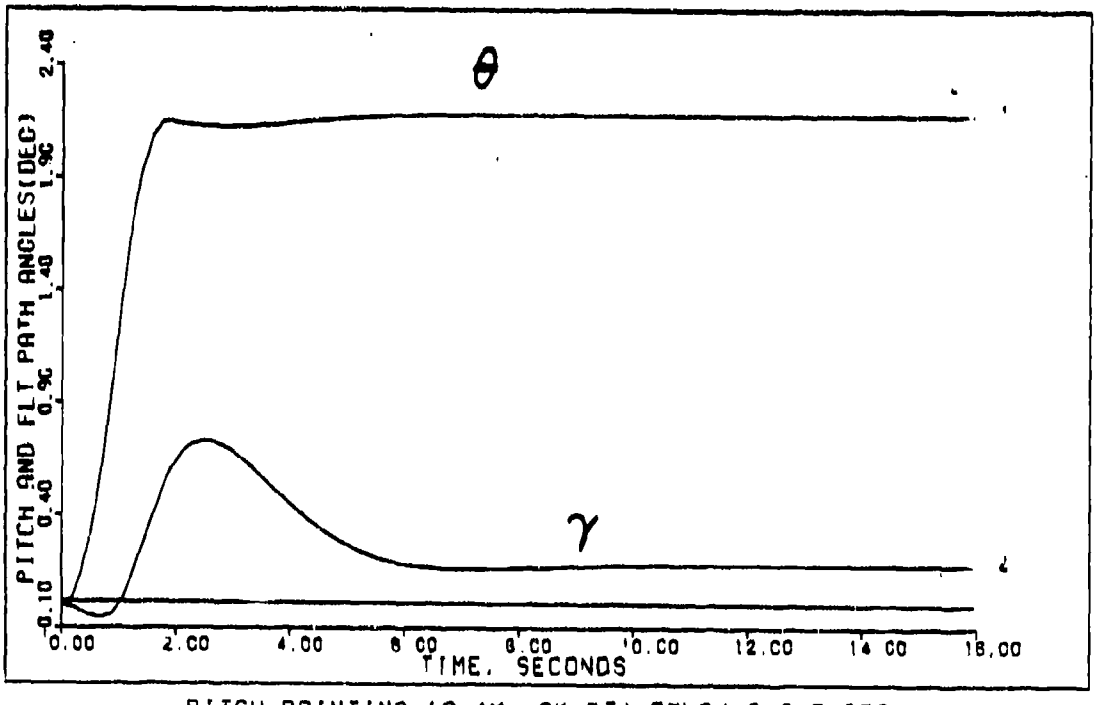

PITCH POINTING (0.4M OK FT) DELAY=0.025 SEC

Figure 5-70

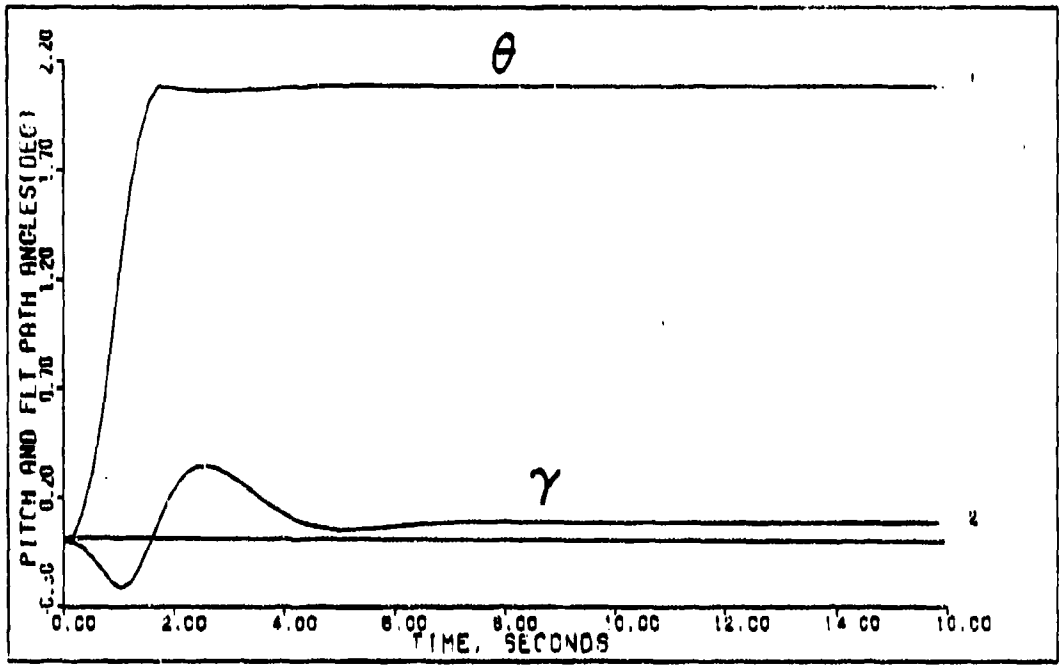

PITCH POINTING (0.4M OK FT) ACTUATORS

Figure 5-71

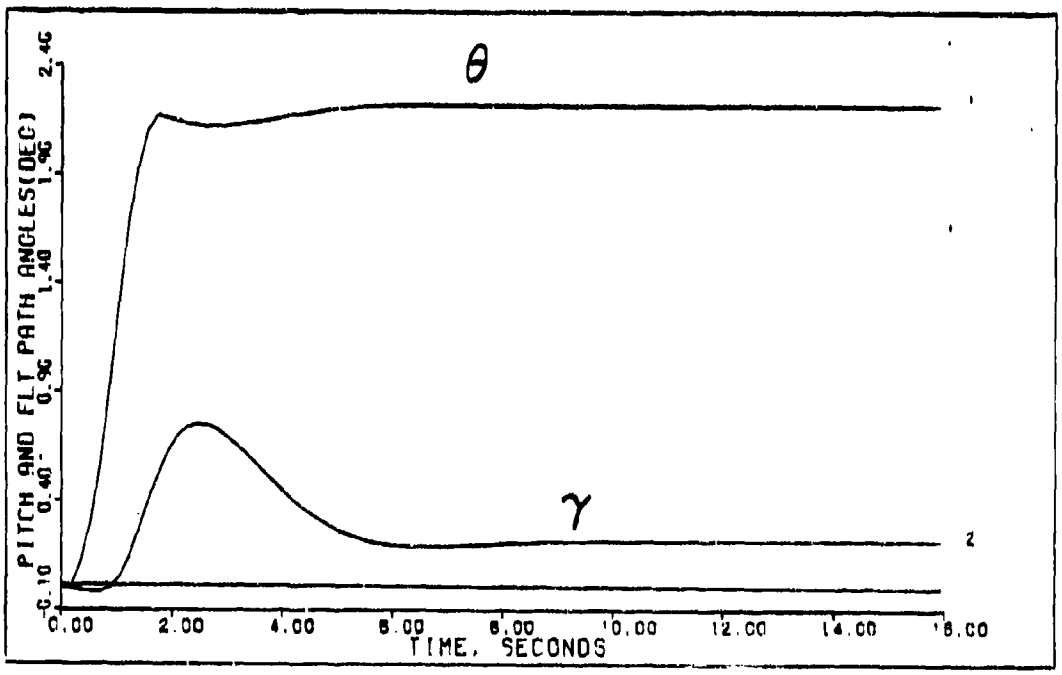

PITCH POINTING (0.4M OK FT) DELAY=0.025 SEC ACTUATORS

Figure 5-72

An analysis of the time history plots for all configurations of actuators and computational time delay show smooth and well behaved responses.

Without actuator dynamics and computational time delay in the simulation, Fig. 5-49 shows the pitch rate response of the aircraft slightly overshoots the pitch rate pulse input command. The overshoot is greater when time delay and/or actuator dynamics are added to the simulation (see Figs. 5-50 through 5-52). As a result, the actual pitch angle response has a steady state value slightly greater than calculated from the pitch rate pulse input signal. However, the angle of attack control input is set equal to the desired (not actual) pitch angle because it is not possible to exactly precompute the actual pitch angle response. The angle of attack is slightly less than the resulting pitch angle depending on the overshoot in the actual pitch rate response. The difference between the pitch angle and angle of attack determines the error in the flight path angle. The flight path angle error ranges from 0.1 degrees for the basic aircraft configuration in Fig. 5-69 to 0.3 degrees with computational time delay and actuator dynamics added to the simulation as illustrated in Fig. 5-72.

A maximum of two degrees of pitch pointing are possible without exceeding the canard and strake deflection limits for 0.5 Mach at sea level. The limits vary,

depending on the flight condition, and are easily calculated using the $\underline{G}(0)^{-1}$ steady state transfer function matrix as described in Chapter 4.

Analysis of the canard and strake flap deflection positions in Fig. 5-61 through 5-64 show the canard and strake correctly generate a positive lift to offset the additional positive lift produced by the increased angle of attack on the main wings.

The velocity control for all cases is excellent with a drop of less than 0.1 feet per second during the transient response (see Figs. 5-53 through 5-56). The thrust increases to offset the increased drag induced by the higher angle of attack as shown in Figs. 5-65 through 5-68.

The pitch angles in Figs. 5-69 through 5-72 increase smoothly to a steady state value with a small overshoot. The steady state value of the pitch angle equals the integral of the pitch rate response.

The responses for the pitch pointing maneuver are also good for the other flight conditions. The design parameters and plots are presented in Appendices D through F.

6. Results for the Lateral Control System Designs

6-1 Introduction

This chapter presents the design data and time history response plots for the X-29 aircraft, implemented with a "Porter configured" error actuated flight control system for the lateral-directional dynamics. Results include control laws for the coordinated turn and beta (sideslip) pointing for five flight conditions as follows:

1. 0.4 Mach at Sea Level
2. 0.9 Mach at Sea Level
3. 0.7 Mach at 15,000 Feet
4. 1.2 Mach at 15,000 Feet
5. 0.9 Mach at 50,000 Feet

For illustration and analysis, results are presented for the two lateral maneuvers at the flight condition of 0.7 Mach at 15,000 feet. Design data and plots for the maneuvers not detailed in this chapter are included in Appendices G and H.

Because the lateral control system is designed by primarily following the design procedure developed in Chapter 4 for the longitudinal controller, a separate chapter on the lateral design procedure is not necessary. However, before presenting the results of the lateral control system designs, this chapter first highlights-

significant information related to major steps in the design procedure and discusses those differences between the lateral and longitudinal design procedure.

6-2 Analysis of Aircraft Model

An analysis of the open-loop transfer functions of the unaugmented aircraft provide insight into the possible difficulty in designing a satisfactory control system. For example, the transfer functions for the lateral equations of motion for the unaugmented aircraft represent a statically unstable system. The following open-loop transfer functions for 0.7 Mach at 15,000 feet clearly illustrate this phenomena:

$$\text{Characteristic Polynomial (C.P)} = (s + 0.1969 \pm j\ 2.960)(s + 2.920)(s - 0.00911) \quad (6\text{-}1)$$

$$\phi/\delta_F = 1.488\ (s + 0.1958 \pm j\ 2.996)/\text{C.P.} \quad (6\text{-}2)$$

$$\phi/\delta_R = 0.2719\ (s - 0.1708 \pm j\ 1.397)/\text{C.P.} \quad (6\text{-}3)$$

$$\beta/\delta_F = -0.0008361\ (s + 8.004 \pm j\ 3.966)(s - 0.1549)/\text{C.P.} \quad (6\text{-}4)$$

$$\beta/\delta_R = .0009071\ (s + 112.3)(s + 2.877)(s - 0.007798)/\text{C.P.} \quad (6\text{-}5)$$

There is an unstable root at 0.00911 in the characteristic polynomial. Also, several of the transfer functions have zeros in the right half plane. Therefore, the plant is a non-minimum phase system. Thus, the successful design of a control system is difficult. This is especially true

when actuator/sensor dynamics and computational time delay are added to the basic equations. These additions may reduce the phase margin and make it a harder task to assure stabilization of the system. Although the lateral equations are statically unstable, they are "more stable" than the longitudinal equations which have poles and zeros farther to the right in the right half s-plane (see Chapter 4-3). As a result, it is less tedious to design a controller for the lateral mode of the aircraft.

6-3 Controlled Variables and Aircraft Controls

For this research effort, the bank angle and the sideslip angle are selected as the controlled variables which are represented by the output vector $\underline{y}$. The rudder and flaperons are the aircraft control surfaces chosen for the control input vector $\underline{u}$.

An attempt to augment the aircraft state equations with actuator dynamics and then control lateral acceleration and roll rate was unsuccessful due to current limitations with the design method.

6-4 Controllability, Observability, and Transmission Zeros

The computer program "Zero" (7) is used to calculate the transmission, input decoupling, and output decoupling zeros of the state and output aircraft plant equations. With the lateral control system configured as described in

the previous section, the aircraft plant is completely controllable and observable; i.e., there are no input decoupling or output decoupling zeros, for all the flight conditions. In addition, the transmission zeros are located in the left half s-plane. For example, at the flight condition of 0.7 Mach at 15,000 feet the transmission zeros occur at -3.3431 and -3.3047 with a measurement matrix of:

$$M = \begin{bmatrix} 0.3 & 0 \\ 0 & 0.3 \end{bmatrix}$$

6-5 Measurement Matrix

A measurement matrix is required for the lateral control system because CB does not have full rank. As explained in Chapter 4-7, the measurement matrix introduces additional transmission zeros. They can be changed by altering the measurement matrix. Since the measurement matrix feeds back the derivatives of the states, the transient error between the control system input vector $\underline{v}$ and the output vector $\underline{y}$ is minimized by reducing the number of measurement matrix elements to the smallest number that provides a satisfactory response. Also, if the input vector is a constant value in the steady state, then the measurement matrix does not affect the steady state error since the derivatives of the states are equal to zero.

For the lateral control system configuration presented in this thesis, a measurement matrix with diagonal elements of 0.1 results in satisfactory performance of the control system only if the basic aircraft equations (without actuator dynamics and computational time delay) are included in the simulation. However, when actuator dynamics and/or computational time delay are added to the closed-loop simulation of control systems, it is necessary to increase the diagonal measurement matrix elements to a value of 0.3 to prevent unbounded oscillations in the output.

6-6 Control Input Magnitudes

In this thesis, the maximum magnitude and duration of the input command vector are adjusted to maintain aircraft movement within the linear region of the aircraft equations of motion. This makes anlaysis of the results easier and more realistic. For example, calculations are made to determine the turn rate generated as a function of the bank angle for a level coordinated turn at a constant airspeed. This calculation is independent of the aircraft and depends on the bank angle of the vehicle. This equation relating the airspeed and bank angle to the yaw rate is derived using the following relationships. First, the lateral g's generated by an aircraft in a level coordinated turn is equal to the tangent of the bank angle. Using this

relationship and the equation for centrifugal acceleration:

$$a = v^2/R \tag{6-6}$$

where

a = acceleration in feet/second^2

v = tangential velocity in feet per second

R = turn radius in feet

the circumference of a circle:

$$C = 2\pi R \tag{6-7}$$

where

C = circumference of circle in feet

R = turn radius of the aircraft in feet

and the constants

1 g = 32.2 feet/second^2

360 degrees in a circle

the following relationship is derived relating bank angle and velocity to yaw rate:

$$r = (360)(32.2) \tan \phi/2\pi v \tag{6-8}$$

where

r = yaw rate in degrees/second

ϕ = bank angle in degrees

v = tangential velocity in feet/second

As an example, for the flight condition of 0.7 Mach (740 feet/second) at 15,000 feet, a 15 degree bank results in a yaw rate of 0.668 degrees/second using the equation above. This agrees closely with the results of 0.652 obtained from the simulation on MULTI. The error increases with greater bank angle because the linear equations of motion approximate the tangent of the bank angle as equal to the bank angle in radians. This is a good approximation only for small angles.

For the beta pointing maneuver the sideslip angle is limited to 10 degrees due to nonlinearities in the drag.

6-7 Results

The introduction to this chapter describes the maneuvers and flight conditions used in the design of the lateral controllers for this research effort. The following sections present the results for the coordinated turn and the beta pointing maneuver for an aircraft with actuator dynamics and computational time delay added to the simulation for the flight condition of 0.7 Mach at 15,000 feet. Data and response plots for the remaining flight conditions are in Appendices G and H.

6-8 Coordinated Turn for 0.7 Mach at 15,000 Feet

The lateral state space matrices for this flight condition are tabulated in Table 6-1. The command vector $\underline{v}$,

TABLE 6-1

LATERAL STATE SPACE MATRICES

FLIGHT CONDITION: 0.7 Mach at 15000 Feet

A (Plant Matrix)

.0000E+00	.0000E+00	.1000E+01	.5710E-01
.4334E-01	-.2210E+00	.5710E-01	-.9984E+00
.0000E+00	-.1793E+02	-.2989E+01	.1090E+01
.0000E+00	.7836E+01	-.9651E-01	-.9504E-01

B (Control Input Matrix)

.0000E+00	.0000E+00
-.8361E-03	.9071E-03
.1493E+01	.2670E+00
.9608E-01	-.8655E-01

C (Output Matrix)

.1000E+01	.0000E+00	.0000E+00	.0000E+00
.0000E+00	.1000E+01	.0000E+00	.0000E+00

Notes

1. States (listed in order) are bank angle, sideslip angle, roll rate, and yaw rate.

2. Control inputs (listed in order) are flaperon and rudder.

3. Outputs (listed in order) are bank angle and sideslip angle.

design parameters, and controller matrices for this maneuver are presented in Table 6-2. Table 6-3 lists the figures of merit. The aircraft time response plots are presented in Figs. 6-1 through 6-4. Note that all angles are converted from radians to degrees before plotting.

In this maneuver the bank angle command is ramped in one second to a steady state value of 15 degrees (see Fig. 6-1). The aircraft response follows the input command very smoothly with a negligible overshoot of only 0.2 degrees. The sideslip angle is commanded to zero. The time response plot (see Fig. 6-2) shows no change in the sideslip angle. The figures of merit in Table 6-3 show that the sideslip angle actually peaks at 0.5 seconds to a very small -0.01 degrees during the transient portion of the maneuver (too small to see on the plot) before returning to zero in the steady state. Figure 6-3 shows a peak flaperon deflection of 0.8 degrees at approximately 0.5 seconds and a peak rudder deflection of 0.1 degrees at 0.9 seconds. The plots for the flaperon and rudder are relatively smooth and easily within the deflection and rate limits for both control surfaces. The roll and yaw rates shown in Fig. 6-4 are smooth and well controlled. The roll rate peaks at 15 degrees per second at 0.5 seconds before returning to zero. The yaw rate peaks at 0.7 degrees/second before settling at 0.652 degrees/second which is

TABLE 6-2

DESIGN PARAMETERS AND CONTROLLER MATRICES
FOR LATERAL CONTROLLERS

MANEUVER: Coordinated Turn

COMMAND VECTOR $\underline{y}$*: 1, 0.2618, 50, 50
0, 0, 0, 0

ALPHA: 1.0 EPSILON: 1.0 SIGMA**: 0.5, 0.5

MEASUREMENT MATRIX**: 0.3, 0.3

PLANT WITH ACTUATOR DYNAMICS AND
COMPUTATIONAL TIME DELAY

Flight Condition	$K_0 = K_1$	
0.4 Mach at Sea Level	.1779E+01	-.4041E+01
	-.5172E+00	.2705E+02
0.9 Mach at Sea Level	.5671E+00	-.1557E+01
	.1405E+00	.7334E+01
0.7 Mach at 15000 Feet	.1088E+01	-.2729E+01
	.1383E+00	.1561E+02
1.2 Mach at 15000 Feet	.1012E+01	-.2528E+01
	.1971E+01	.1247E+02
0.9 Mach at 50000 Feet	.4174E+01	-.1032E+02
	-.1387E+01	.4071E+02

Notes

*Each pulse entry in y has four parts:
1. The time in seconds the input reaches steady state;
2. Steady state value (angle in radians);
3. Time the input leaves steady state; and
4. Time input reaches zero.

**Diagonal element values of the matrix.

TABLE 6-3

LATERAL FIGURES OF MERIT

MANEUVER: Coordinated Turn

COMMAND VECTOR $\underline{y}^*$: 1, 0.2618, 50, 50
0, 0, 0, 0

PLANT WITH ACTUATOR DYNAMICS AND COMPUTATIONAL TIME DELAY

Flight Condition: 0.4 Mach at Sea Level

Output	Peak Value**	Peak Time	Settling Time
Bank Angle	15.2	2.1	1.5
Sideslip Angle	-0.01	0.5	***
Roll Rate	15.0	0.5	***
Yaw Rate	2.0	1.0	1.5

Flight Condition: 0.9 Mach at Sea Level

Output	Peak Value**	Peak Time	Settling Time
Bank Angle	16.08	2.3	3.9
Sideslip Angle	-.02	1.3	***
Roll Rate	15.0	1.0	***
Yaw Rate	1.0	1.0	1.8

Flight Condition: 0.7 Mach at 15000 Feet

Output	Peak Value**	Peak Time	Settling Time
Bank Angle	15.3	2.2	1.5
Sideslip Angle	-0.006	0.8	***
Roll Rate	15.0	0.5	***
Yaw Rate	0.7	1.1	1.5

TABLE 6-3--Continued

Flight Condition: 1.2 Mach at 15000 Feet

Output	Peak Value**	Peak Time	Settling Time
Bank Angle	15.9	2.3	3.7
Sideslip Angle	-0.04	1.4	***
Roll Rate	15.1	1.0	***
Yaw Rate	1.0	1.1	1.9

Flight Condition: 0.9 Mach at 50000 Feet

Output	Peak Value**	Peak Time	Settling Time
Bank Angle	15.08	2.2	1.9
Sideslip Angle	.02	0.7	***
Roll Rate	17.0	0.5	***
Yaw Rate	1.9	0.4	1.8

Notes

1. Figures of merit for the roll rate and the yaw rate are estimated for the response plots.

2. Bank angle and sideslip angle are components of the output vector $\underline{y}$.

*Commanded inputs in order are:
(1) bank angle in radians; and
(2) side slip angle in radians.

**Angles are converted from radians to degrees prior to calculating the figures of merit.

***Final value of the output is zero. Settling time is undefined using the definition of 2 percent of final value.

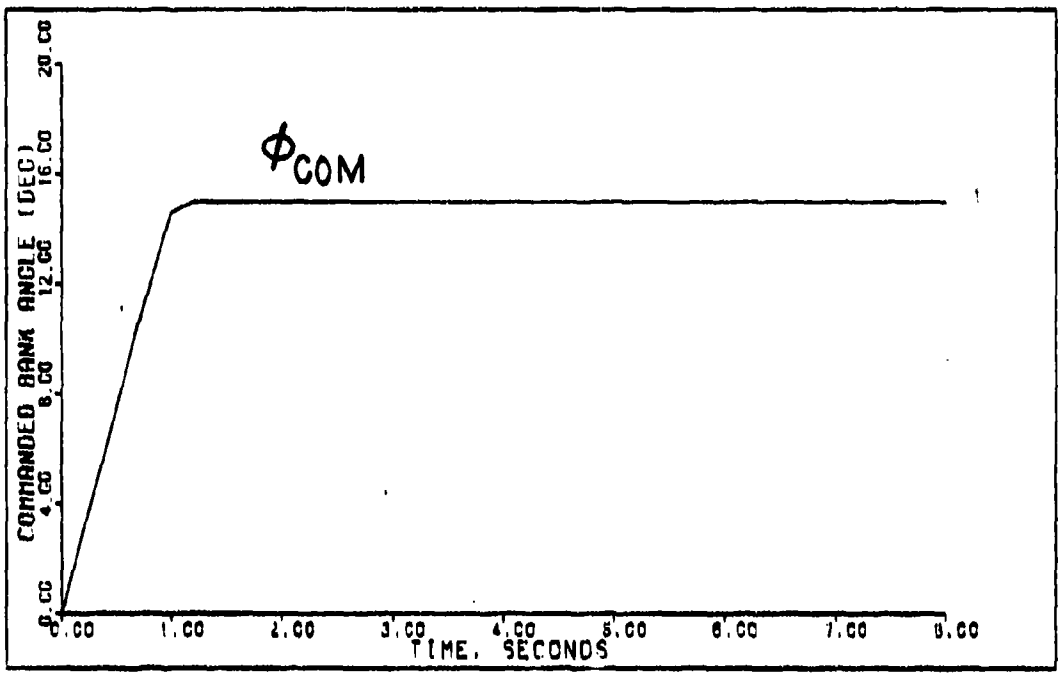

COORDINATED TURN (0./M 15K FT) DELAY=0.025 SEC ACTUATORS

Figure 6-1

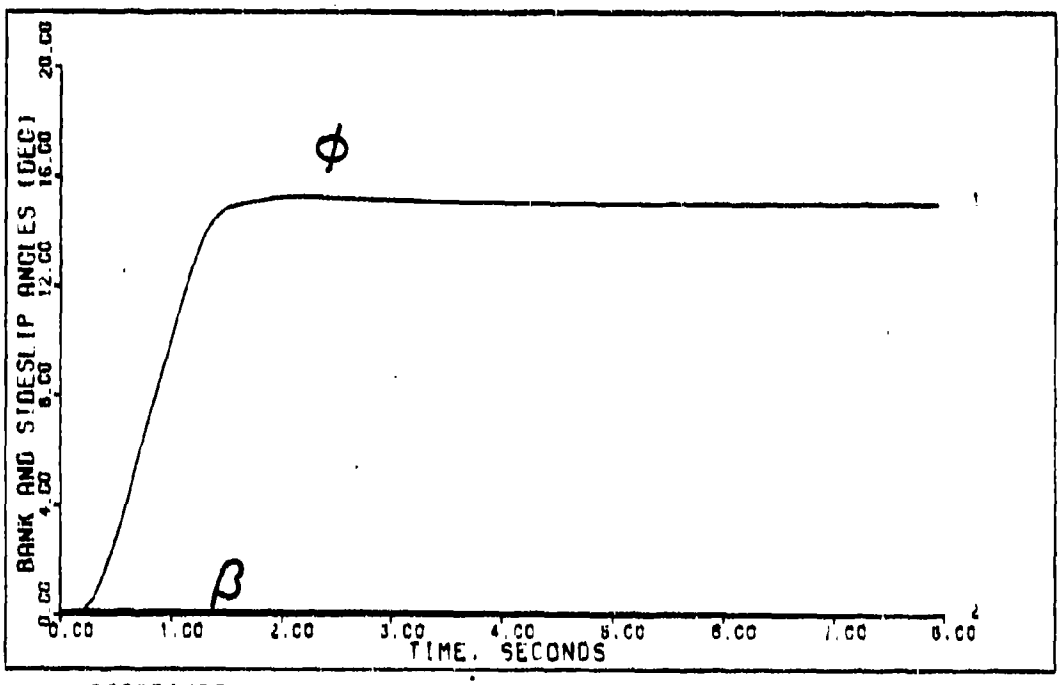

COORDINATED TURN (0./M 15K FT) DELAY=0.025 SEC ACTUATORS

Figure 6-2

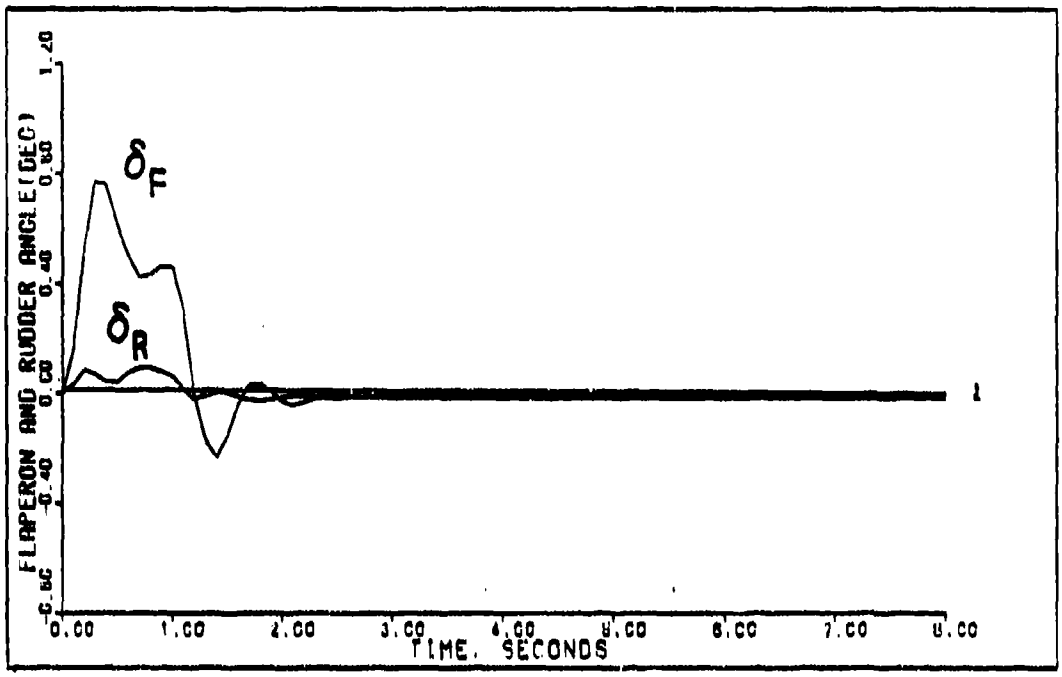

COORDINATED TURN (0.7M 15K FT) DELAY=0.025 SEC ACTUATORS

Figure 6-3

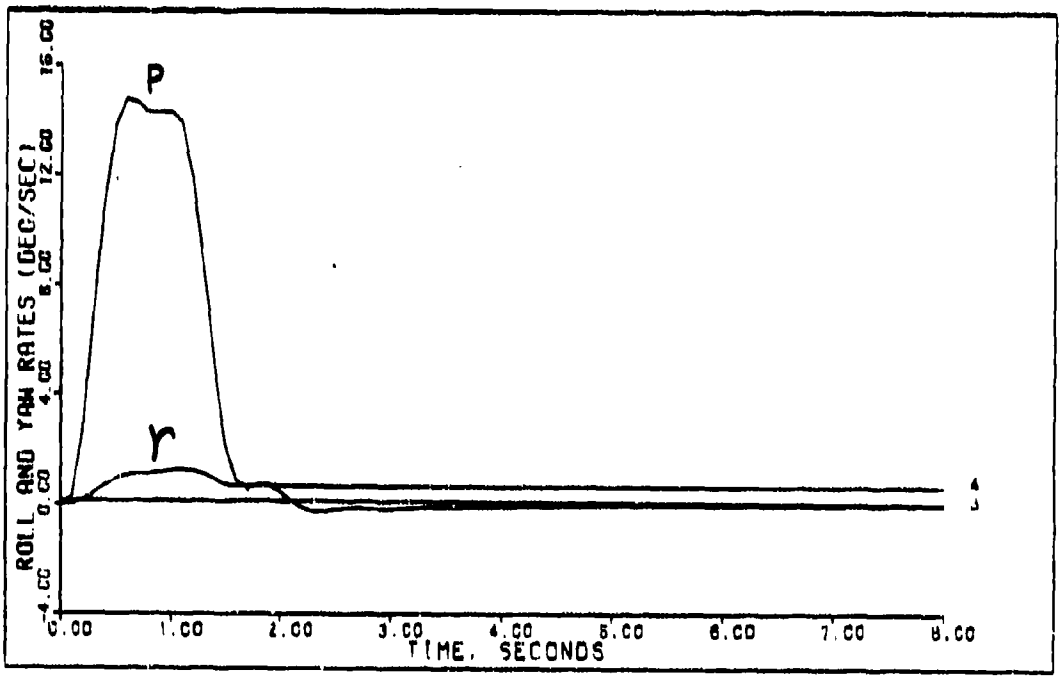

COORDINATED TURN (0.7M 15K FT) DELAY=0.025 SEC ACTUATORS

Figure 6-4

very close to the computed value of 0.668 degrees/second as discussed in Chapter 6-6.

Analysis of the time histories for the other flight conditions also show good aircraft responses. The data is presented in Appendices G and H.

6-9 Beta Pointing Maneuver for 0.7 Mach at 15,000 Feet

The aircraft lateral equations of motion are tabulated in Table 6-1. The command vector $\underline{v}$, design parameters, and controller matrices for this maneuver are presented in Table 6-4. The figures of merit are listed in Table 6-5.

The object of this maneuver is to sideslip the aircraft while maintaining a wings level flight attitude. The sideslip angle is the angle formed between the velocity vector and the nose of the aircraft. Pilots often use the maneuver during crosswind landings. The aircraft is sideslipped into the wind to maintain the desired ground track while simultaneously keeping the nose of the aircraft pointed toward the runway, the fuselage of the aircraft parallel to the centerline, and the wings in level flight. Beta pointing is also helpful for making minor corrections during formation and air refueling and is used in certain combat maneuvers and tracking tasks.

In this maneuver, a ramp-to-hold input signal commands the sideslip angle to 10 degrees (see Fig. 6-5). In addition, the bank angle is commanded to zero.

TABLE 6-4

DESIGN PARAMETERS AND CONTROLLER MATRICES
FOR LATERAL CONTROLLERS

MANEUVER: Beta Pointing

COMMAND VECTOR $\underline{v}$*: 0, 0, 0, 0
1, 0.17453, 50, 50

ALPHA: 1.0 EPSILON: 1.0

MEASUREMENT MATRIX: 0.3, 0.3

PLANT WITH ACTUATOR DYNAMICS AND
COMPUTATIONAL TIME DELAY

Flight Condition	Sigma**	$K_0 = K_1$	
0.4 Mach at Sea Level	0.1, 1.5	.3557E+00	-.1212E+02
		-.1034E+00	.8116E+02
0.9 Mach at Sea Level	1.0, 2.4	.1134E+01	-.7473E+01
		.2809E+00	.3520E+02
0.7 Mach at 15000 Feet	0.4, 1.5	.8704E+00	-.8187E+01
		.1106E+00	.4682E+02
1.2 Mach at 15000 Feet	1.0, 2.4	.2023E+01	-.1213E+02
		.3942E+01	.5983E+02
0.9 Mach at 50000 Feet	1,0, 2.4	.8349E+01	-.4954E+02
		-.2775E+01	.1954E+03

Notes

*Each pulse entry in $\underline{v}$ has four parts:
1. The time in seconds the input reaches steady state;
2. Steady state value (angle in radians);
3. Time the input leaves steady state; and
4. Time input reaches zero.

**Diagonal element values of the matrix.

TABLE 6-5

LATERAL FIGURES OF MERIT

MANEUVER: Beta Pointing

COMMAND VECTOR $\underline{y}^*$: 0, 0, 0, 0
1, 0.17453, 50, 50

PLANT WITH ACTUATOR DYNAMICS AND COMPUTATIONAL TIME DELAY

Flight Condition: 0.4 Mach at Sea Level

Output	Peak Value**	Peak Time	Settling Time
Bank Angle	-7.9	1.7	***
Sideslip Angle	10.0	10.0	2.5
Roll Rate	-9.5	1.2	***
Yaw Rate	-10.5	1.0	2.0

Flight Condition: 0.9 Mach at Sea Level

Output	Peak Value**	Peak Time	Settling Time
Bank Angle	-4.5	1.4	***
Sideslip Angle	10.0	10.0	3.3
Roll Rate	-5.0	1.2	***
Yaw Rate	-11.0	1.0	2.0

Flight Condition: 0.7 Mach at 15000 Feet

Output	Peak Value**	Peak Time	Settling Time
Bank Angle	-3.45	1.3	***
Sideslip Angle	10.0	10.0	2.8
Roll Rate	-4.5	0.5	***
Yaw Rate	-10.0	0.9	2.1

TABLE 6-5--Continued

Flight Condition: 1.2 Mach at 15000 Feet

Output	Peak Value**	Peak Time	Settling Time
Bank Angle	-6.6	1.4	***
Sideslip Angle	10.0	10.0	3.3
Roll Rate	-7.5	1.2	***
Yaw Rate	-11.0	1.1	2.0

Flight Condition: 0.9 Mach at 50000 Feet

Output	Peak Value**	Peak Time	Settling Time
Bank Angle	-0.7	1.0	***
Sideslip Angle	10.0	10.0	2.1
Roll Rate	-4.0	0.5	***
Yaw Rate	-10.0	0.9	2.1

Notes

1. Figures of merit for the roll rate and the yaw rate are estimated for the response plots.

2. Bank angle and sideslip angle are components of the output vector $\underline{y}$.

*Commanded inputs in order are:
(1) bank angle in radians; and
(2) side slip angle in radians.

**Angles are converted from radians to degrees prior to calculating the figures of merit.

***Final value of the output is zero. Settling time is undefined using the definition of 2 percent of final value.

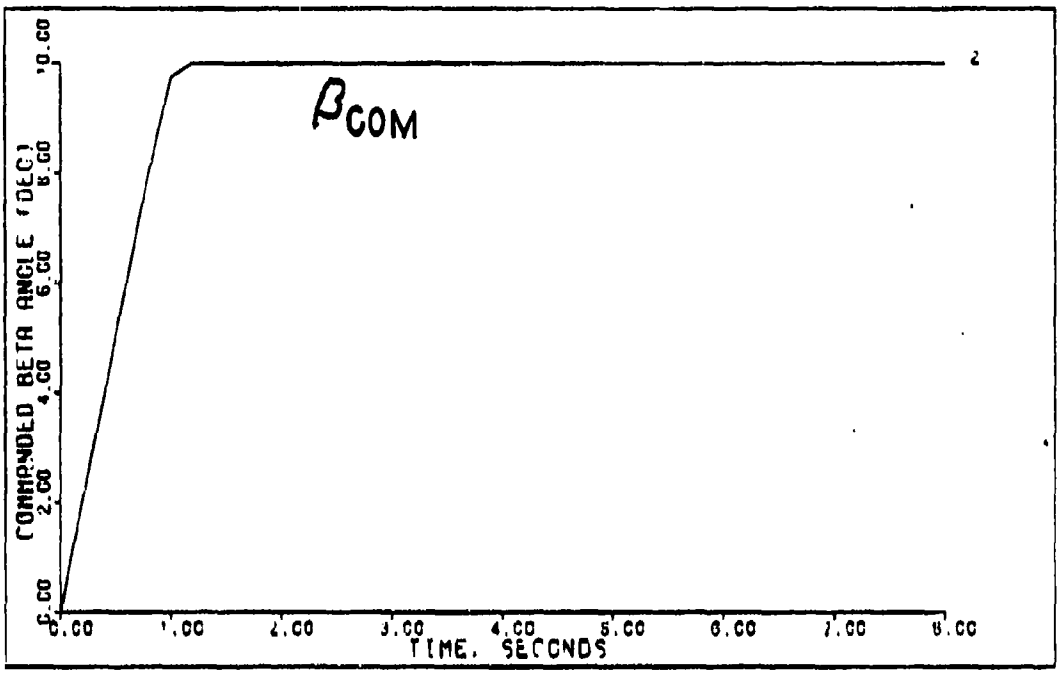

BETA POINTING (0./M 15K FT) DELAY=0.025 SEC ACTUATORS.

Figure 6-5

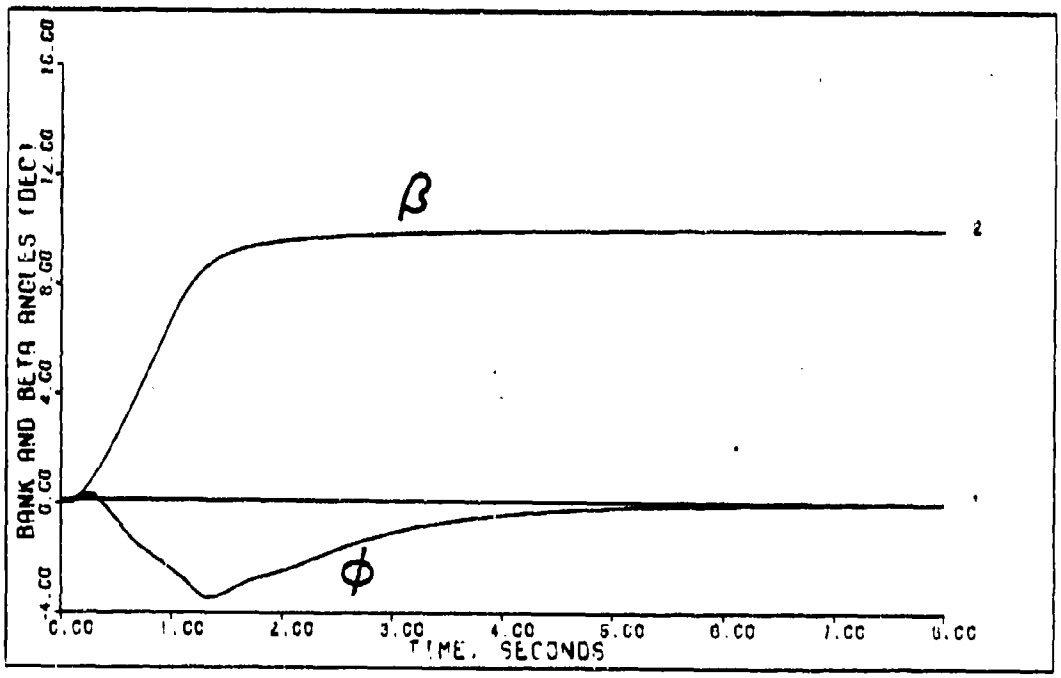

BETA POINTING (0./M 15K FT) DELAY=0.025 SEC ACTUATORS

Figure 6-6

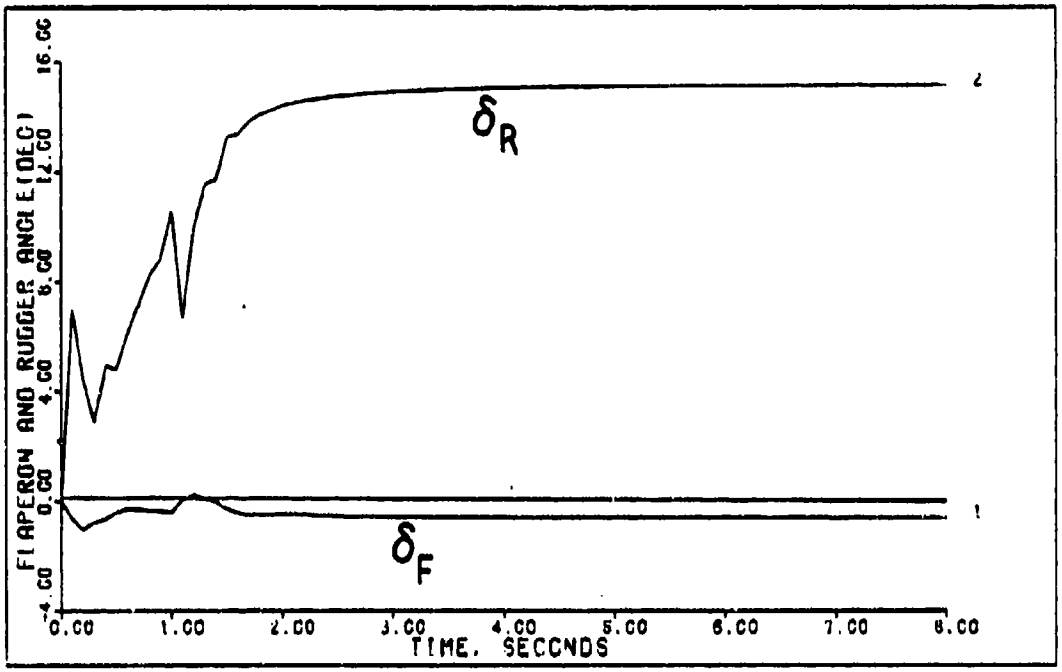

BETA POINTING (0.7M 15K FT) DELAY=0.025 SEC ACTUATORS

Figure 6-7

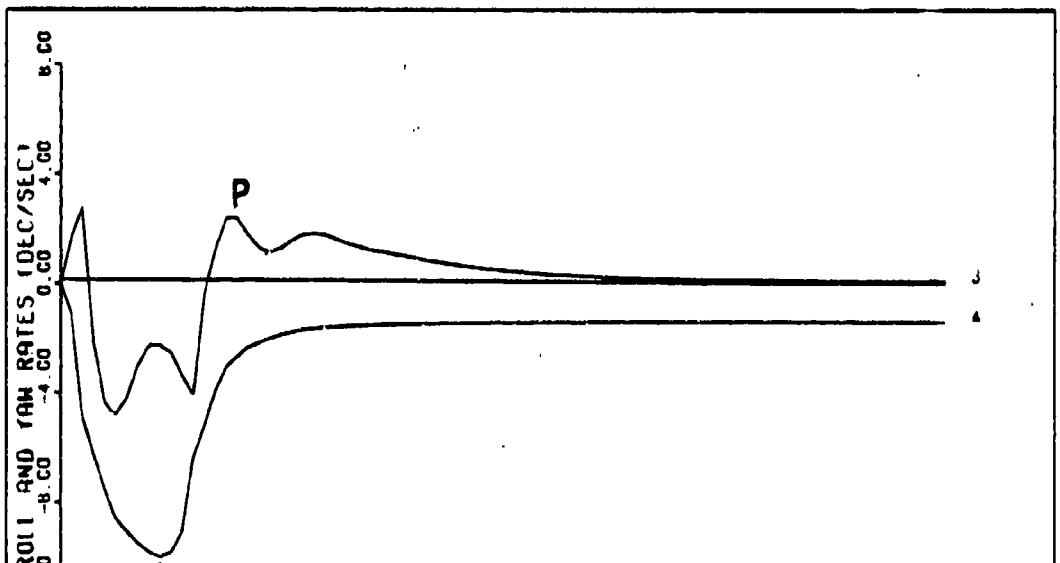

BETA POINTING (0.7M 15K FT) DELAY=0.025 SEC ACTUATORS

Figure 6-8

Figure 6-6 shows the aircraft smoothly follows the commanded beta angle without an overshoot. As expected, the rudder deflection required to establish the sideslip angle causes a negative moment about the x axis. This causes the bank angle to momentarily change during the transient response until corrective aileron is applied by the control system. For this flight condition, the bank angle peaks at -3.45 degrees (see Table 6-5) before returning to a steady state value of zero. When the bank angle feedback element in the sigma matrix is increased to reduce the maximum bank angle, the wings begin to rock in an attempt to maintain a zero bank angle. Pilots often perform the beta pointing maneuver with manual inputs to the aileron and rudder in conventional aircraft and expect the bank angle to change momentarily during the transient portion of the maneuver. Therefore, it is preferred to accept a slightly larger error during the transient as long as it is non-oscillatory. When the wings rock or flutter at relatively high frequencies, pilots may falsely perceive that the aircraft is unstable and uncontrollable which is not desirable.

Figure 6-7 shows the time history of the rudder and flaperon deflection angles. Although the plots are not as smooth as those for the coordinated turn, the rudder is still operating within the rate limit of 141 degrees per second. The resulting roll and yaw rates are well controlled as shown in Fig. 6-8.

Analysis of the plots for this maneuver at the other four flight conditions shows good aircraft responses. The data is presented in Appendices G and H.

6-10 Summary

This chapter begins with a description of the design procedure used to obtain the lateral control laws. Emphasis is placed on an analysis of the aircraft open-loop transfer functions including the location of the zeros and poles and the controllability and observability of the system. Also discussed is the effect of the measurement matrix on the transmission zeros and the transient response. Then the data for the coordinated turn and beta pointing maneuvers are presented for the flight condition of 0.7 Mach at 15,000 feet. The chapter concludes with a brief description of the maneuvers and an analysis of the time history plots.

7. Conclusions and Recommendations

7-1 Comments on the Results

The major objective of this thesis is accomplished with the successful design of flight control laws for the statically unstable longitudinal and lateral modes on the X-29 aircraft. The control laws are implemented with controller matrices that have configurations and gains determined by applying the multivariable control theory of Professor Brian Porter.

Very good results are obtained with and without actuator dynamics and computational delay added to the system. The time responses are smooth and well controlled and meet established requirements such as control surface deflection and rate limits. The designs are not optimum in every sense, but the Porter technique provides a relatively straightforward and quick procedure for developing the control laws. The method has many advantages over other multivariable design techniques from a practical application point of view. These advantages are listed as follows:

1. Analog and digital designs are developed using essentially the same design procedure.

2. The method uses output feedback without requiring full state information.

3. A high degree of decoupling between the outputs is easily obtainable.

4. Computer assisted software provides the capability to iteratively fine tune the design to obtain the best possible responses.

Although there are many advantages to the Porter method, this research effort encounters some limitations which must be overcome to make this technique a truly superior way to solve actual aircraft flight control problems. These limitations are discussed in the next section.

7-2 Improving the Design Process

Refinement and expansion of Porter's control law theory is desirable to overcome some problems that are encountered in this research effort when applying the Porter method in a practical way to an aircraft with serious flight control problems.

First, theory should be developed to determine a method of selecting initial sigma weighting matrices for a non-minimum phase plant that will result in a stable response. Currently, trial and error is the only method available, which proves to be very time consuming and not always successful.

Another limitation occurs when actuator dynamics are implemented into the state equations of the aircraft plant. Then a measurement matrix becomes necessary and

derivatives of the states must be fed back. This is often undesirable. For example, in this research effort the measurement matrix generates additional transmission zeros which are in the right half s-plane and the result is an inability to achieve a stable design. See Appendix I for additional details. Until theory can be expanded to permit a feedforward D matrix, acceleration cannot be assigned as an output variable without implementing actuators into the state matrix.

Third, the Porter method can be more useful in practical application if some of the inputs can float for certain maneuvers. Currently, a Porter "configured" flight control system requires every input to have a specific command irrespective of the maneuver. Thus, for some maneuvers, nonessential inputs require precomputation or the output C matrix must be changed.

Finally, the theory needs expanding so weighting can be assigned to control surfaces prior to calculating the control matrices. This will eliminate overdriving less effective control surfaces when other control surfaces still have unused control power remaining.

7-3 MULTI Improvements

Recommendations to the MULTI program are based on its extensive use during this research effort.

Ultimately the MULTI program should be rewritten using structured programming techniques along with adequate documentation.

The ZERO program, which calculates the input decoupling, output decoupling, and transmission zeros, should be added to the MULTI program. This will save time and eliminate duplicate entries of system matrices into each program.

An option should be added to MULTI to provide the capability to plot aircraft control input rates on the terminal screen and Calcomp plotter. Also, control input rate limiting needs to be added to the simulation.

Option 28 needs expansion so figures of merit can be calculated not only for the outputs but also for the states, any combination of states, and the control inputs.

7-4 Proposed Future Work

In general, it is highly desirable to control rates and accelerations as opposed to angles which are often difficult to measure. Angle information is generally provided by inertial navigation systems which have lower hardware reliability than the flight control system. Also pilots control rates in conventional aircraft and feel accelerations.

Therefore, future work on the X-29 should concentrate on controlling rates and accelerations. Rates as output variables generally cause transmission zeros to

occur at the origin which usually makes stabilizaiton of the system more tedious but not impossible.

An unsuccessful attempt to control acceleration in this research effort results from the inability to find a stable design when actuators are implemented in the state equations. Future research efforts should attempt to overcome this problem by finding an easy way to implement a D matrix into the design procedure.

Limiting the bandwidth of the control system reduces susceptibility to noise and other objectionable high frequency disturbances. Therefore, it is desirable to investigate the loop transmission frequency of the final control system design.

Appendix A: Multivariable Control Theory

(Reproduced from Reference 4)

This thesis utilizes the multivariable design method of Professor Brian Porter of the University of Salford, England (10). The design method uses output feedback with high-gain error-actuated controllers. Output feedback is advantagous since state variables may be difficult to measure while system response data are more readily available.

System State Equations

Porter's method works equally well for either continuous or discrete systems, but it is often easier to first examine a system in the continous time domain. This is because designs can be more easily visualized in the s-plane than in the z-plane. A continuous time system is represented by the state space model:

$$\dot{\underline{x}} = \underline{A}\underline{x} + \underline{B}\underline{u}$$
$$\underline{y} = \underline{C}\underline{x} \qquad \text{(A-1)}$$

where

$\underline{A}$ = continuous plant matrix (n x n)

$\underline{B}$ = continuous input control matrix (n x m)

$\underline{C}$ = continuous output matrix (ℓ x n)

$\underline{x}$ = state variable vector with n states

$\underline{u}$ = input vector with m inputs

$\underline{y}$ = output vector with ℓ outputs

The system inputs for an aircraft are the control surface deflections or actuator input commands, and the system outputs are aircraft responses affected by the inputs.

The method does not allow for a feedforward, $\underline{D}$, matrix. If such a matrix is present in the original state space model, the control inputs must be redefined as states so that the $\underline{D}$ matrix is absorbed into the $\underline{C}$ matrix. This can be accomplished by incorporating the actuator dynamics into the plant model. Actuator inputs then become control inputs.

To employ Porter's method, it is desirable (but not necessary) to partition the system state equations as follows:

$$\begin{bmatrix} \dot{\underline{x}}_1 \\ \hline \dot{\underline{x}}_2 \end{bmatrix} = \left[\begin{array}{c|c} \underline{A}_{11} & \underline{A}_{12} \\ \hline \underline{A}_{21} & \underline{A}_{22} \end{array}\right] \begin{bmatrix} \underline{x}_1 \\ \hline \underline{x}_2 \end{bmatrix} + \begin{bmatrix} \underline{B}_1 \\ \hline \underline{B}_2 \end{bmatrix} \underline{u}$$

$$\underline{y} = \begin{bmatrix} \underline{C}_1 & | & \underline{C}_2 \end{bmatrix} \begin{bmatrix} \underline{x}_1 \\ \hline \underline{x}_2 \end{bmatrix} \qquad \text{(A-2)}$$

The equations are partitioned so that $\underline{B}_2$ and $\underline{C}_2$ are square ($m \times m$) and ($\ell \times \ell$) matrices, respectively. The method requires that the number of inputs to the system equals the number of outputs which means $m = \ell$, and therefore the dimension of $\underline{B}_2$ equals the dimension of $\underline{C}_2$. It is often possible to form the state equations so that $\underline{B}_1 = \underline{0}$.

For the discrete case the system equations are written as follows:

$$\underline{x}[(k+1)T] = \underline{\Phi x}(kT) + \underline{\Psi u}(kT)$$
$$\underline{y}(kT) = \underline{\Gamma x}(kT) \qquad \text{(A-3)}$$

where

$\underline{\Phi} = \exp(\underline{A}T)$ = discrete plant matrix

$\underline{\Psi} = \int_0^T \exp(\underline{A}T)\underline{B}dt$ = discrete input control matrix

$\underline{\Gamma} = \underline{C}$ = discrete output matrix

In the above equations T is the sampling period, and k takes on integer values from zero to plus infinity.

System With Output Feedback

Figure A-1 shows the block diagram for a continuous output feedback system, where $\underline{v}$ is the command input vector, and $\underline{y}$ is the desired output vector. The blocks for the plant are derived directly from the system state equations, Equation (A-1). The proportional plus integral controller has three parameters, $\underline{K}_0$, $\underline{K}_1$, and g, which must be determined by the designer. The output signal of the controller, $\underline{u}$, is given in the following control law equation:

$$\underline{u} = g(\underline{K}_0\underline{e} + \underline{K}_1\int\underline{e}dt) \qquad \text{(A-4)}$$

where

$\underline{u}$ is the output signal of the controller

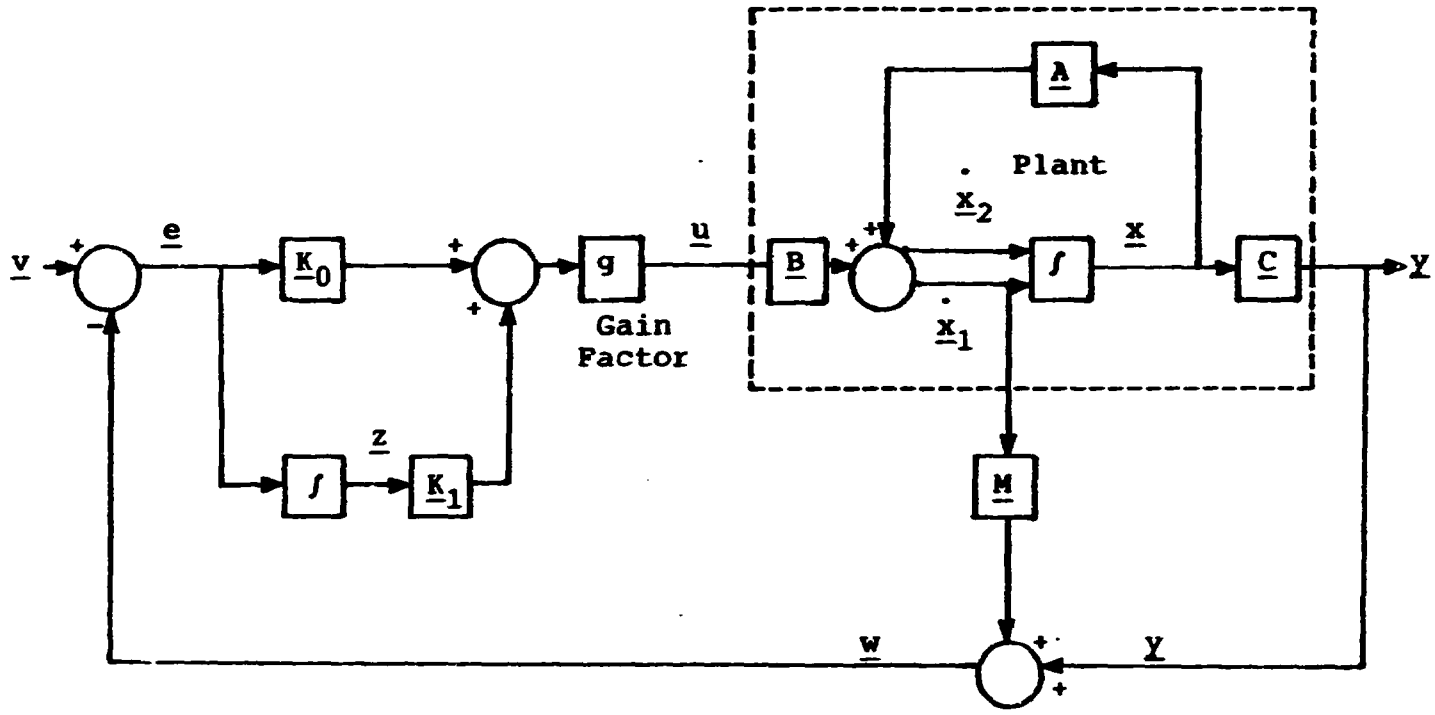

Figure A-1. System block Diagram -- Continuous Case

$\underline{e}$ is the error signal at the input of the controller

$\underline{K}_0$ is the proportional gain matrix

$\underline{K}_1$ is the gain matrix for the integral term

g is the scalar forward path gain

A measurement matrix $\underline{M}$ is included in the system if the plant is irregular. Regular and irregular plants are discussed later.

The discrete system block diagram, shown in Figure A-2, is similar to the continuous system, but Equation (A-4) becomes

$$\underline{u}(kT) = (1/T)[\underline{K}_0\underline{e}(kT) + \underline{K}_1\underline{z}(kT)] \qquad (A-5)$$

where the forward path gain g equals the sampling frequency, (1/T). The $\underline{z}(kT)$ matrix is derived from the backward difference equation,

$$\underline{z}[(k+1)T] = \underline{z}(kT) + T\underline{e}(kT) \qquad (A-6)$$

The steps to be taken next in the design method depend on whether or not $[\underline{CB}]$ has full rank, i.e., does it have an inverse. If the matrix $[\underline{CB}]$ has full rank, the plant is called "regular" and no measurement matrix $\underline{M}$ is needed. However, if $[\underline{CB}]$ does not have full rank, the plant is called "irregular" and $\underline{M}$ is needed to form a new matrix $[\underline{FB}]$ (see Equations (A-12) through (A-14)) which does have an inverse. This is explained in more detail in the next sections. When the partitioned $\underline{B}$ matrix in Equation (A-2)

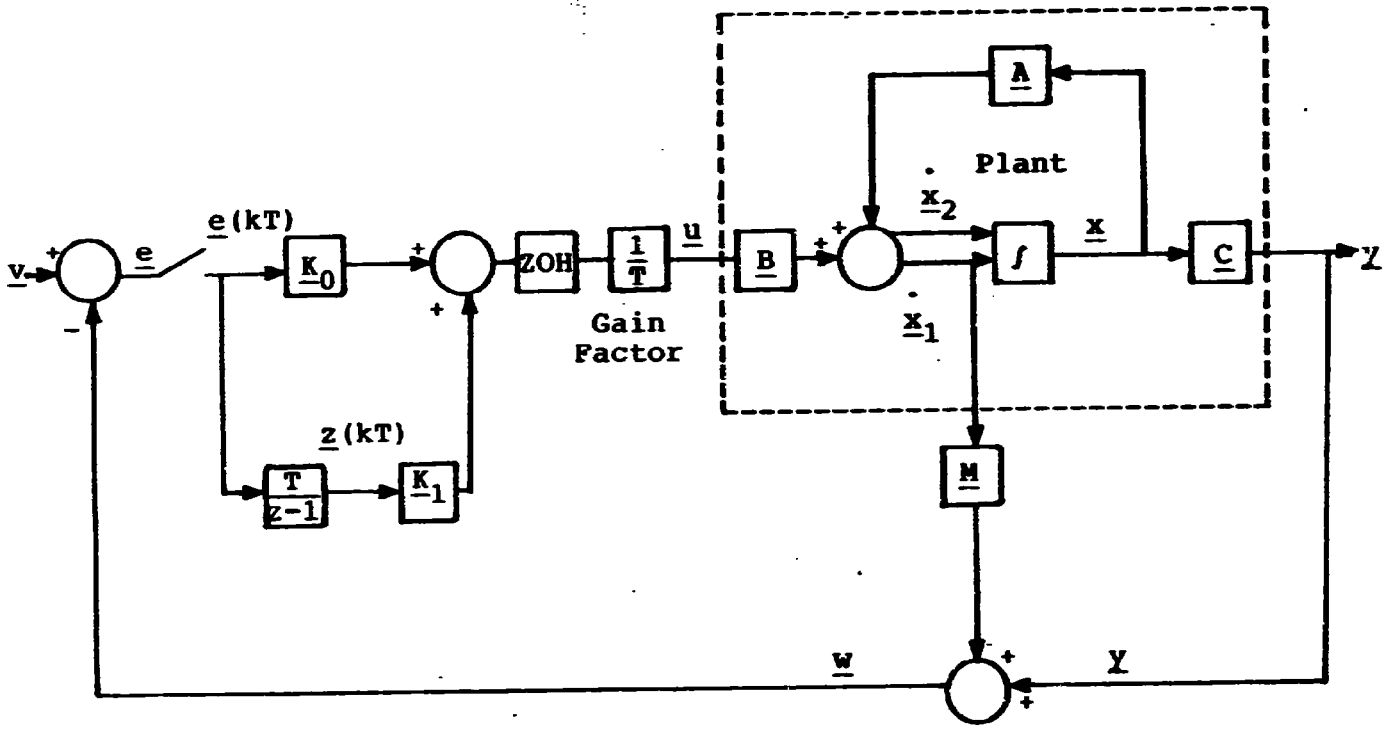

Figure A-2. System Block Diagram -- Discrete Case

has the form

$$\begin{bmatrix} \underline{0} \\ \hline \underline{B}_2 \end{bmatrix} \tag{A-7}$$

then

$$[\underline{CB}] = [\underline{C}_2\underline{B}_2] \tag{A-8}$$

$$[\underline{FB}] = [\underline{F}_2\underline{B}_2] \tag{A-9}$$

Regular Plant

For the system to be classified as "regular" the first Markov parameter $[\underline{CB}]$ must have full rank. If this is true the gain matricies can be found from

$$\underline{K}_0 = [\underline{CB}]^{-1}\underline{\Sigma} \tag{A-10}$$

and

$$\underline{K}_1 = \bar{\alpha}[\underline{CB}]^{-1}\underline{\Sigma} \tag{A-11}$$

where

$\bar{\alpha}$ is a constant which assigns the ratio of proportional to integral control

$\underline{\Sigma}$ is the diagonal weighting matrix

The diagonal weighting matrix, $\underline{\Sigma} = \text{diag}\ \{\sigma_1, \sigma_2, \ldots, \sigma_\ell\}$, is specified by the designer. Each σ_i $(i = 1,\ldots,\ell)$ determines the weighting of the effect of a particular error signal on each control input.

Irregular Plant

If the first Markov parameter [$\underline{CB}$] is rank deficient, then the plant is called "irregular". In this case, the $\underline{C}$ matrix must be replaced by

$$\underline{F} = [\underline{F}_1 \mid \underline{F}_2] \tag{A-12}$$

where

$$\underline{F}_1 = [\underline{C}_1 + \underline{MA}_{11}] \tag{A-13}$$

$$\underline{F}_2 = [\underline{C}_2 + \underline{MA}_{12}] \tag{A-14}$$

The matrix $\underline{M}$ in the above equations is a measurement matrix which is chosen such that the matrix [$\underline{FB}$] has full rank. The designer chooses the measurement matrix so that it is as sparse as possible, thus the smallest number of additional measurements are required. Reference 13 gives an approach for selecting the measurement matrix to achieve optimal decoupling. Once $\underline{M}$ is formed, $\underline{K}_0$ and $\underline{K}_1$ are computed by

$$\underline{K}_0 = [\underline{FB}]^{-1}\underline{\Sigma} \tag{A-15}$$

$$\underline{K}_1 = \bar{\alpha}[\underline{FB}]^{-1}\underline{\Sigma} \tag{A-16}$$

which are similar to Equations (A-10) and (A-11).

For irregular plants the error vector $\underline{e}$ is defined as

$$\underline{e} = \underline{v} - \underline{w} \tag{A-17}$$

where

$$\underline{w} = \underline{y} + \underline{M}\dot{\underline{x}}_1 \qquad \text{(A-18)}$$

For step inputs the values of the rates, $\dot{\underline{x}}_1$, become zero in the steady state because they represent kinematic variables.

Asymptotic Characteristics

As the gain factor of the system, g (or 1/T for the discrete case), approaches infinity, the system transfer function matrix G(s) assumes the asymptotic form

$$\underline{\Gamma}(\lambda) = \tilde{\underline{\Gamma}}(\lambda) + \hat{\underline{\Gamma}}(\lambda) \qquad \text{(A-19)}$$

where

$\tilde{\underline{\Gamma}}(\lambda)$ is the slow transfer function matrix

$\hat{\underline{\Gamma}}(\lambda)$ is the fast transfer function matrix

The roots of the asymptotic closed-loop transfer function may be grouped into three sets: $\underline{Z}_1$, $\underline{Z}_2$, and $\underline{Z}_3$. Table A-1 gives the equations for finding these asymptotic roots. Sets $\underline{Z}_1$ and $\underline{Z}_2$ correspond to the slow modes of the system, where the modes associated with the roots in $\underline{Z}_1$ become uncontrollable, and, for regular plants, the modes associated with the roots in $\underline{Z}_2$ become unobservable as the gain increases. Set $\underline{Z}_3$, the infinite roots, are associated with the fast modes of the system which become dominant as the gain increases.

The roots in set $\underline{Z}_2$ correspond to the transmission zeros of the system which are not altered by output feedback. Since infinite gain cannot be implemented, and is not

Table A-1

Asymptotic Equations for Zero-$\underline{B}_2$ Form

System represented by:

$$\begin{bmatrix} \dot{\underline{x}}_1 \\ \hline \dot{\underline{x}}_2 \end{bmatrix} = \left[\begin{array}{c|c} \hat{\underline{A}}_{11} & \hat{\underline{A}}_{12} \\ \hline \hat{\underline{A}}_{21} & \hat{\underline{A}}_{22} \end{array}\right] \begin{bmatrix} \underline{x}_1 \\ \hline \underline{x}_2 \end{bmatrix} + \begin{bmatrix} \underline{0} \\ \hline \hat{\underline{B}}_2 \end{bmatrix} \underline{u} \qquad \text{and} \qquad \underline{y} = \left[\hat{\underline{C}}_1 \mid \hat{\underline{C}}_2\right] \begin{bmatrix} \underline{x}_1 \\ \hline \underline{x}_2 \end{bmatrix}$$

	Continuous Case (s-plane)	Discrete Case (z-plane)
	Gain Factor = q	Gain Factor = $1/T$
	$\underline{\Gamma}(\lambda) = \underline{C}_0(\lambda \underline{I}_n - \underline{A}_0)^{-1}\underline{B}_0$	$\underline{\Gamma}(\lambda) = \underline{C}_0(\lambda \underline{I}_n - \underline{A}_0)^{-1}\underline{B}_0$
	$\hat{\underline{\Gamma}}(\lambda) = (\lambda \underline{I}_m + q\hat{\underline{C}}_2\hat{\underline{B}}_2\underline{K}_0)^{-1} q\hat{\underline{C}}_2\hat{\underline{B}}_2\underline{K}_0$	$\hat{\underline{\Gamma}}(\lambda) = (\lambda \underline{I}_m - \underline{I}_m + \hat{\underline{C}}_2\hat{\underline{B}}_2\underline{K}_0)^{-1}\hat{\underline{C}}_2\hat{\underline{B}}_2\underline{K}_0$
Finite Roots		
$\underline{z}_1$	$\{\lvert \lambda \underline{K}_0 + \underline{K}_1 \rvert = \underline{0}\}$	$\{\lvert \lambda \underline{I}_m - \underline{I}_m + T\underline{K}_0^{-1}\underline{K}_1 \rvert = \underline{0}\}$
$\underline{z}_2$	$\{\lvert \lambda \underline{I}_{n-m} - \hat{\underline{A}}_{11} + \hat{\underline{A}}_{12}\hat{\underline{C}}_2^{-1}\hat{\underline{C}}_1 \rvert = \underline{0}\}$	$\{\lvert \lambda \underline{I}_{n-m} - T\hat{\underline{A}}_{11} + \hat{\underline{A}}_{12}\hat{\underline{C}}_2^{-1}\hat{\underline{C}}_1 \rvert = \underline{0}\}$
Infinite Roots		
$\underline{z}_3$	$\{\lvert \lambda \underline{I}_m + q\hat{\underline{C}}_2\hat{\underline{B}}_2\underline{K}_0 \rvert = \underline{0}\}$	$\{\lvert \lambda \underline{I}_m - \underline{I}_m + \hat{\underline{C}}_2\hat{\underline{B}}_2\underline{K}_0 \rvert = \underline{0}\}$

where

$$\underline{A}_0 = \left[\begin{array}{c|c} -\underline{K}_0^{-1}\underline{K}_1 & \underline{0} \\ \hline \hat{\underline{A}}_{12}\hat{\underline{C}}_2^{-1}\underline{K}_0^{-1}\underline{K}_1 & \hat{\underline{A}}_{11} - \hat{\underline{A}}_{12}\hat{\underline{C}}_2^{-1}\hat{\underline{C}}_1 \end{array}\right]$$

$$\underline{B}_0 = \begin{bmatrix} \underline{0} \\ \hline \hat{\underline{A}}_{12}\hat{\underline{C}}_2^{-1} \end{bmatrix}$$

Regular Design	Irregular Design
$\underline{C}_0 = \left[\underline{K}_0^{-1}\underline{K}_1 \mid \underline{0}\right]$	$\underline{C}_0 = \left[\hat{\underline{C}}_2\underline{F}_2^{-1}\underline{K}_0^{-1}\underline{K}_1 \mid \hat{\underline{C}}_1 - \hat{\underline{C}}_2\underline{F}_2^{-1}\underline{F}_1\right]$

desirable, the closed-loop roots of the system tend to migrate toward the transmission zeros. This may adversely affect the system stability if the location of these zeros is in the unstable region. Reference 12 gives a procedure for locating the transmission zeros of a system.

As the gain increases the system output responses become increasingly decoupled. The asymptotic closed-loop transfer function for the continuous case has the form

$$\underline{\Gamma}(\lambda) = \text{diag}\left\{\frac{g\sigma_1}{\lambda+g\sigma_1}, \frac{g\sigma_2}{\lambda+g\sigma_2}, \ldots, \frac{g\sigma_\ell}{\lambda+g\sigma_\ell}\right\} \qquad \text{(A-20)}$$

For the discrete case the form is

$$\underline{\Gamma}(\lambda) = \text{diag}\left\{\frac{\sigma_1}{\lambda-1+\sigma_1}, \frac{\sigma_2}{\lambda-1+\sigma_2}, \ldots, \frac{\sigma_\ell}{\lambda-1+\sigma_\ell}\right\} \qquad \text{(A-21)}$$

where the σ_i $(i = 1,\ldots,\ell)$ are determined by the weighting matrix, $\underline{\Sigma}$.

The computer program MULTI is of great value in reducing the time required to achieve a satisfactory design. The MULTI User's Manual (8) describes the program and its operation.

Appendix B: Forming G(0) and $G(0)^{-1}$ Matrices for Calculating Steady State Vectors

Introduction

This additional improvement to MULTI provides the capability to calculate the G(0) and $G(0)^{-1}$ matrices directly from A, B, and C matrices of the plant. Also, the user is given the option:

1. to enter the plant steady state output vector y and have MULTI automatically calculate the steady state input vector u using the G(0) inverse matrix;

2. to enter the plant steady state input vector u and have MULTI automatically calculate the steady state output vector y using the G(0) matrix.

User's Guide

First the A, B, and C matrices of the plant are entered into MULTI using Options 2 and 3 or 9. Then the user selects Option 6 and the following prompt appears:

```
FOR OPEN-LOOP TRANSFER FUNCTION ENTER 1 >
FOR CLOSED-LOOP TRANSFER FUNCTION ENTER 2 >
FOR G(0) AND G(0) INVERSE MATRICES ENTER 3 >
```

If 3 is entered, the matrices are computed and printed like the example which follows:

THE G(0) MATRIX IS:

```
-.3192E-01      .1453E-01      .8929E+00
 .8212E+02     -.3726E+02     -.1225E+03
-.1039E-01      .3564E-02      .1213E-01
```

THE G(0) INVERSE MATRIX IS:

```
 .1922E+01     -.3769E-01     -.3949E+03
-.3467E+01     -.1114E+00     -.8705E+03
 .1183E+01      .4658E-03      .4607E-01
```

Next the following prompt automatically appears:

```
TO USE THE G(0) INVERSE MATRIX OR G(0) MATRIX
TO CALCULATE THE STEADY STATE VALUE OF THE:

PLANT INPUT VECTOR U            ENTER >1
PLANT OUTPUT VECTOR Y           ENTER >2
TERMINATE CALCULATIONS          ENTER >3
```

If 1 is entered the following prompt appears:

```
ENTER THE "N" ELEMENTS OF THE
PLANT OUTPUT VECTOR Y:
```

For example, enter 1,1,1 and the following appears:

```
THE PLANT OUTPUT VECTOR Y
JUST ENTERED IS:

1.
1.
1.

THE PLANT INPUT VECTOR

U = G(0) INVERSE * Y IS

-394.71625
-874.03421
1.22980556
```

then the following prompt automatically reappears and the process is repeated until the calculations are terminated by entering 3:

```
TO USE THE G(0) INVERSE MATRIX OR G(0) MATRIX
TO CALCULATE THE STEADY STATE VALUE OF THE:

PLANT INPUT VECTOR U          ENTER  1
PLANT OUTPUT VECTOR Y         ENTER  2
TERMINATE CALCULATIONS        ENTER  3
```

Programmer's Guide

The following FORTRAN 77 code is added to the MULTI Option 6 Overlay. Comments explain each portion of the program.

```
        PRINT$, 'FOR G(0) AND G(0) INVERSE MATRICES ENTER 3 > '
      READ$, TFTYPE
C$$$$$$$$$$$$$$$$$$$$$$$$$$$$$$$$$$$$$$$$$$$$$$$$$$$$$$$$$$$$$$$$$$$$$$$$$$$
C$$$$$$$$$$THIS SECTION CALCULATES THE G(0) AND G(0) INVERSE MATRICES$$$$$$$
      IF(TFTYPE.EQ.3) THEN
      DO 162 I=1,20
         BT(I)=0.
         CT(I)=0.
 162  CONTINUE
C$$$$$$FOLLOWING SETS DUMMY VARIABLE L=N (DIMENSION OF MATRIX A)$$$$$$$$$$
      L=N
C$$$$$$FOLLOWING COPIES MATRIX A TO DUMMY MATRIX VARIABLE ACL$$$$$$$$$$$$$$
      DO 164 I=1,N
         DO 163 J=1,N
              ACL(I,J)=A(I,J)
 163     CONTINUE
 164  CONTINUE
C$$$$$$FOLLOWING CALCULATES DENOMINATOR POLYNOMIAL OF C$[SI-A] INVERSE $ B
      CALL PHOFB (ACL,L,L,DET)
C$$$$$$FOLLOWING CALCULATES NUMERATOR POLYNOMIAL OF C$[SI-A] INVERSE $ B
      DO 170 IP=1,P
         DO 169 IN=1,N
              DO 168 I=1,N
                        BT(I)=B(I,IN)
                        CT(I)=C(IP,I)
```

```
 168            CONTINUE
                CALL CADJB (CT,BT,GP,L)
C$$$$$$$$FOLLOWING CALCULATES ELEMENTS OF MATRIX G(0)$$$$$$$$$$$$$$$$$$$$$$$$
                GZ(IP,IM)=GP(1)/DET(1)
 169      CONTINUE
 170  CONTINUE
      PRINT$,' '
      PRINT$,' '
      PRINT$,'THE G(0) MATRIX IS:'
      PRINT$,' '
      PRINT$,' '
      CALL MATPR(GZ,P,M)
      PRINT$,' '
      PRINT$, 'THE G(0) INVERSE MATRIX IS:'
      PRINT$,' '
      PRINT$,' '
C$$$$$$$$$$FOLLOWING CALCULATES MATRIX G(0) INVERSE$$$$$$$$$$$$$$$$$$$$$$$$$
      IDGT=10
      IA=10
      CALL LINV2F (GZ,P,IA,GZINV,IDGT,WKAREA,IER)
      IF (IER.EQ.34) THEN
          PRINT$,'ACCURACY TEST FAILED....DATA MAY BE SUSPECT'
      ELSE IF (IER.EQ.131) THEN
          PRINT$,'MATRIX TOO ILL-CONDITIONED FOR ITERATIVE'
          PRINT$,'IMPROVEMENT TO BE EFFECTIVE'
      ELSE IF (IER.EQ.129) THEN
          PRINT$,'SINGULAR AND CANNOT BE INVERTED'
      ELSE
          CALL MATPR (GZINV,P,M)
          PRINT$,' '
          PRINT$,' '
 171      PRINT$,'TO USE THE G(0) INVERSE MATRIX OR G(0) MATRIX'
          PRINT$,'TO CALCULATE THE STEADY-STATE VALUE OF THE:'
          PRINT$,' '
          PRINT$,'PLANT INPUT VECTOR U      ENTER >1'
          PRINT$,'PLANT OUTPUT VECTOR Y     ENTER >2'
          PRINT$,'TERMINATE CALCULATIONS    ENTER >3'
          READ$,IIYES
          IF (IIYES.EQ.1) THEN
                PRINT$,' '
                PRINT$,'ENTER THE ',P,' COLUMN ELEMENTS OF THE'
                PRINT$,'PLANT OUTPUT VECTOR Y'
                READ$,((YYY(I,J),J=1,1),I=1,P)
                PRINT$,' '
                PRINT$,'THE PLANT OUTPUT VECTOR Y'
                PRINT$,'JUST ENTERED IS:'
                PRINT$,' '
                PRINT$,' '
```

```
                PRINT$,' '
              DO 172 I=1,P
                      PRINT$,'   ',YYY(I,1)
172           CONTINUE
              IA=10
              CALL VMULFF(GZINV,YYY,P,P,J,IA,IA,UUU,IA,IER)
              PRINT$,' '
              PRINT$,' '
              PRINT$,'THE PLANT INPUT VECTOR'
              PRINT$,'U = G(0) INVERSE * Y   IS'
              PRINT$,' '
              PRINT$,' '
              DO 173 I=1,P
                      PRINT$,'   ',UUU(I,1)
173           CONTINUE
              PRINT$,' '
              PRINT$,' '
              GO TO 171
          ELSE IF (IIYES.EQ.2) THEN
              PRINT$,' '
              PRINT$,'ENTER THE ',P,' COLUMN ELEMENTS OF THE'
              PRINT$,'PLANT INPUT VECTOR U'
              READ$,((UUU(I,J),J=1,1),I=1,P)
              PRINT$,' '
              PRINT$,'THE PLANT INPUT VECTOR U'
              PRINT$,'JUST ENTERED IS'
              PRINT$,' '
              PRINT$,' '
              DO 174 I=1,P
                      PRINT$,'   ',UUU(I,1)
174           CONTINUE
              IA=10
              CALL VMULFF(GZ,UUU,P,P,J,IA,IA,YYY,IA,IER)
              PRINT$,' '
              PRINT$,' '
              PRINT$,'THE PLANT OUTPUT VECTOR'
              PRINT$,'Y = G(0) * U   IS'
              PRINT$,' '
              PRINT$,' '
              DO 175 I=1,P
                      PRINT$,'   ',YYY(I,1)
175           CONTINUE
              PRINT$,' '
              PRINT$,' '
              GO TO 171
          END IF
      END IF
          GO TO 8017
      END IF
```

Appendix C: Converting Radians to Degrees for Plotting

Introduction

This addition to MULTI provides the capability to selectively convert the vectors and states of the simulation output from radians to degrees prior to plotting the data or calculating the figures of merit. This is useful because the equations of motion for aircraft often have the variables describing angles with dimensional units in radians and control surface deflections in dimensional units of degrees.

User's Guide

Option 26 is executed to generate the simulation data. After the calculations are completed the following prompt appears:

```
CONVERT RADIANS TO DEGREES?   1-YES,   0-NO
```

If 0 is entered the option is skipped. If 1 is entered, then prompts appear as shown in the following example:

```
ENTER # OF OUTPUTS (Y VECTOR) TO CONVERT
? 2

ENTER INTEGERS FOR Y VECTOR CHOICES
? 1,3
```

```
ENTER # OF INPUTS (V VECTOR) TO CONVERT
? 2

ENTER INTEGERS FOR V VECTOR CHOICES
? 1,3

ENTER # OF STATES TO CONVERT
? 3

ENTER INTEGERS FOR STATE VECTOR CHOICES
? 1,3,4
```

Programmer's Guide

The following FORTRAN 77 code is added to the Option 26 overlay. Comments explain each section of the code.

```
      PRINT$,'CONVERT RADIANS TO DEGREES? 1-YES, 0-NO'
      READ$,IYES
      IF(IYES.NE.1) THEN
         GO TO 8990
      ELSE
         PRINT$,'ENTER # OF OUTPUTS (Y VECTOR) TO CONVERT'
         READ$,NUMBER
      END IF
      IF(NUMBER.EQ.0) THEN
         GO TO 8850
      ELSE
         PRINT$,'ENTER INTEGERS FOR Y VECTOR CHOICES'
         READ$,(ICLMS(QN),QN=1,NUMBER)
         DO 8800 QN=1,NUMBER
               DO 8700 I=1,NT
               YP(I,(ICLMS(QN)+1))=YP(I,(ICLMS(QN)+1))*57.2958
8700           CONTINUE
8800     CONTINUE
      END IF
8850  PRINT$,'ENTER # OF INPUTS (V VECTOR) TO CONVERT'
      READ$,NUMBER
      IF(NUMBER.EQ.0) THEN
          GO TO 8900
      ELSE
         PRINT$,'ENTER INTEGERS FOR V VECTOR CHOICES'
         READ$,(ICLMS(QN),QN=1,NUMBER)
         DO 8870 QN=1,NUMBER
               DO 8860 I=1,NT
               VP(I,(ICLMS(QN)+1))=VP(I,(ICLMS(QN)+1))*57.2958
8860           CONTINUE
8870     CONTINUE
      END IF
```

```
8900 PRINT$,'ENTER # OF STATES TO CONVERT'
     READ$,NUMBER
     IF(NUMBER.EQ.0) THEN
         GO TO 8990
     ELSE
         PRINT$,'ENTER INTEGERS FOR STATE VECTOR CHOICES'
         READ$,(ICLMS(QN),QN=1,NUMBER)
         DO 8970 QN=1,NUMBER
               DO 8760 I=1,NT
               XP(I,(ICLMS(QN)+1))=XP(I,(ICLMS(QN)+1))$57.2958
8760 CONTINUE
8970 CONTINUE
     END IF
8990 CONTINUE
     GO TO 8007
```

Appendix D: Longitudinal State Space Matrices

Tables in this appendix list the linearized longitudinal state space matrices of the X-29 aircraft for the following flight conditions:

(1) 0.4 Mach at Sea Level

(2) 0.7 Mach at 15000 Feet

(3) 1.2 Mach at 15000 Feet

TABLE D-1

LONGITUDINAL STATE SPACE MATRICES

FLIGHT CONDITION: 0.4 Mach at Sea Level

A (Plant Matrix)

.0000E+00	.0000E+00	.0000E+00	.1000E+01
-.3217E+02	-.1660E-01	.4880E-01	-.4273E+00
.0000E+00	-.3172E-03	-.1001E+01	.9880E+00
.0000E+00	.2823E-03	.1012E+02	-.4340E+00

B (Control Input Matrix)

.0000E+00	.0000E+00	.0000E+00
-.4891E-01	.2592E-01	.3779E+02
-.9426E-03	-.8021E-03	-.6761E-02
.9328E-01	-.3603E-01	-.2679E+00

C (Output Matrix)

.0000E+01	.0000E+00	.0000E+00	.1000E+01
.0000E+00	.1000E+01	.0000E+00	.0000E+00
.0000E+00	.0000E+00	.1000E+01	.0000E+00

Notes

1. States (listed in order) are pitch angle, change in forward velocity, angle-of-attack, and pitch rate.

2. Control inputs (listed in order) are canards, strake flaps, and thrust.

3. Outputs (listed in order) are pitch rate, change in forward velocity, and angle of attack.

TABLE D-2

LONGITUDINAL STATE SPACE MATRICES

FLIGHT CONDITION: 0.7 Mach at 15000 Feet

A (Plant Matrix)

.0000E+00	.0000E+00	.0000E+00	.1000E+01
-.3213E+02	-.1199E-01	-.1718E+01	-.3504E+00
-.3243E-06	-.1298E-03	-.1138E+01	.9917E+00
.0000E+00	.2986E-03	.1892E+02	-.4928E+00

B (Control Input Matrix)

.0000E+00	.0000E+00	.0000E+00
-.5895E-01	.2621E-01	.2724E+02
-.1161E-02	-.7808E-03	-.2099E-02
.1720E+00	-.5630E-01	-.1929E+00

C (Output Matrix)

.0000E+00	.0000E+00	.0000E+00	.1000E+01
.0000E+00	.1000E+01	.0000E+00	.0000E+00
.0000E+00	.0000E+00	.1000E+01	.0000E+00

Notes

1. States (listed in order) are pitch angle, change in forward velocity, angle-of-attack, and pitch rate.

2. Control inputs (listed in order) are canards, strake flaps, and thrust.

3. Outputs (listed in order) are pitch rate, change in forward velocity, and angle of attack.

TABLE D-3

LONGITUDINAL STATE SPACE MATRICES

FLIGHT CONDITION: 1.2 Mach at 15000 Feet

A (Plant Matrix)

.0000E+00	.0000E+00	.0000E+00	.1000E+01
-.3213E+02	-.1083E+00	-.2668E+02	-.3814E+00
-.1892E-06	-.6824E-04	-.2461E+01	.9930E+00
.0000E+00	-.7393E-02	.1920E+02	-.9340E+00

B (Control Input Matrix)

.0000E+00	.0000E+00	.0000E+00
-.2959E+00	.3583E-01	.1079E+03
-.3266E-02	-.7448E-03	-.3645E-02
.3880E+00	-.1195E+00	-.7638E+00

C (Output Matrix)

.0000E+00	.0000E+00	.0000E+00	.1000E+01
.0000E+00	.1000E+01	.0000E+00	.0000E+00
.0000E+00	.0000E+00	.1000E+01	.0000E+00

Notes

1. States (listed in order) are pitch angle, change in forward velocity, angle-of-attack, and pitch rate.

2. Control inputs (listed in order) are canards, strake flaps, and thrust.

3. Outputs (listed in order) are pitch rate, change in forward velocity, and angle of attack.

Appendix E: Longitudinal Design Parameters, Controller Matrices, and Figures of Merit

Two sets of tables in this appendix tabulate the design parameters, controller matrices, and figures of merit for the following longitudinal maneuvers and flight conditions:

Direct Climb

1. 0.4 Mach at Sea Level
2. 1.2 Mach at 15000 Feet

Vertical Translation

1. 0.7 Mach at 15000 Feet
2. 1.2 Mach at 15000 Feet

Pitch Pointing

1. 0.7 Mach at 15000 Feet
2. 1.2 Mach at 15000 Feet

TABLE E-1

DESIGN PARAMETERS AND CONTROLLER MATRICES
FOR LONGITUDINAL CONTROLLERS

FLIGHT CONDITION: 0.4 Mach at Sea Level
MANEUVER: Direct Climb
COMMAND VECTOR $\underline{v}$*: 1.1, 0.0436, 3, 4.1
0, 0, 0, 0
0, 0, 0, 0

Plant Only

Alpha	Epsilon	Sigma**	$\underline{K}_0$***		
		1.7	.1253E+02	-.8427E-02	-.3313E+01
0.714	1.4	1.2	-.1495E+02	-.2592E+00	-.8588E+01
		0.01	.2647E-01	.3192E-01	.1603E-02

Plant and Computational Time Delay

Alpha	Epsilon	Sigma**	$\underline{K}_0$***		
		1.9	.1400E+02	-.8427E-02	-.6625E+01
0.714	1.4	1.2	-.1670E+02	-.2592E+00	-.1718E+02
		0.02	.2958E-01	.3192E-01	.3206E-02

Plant with Actuator Dynamics

Alpha	Epsilon	Sigma**	$\underline{K}_0$***		
		2.0	.1474E+02	-.8427E-02	-.3313E+01
0.714	1.4	1.2	-.1758E+02	-.2592E+00	-.8588E+01
		0.01	.3114E-01	.3192E-01	.1603E-02

Plant with Actuator Dynamics and Computational Time Delay

Alpha	Epsilon	Sigma**	$\underline{K}_0$***		
		2.1	.1548E+02	-.7022E-02	-.4969E+01
.555	1.8	1.0	-.1846E+02	-.2160E+00	-.1288E+02
		0.015	.3269E-01	.2660E-01	.2405E-02

Notes

*Each pulse entry in $\underline{v}$ has four parts:
1. The time in seconds the input reaches steady-state;
2. Steady-state value (angles in radians);
3. Time the input leaves steady-state; and
4. Time the input reaches zero.

**Diagonal element values of the matrix.

***$\underline{K}_0$ = alpha * $\underline{K}_1$.

TABLE E-2

DESIGN PARAMETERS AND CONTROLLER MATRICES
FOR LONGITUDINAL CONTROLLERS

FLIGHT CONDITION: 1.2 Mach at 15000 Feet
MANEUVER: Direct Climb
COMMAND VECTOR $\underline{v}$*: 1.1, 0.0436, 3.0, 4.1
0, 0, 0, 0
0, 0, 0, 0

Plant Only

Alpha	Epsilon	Sigma**	$\underline{K}_0$***		
		1.7	.1866E+01	.1094E-02	-.1760E+01
0.7143	1.4	0.6	-.8219E+01	-.3208E-01	-.5695E+01
		0.01	.7845E-02	.5574E-02	-.2935E-02

Plant and Computational Time Delay

Alpha	Epsilon	Sigma**	$\underline{K}_0$***		
		1.9	.2085E+01	.1094E-02	-.3520E+01
0.7143	1.4	0.6	-.9186E+01	-.3208E-01	-.1139E+02
		0.02	.8768E-02	.5574E-02	-.5870E-02

Plant with Actuator Dynamics

Alpha	Epsilon	Sigma**	$\underline{K}_0$***		
		2.0	.2195E+01	.1094E-02	-.1760E+01
0.7143	1.4	0.6	-.9669E+01	-.3208E-01	-.5695E+01
		0.01	.9230E-02	.5574E-02	-.2935E-02

Plant with Actuator Dynamics and Computational Time Delay

Alpha	Epsilon	Sigma**	$\underline{K}_0$***		
		2.1	.2304E+01	.1094E-02	-.2639E+01
.555	1.8	0.6	-.1015E+02	-.3207E-01	-.8542E+01
		0.015	.9690E-02	.5574E-02	-.4402E-02

Notes

*Each pulse entry in $\underline{v}$ has four parts:
1. The time in seconds the input reaches steady-state;
2. Steady-state value (angles in radians);
3. Time the input leaves steady-state; and
4. Time the input reaches zero.

**Diagonal element values of the matrix.

***$\underline{K}_0$ = alpha * $\underline{K}_1$.

TABLE E-3

DESIGN PARAMETERS AND CONTROLLER MATRICES
FOR LONGITUDINAL CONTROLLERS

FLIGHT CONDITION: 0.7 Mach at 15000 Feet
MANEUVER: Vertical Translation
COMMAND VECTOR $\underline{v}$*: 0, 0, 0, 0
0, 0, 0, 0
1.1, -0.0349, 50, 50

Plant Only

Alpha	Epsilon	Sigma**	$\underline{K}_0$***		
		1.9	.7435E+01	.5984E-02	-.4229E+01
.4545	2.2	1.0	-.1113E+02	-.1079E+00	-.1293E+02
		0.015	.2679E-01	.3683E-01	.3290E-02

Plant and Computational Time Delay

Alpha	Epsilon	Sigma**	$\underline{K}_0$***		
		1.9	.7435E+01	.5984E-02	-.8458E+01
.4545	2.2	1.0	-.1113E+02	-.1079E+00	-.2586E+02
		0.03	.2679E-01	.3683E-01	.6581E-02

Plant with Actuator Dynamics

Alpha	Epsilon	Sigma**	$\underline{K}_0$***		
		2.0	.7826E+01	.5984E-02	-.4229E+01
.4545	2.2	1.0	-.1171E+02	-.1079E+00	-.1293E+02
		0.015	.2821E-01	.3683E-01	.3290E-02

Plant with Actuator Dynamics and Computational Time Delay

Alpha	Epsilon	Sigma**	$\underline{K}_0$***		
		1.9	.7435E+01	.8976E-02	-.7049E+01
.4545	2.2	1.5	-.1113E+02	-.1618E+00	-.2155E+02
		0.025	.2679E-01	.5524E-01	.5484E-02

Notes

*Each pulse entry in $\underline{v}$ has four parts:
1. The time in seconds the input reaches steady-state;
2. Steady-state value (angles in radians);
3. Time the input leaves steady-state; and
4. Time the input reaches zero.

**Diagonal element values of the matrix.

***$\underline{K}_0$ = alpha * $\underline{K}_1$.

TABLE E-4

DESIGN PARAMETERS AND CONTROLLER MATRICES
FOR LONGITUDINAL CONTROLLERS

FLIGHT CONDITION: 1.2 Mach at 15000 Feet
MANEUVER: Vertical Translation
COMMAND VECTOR $\underline{v}$*: 0, 0, 0, 0
0, 0, 0, 0
0, 1.1, -0.0218, 50, 50

Plant Only

Alpha	Epsilon	Sigma**	$\underline{K}_0$***		
		1.8	.1975E+01	.1823E-02	-.8799E+01
0.4545	1.8	1.0	-.8702E+01	-.5346E-01	-.2848E+02
		0.05	.8307E-02	.9291E-02	-.1467E-01

Plant and Computational Time Delay

Alpha	Epsilon	Sigma**	$\underline{K}_0$***		
		1.8	.1975E+01	.1823E-02	-.1760E+02
0.4545	1.8	1.0	-.8702E+01	-.5346E-01	-.5695E+02
		0.1	.8307E-02	.9291E-02	-.2935E-01

Plant with Actuator Dynamics

Alpha	Epsilon	Sigma**	$\underline{K}_0$***		
		1.8	.1975E+01	.1823E-02	-.1056E+02
0.4545	1.8	1.0	-.8702E+01	-.5346E-01	-.3417E+02
		0.06	.8307E-02	.9291E-02	-.1761E-01

Plant with Actuator Dynamics and Computational Time Delay

Alpha	Epsilon	Sigma**	$\underline{K}_0$***		
		1.8	.1975E+01	.1823E-02	-.1232E+02
0.4545	1.8	1.0	-.8702E+01	-.5346E-01	-.3987E+02
		0.07	.8307E-02	.9291E-02	-.2054E-01

Notes

*Each pulse entry in $\underline{v}$ has four parts:
1. The time in seconds the input reaches steady-state;
2. Steady-state value (angles in radians);
3. Time the input leaves steady-state; and
4. Time the input reaches zero.

**Diagonal element values of the matrix.

***$\underline{K}_0$ = alpha * $\underline{K}_1$.

TABLE E-5

DESIGN PARAMETERS AND CONTROLLER MATRICES
FOR LONGITUDINAL CONTROLLERS

FLIGHT CONDITION: 0.7 Mach at 15000 Feet
MANEUVER: Pitch Pointing
COMMAND VECTOR $\underline{v}$*: 0, 0.8, 0.0349, 1.0, 1.8
0, 0, 0, 0
0, 0.8, 0.0349, 50, 50

Plant Only

Alpha	Epsilon	Sigma**	$\underline{K}_0$***		
		1.9	.7432E+01	.5982E-02	-.5637E+01
0.357	2.8	1.0	-.1112E+02	-.1079E+00	-.1724E+02
		0.02	.2678E-01	.3681E-01	.4385E-02

Plant and Computational Time Delay

Alpha	Epsilon	Sigma**	$\underline{K}_0$***		
		1.9	.7432E+01	.5982E-02	-.7046E+01
0.357	2.8	1.0	-.1112E+02	-.1079E+00	-.2154E+02
		0.025	.2678E-01	.3681E-01	.5482E-02

Plant with Actuator Dynamics

Alpha	Epsilon	Sigma**	$\underline{K}_0$***		
		1.9	.7432E+01	.5982E-02	-.4227E+01
0.357	2.8	1.0	-.1112E+02	-.1079E+00	-.1293E+02
		0.015	.2678E-01	.3681E-01	.3289E-02

Plant with Actuator Dynamics and Computational Time Delay

Alpha	Epsilon	Sigma**	$\underline{K}_0$***		
		1.7	.6649E+01	.5982E-02	-.4227E+01
0.357	2.8	1.0	-.9951E+01	-.1079E+00	-.1293E+02
		0.015	.2396E-01	.3681E-01	.3289E-02

Notes

*Each pulse entry in $\underline{v}$ has four parts:
1. The time in seconds the input reaches steady-state;
2. Steady-state value (angles in radians);
3. Time the input leaves steady-state; and
4. Time the input reaches zero.

**Diagonal element values of the matrix.

***$\underline{K}_0$ = alpha * $\underline{K}_1$.

TABLE E-6

DESIGN PARAMETERS AND CONTROLLER MATRICES
FOR LONGITUDINAL CONTROLLERS

FLIGHT CONDITION: 1.2 Mach at 15000 Feet
MANEUVER: Pitch Pointing
COMMAND VECTOR $\underline{v}$*: 0.8, 0.0218, 1.0, 1.8
0, 0, 0, 0
0.8, 0.0218, 50, 50

Plant Only

Alpha	Epsilon	Sigma**	$\underline{K}_0$***		
		1.9	.2084E+01	.3645E-03	-.1231E+02
0.357	2.8	0.2	-.9182E+01	-.1069E-01	-.3985E+02
		0.07	.8765E-02	.1857E-02	-.2054E-01

Plant and Computational Time Delay

Alpha	Epsilon	Sigma**	$\underline{K}_0$***		
		1.9	.2084E+01	.3645E-03	-.2815E+02
0.357	2.8	0.2	-.9182E+01	-.1069E-01	-.9109E+02
		0.16	.8765E-02	.1857E-02	-.4694E-01

Plant with Actuator Dynamics

Alpha	Epsilon	Sigma**	$\underline{K}_0$***		
		1.9	.2084E+01	.3645E-03	-.8796E+01
0.357	2.8	0.2	-.9182E+01	-.1069E-01	-.2846E+02
		0.05	.8765E-02	.1857E-02	-.1467E-01

Plant with Actuator Dynamics and Computational Time Delay

Alpha	Epsilon	Sigma**	$\underline{K}_0$***		
		1.9	.2084E+01	.3645E-03	-.1231E+02
0.357	2.8	0.2	-.9182E+01	-.1069E-01	-.3985E+02
		0.07	.8765E-02	.1857E-02	-.2054E-01

Notes

*Each pulse entry in $\underline{v}$ has four parts:
1. The time in seconds the input reaches steady-state;
2. Steady-state value (angles in radians);
3. Time the input leaves steady-state; and
4. Time the input reaches zero.

**Diagonal element values of the matrix.

***$\underline{K}_0$ = alpha * $\underline{K}_1$.

TABLE E-7

LONGITUDINAL FIGURES OF MERIT

FLIGHT CONDITION: 0.4 Mach at Sea Level

MANEUVER: Direct Climb

COMMAND VECTOR $\underline{v}$:* 1.1, 0.0436, 3, 4.1
0, 0, 0, 0
0, 0, 0, 0

Plant Only

Output	Peak Value**	Peak Time	Settling Time
Pitch Rate	2.59	1.4	***
Forward Velocity	-0.0203	2.975	***
Angle of Attack	1.27	1.925	***
Pitch Angle	7.6	4.0	4.1
Flight Path Angle	8.3	5.2	9.5

Plant and Computational Time Delay

Output	Peak Value**	Peak Time	Settling Time
Pitch Rate	2.56	1.4	***
Forward Velocity	-0.02	2.975	***
Angle of Attack	0.918	1.575	***
Pitch Angle	7.6	3.9	3.9
Flight Path Angle	8.2	4.9	8.8

TABLE E-7 --Continued

Plant with Actuator Dynamics

Output	Peak Value**	Peak Time	Settling Time
Pitch Rate	2.6	1.575	***
Forward Velocity	-0.02	2.8	***
Angle of Attack	1.34	1.925	***
Pitch Angle	7.7	4.0	7.8
Flight Path Angle	8.4	5.2	8.0

Plant with Actuator Dynamics and Computational Time Delay

Output	Peak Value**	Peak Time	Settling Time
Pitch Rate	2.7	1.225	***
Forward Velocity	-0.038	2.45	***
Angle of Attack	1.45	1.925	***
Pitch Angle	7.7	3.9	4.0
Flight Path Angle	8.4	5.2	8.2

Notes

1. Figures of merit for the pitch angle and the flight path angle are estimated from the response plots.

2. Pitch rate, forward velocity, and angle of attack are components of the output vector $\underline{y}$.

3. Pitch rate and angle of attack are commanded to achieve desired responses in the pitch angle and the flight path angle for each maneuver.

*Commanded inputs in order:
(1) pitch rate in radians per second;
(2) forward velocity in feet per second; and
(3) angle of attack in radians.

**Angles are converted from radians to degrees prior to calculating the figures of merit.

***Final value of the output is zero. Settling time undefined using definition of 2 percent of final value.

TABLE E-8

LONGITUDINAL FIGURES OF MERIT

FLIGHT CONDITION: 1.2 Mach at 15000 Feet

MANEUVER: Direct Climb

COMMAND VECTOR $\underline{v}$:* 1.1, 0.0436, 3, 4.1
0, 0, 0, 0
0, 0, 0, 0

Plant Only

Output	Peak Value**	Peak Time	Settling Time
Pitch Rate	2.59	1.4	***
Forward Velocity	-0.04	2.275	***
Angle of Attack	0.756	1.75	***
Pitch Angle	7.6	3.9	3.9
Flight Path Angle	7.9	4.4	4.6

Plant and Computational Time Delay

Output	Peak Value**	Peak Time	Settling Time
Pitch Rate	2.66	1.225	***
Forward Velocity	-0.08	2.1	***
Angle of Attack	0.78	1.75	***
Pitch Angle	7.7	3.9	4.0
Flight Path Angle	7.9	4.2	4.5

TABLE E-8 --Continued

Plant with Actuator Dynamics

Output	Peak Value**	Peak Time	Settling Time
Pitch Rate	2.64	1.4	***
Forward Velocity	-0.039	1.925	***
Angle of Attack	0.77	1.575	***
Pitch Angle	7.6	3.9	3.9
Flight Path Angle	7.8	4.2	5.5

Plant with Actuator Dynamics and Computational Time Delay

Output	Peak Value**	Peak Time	Settling Time
Pitch Rate	2.79	1.225	***
Forward Velocity	-0.069	1.4	***
Angle of Attack	0.825	1.575	***
Pitch Angle	7.7	3.9	4.0
Flight Path Angle	7.8	4.2	5.5

Notes

1. Figures of merit for the pitch angle and the flight path angle are estimated from the response plots.

2. Pitch rate, forward velocity, and angle of attack are components of the output vector $\underline{y}$.

3. Pitch rate and angle of attack are commanded to achieve desired responses in the pitch angle and the flight path angle for each maneuver.

*Commanded inputs in order:
(1) pitch rate in radians per second;
(2) forward velocity in feet per second; and
(3) angle of attack in radians.

**Angles are converted from radians to degrees prior to calculating the figures of merit.

***Final value of the output is zero. Settling time undefined using definition of 2 percent of final value.

TABLE E-9

LONGITUDINAL FIGURES OF MERIT

FLIGHT CONDITION: 0.7 Mach at 15000 Feet

MANEUVER: Vertical Translation

COMMAND VECTOR $\underline{v}$:* 0, 0, 0, 0
0, 0, 0, 0
1.1, -0.0349, 50, 50

Plant Only

Output	Peak Value**	Peak Time	Settling Time
Pitch Rate	-0.11	1.575	***
Forward Velocity	0.009	1.925	***
Angle of Attack	-2.03	4.025	4.55
Pitch Angle	-0.25	3.6	3.7
Flight Path Angle	1.8	3.6	3.7

Plant and Computational Time Delay

Output	Peak Value**	Peak Time	Settling Time
Pitch Rate	-0.229	1.575	***
Forward Velocity	0.003	1.925	***
Angle of Attack	-2.01	3.85	2.975
Pitch Angle	-0.4	3.6	3.7
Flight Path Angle	1.7	3.7	3.8

TABLE E-9 --Continued

Plant with Actuator Dynamics

Output	Peak Value**	Peak Time	Settling Time
Pitch Rate	-0.18	1.575	***
Forward Velocity	.002	1.75	***
Angle of Attack	-2.08	3.5	4.55
Pitch Angle	-0.2	3.5	3.5
Flight Path Angle	1.9	3.5	3.5

Plant with Actuator Dynamics and Computational Time Delay

Output	Peak Value**	Peak Time	Settling Time
Pitch Rate	-0.394	1.575	***
Forward Velocity	0.004	1.925	***
Angle of Attack	-2.007	3.675	2.975
Pitch Angle	-0.4	4.0	4.1
Flight Path Angle	1.6	3.6	3.7

Notes

1. Figures of merit for the pitch angle and the flight path angle are estimated from the response plots.

2. Pitch rate, forward velocity, and angle of attack are components of the output vector $\underline{y}$.

3. Pitch rate and angle of attack are commanded to achieve desired responses in the pitch angle and the flight path angle for each maneuver.

*Commanded inputs in order:
(1) pitch rate in radians per second;
(2) forward velocity in feet per second; and
(3) angle of attack in radians.

**Angles are converted from radians to degrees prior to calculating the figures of merit.

***Final value of the output is zero. Settling time undefined using definition of 2 percent of final value.

TABLE E-10

LONGITUDINAL FIGURES OF MERIT

FLIGHT CONDITION: 1.2 Mach at 15000 Feet

MANEUVER: Vertical Translation

COMMAND VECTOR $\underline{y}$:* 0, 0, 0, 0
0, 0, 0, 0
1.1, -0.0218, 50, 50

Plant Only

Output	Peak Value**	Peak Time	Settling Time
Pitch Rate	-0.09	1.225	***
Forward Velocity	0.004	1.225	***
Angle of Attack	-1.25	15.9	5.575
Pitch Angle	0.16	3.0	3.0
Flight Path Angle	1.19	3.2	3.2

Plant and Computational Time Delay

Output	Peak Value**	Peak Time	Settling Time
Pitch Rate	-0.19	1.225	***
Forward Velocity	0.10	1.225	***
Angle of Attack	-1.25	15.9	5.9
Pitch Angle	-0.30	3.1	3.1
Flight Path Angle	.95	3.1	3.1

TABLE E-10--Continued

Plant with Actuator Dynamics

Output	Peak Value**	Peak Time	Settling Time
Pitch Rate	0.424	0.175	***
Forward Velocity	0.009	1.4	***
Angle of Attack	-1.25	15.9	6.1
Pitch Angle	-0.2	2.1	2.3
Flight Path Angle	1.9	1.6	1.8

Plant with Actuator Dynamics and Computational Time Delay

Output	Peak Value**	Peak Time	Settling Time
Pitch Rate	-0.68	1.4	***
Forward Velocity	0.18	1.4	***
Angle of Attack	1.25	15.7	6.0
Pitch Angle	-0.3	2.0	2.1
Flight Path Angle	1.0	1.75	3.0

Notes

1. Figures of merit for the pitch angle and the flight path angle are estimated from the response plots.

2. Pitch rate, forward velocity, and angle of attack are components of the output vector $\underline{y}$.

3. Pitch rate and angle of attack are commanded to achieve desired responses in the pitch angle and the flight path angle for each maneuver.

*Commanded inputs in order:
(1) pitch rate in radians per second;
(2) forward velocity in feet per second; and
(3) angle of attack in radians.

**Angles are converted from radians to degrees prior to calculating the figures of merit.

***Final value of the output is zero. Settling time undefined using definition of 2 percent of final value.

TABLE E-11

LONGITUDINAL FIGURES OF MERIT

FLIGHT CONDITION: 0.7 Mach at 15000 Feet

MANEUVER: Pitch Pointing

COMMAND VECTOR $\underline{y}$:* 0, 0.8, 0.0349, 1.0, 1.8
0, 0, 0, 0
0, 0.8, 0.0349, 50, 51

Plant Only

Output	Peak Value**	Peak Time	Settling Time
Pitch Rate	2.16	0.875	***
Forward Velocity	-0.01	1.225	***
Angle of Attack	2.025	1.4	4.025
Pitch Angle	2.2	1.9	2.0
Flight Path Angle	0.5	2.3	4.0

Plant and Computational Time Delay

Output	Peak Value**	Peak Time	Settling Time
Pitch Rate	2.36	1.05	***
Forward Velocity	-0.02	1.225	***
Angle of Attack	2.01	5.775	4.6
Pitch Angle	2.3	1.95	2.0
Flight Path Angle	0.7	2.5	5.0

TABLE E-11--Continued

Plant with Actuator Dynamics

Output	Peak Value**	Peak Time	Settling Time
Pitch Rate	2.28	1.05	***
Forward Velocity	-0.01	1.05	***
Angle of Attack	2.03	5.075	4.75
Pitch Angle	2.1	1.95	2.5
Flight Path Angle	0.4	2.3	4.3

Plant with Actuator Dynamics and Computational Time Delay

Output	Peak Value**	Peak Time	Settling Time
Pitch Rate	2.42	1.05	***
Forward Velocity	-0.023	1.05	***
Angle of Attack	2.002	7.7	5.6
Pitch Angle	2.0	1.95	5.5
Flight Path Angle	0.9	2.3	5.6

Notes

1. Figures of merit for the pitch angle and the flight path angle are estimated from the response plots.

2. Pitch rate, forward velocity, and angle of attack are components of the output vector $\underline{y}$.

3. Pitch rate and angle of attack are commanded to achieve desired responses in the pitch angle and the flight path angle for each maneuver.

*Commanded inputs in order:
(1) pitch rate in radians per second;
(2) forward velocity in feet per second; and
(3) angle of attack in radians.

**Angles are converted from radians to degrees prior to calculating the figures of merit.

***Final value of the output is zero. Settling time undefined using definition of 2 percent of final value.

TABLE E-12

LONGITUDINAL FIGURES OF MERIT

FLIGHT CONDITION: 1.2 Mach at 15000 Feet

MANEUVER: Pitch Pointing

COMMAND VECTOR $\underline{v}$:* 0.8, 0.0218, 1.0, 1.8
0, 0, 0, 0
0.8, 0.0218, 50, 50

Plant Only

Output	Peak Value**	Peak Time	Settling Time
Pitch Rate	1.36	0.875	***
Forward Velocity	-0.05	1.05	***
Angle of Attack	1.25	15.9	2.975
Pitch Angle	1.35	1.9	1.9
Flight Path Angle	-0.40	1.0	2.5

Plant and Computational Time Delay

Output	Peak Value**	Peak Time	Settling Time
Pitch Rate	1.47	1.05	***
Forward Velocity	-0.12	1.225	***
Angle of Attack	1.253	1.225	2.8
Pitch Angle	1.4	1.9	2.0
Flight Path Angle	-0.4	1.0	2.5

TABLE E-12--Continued

Plant with Actuator Dynamics

Output	Peak Value**	Peak Time	Settling Time
Pitch Rate	1.7	1.05	***
Forward Velocity	-0.085	1.05	***
Angle of Attack	1.28	1.225	3.15
Pitch Angle	1.25	1.9	3.0
Flight Path Angle	-0.4	1.0	2.5

Plant with Actuator Dynamics and Computational Time Delay

Output	Peak Value**	Peak Time	Settling Time
Pitch Rate	2.23	1.05	***
Forward Velocity	-0.205	1.225	***
Angle of Attack	1.28	1.225	3.85
Pitch Angle	1.35	2.5	3.0
Flight Path Angle	0.3	1.9	2.5

Notes

1. Figures of merit for the pitch angle and the flight path angle are estimated from the response plots.

2. Pitch rate, forward velocity, and angle of attack are components of the output vector y.

3. Pitch rate and angle of attack are commanded to achieve desired responses in the pitch angle and the flight path angle for each maneuver.

*Commanded inputs in order:
(1) pitch rate in radians per second;
(2) forward velocity in feet per second; and
(3) angle of attack in radians.

**Angles are converted from radians to degrees prior to calculating the figures of merit.

***Final value of the output is zero. Settling time undefined using definition of 2 percent of final value.

Appendix F: Longitudinal Controller Response Plots

This appendix includes longitudinal response plots for the X-29 closed-loop flight control system incorporating a controller designed with the Porter method. Response plots are provided for the following maneuvers and flight conditions:

Direct Climb

(1) 0.4 Mach at Sea Level

(2) 1.2 Mach at 15000 Feet

Vertical Translation

(1) 0.7 Mach at 15000 Feet

(2) 1.2 Mach at 15000 Feet

Pitch Pointing

(1) 0.7 Mach at 15000 Feet

(2) 1.2 Mach at 15000 Feet

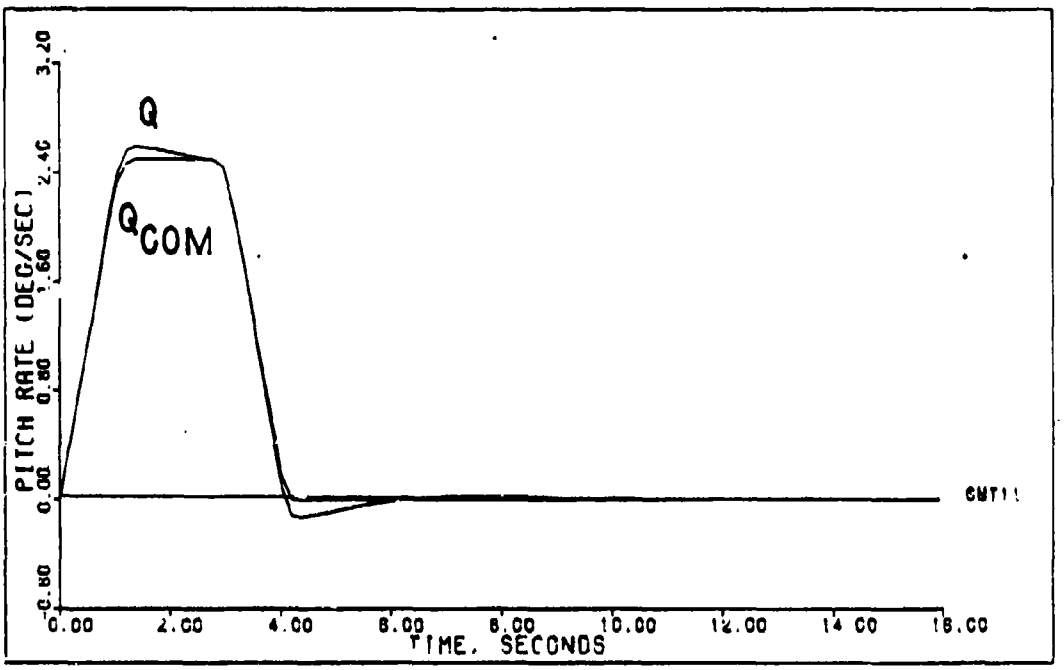

DIRECT CLIMB (0.4M OK FT)

Figure F-1

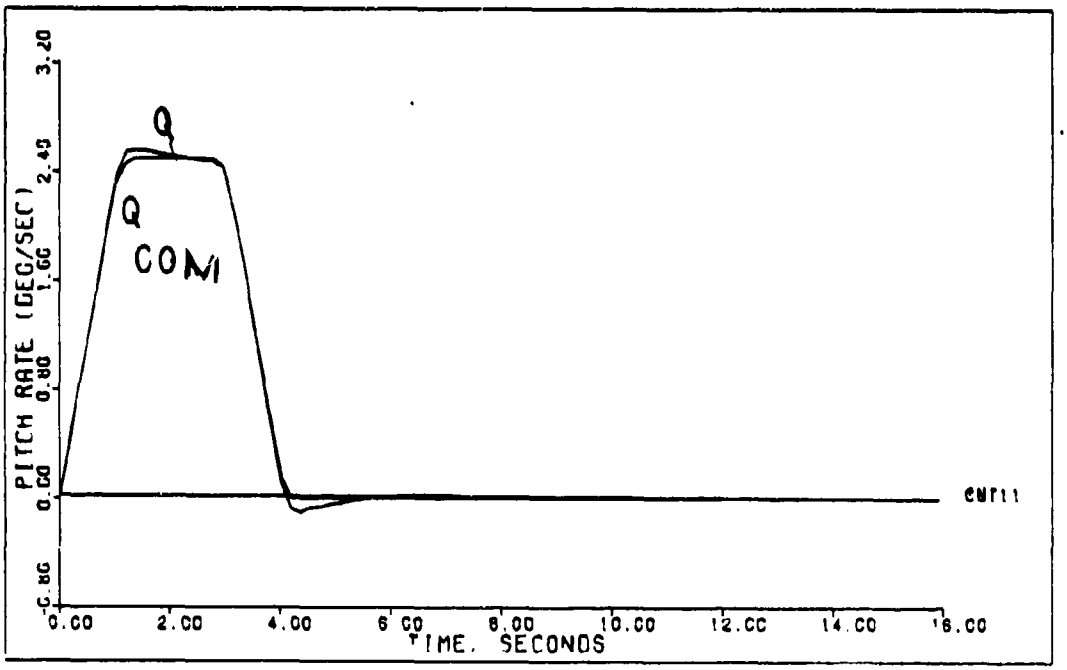

DIRECT CLIMB (0.4M OK FT) DELAY=0.025 SEC

Figure F-2

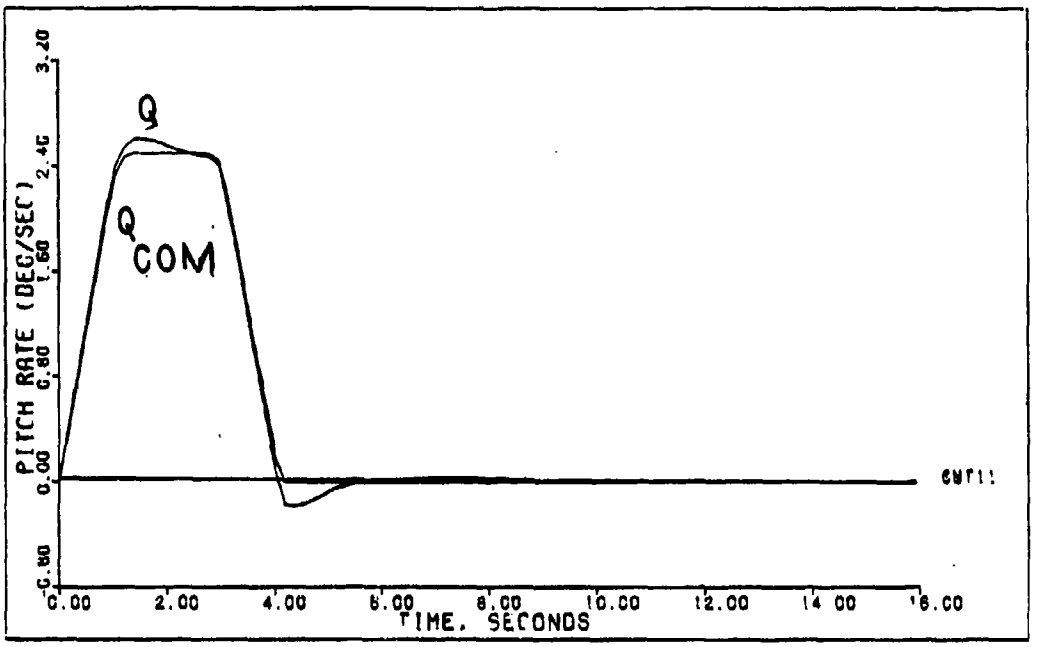

DIRECT CLIMB (0.4M OK FT) ACTUATORS

Figure F-3

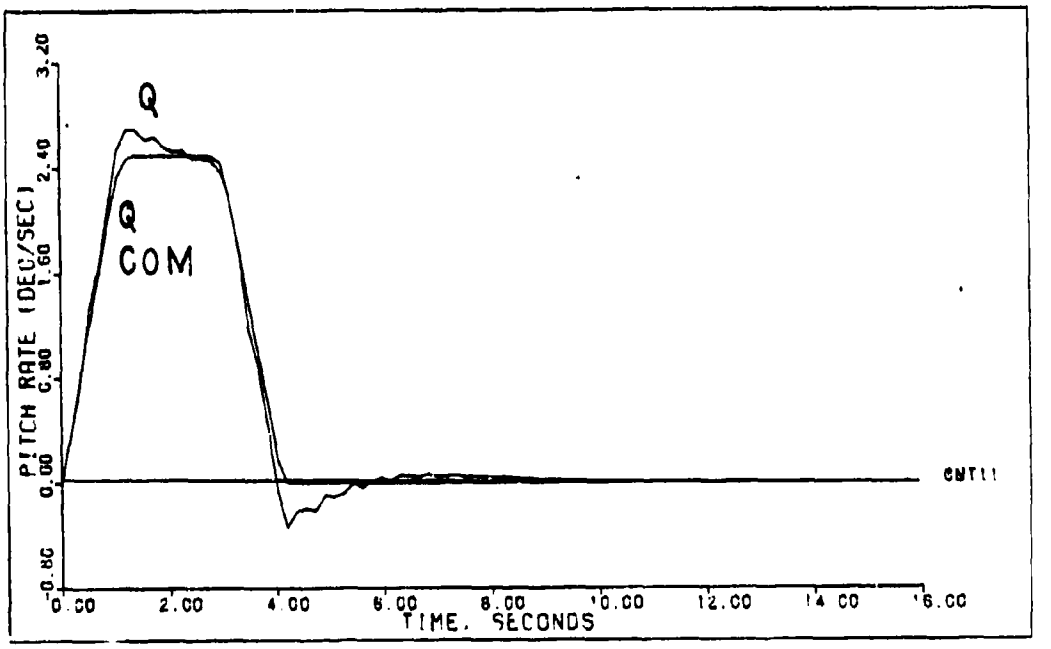

DIRECT CLIMB (0.4M OK FT) DELAY=0.025 SEC ACTUATORS

Figure F-4

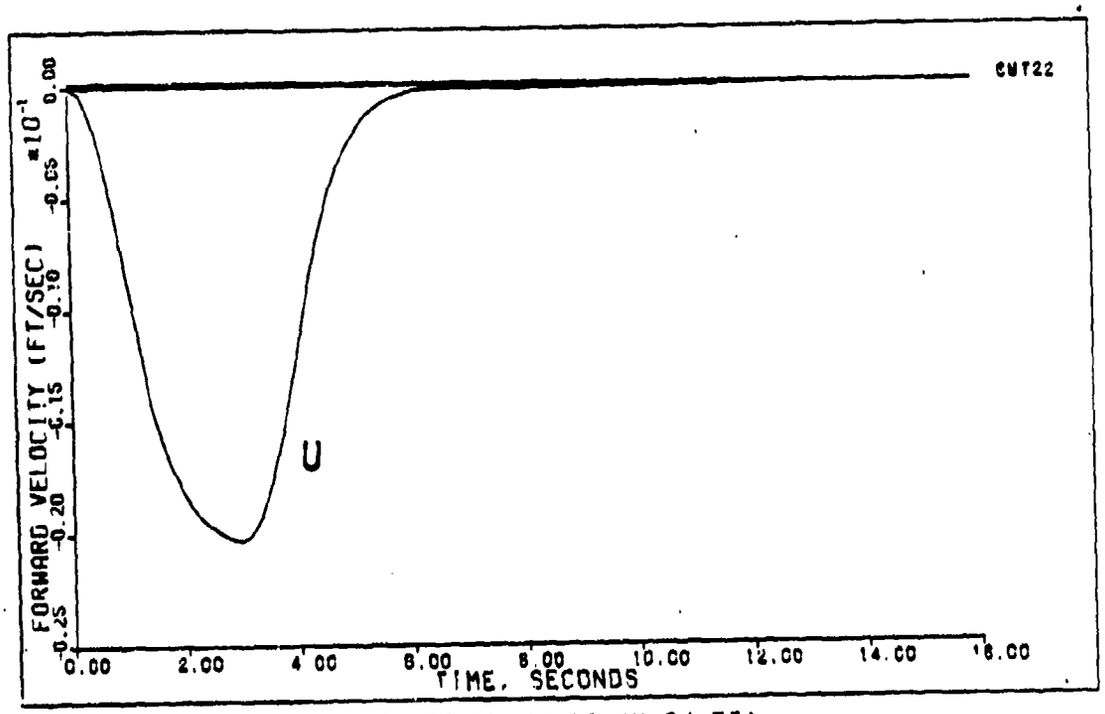

DIRECT CLIMB (0.4M OK FT)

Figure F-5

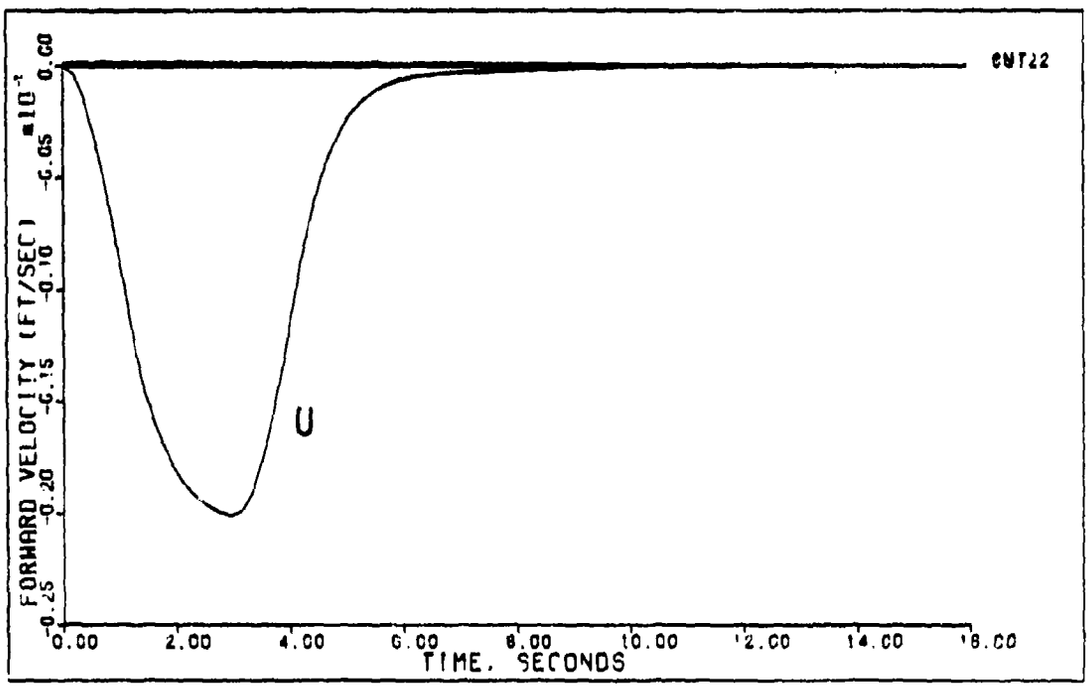

DIRECT CLIMB (0.4M OK FT) DELAY=0.025 SEC

Figure F-6

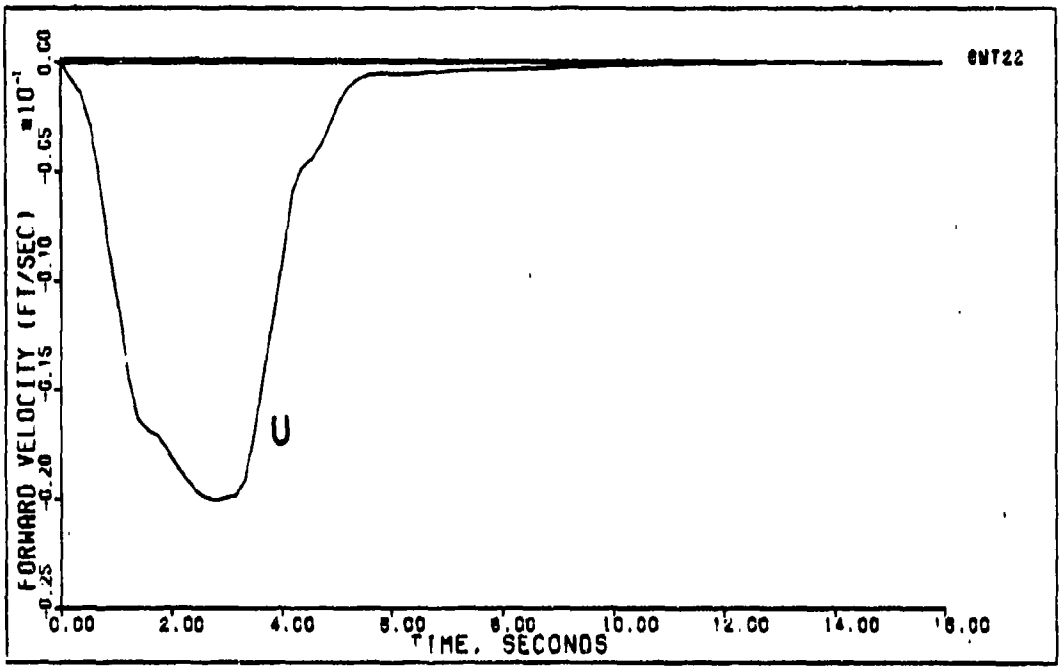

DIRECT CLIMB (0.4M 0K FT) ACTUATORS

Figure F-7

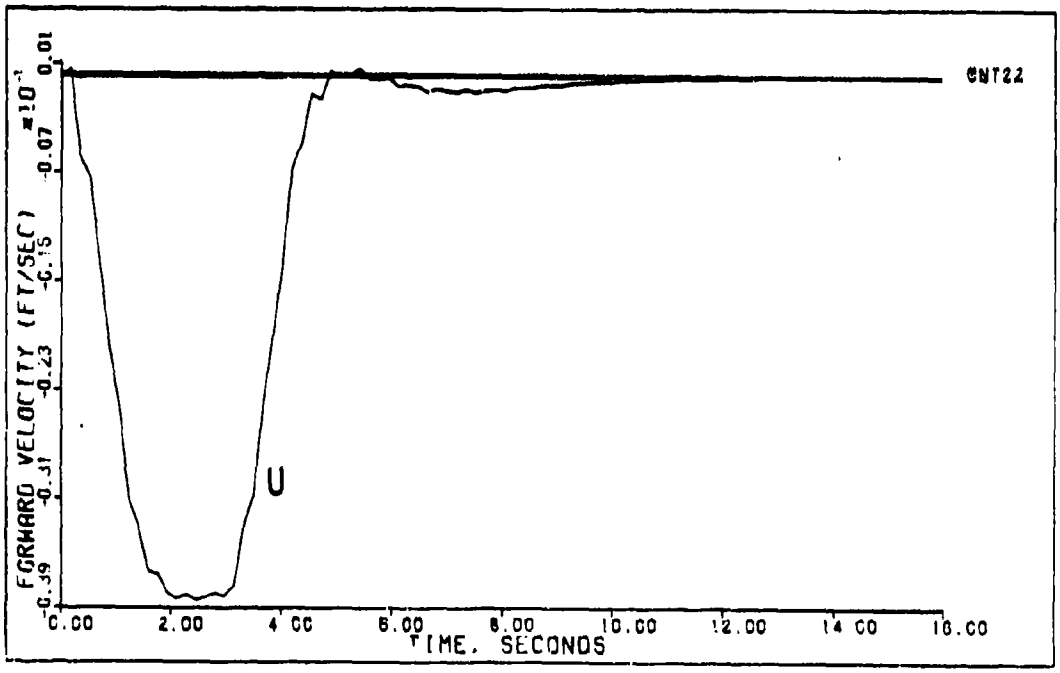

DIRECT CLIMB (0.4M 0K FT) DELAY=0.025 SEC ACTUATORS

Figure F-8

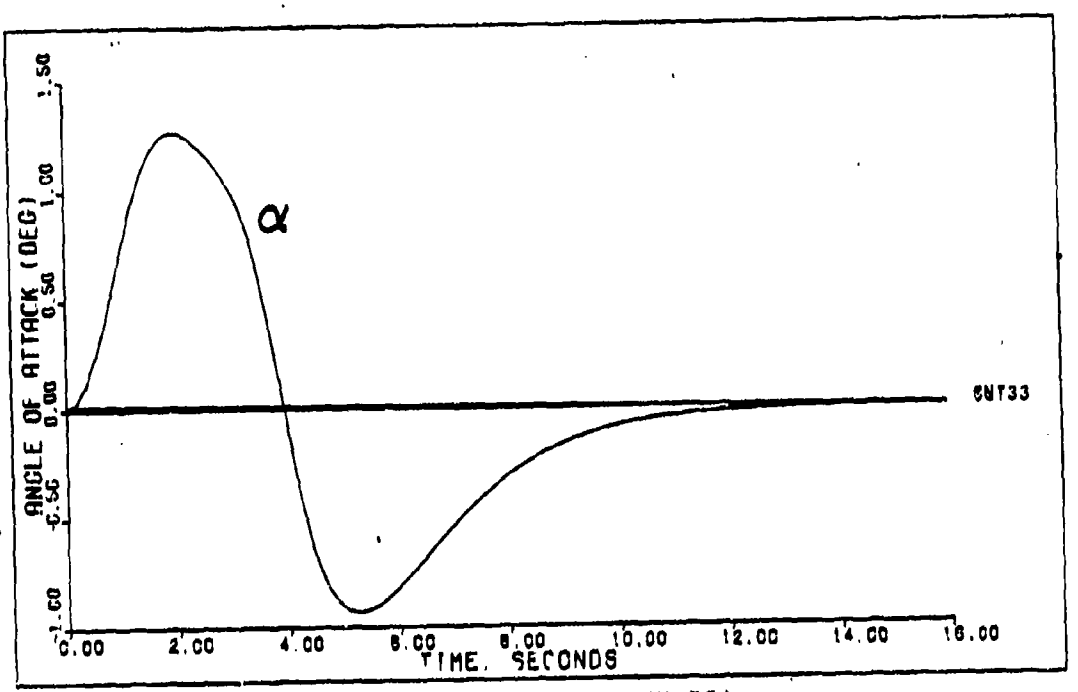

DIRECT CLIMB (0.4M OK FT)

Figure F-9

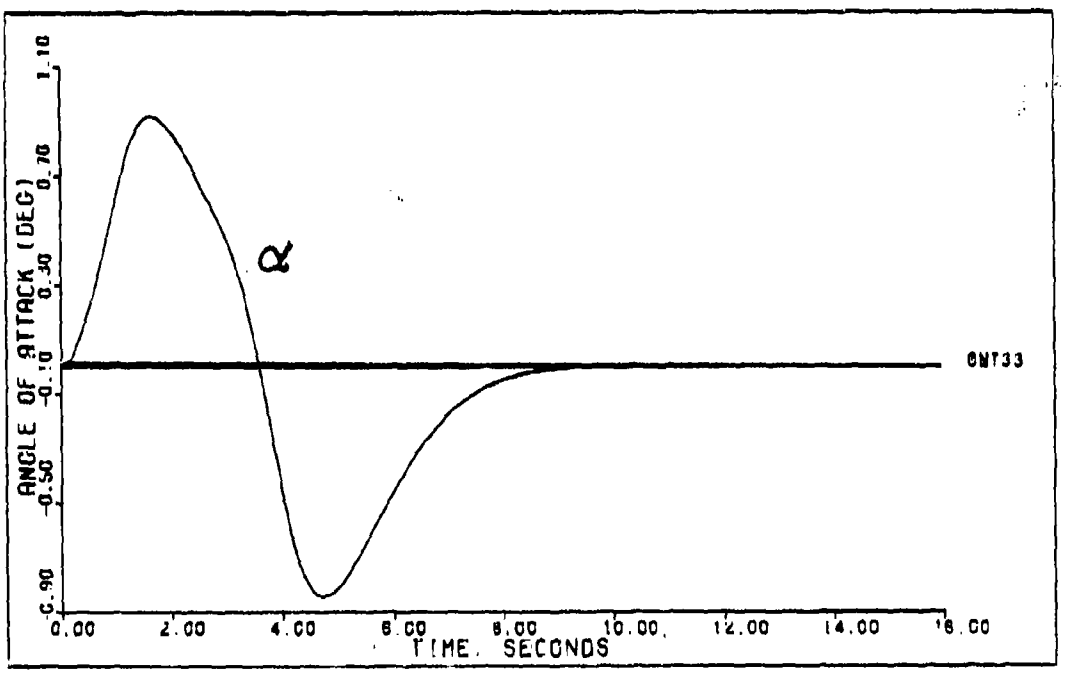

DIRECT CLIMB (0.4M OK FT) DELAY=0.025 SEC

Figure F-10

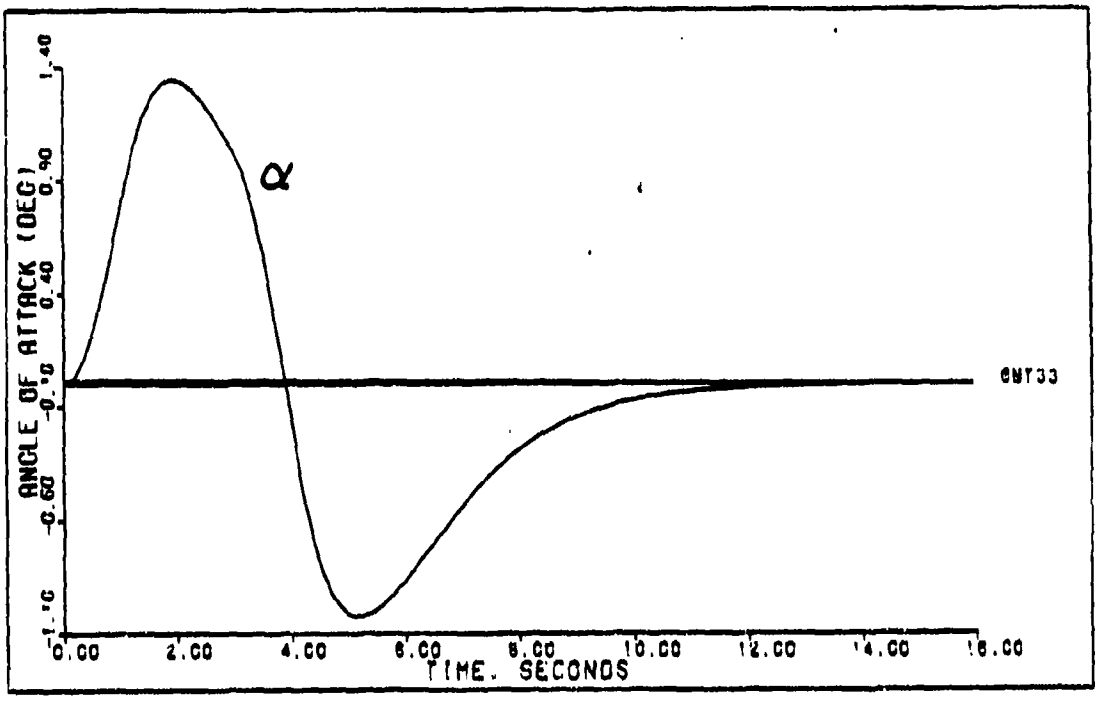

DIRECT CLIMB (0.4M OK FT) ACTUATORS

Figure F-11

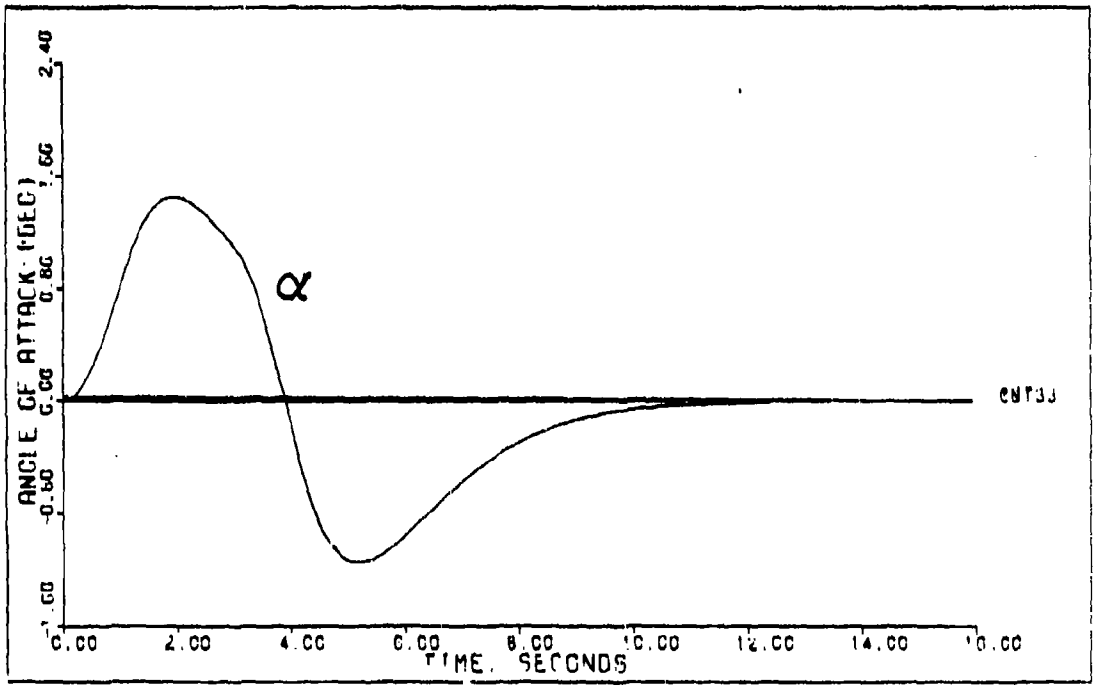

DIRECT CLIMB (0.4M OK FT) DELAY=0.025 ACTUATORS

Figure F-12

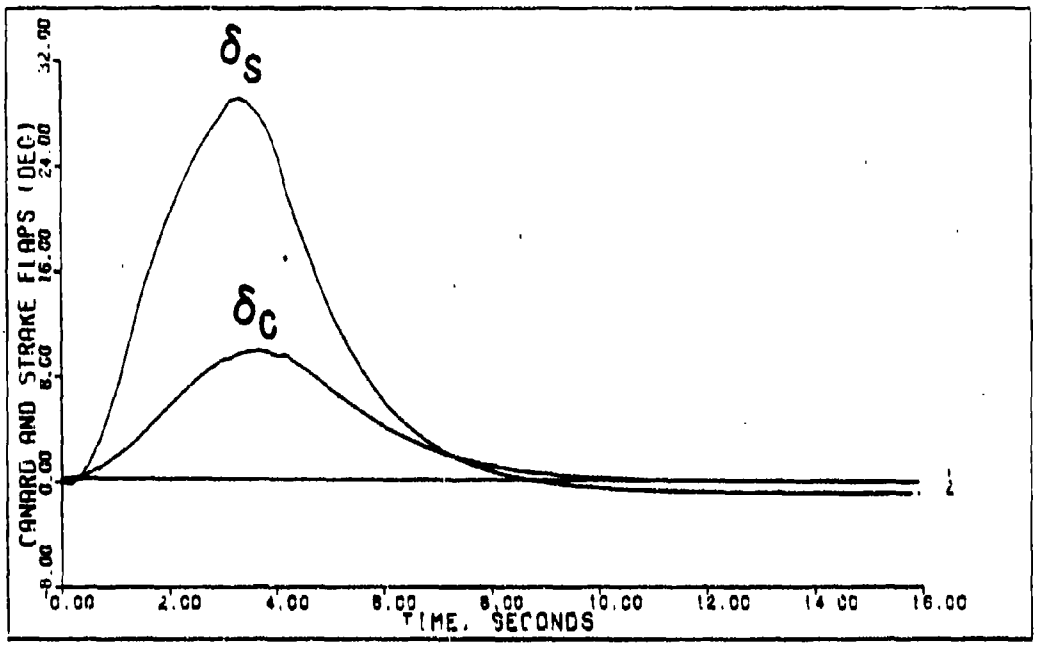

DIRECT CLIMB (0.4M OK FT)

Figure F-13

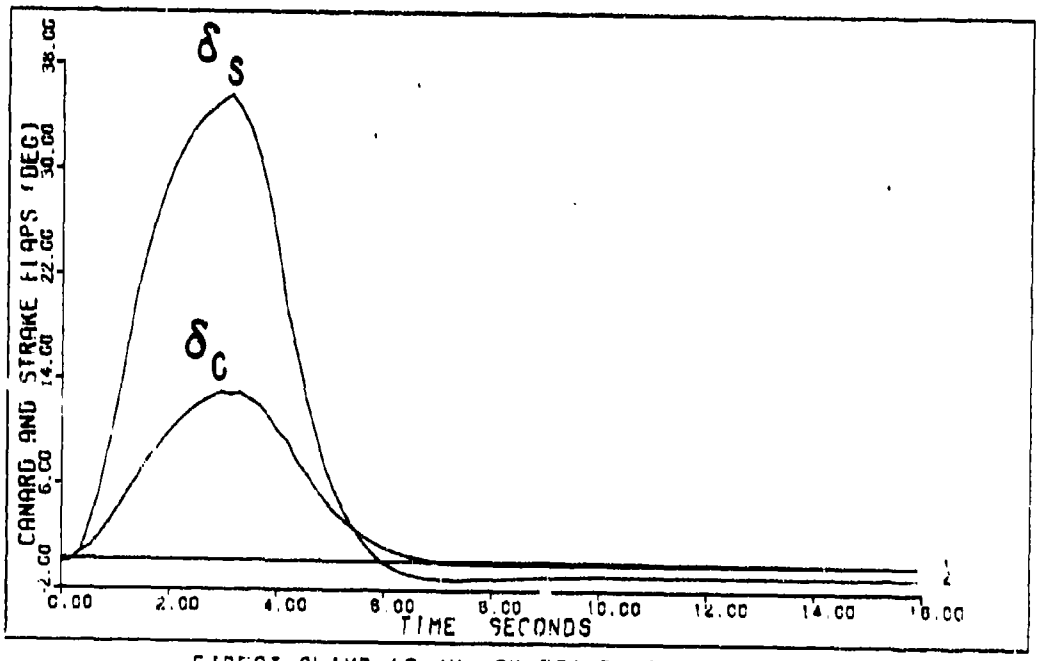

DIRECT CLIMB (0.4M OK FT) DELAY=0.025 SEC

Figure F-14

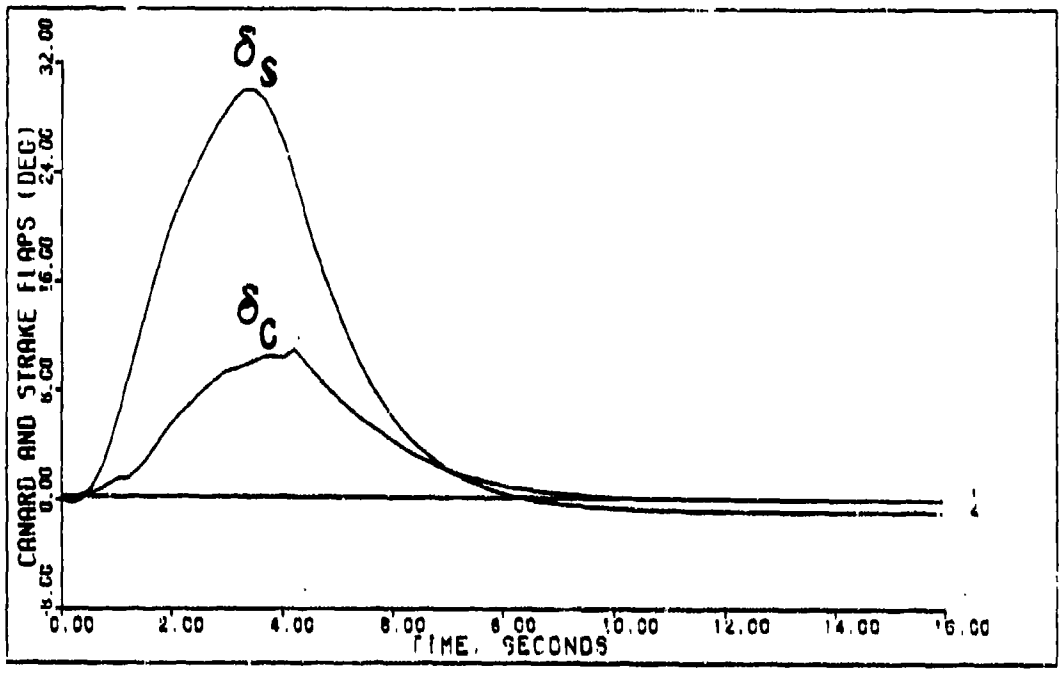

DIRECT CLIMB (0.4M OK FT) ACTUATORS

Figure F-15

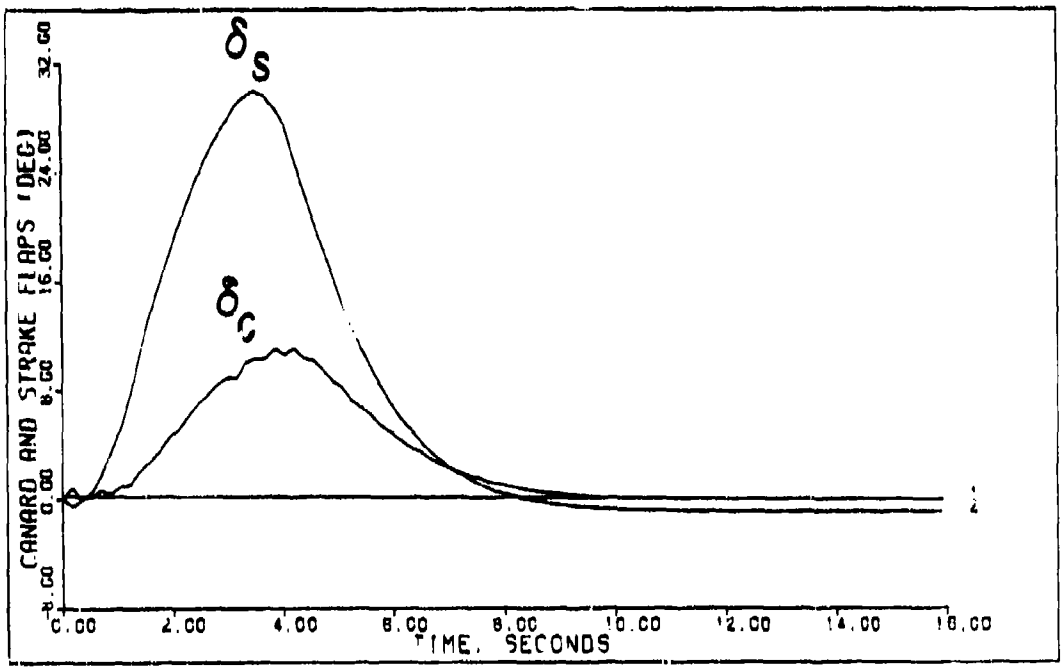

DIRECT CLIMB (0.4M OK FT) DELAY=0.025 ACTUATORS

Figure F-16

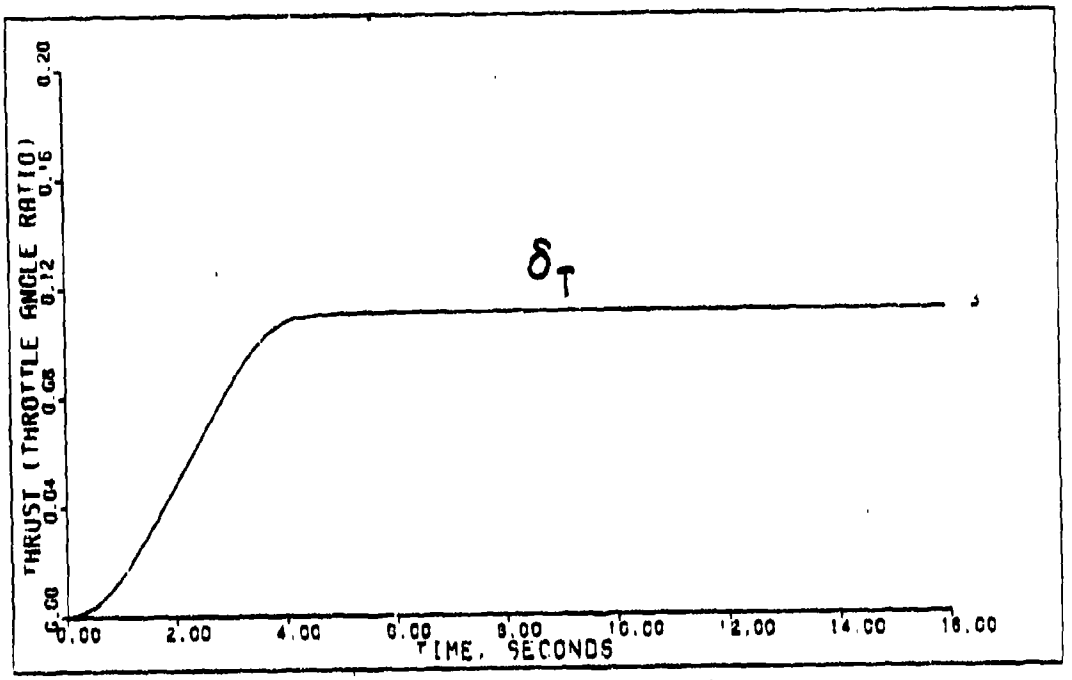

DIRECT CLIMB (0.4M OK FT)

Figure F-17

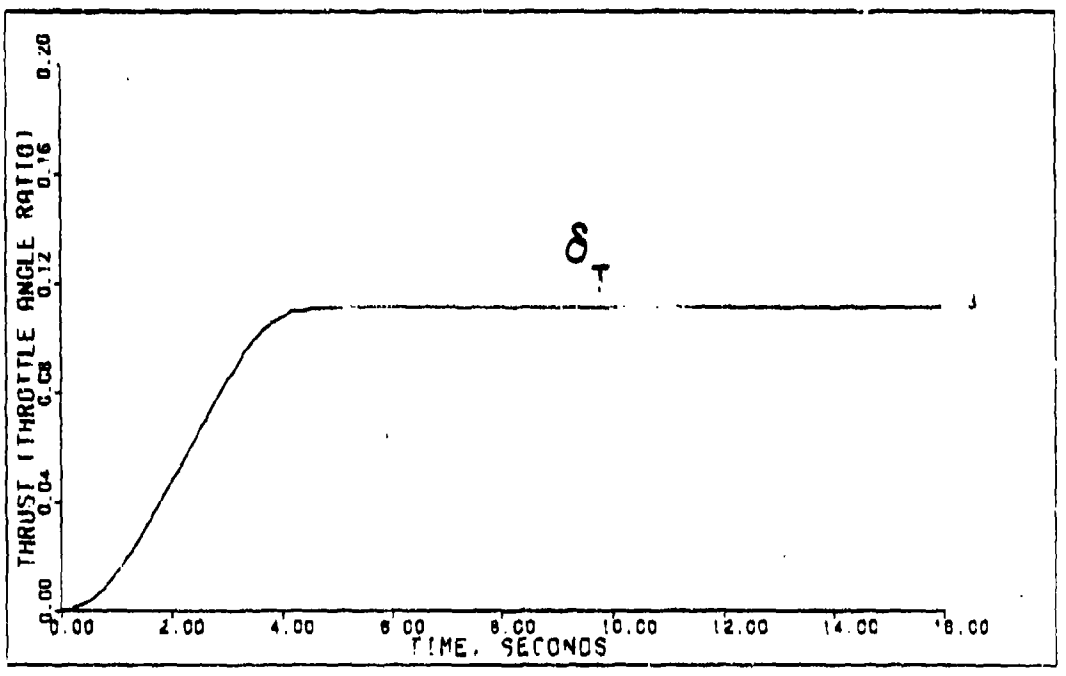

DIRECT CLIMB (0.4M OK FT) DELAY=0.025 SEC

Figure F-18

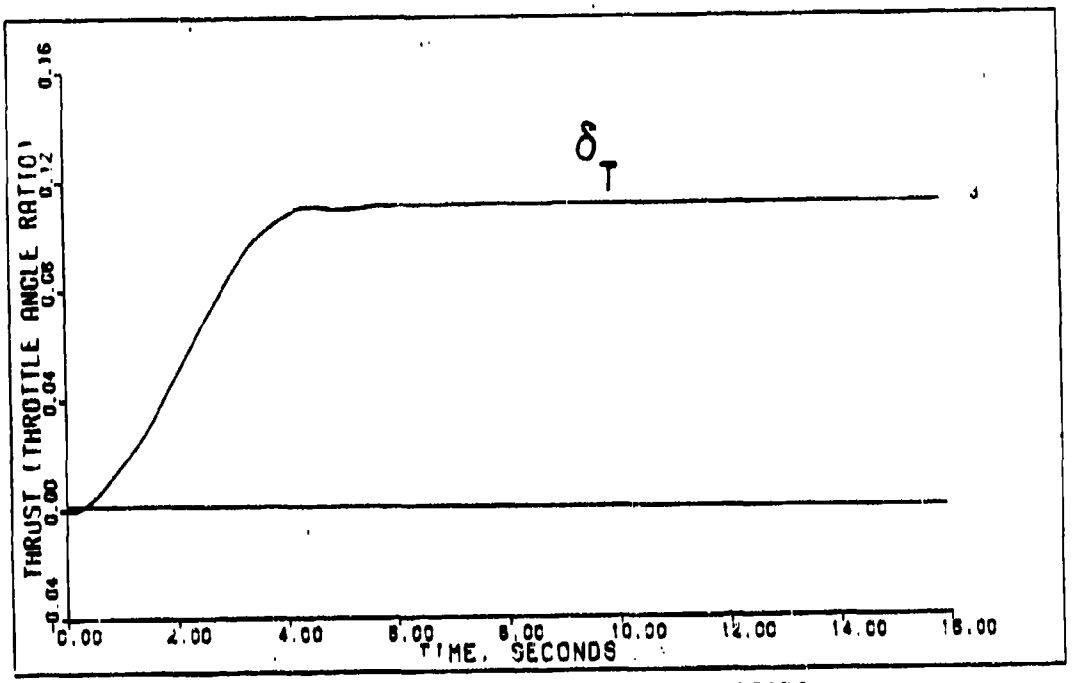

DIRECT CLIMB (0.4M OK FT) ACTUATORS

Figure F-19

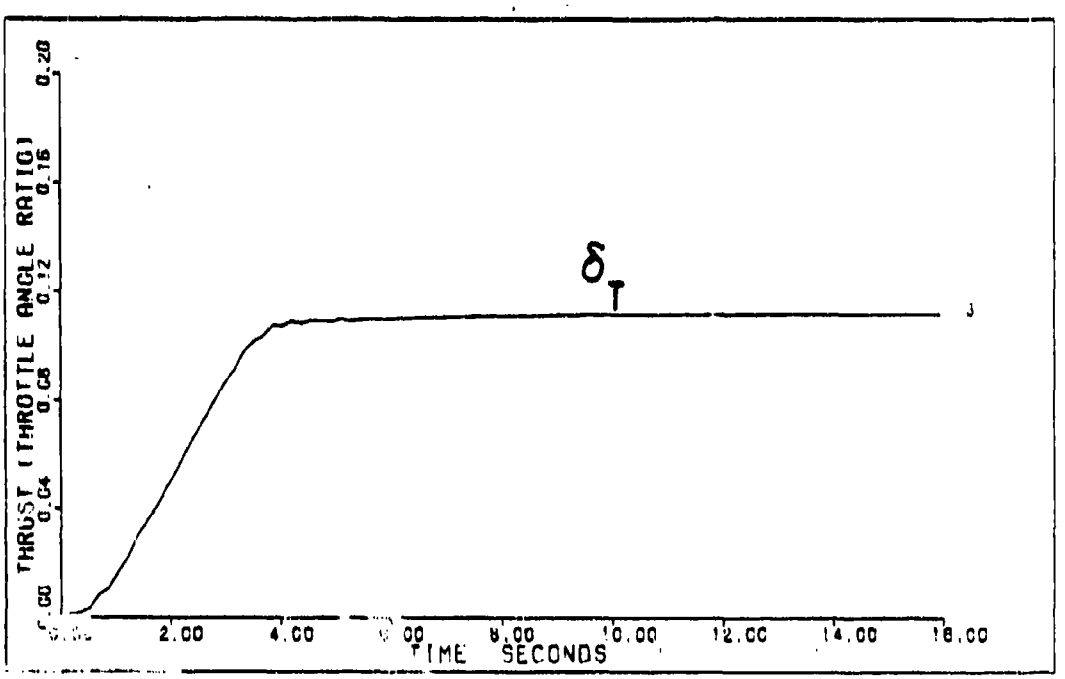

DIRECT CLIMB (0.4M OK FT) DELAY=0.025 ACTUATORS

Figure F-20

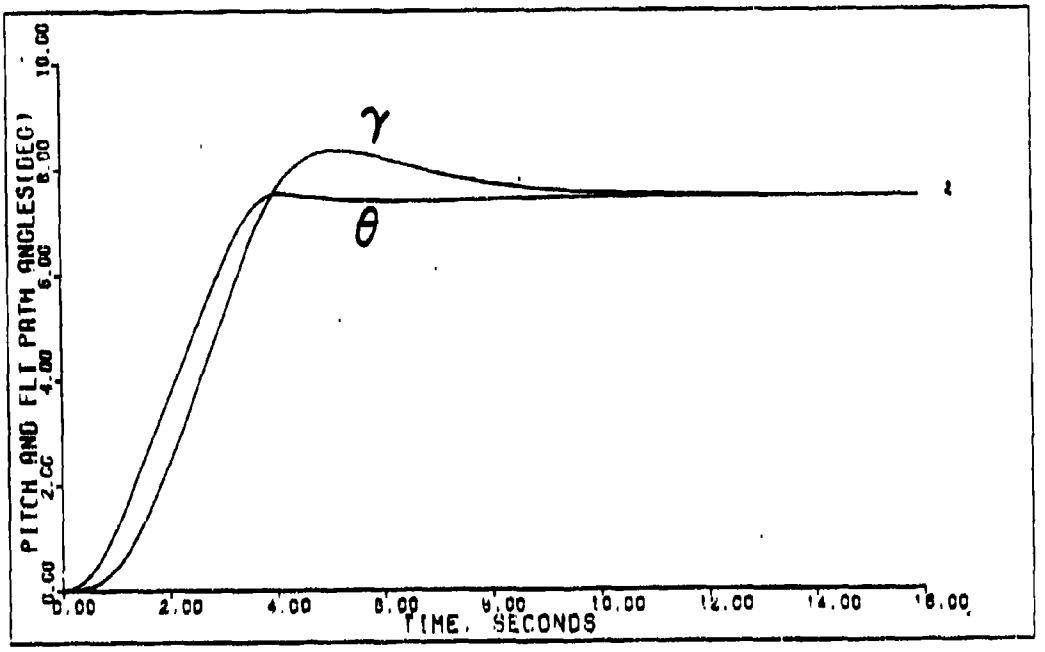

DIRECT CLIMB (0.4M OK FT)

Figure F-21

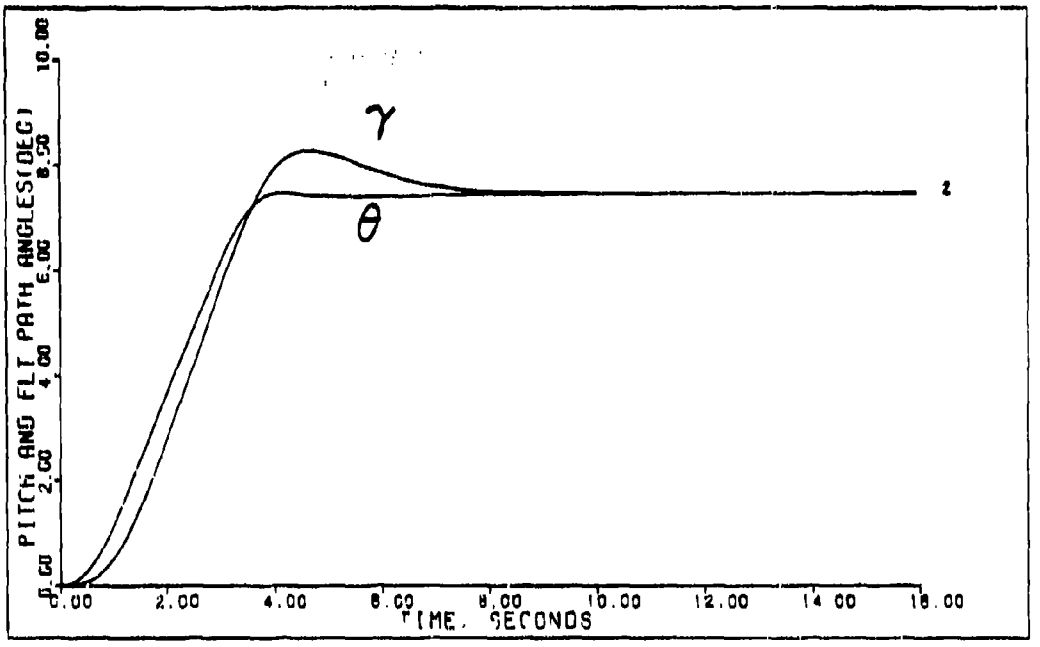

DIRECT CLIMB (0.4M OK FT) DELAY=0.025 SEC

Figure F-22

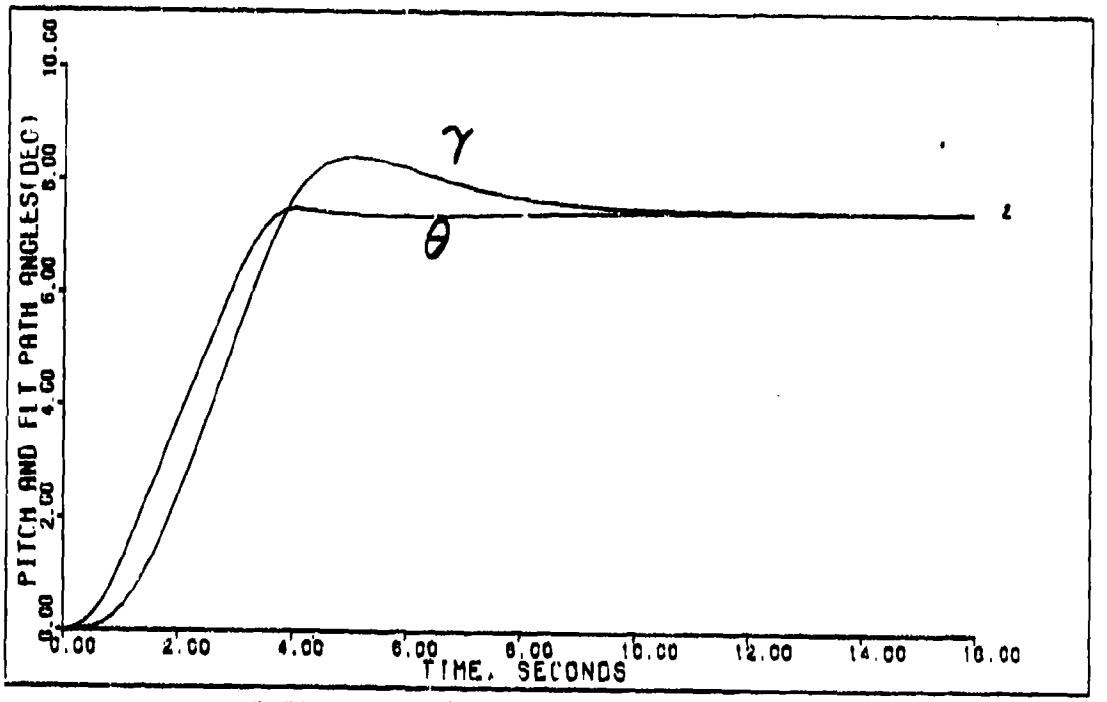

DIRECT CLIMB (0.4M OK FT) ACTUATORS

Figure F-23

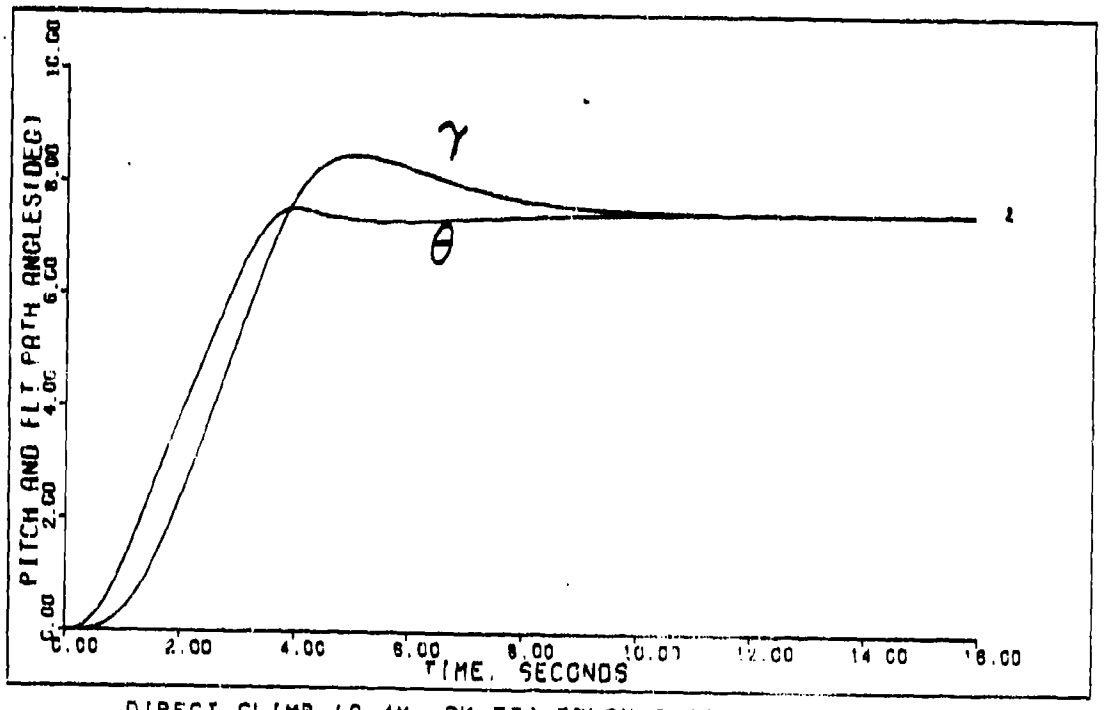

DIRECT CLIMB (0.4M OK FT) DELAY=0.025 SEC ACTUATORS

Figure F-24

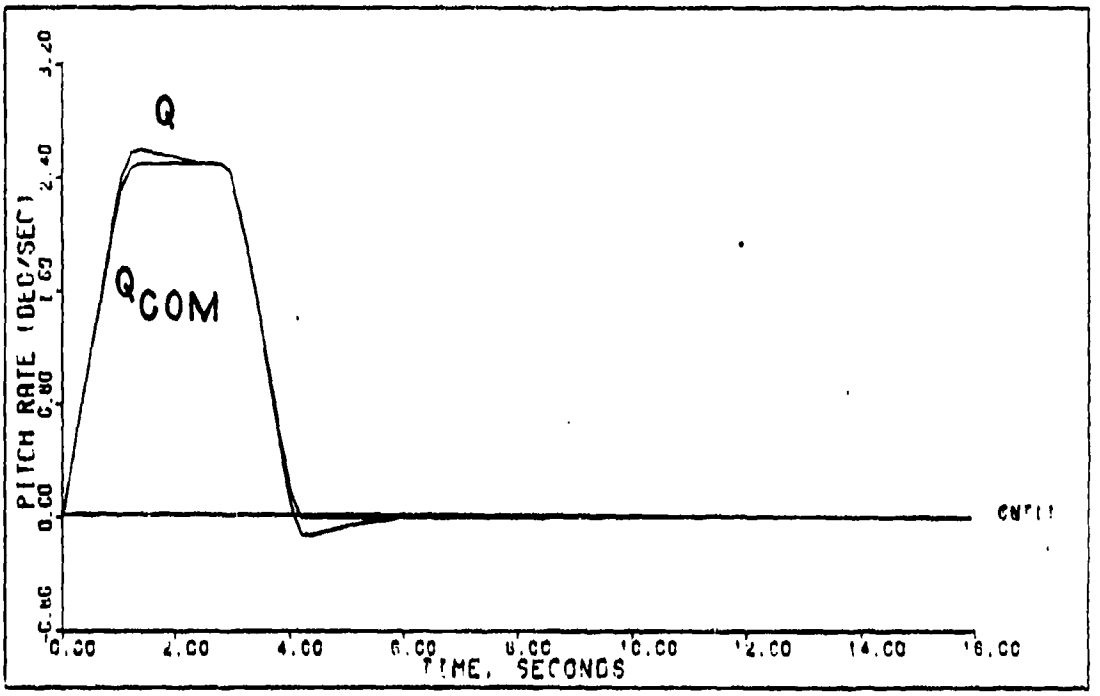

DIRECT CLIMB (1.2M 15K FT)

Figure F-25

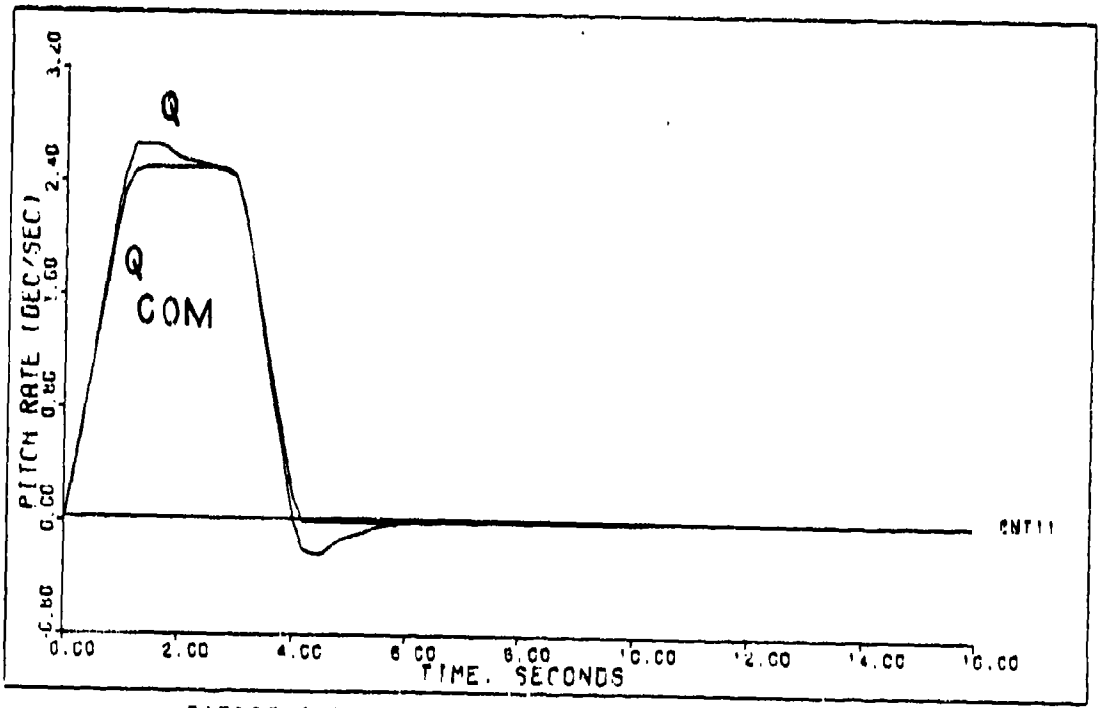

DIRECT CLIMB (1.2M 15K FT) DELAY=0.025 SEC

Figure F-26

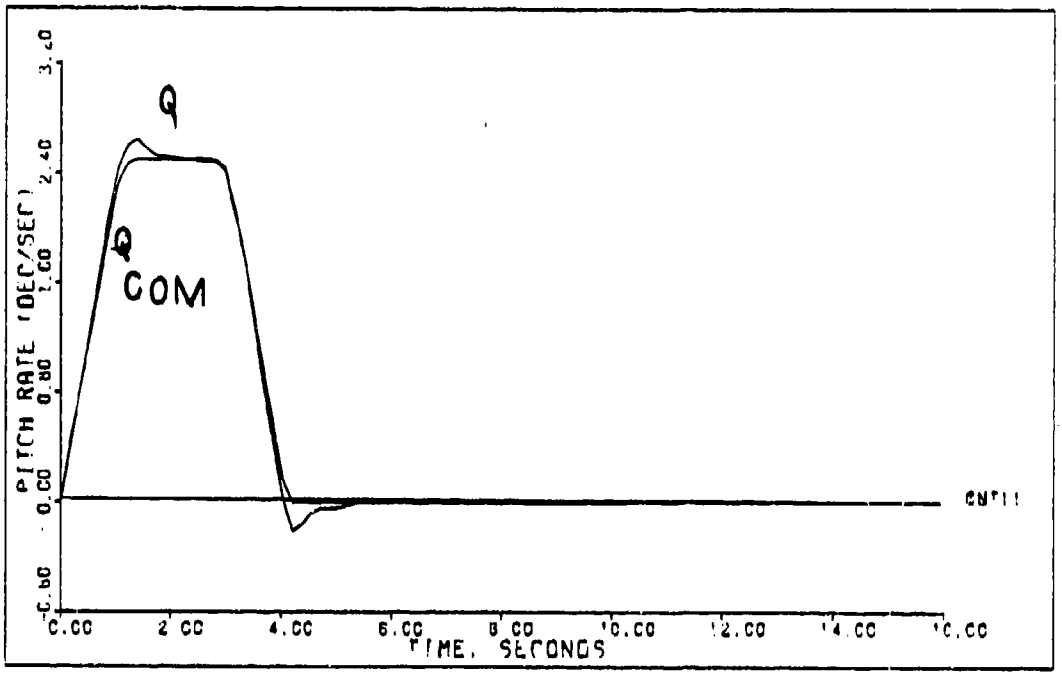

DIRECT CLIMB (1.2M 15K FT) ACTUATORS

Figure F-27

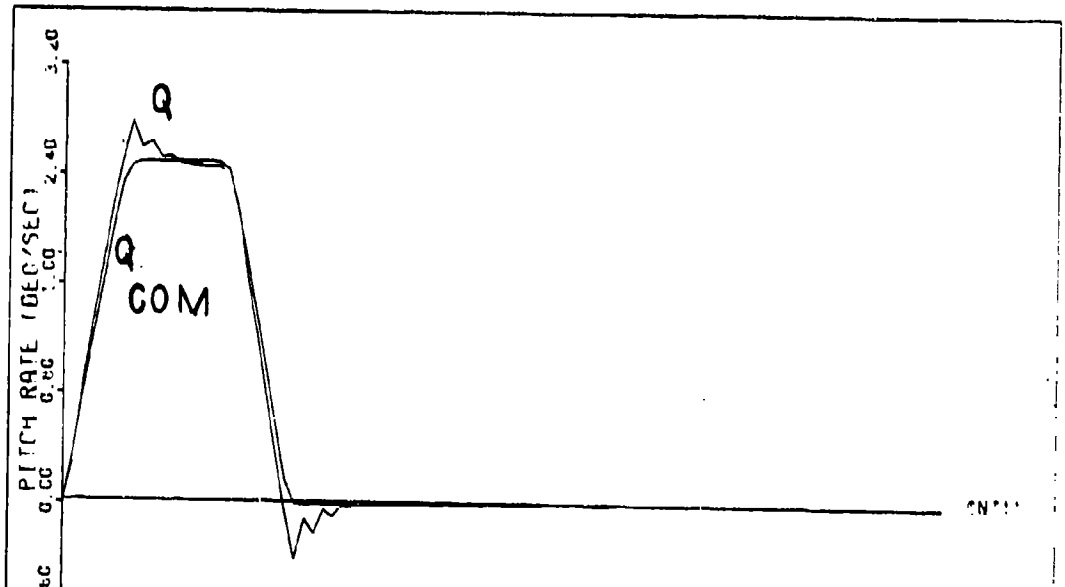

DIRECT CLIMB (1.2M 15K FT) DELAY=0.025 SEC ACTUATORS

Figure F-28

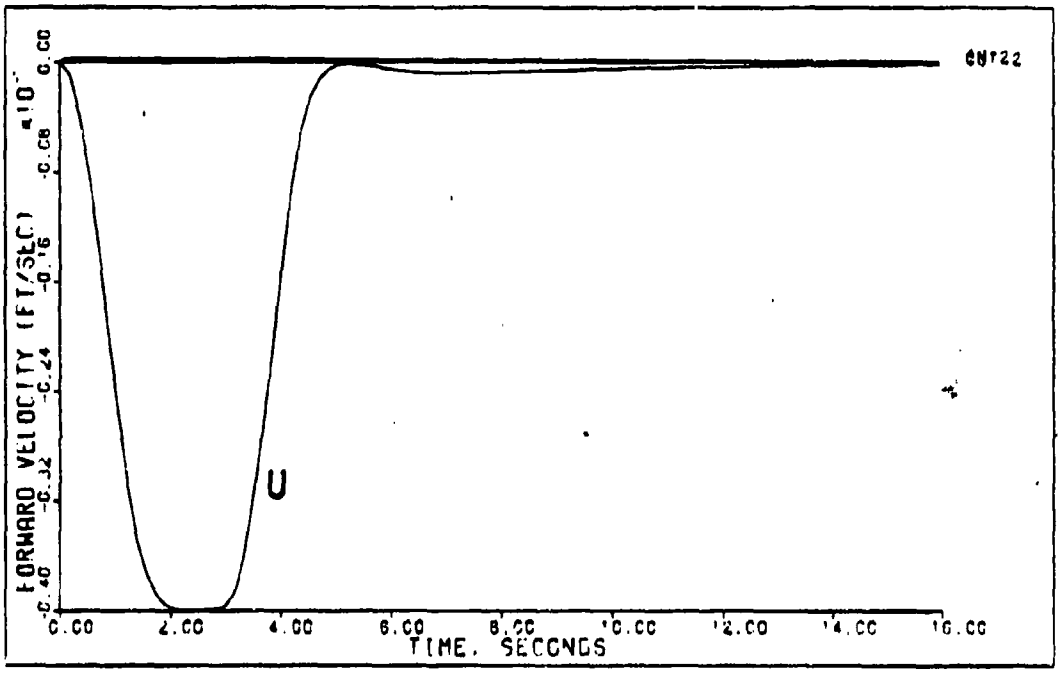

DIRECT CLIMB (1.2M 15K FT)

Figure F-29

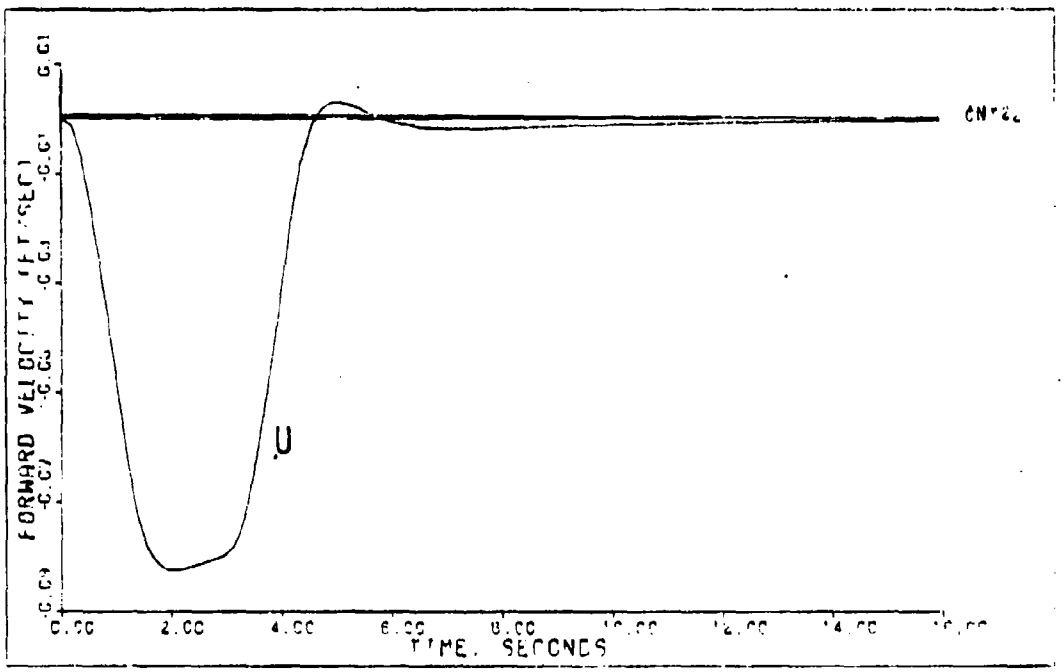

DIRECT CLIMB (1.2M 15K FT) DELAY=0.025 SEC

Figure F-30

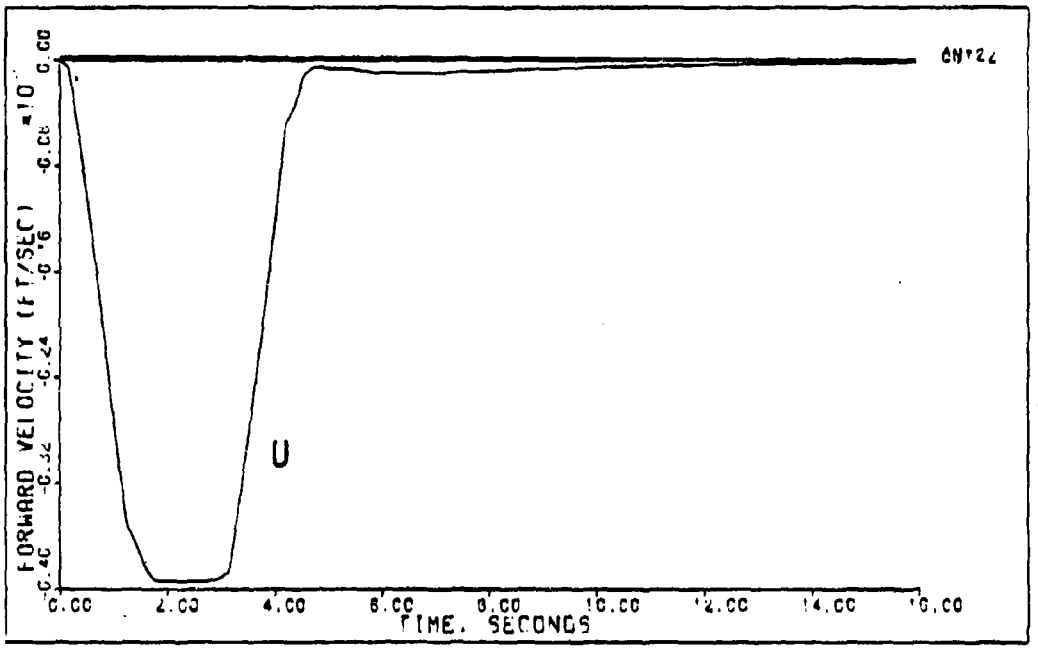

DIRECT CLIMB (1.2M 15K FT) ACTUATORS

Figure F-31

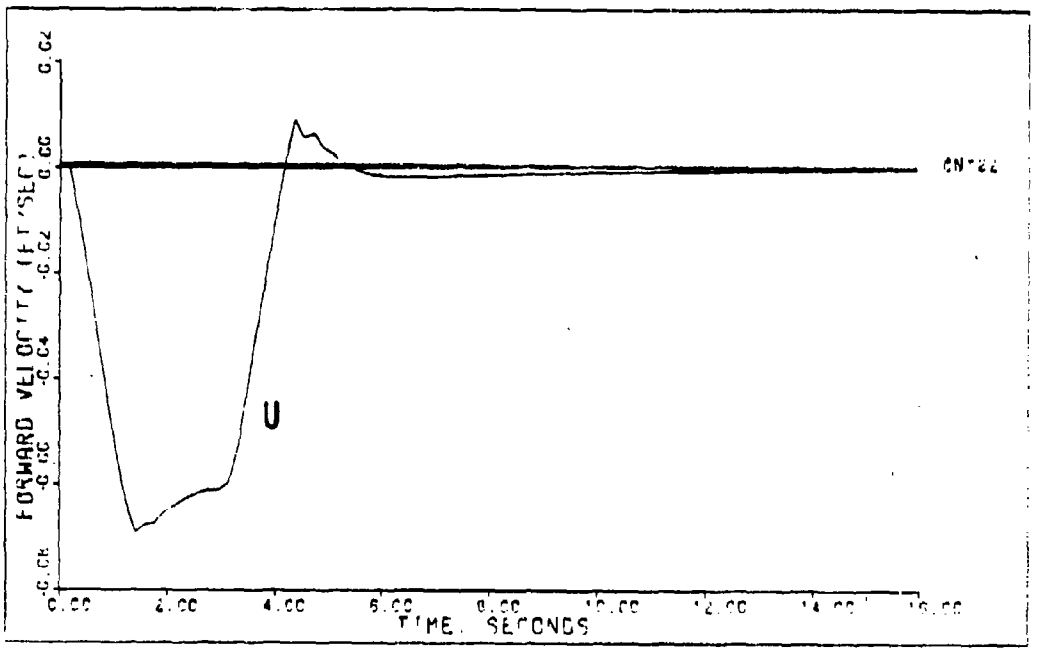

DIRECT CLIMB (1.2M 15K FT) DELAY=0.025 SEC ACTUATORS

Figure F-32

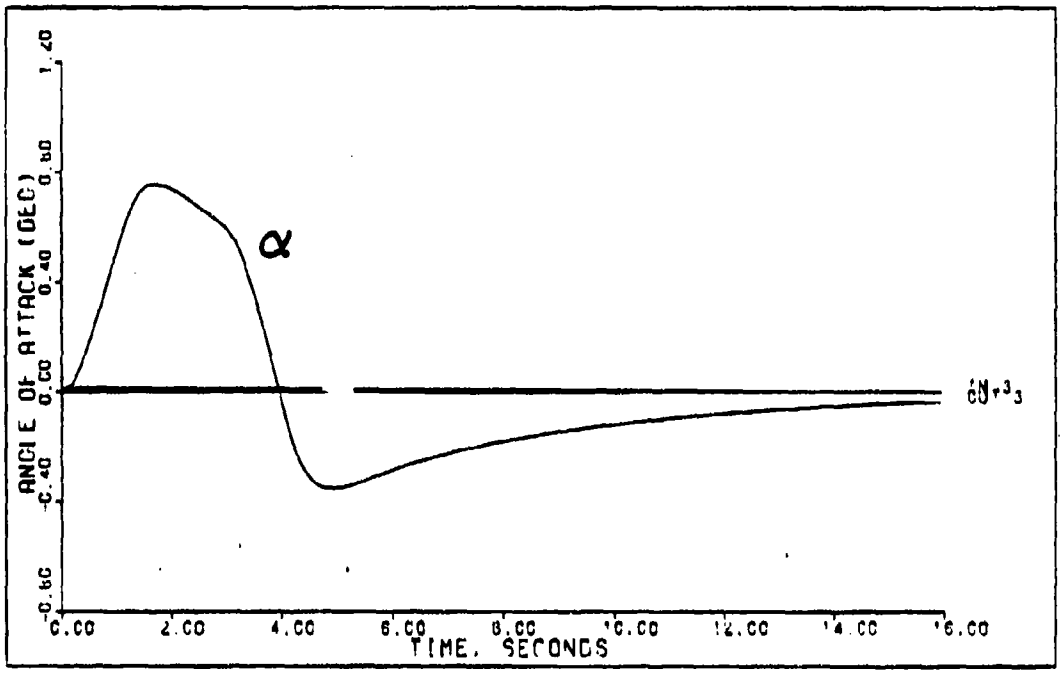

DIRECT CLIMB (1.2M 15K FT)

Figure F-33

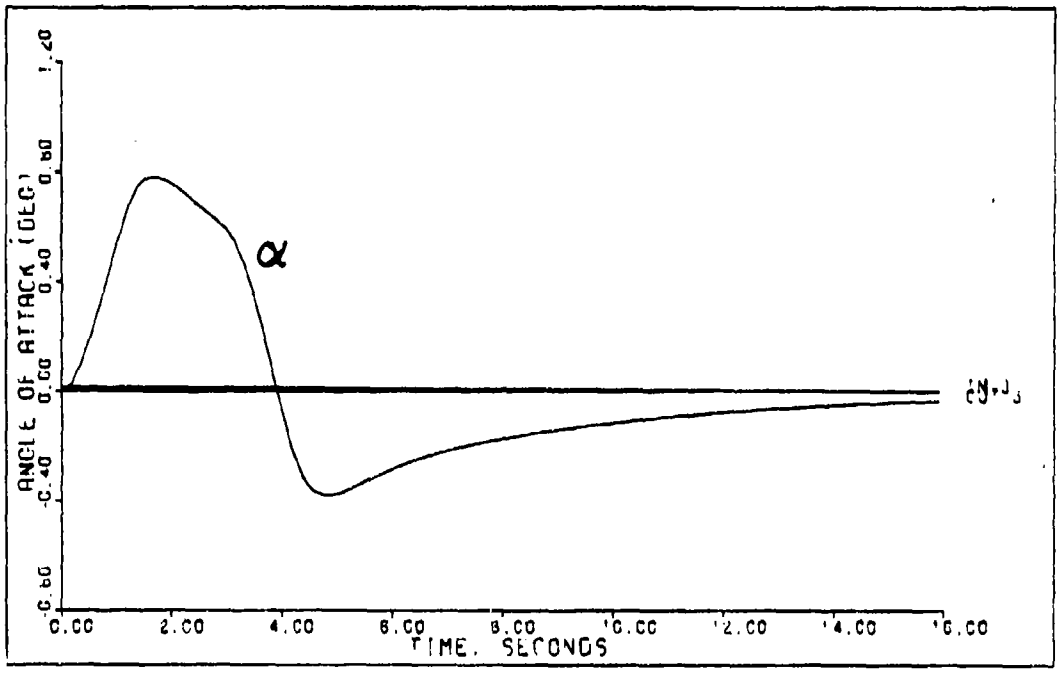

DIRECT CLIMB (1.2M 15K FT) DELAY=0.025 SEC

Figure F-34

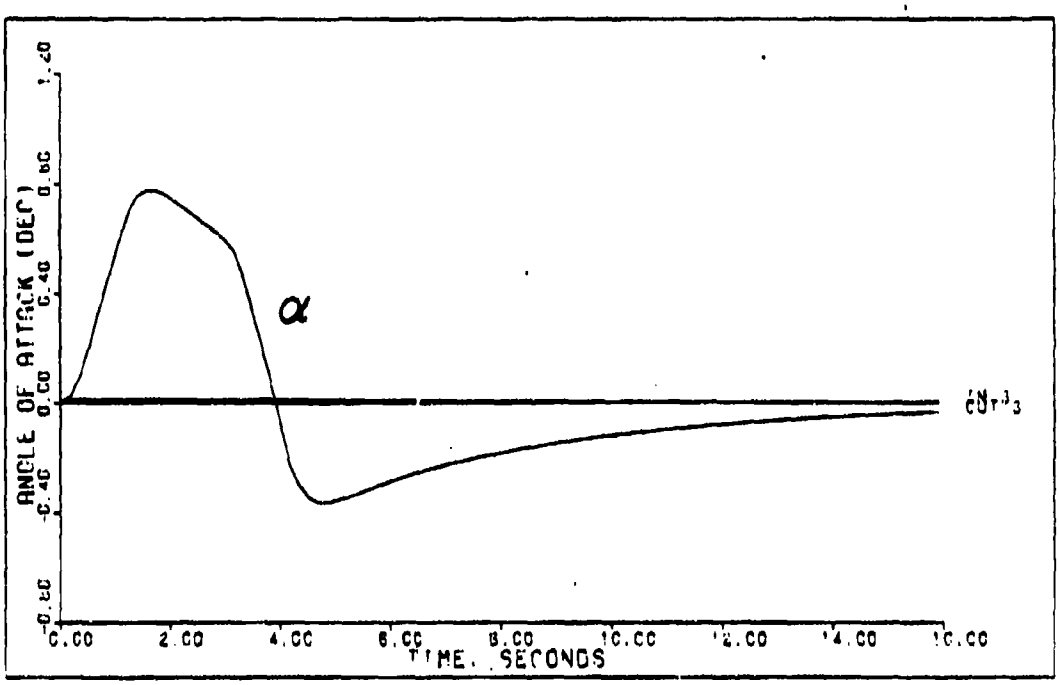

DIRECT CLIMB (1.2M 15K FT) ACTUATORS

Figure F-35

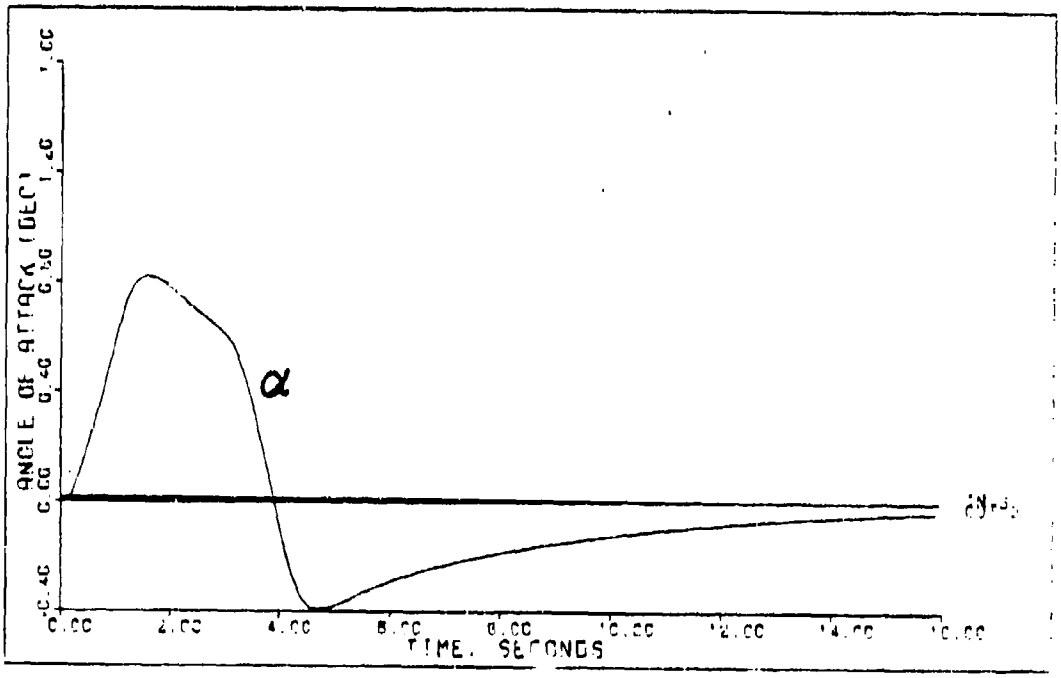

DIRECT CLIMB (1.2M 15K FT) DELAY=0.025 SEC ACTUATORS

Figure F-36

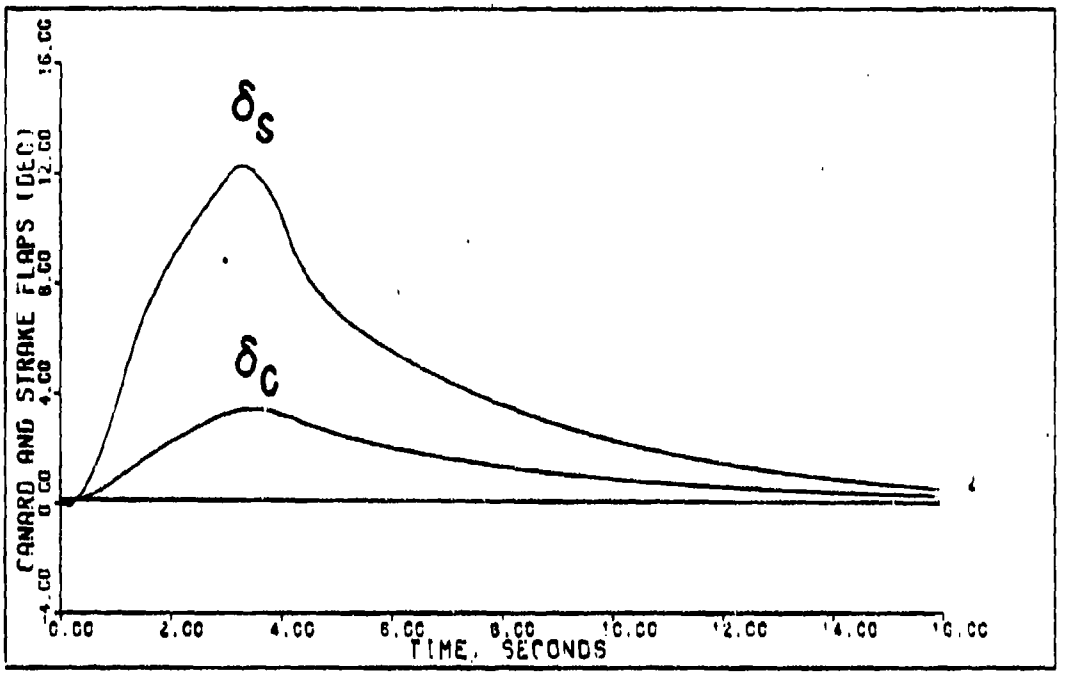

DIRECT CLIMB (1.2M 15K FT)

Figure F-37

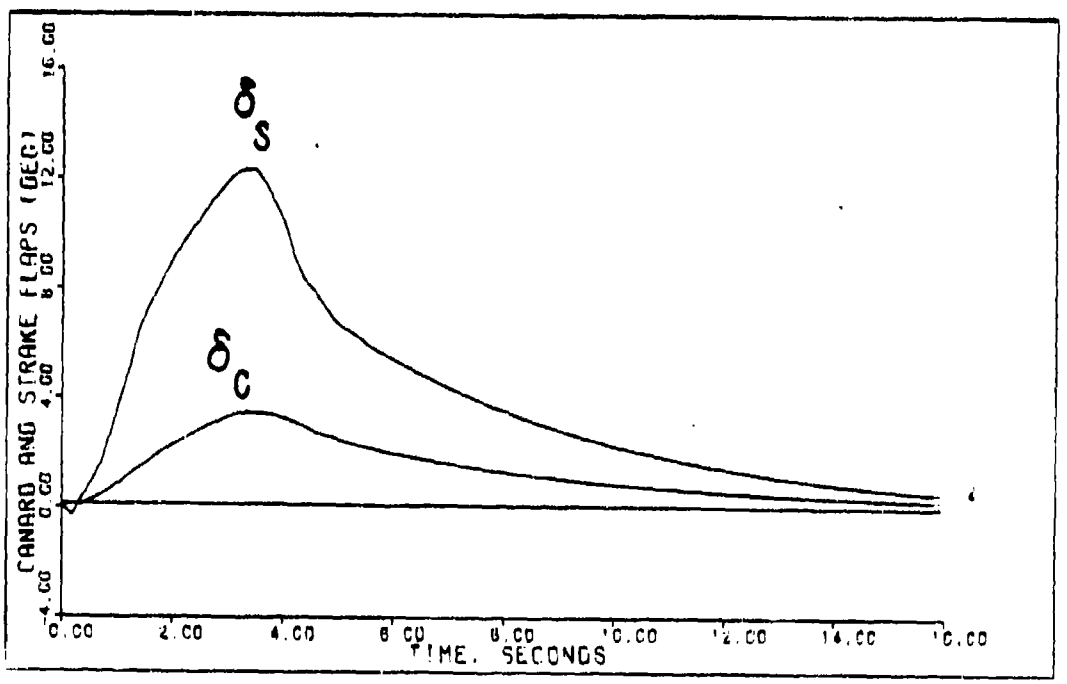

DIRECT CLIMB (1.2M 15K FT) DELAY=0.025 SEC

Figure F-38

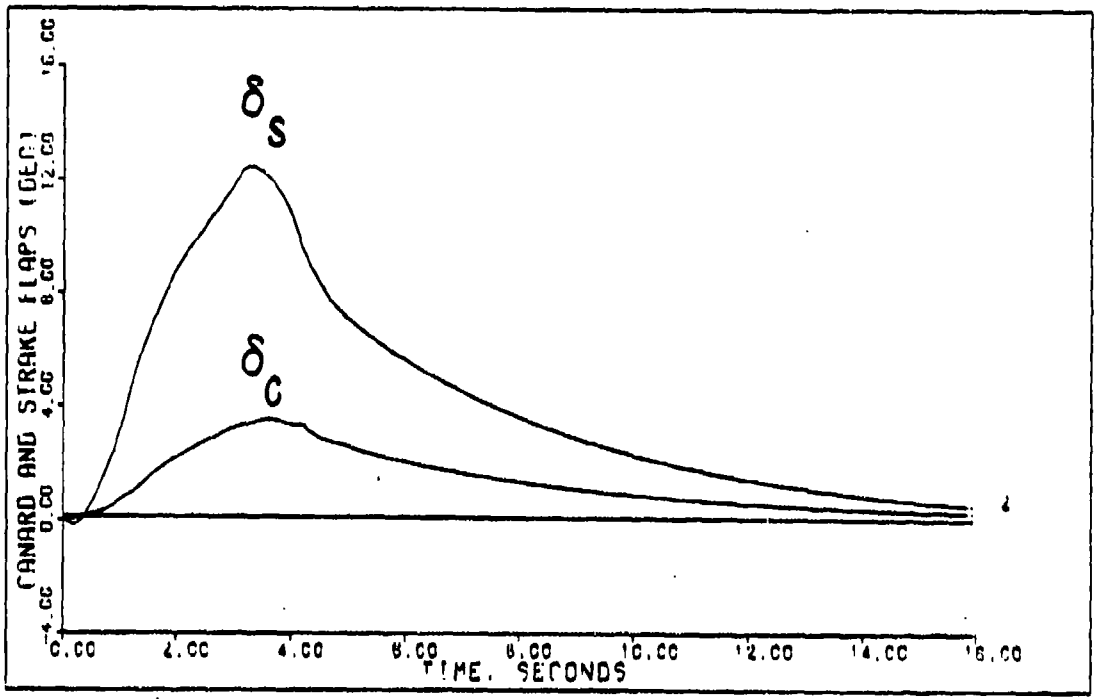

DIRECT CLIMB (1.2M 15K FT) ACTUATORS

Figure F-39

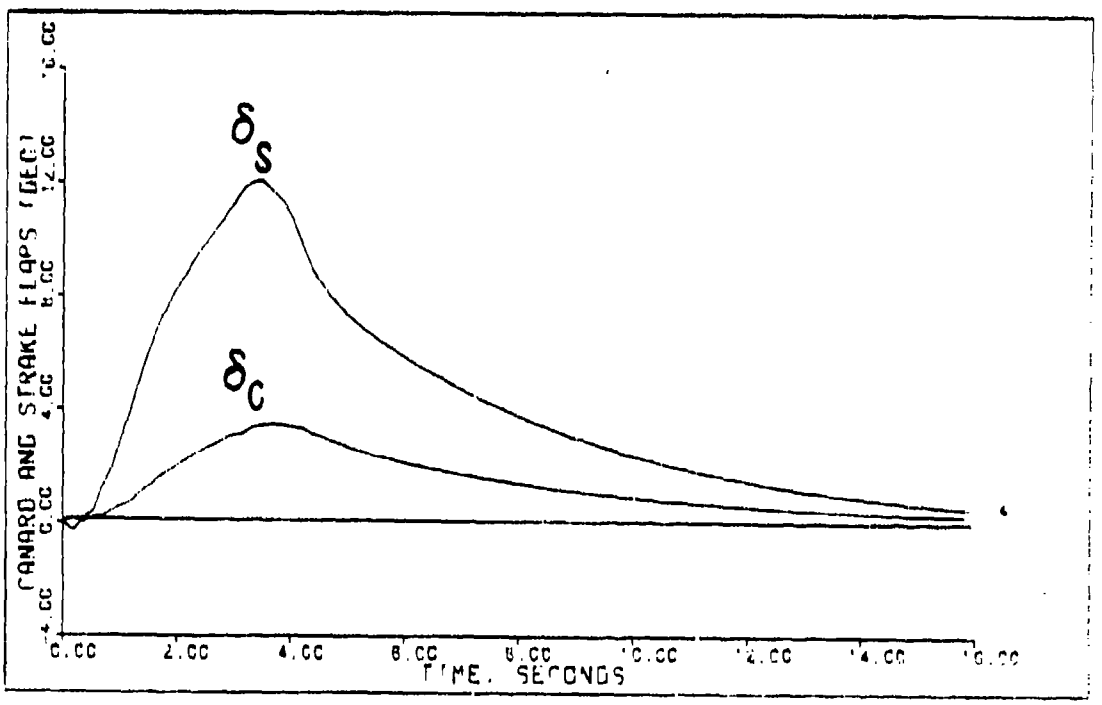

DIRECT CLIMB (1.2M 15K FT) DELAY=0.025 SEC ACTUATORS

Figure F-40

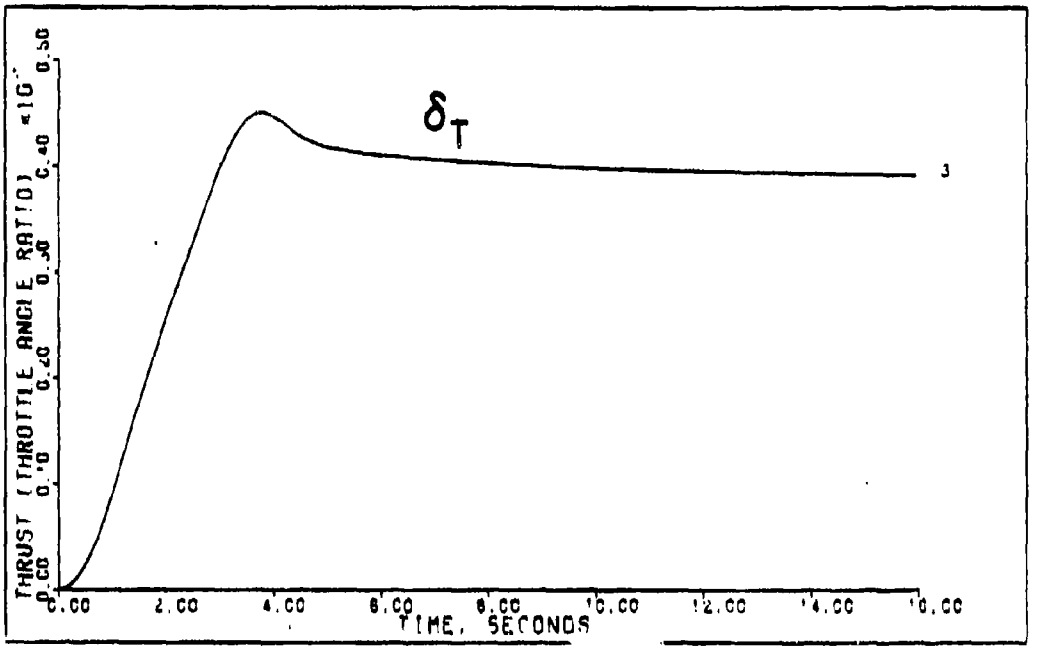

DIRECT CLIMB (1.2M [illegible] FT)

Figure F-

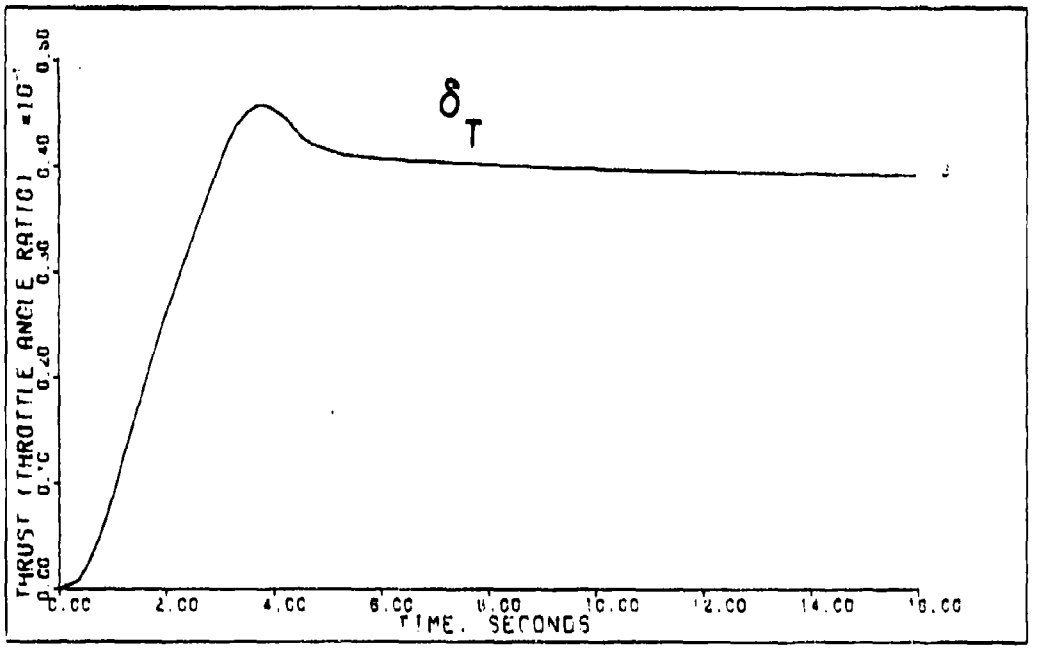

DIRECT CLIMB (1.2M 15K FT) DELAY=0.025 SEC

Figure F-42

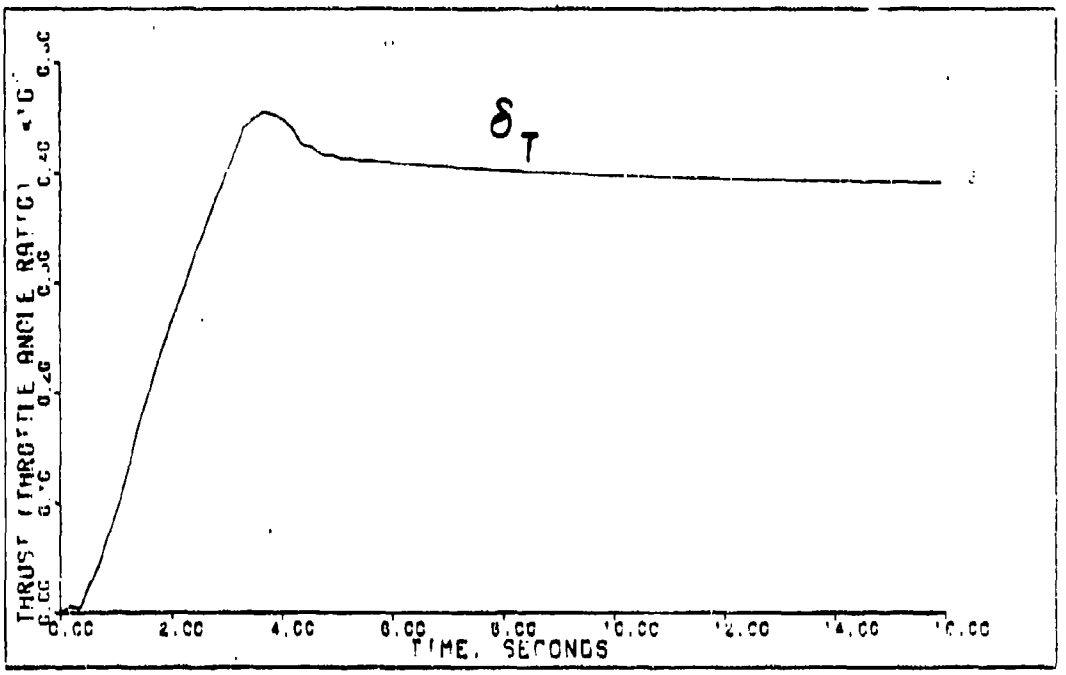

DIRECT CLIMB (1.2M 15K FT) DELAY=0.025 SEC ACTUATORS

Figure F-43

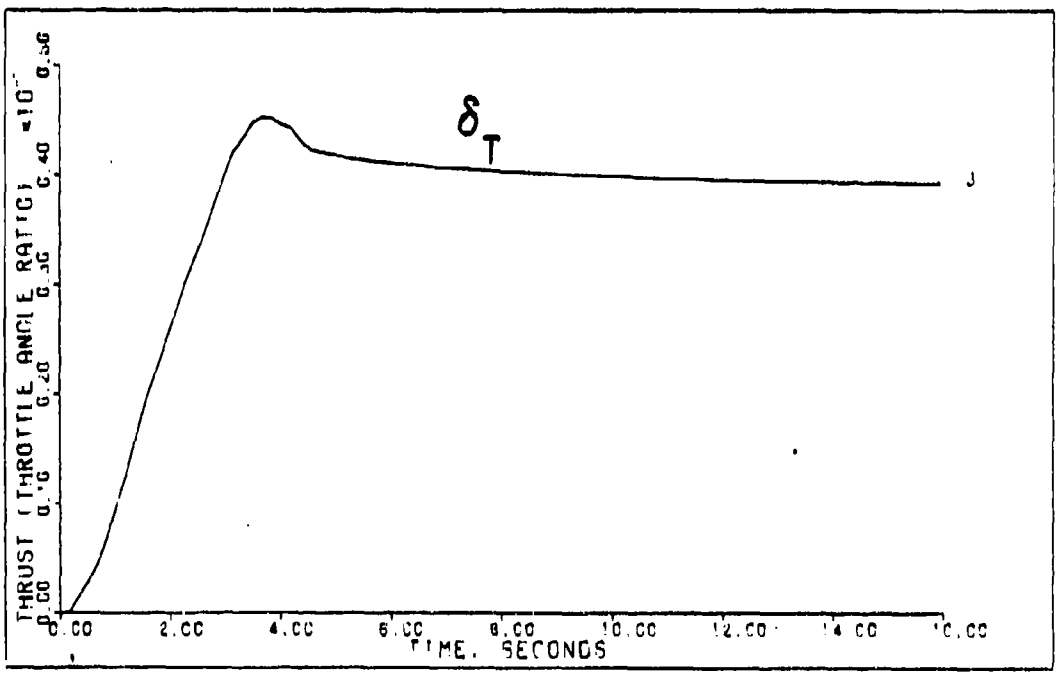

DIRECT CLIMB (1.2M 15K FT) ACTUATORS

Figure F-44

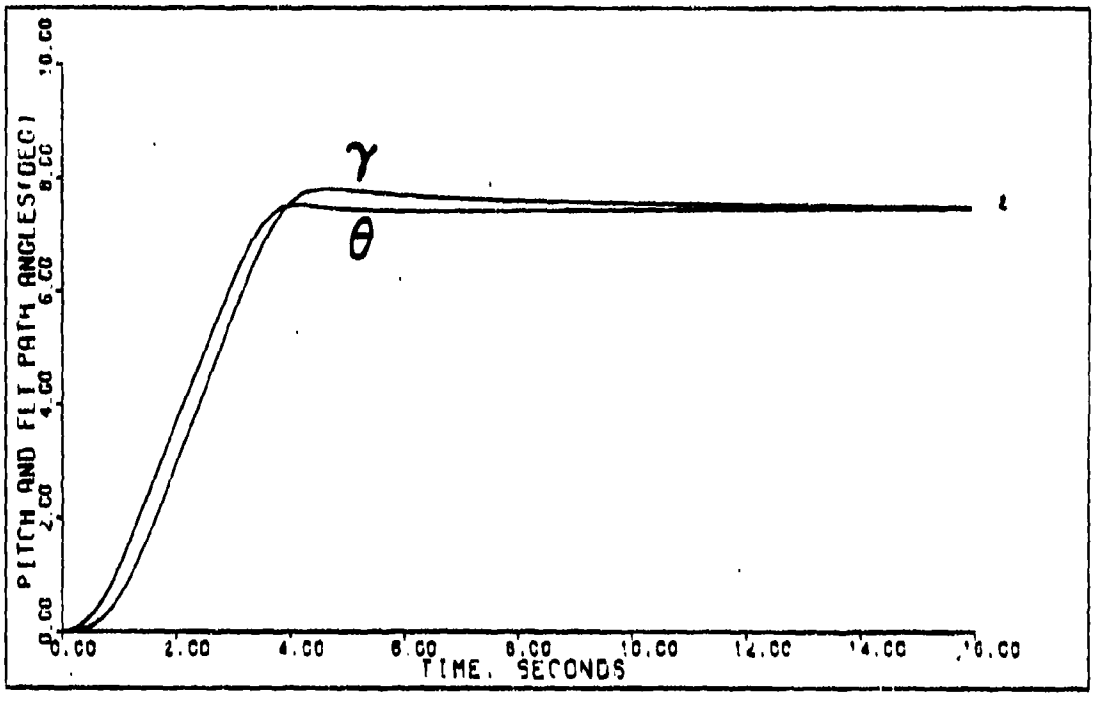

DIRECT CLIMB (1.2M 15K FT)

Figure F-45

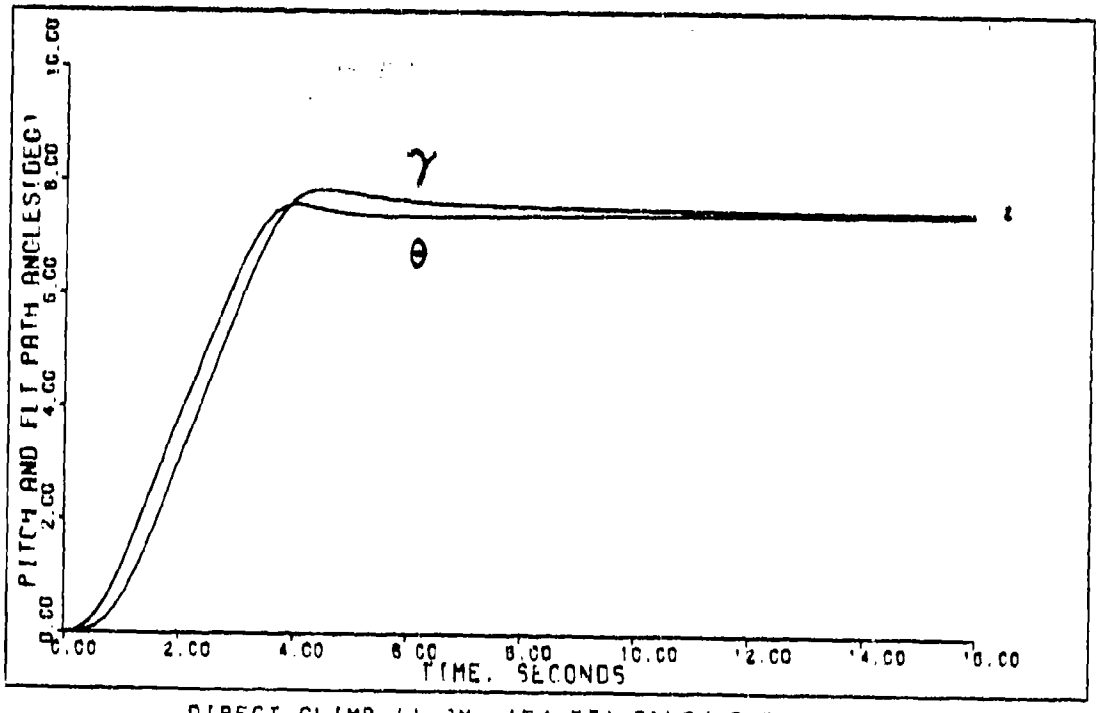

DIRECT CLIMB (1.2M 15K FT) DELAY=0.025 SEC

Figure F-46

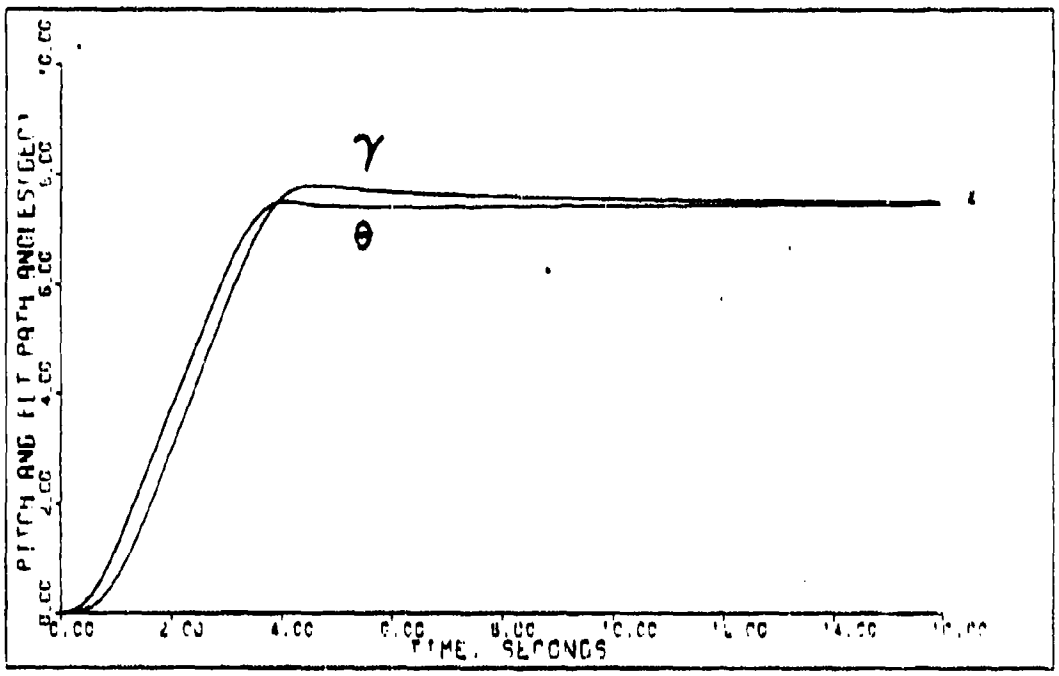

DIRECT CLIMB (1.2M 16K FTI ACTUATORS

Figure F-47

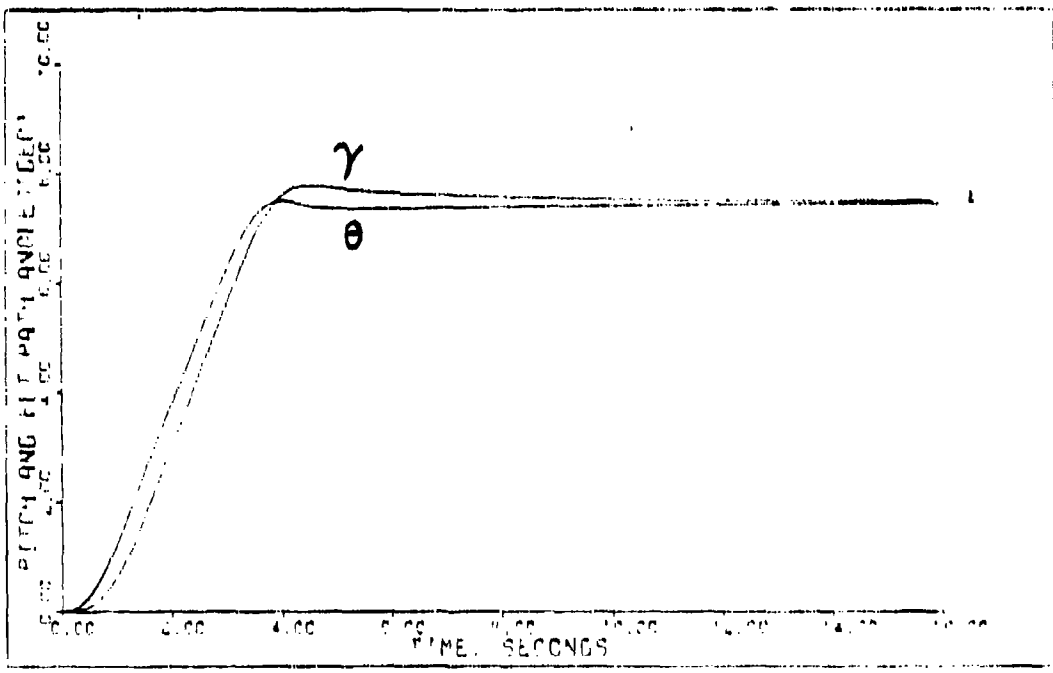

DIRECT CLIMB (1.2M 16K FTI DELTA/0.020 SEC ACTUATORS

Figure F-48

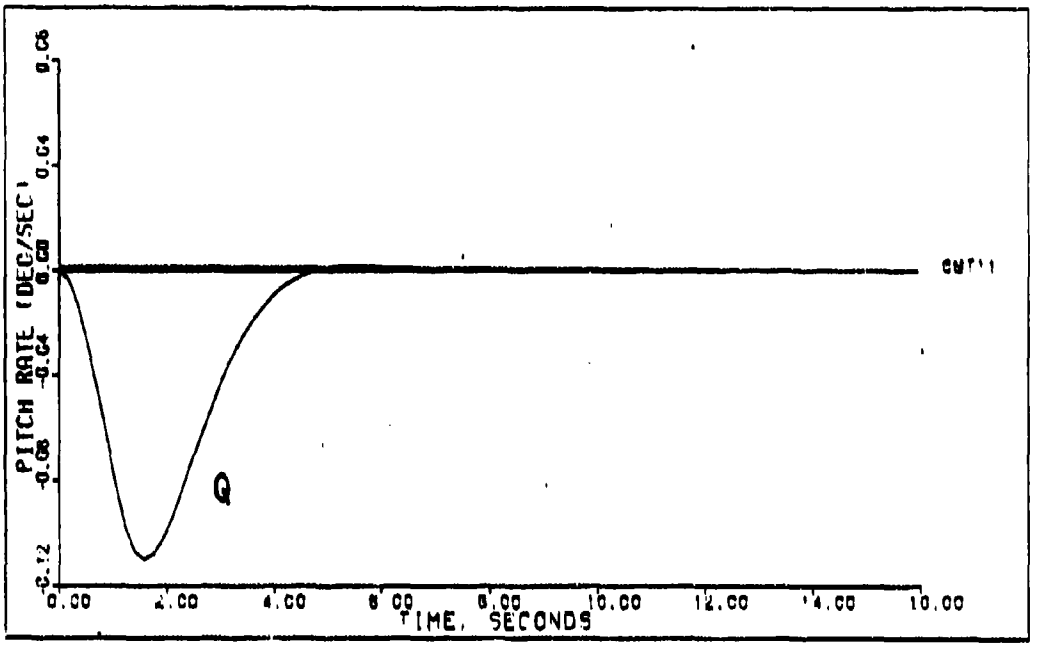

VERTICAL TRANSLATION (0.7M 15K FT)

Figure F-49

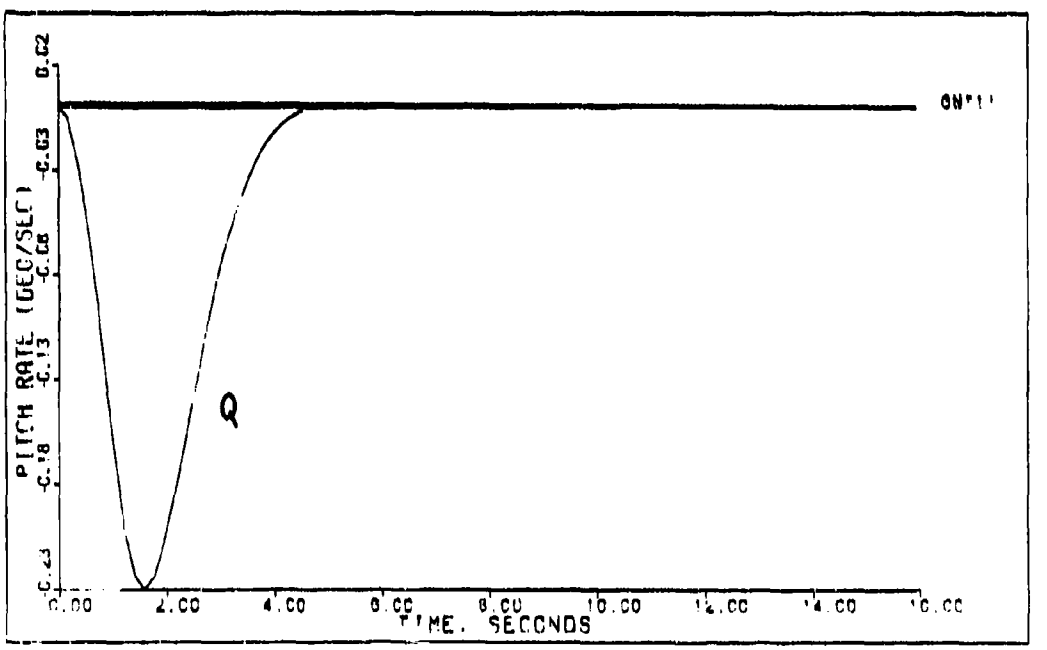

VERTICAL TRANSLATION (0.7M 15K FT) DELAY=0.025 SEC

Figure F-50

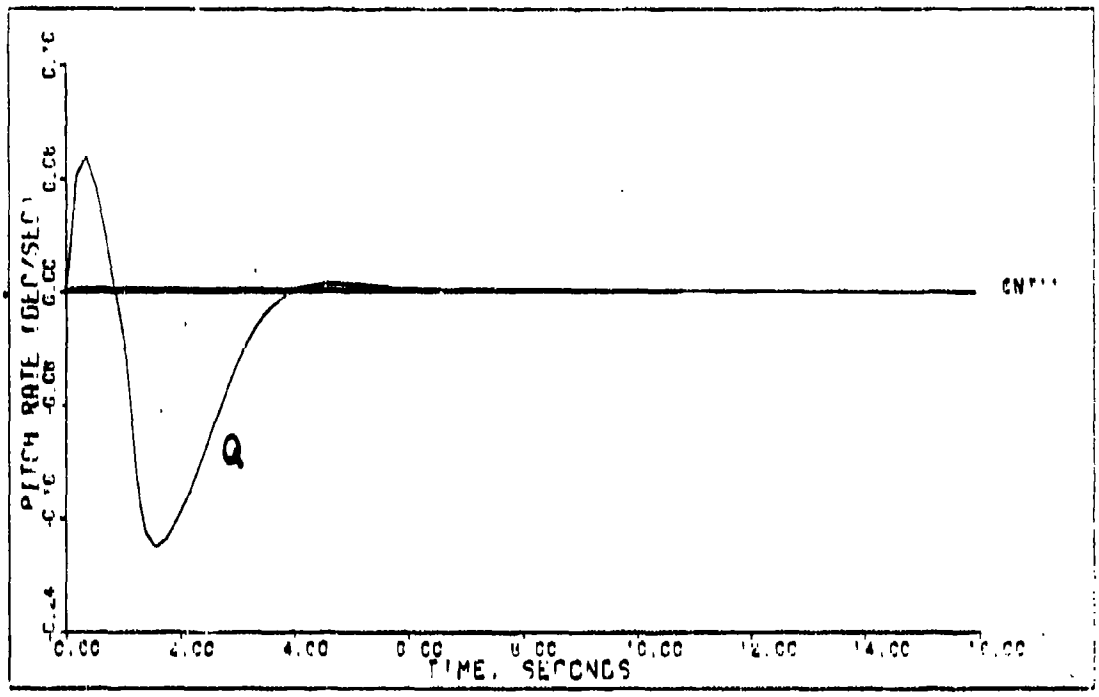

VERTICAL TRANSLATION (0.7M 15K FT) ACTUATORS

Figure F-51

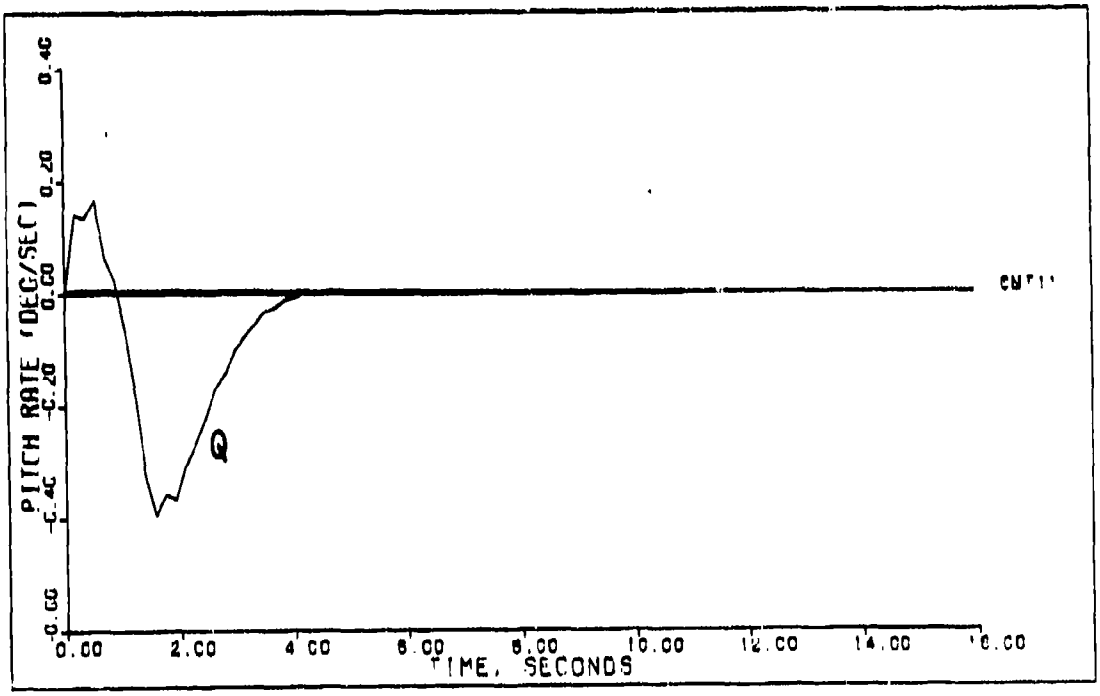

VERTICAL TRANSLATION (0.7M 15K FT) DELAY=0.025 SEC ACTUATORS

Figure F-52

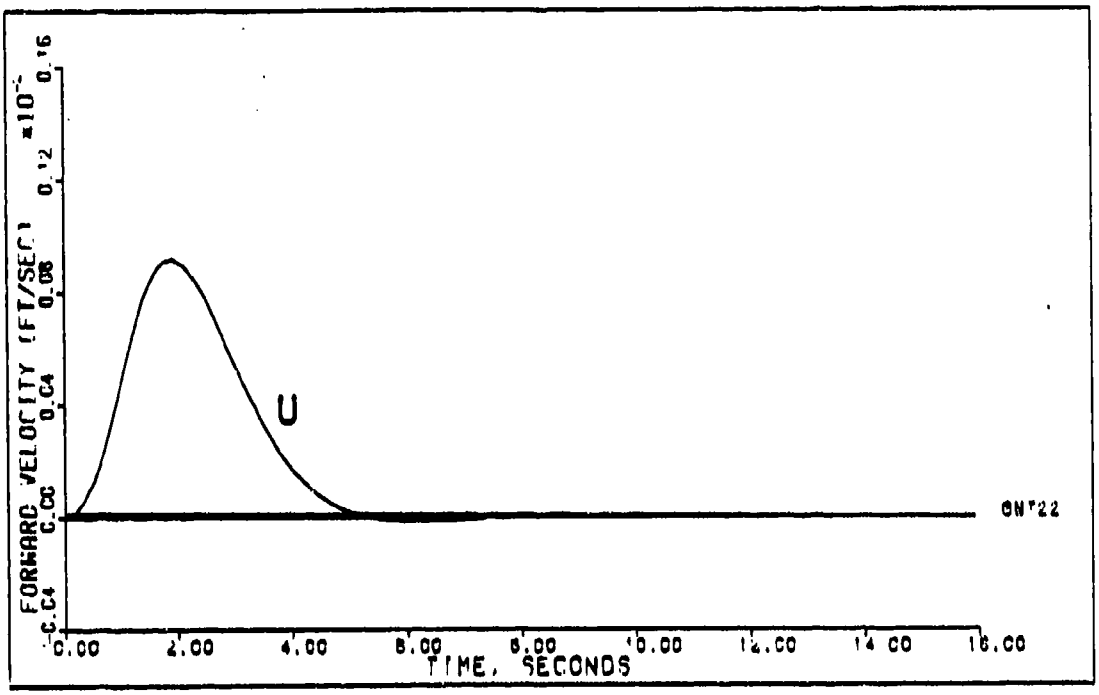

VERTICAL TRANSLATION (0./M 15K FT)

Figure F-53

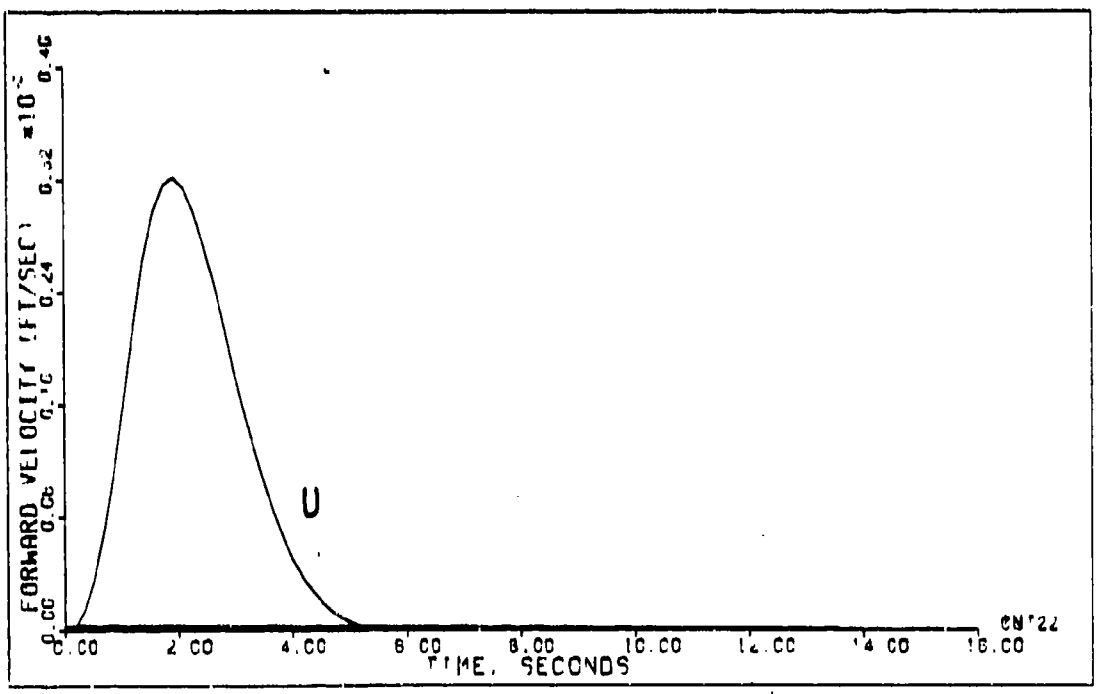

VERTICAL TRANSLATION (0./M 15K FT) DELAY=0.025 SEC

Figure F-54

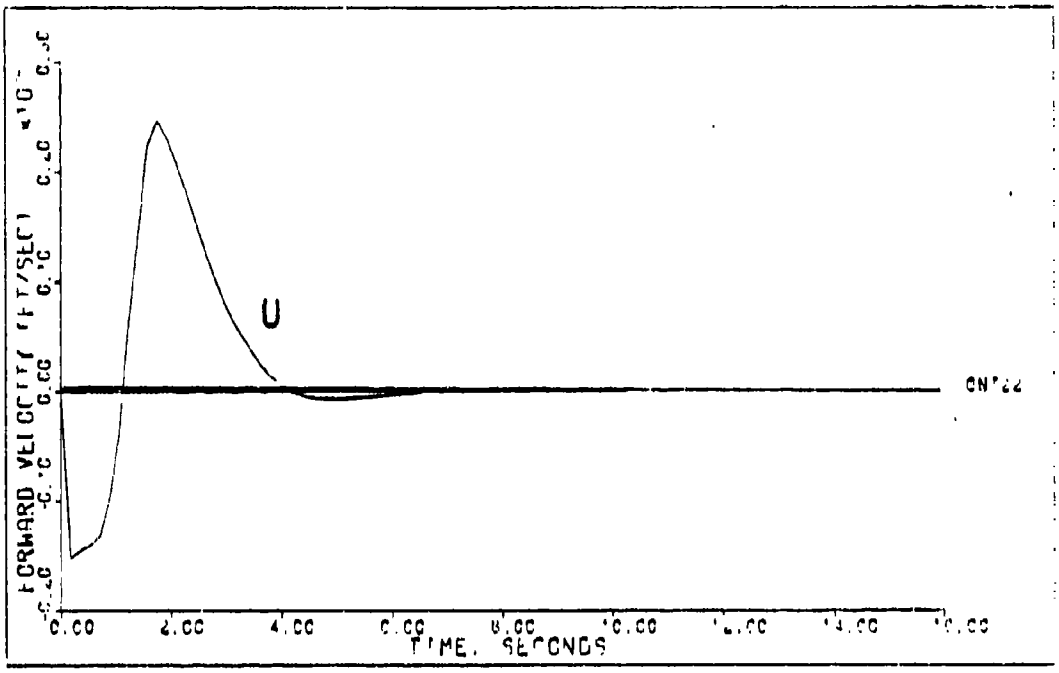

VERTICAL TRANSLATION (0.7M 15K FT) ACTUATORS

Figure F-55

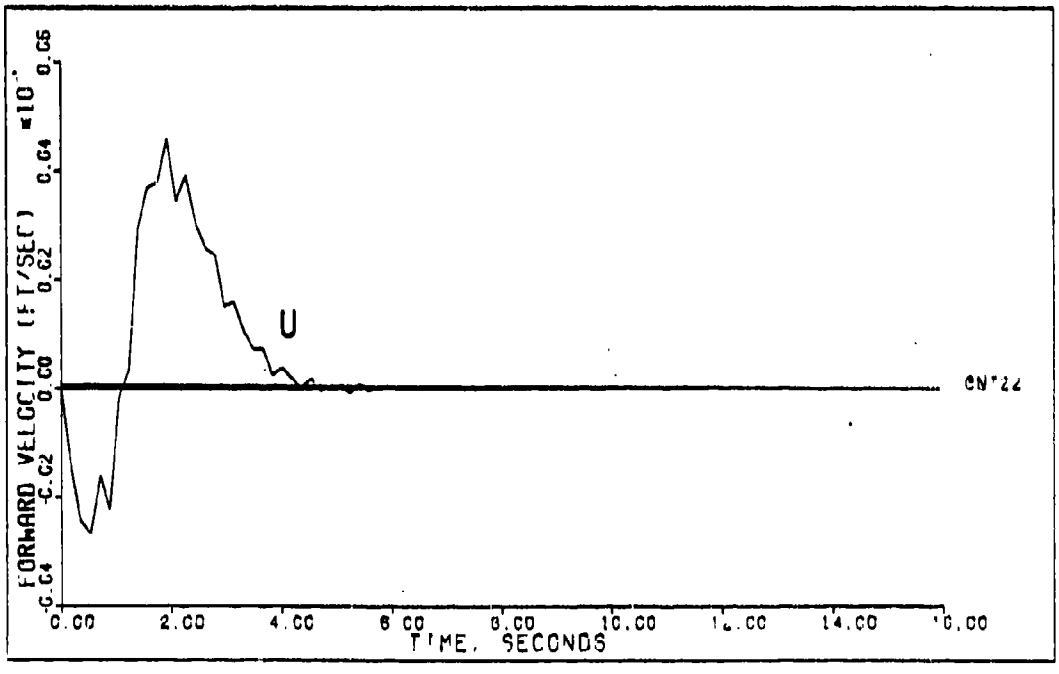

VERTICAL TRANSLATION (0.7M 15K FT) DELAY=0.025 SEC ACTUATORS

Figure F-56

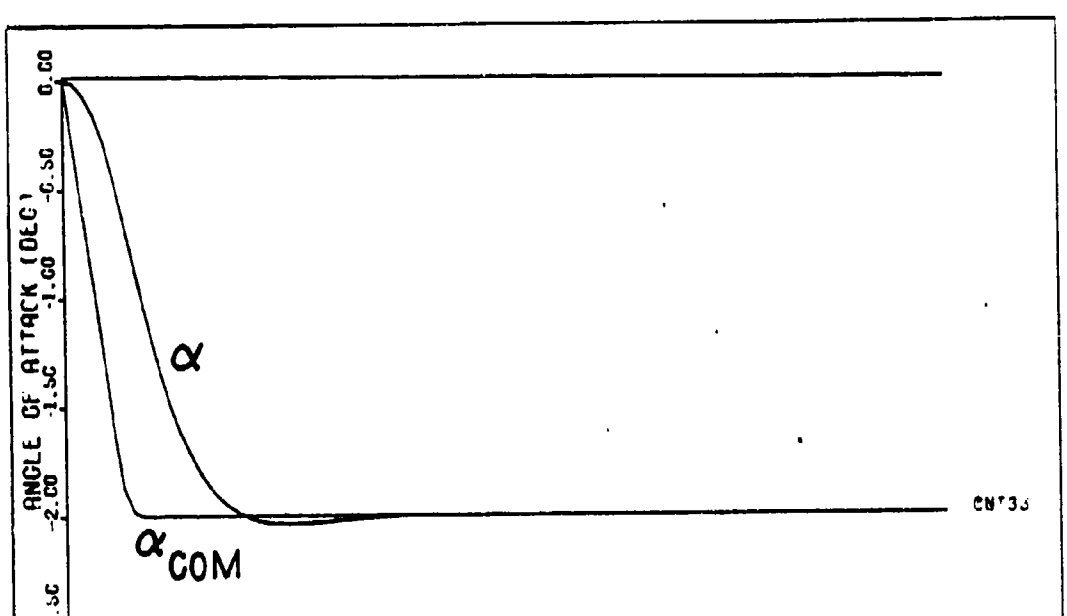

VERTICAL TRANSLATION (0.7M 15K FT)

Figure F-57

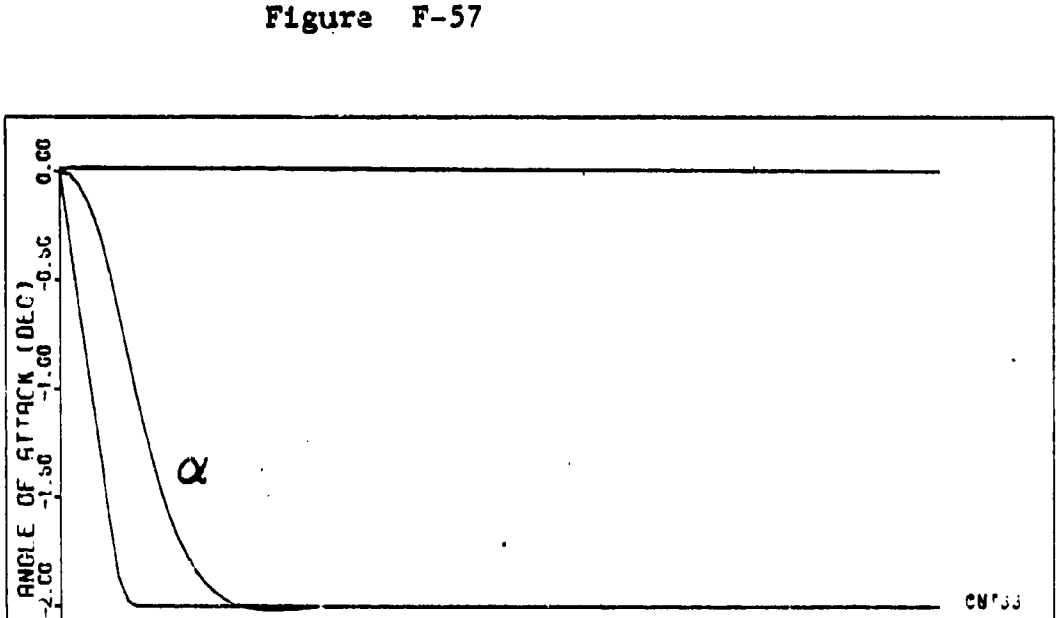

VERTICAL TRANSLATION (0.7M 15K FT) DELAY=0.025 SEC

Figure F-58

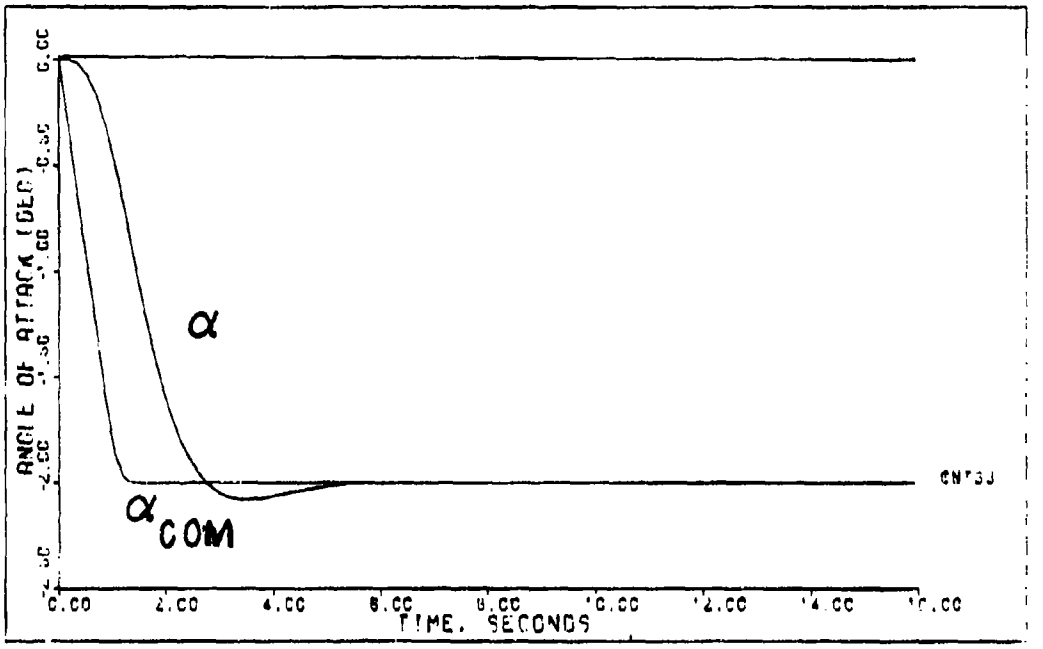

VERTICAL TRANSLATION (0.7M 15K FT) ACTUATORS

Figure F-59

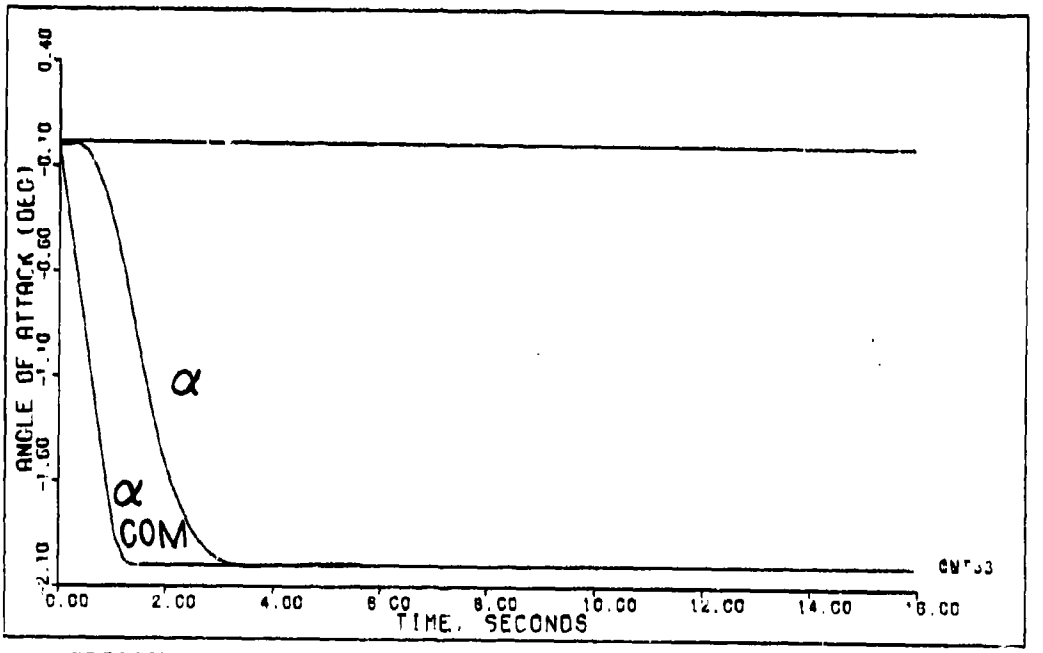

VERTICAL TRANSLATION (0.7M 15K FT) DELAY=0.025 SEC ACTUATORS

Figure F-60

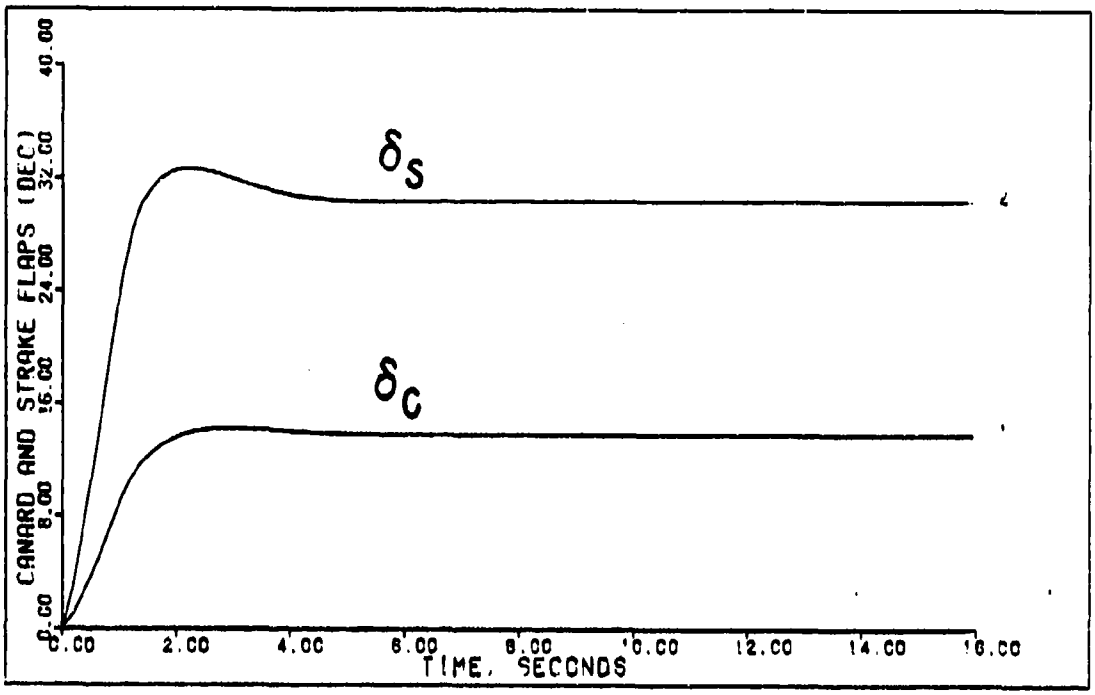

VERTICAL TRANSLATION (0.7M 15K FT)

Figure F-61

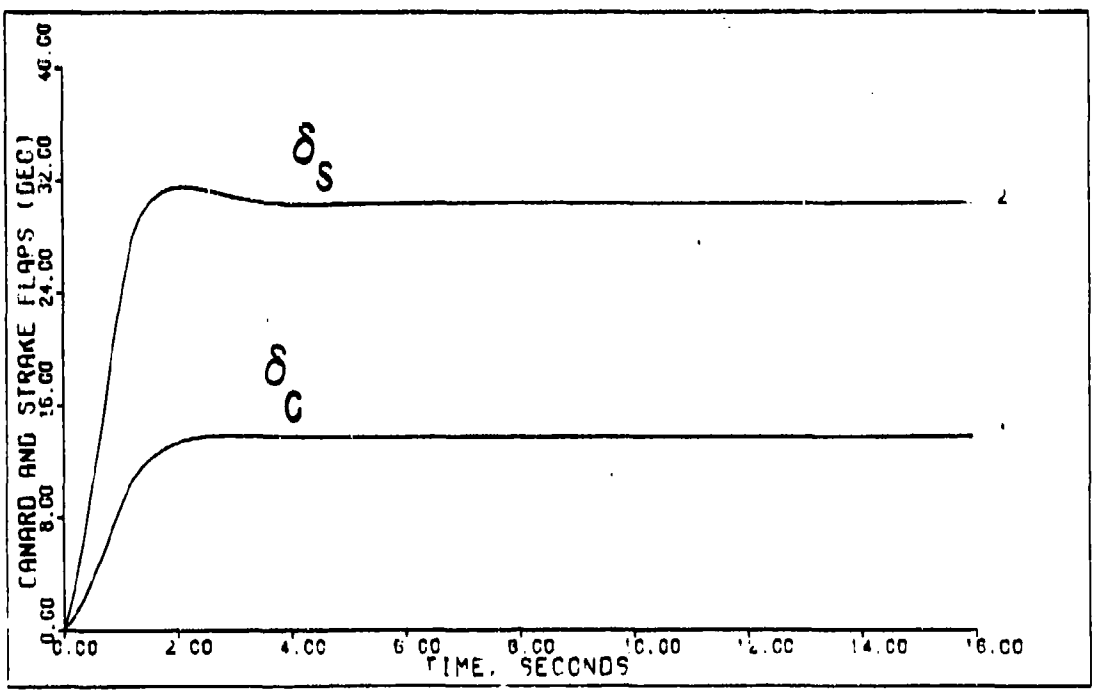

VERTICAL TRANSLATION (0.7M 15K FT) DELAY=0.025 SEC

Figure F-62

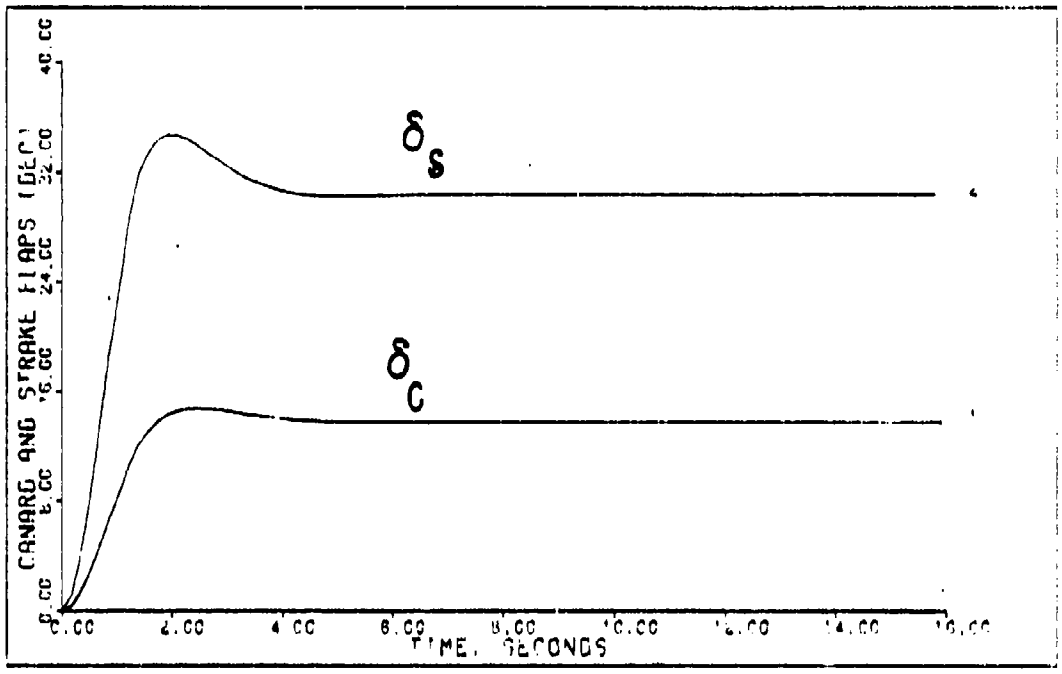

VERTICAL TRANSLATION (0.7M 15K FT) ACTUATORS

Figure F-63

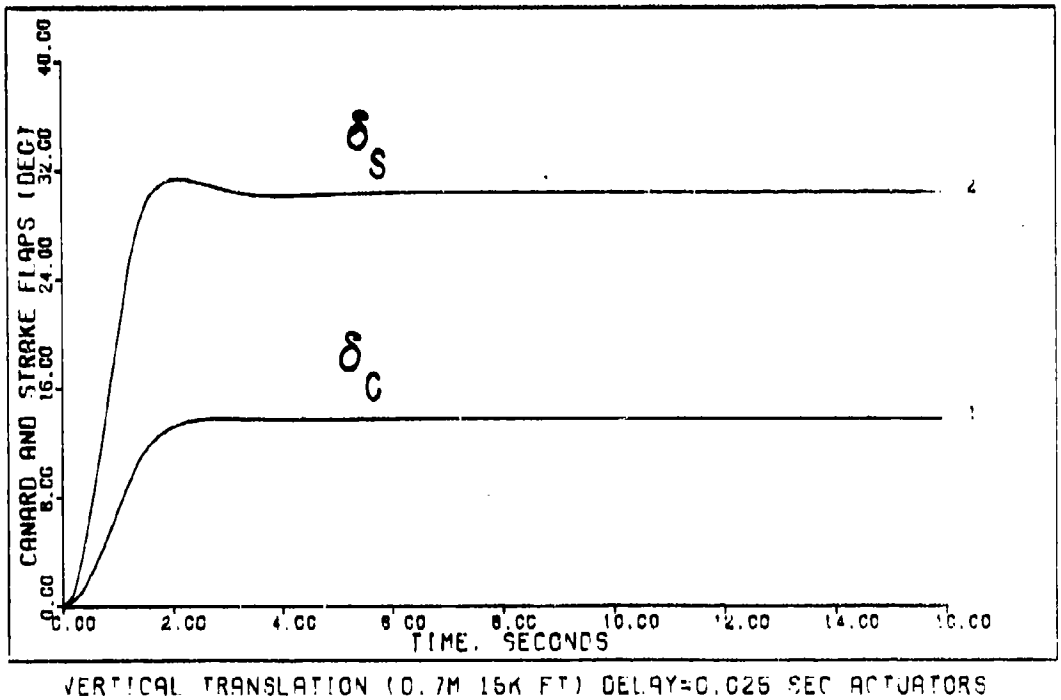

VERTICAL TRANSLATION (0.7M 15K FT) DELAY=0.025 SEC ACTUATORS

Figure F-64

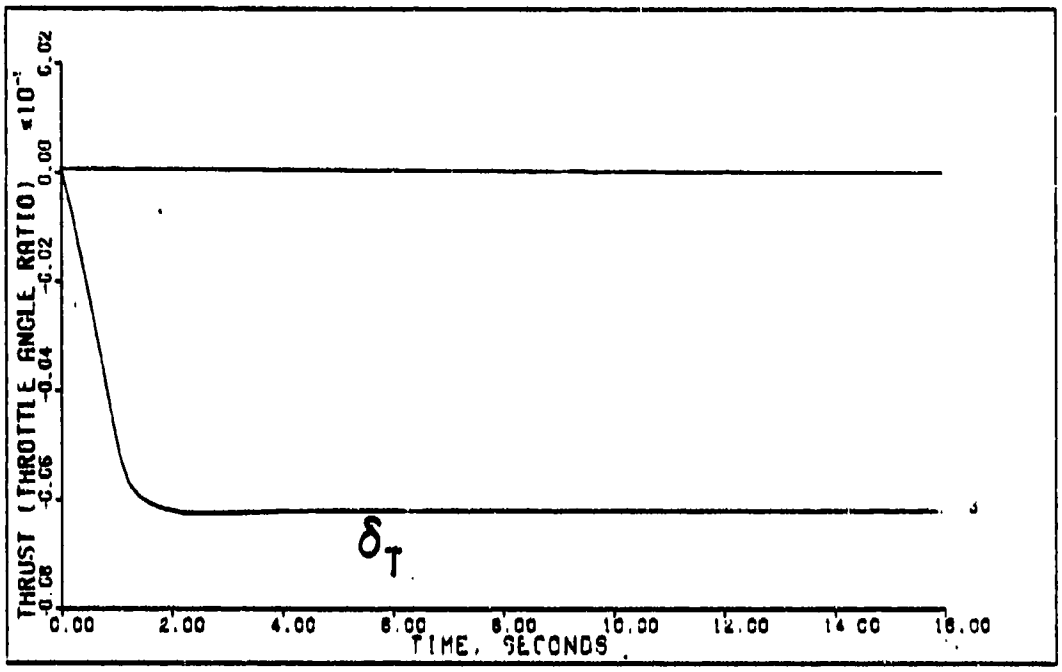

VERTICAL TRANSLATION (0.7M 15K FT)

Figure F-65

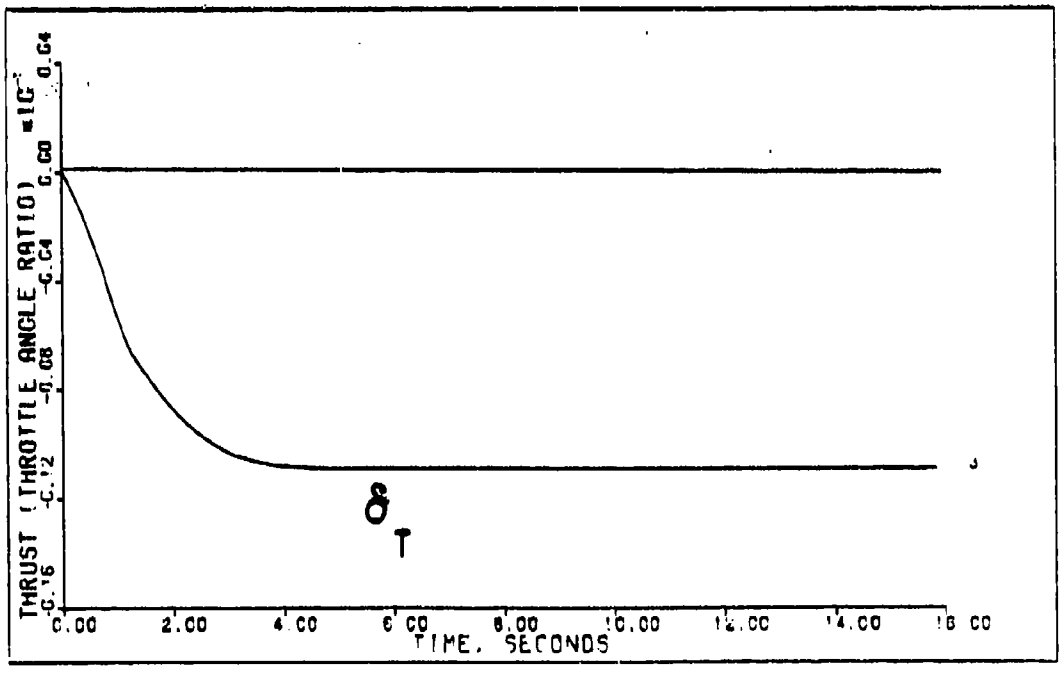

VERTICAL TRANSLATION (0.7M 15K FT) DELAY=0.025 SEC

Figure F-66

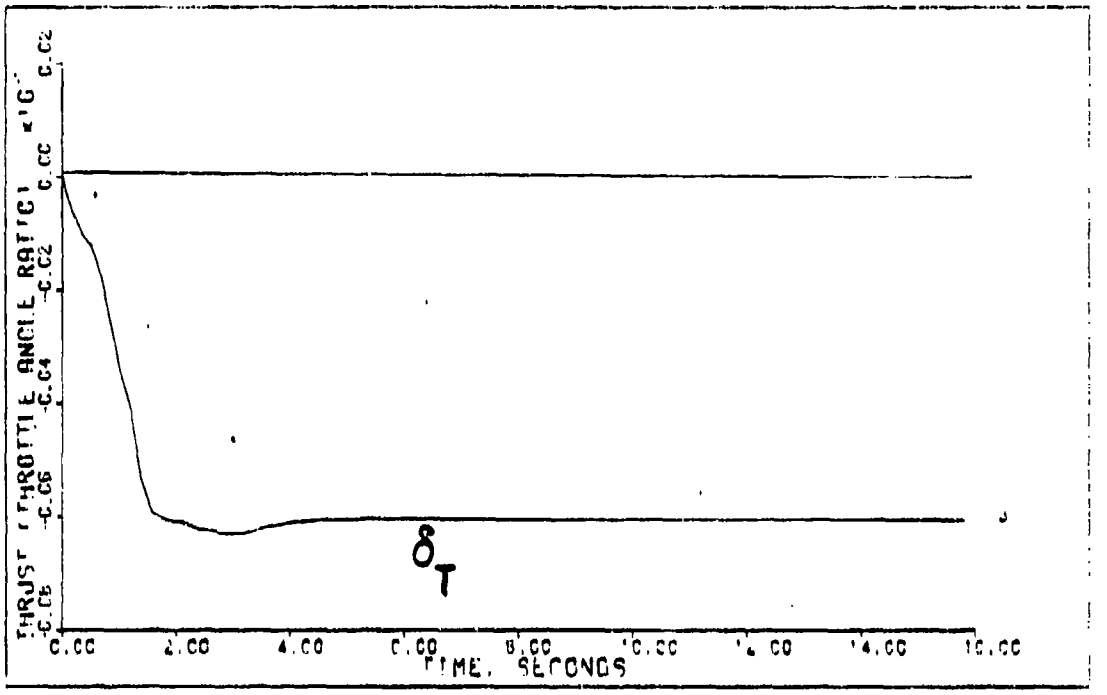

VERTICAL TRANSLATION (0.7M 15K FT) ACTUATORS

Figure F-67

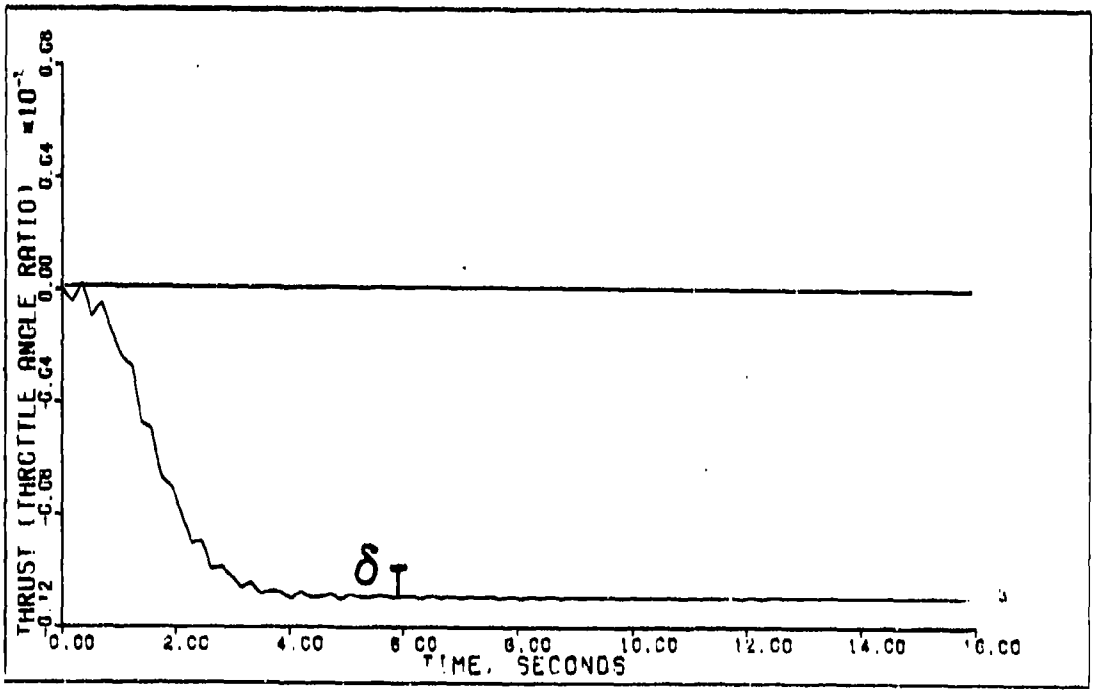

VERTICAL TRANSLATION (0.7M 15K FT) DELAY=0.025 SEC ACTUATORS

Figure F-68

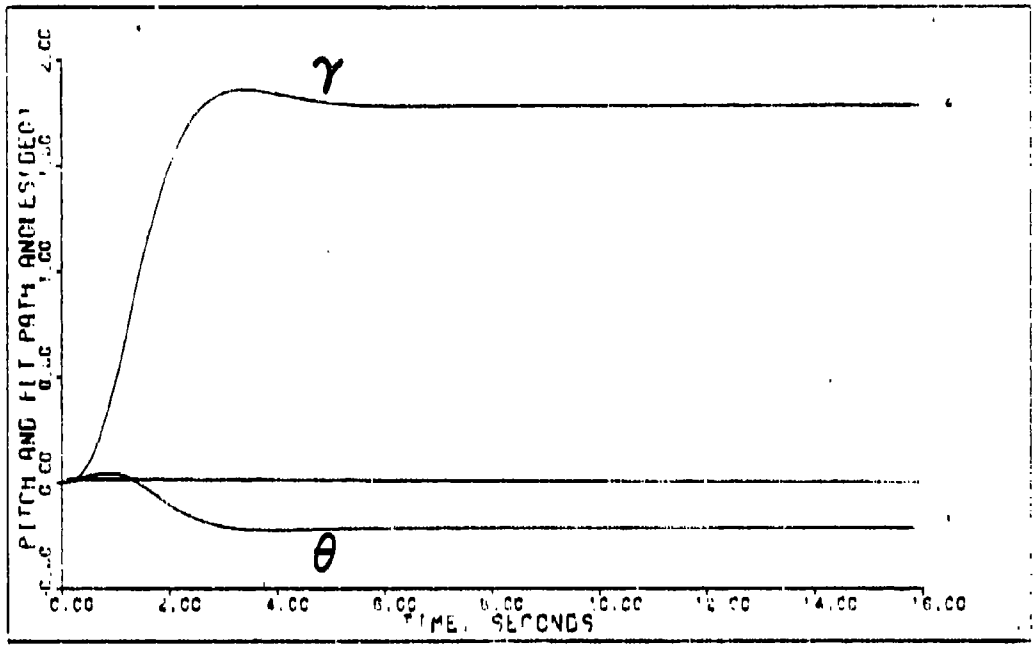

VERTICAL TRANSLATION (0.7M 15K FT) ACTUATORS

Figure F-69

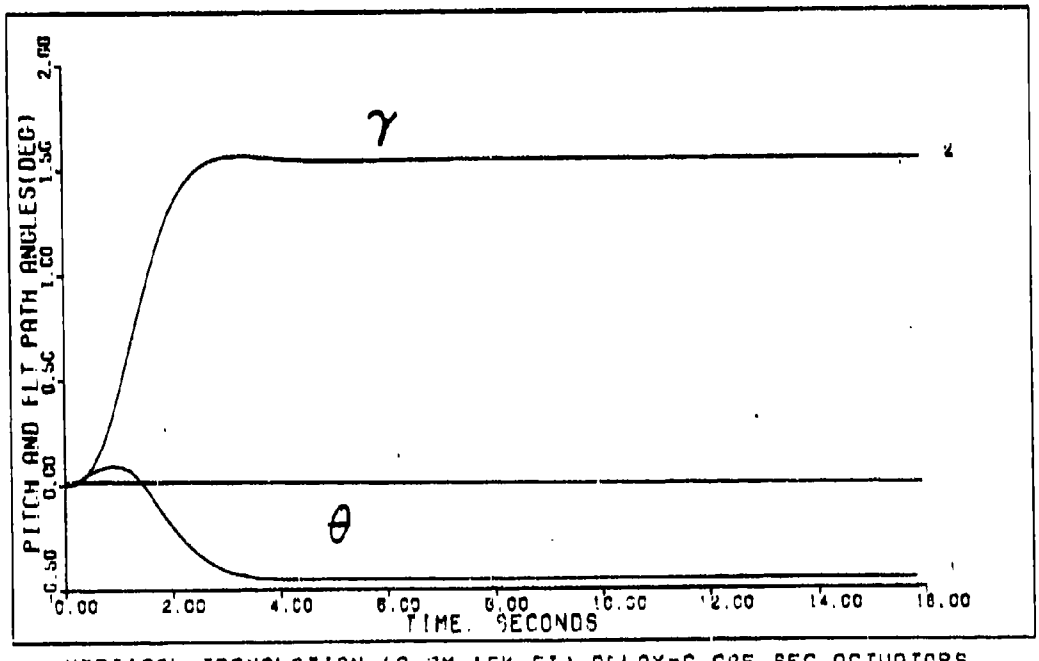

VERTICAL TRANSLATION (0.7M 15K FT) DELAY=0.025 SEC ACTUATORS

Figure F-70

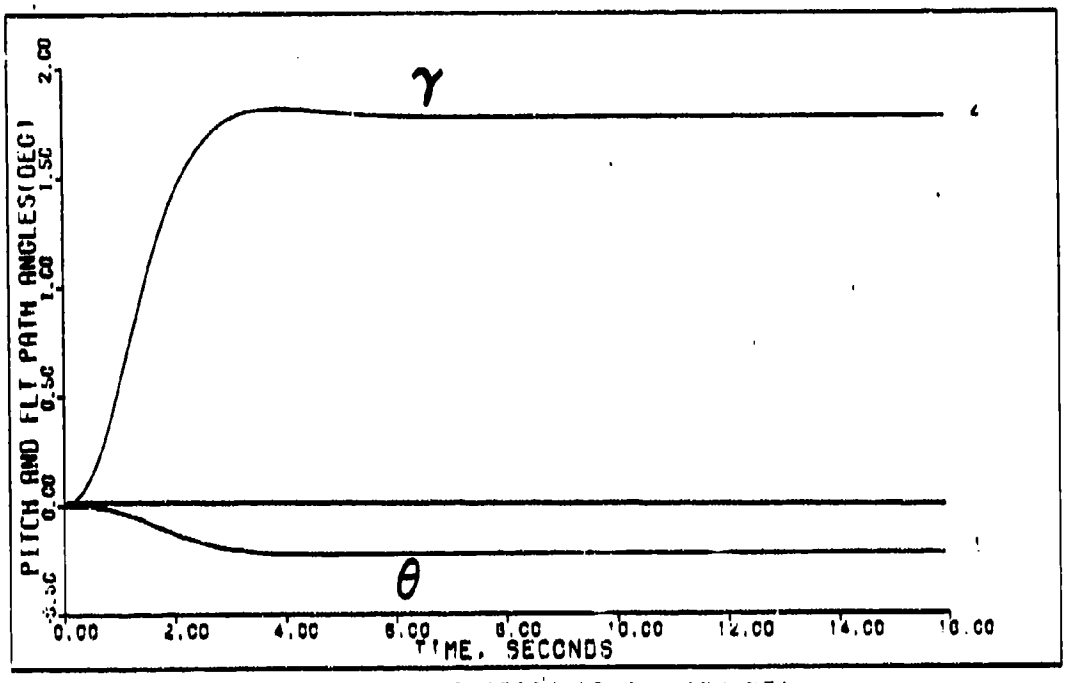

VERTICAL TRANSLATION (0.7M 15K FT)

Figure F-71

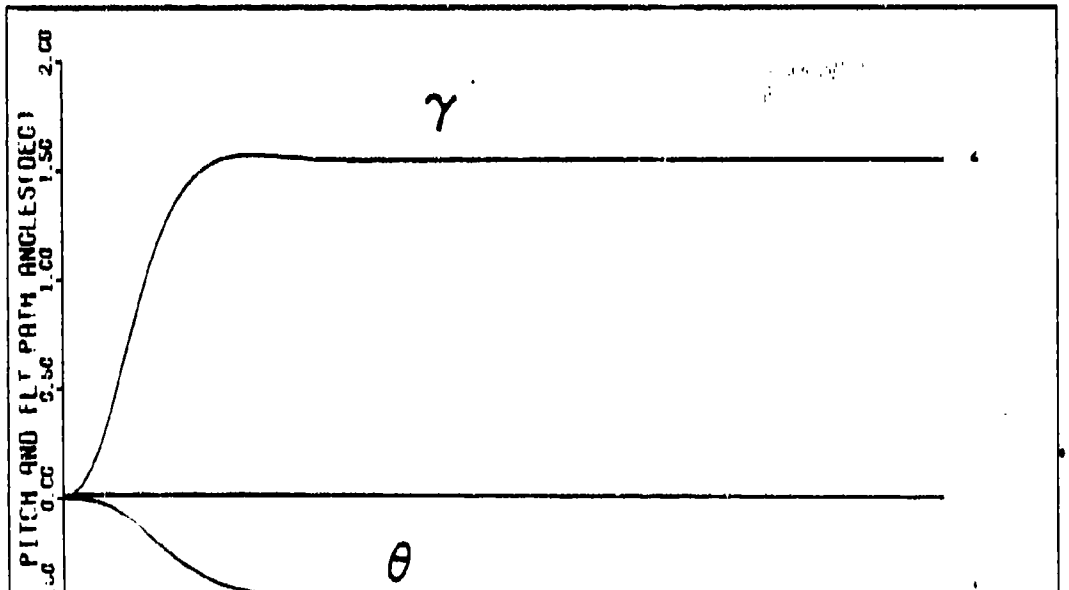

VERTICAL TRANSLATION (0.7M 15K FT) DELAY=0.025 SEC

Figure F-72

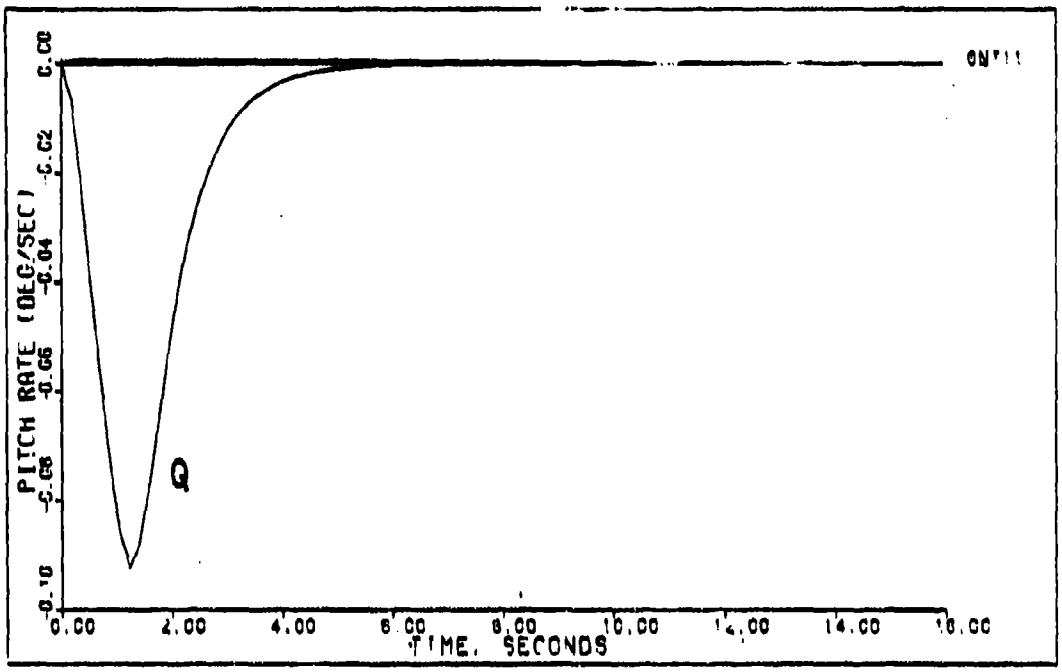

VERTICAL TRANSLATION (1.2M 15K FT)

Figure F-73

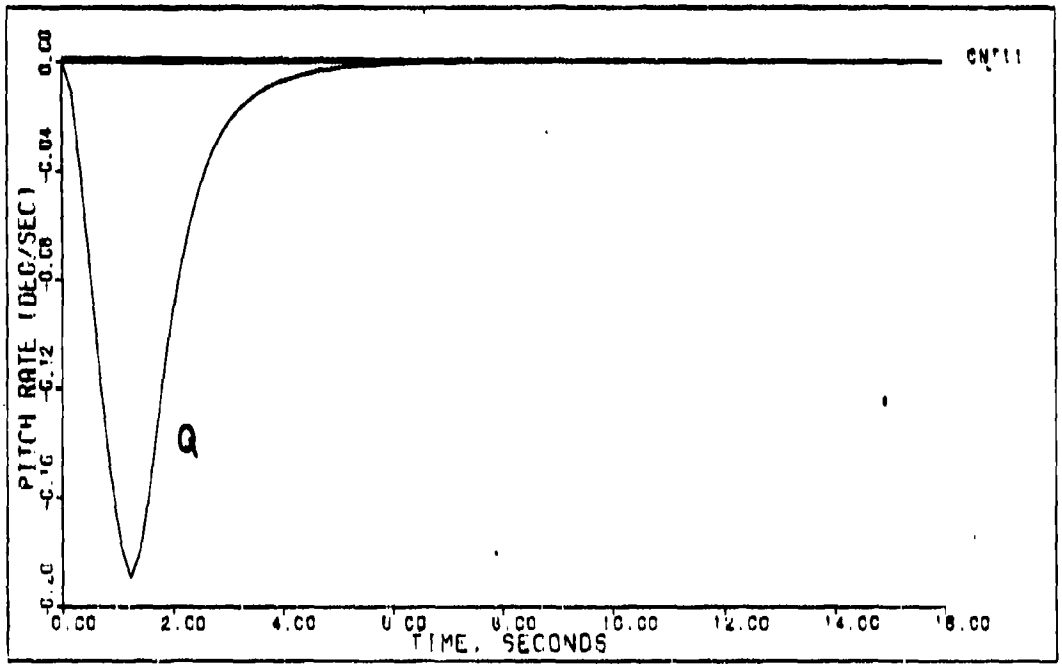

VERTICAL TRANSLATION (1.2M 15K FT) DELAY=0.025 SEC

Figure F-74

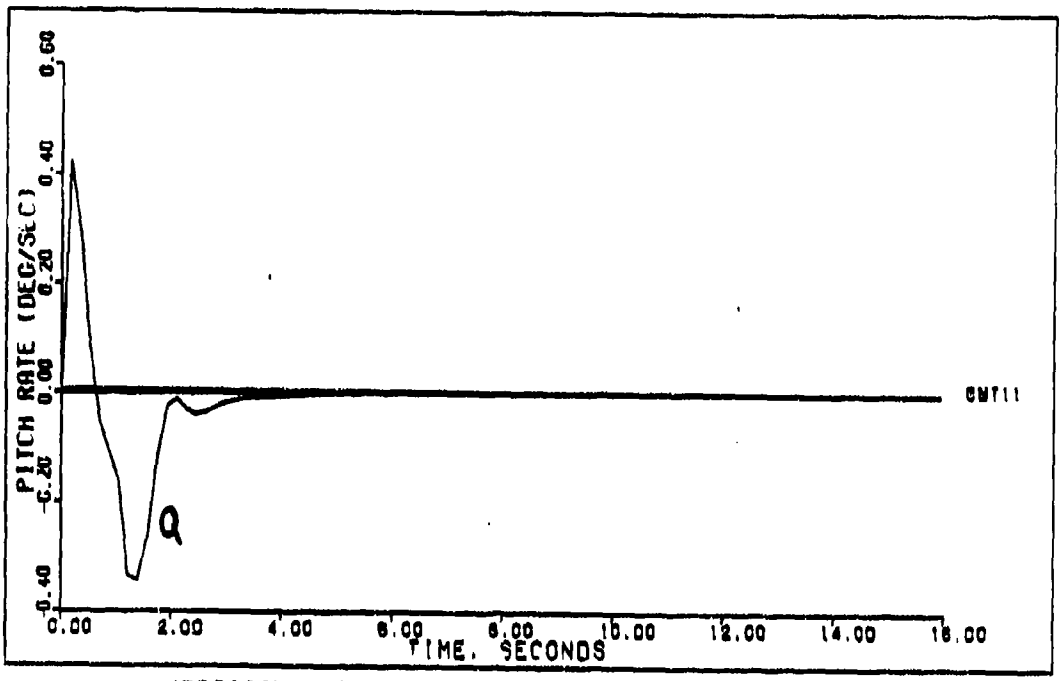

VERTICAL TRANSLATION (1.2M 15K FT) ACTUATORS

Figure F-75

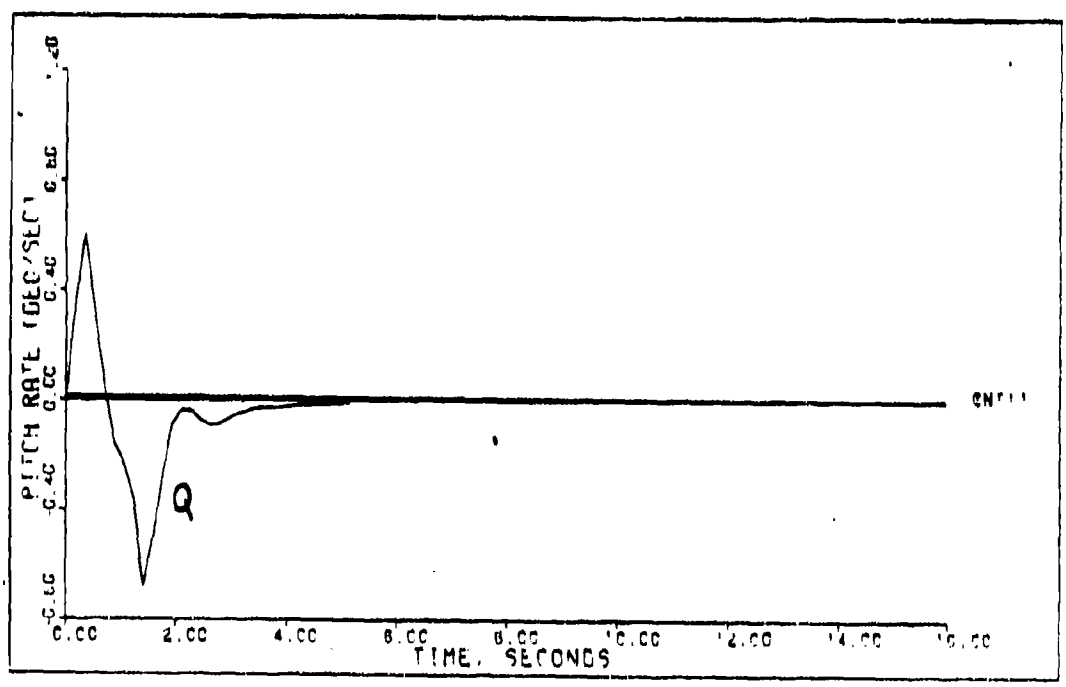

VERTICAL TRANSLATION (1.2M 15K FT) DELAY=0.025 SEC ACTUATORS

Figure F-76

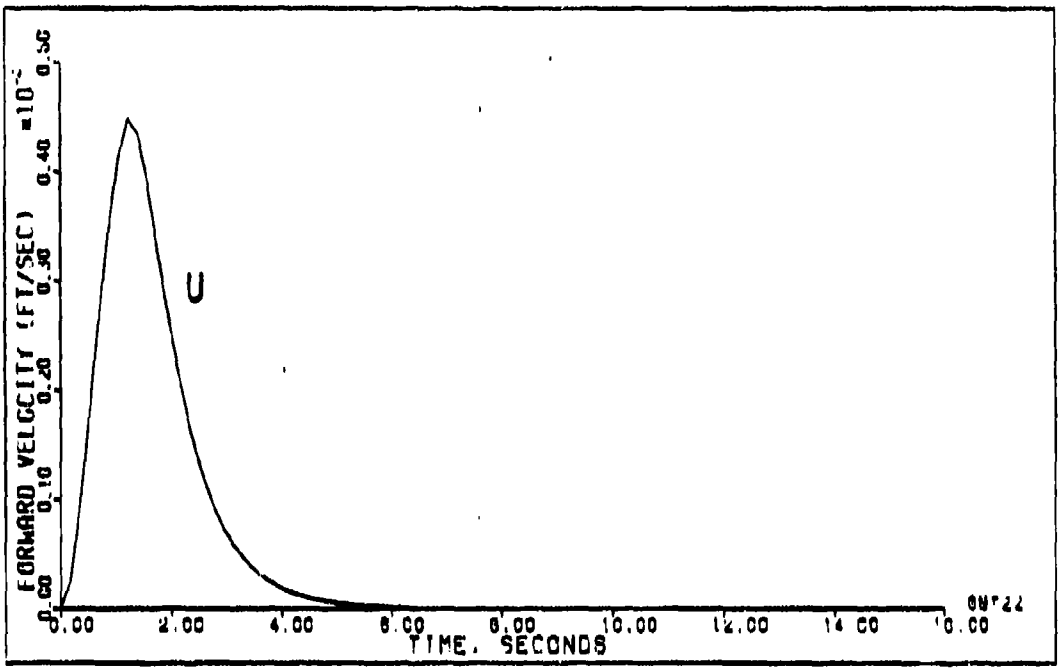

VERTICAL TRANSLATION (1.2M 15K FT)

Figure F-77

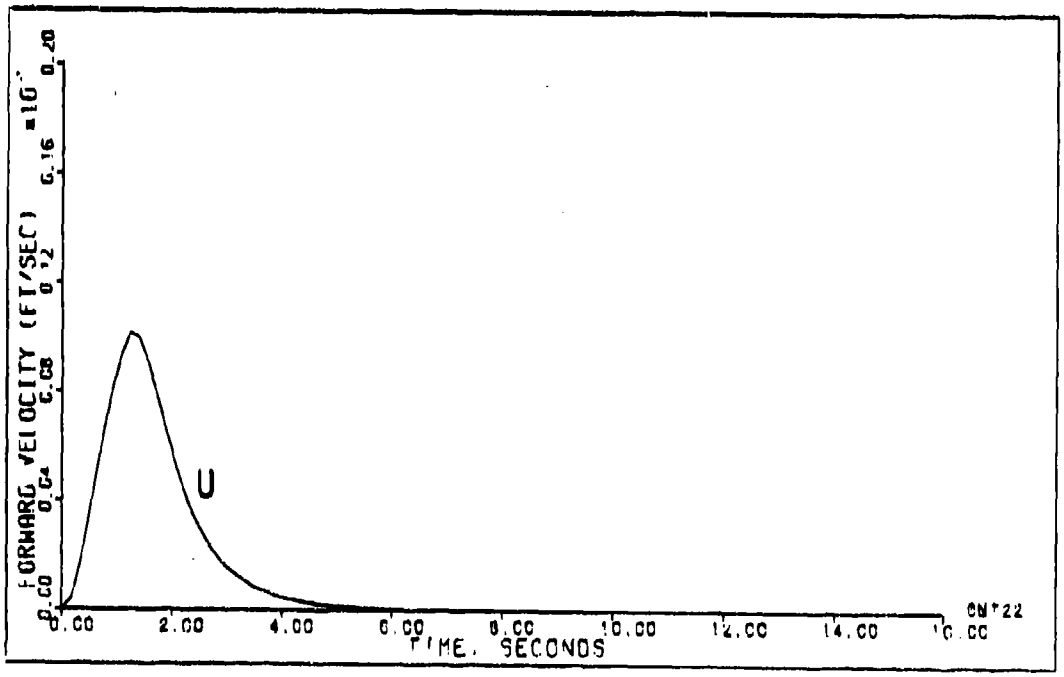

VERTICAL TRANSLATION (1.2M 15K FT) DELAY=0.025 SEC

Figure F-78

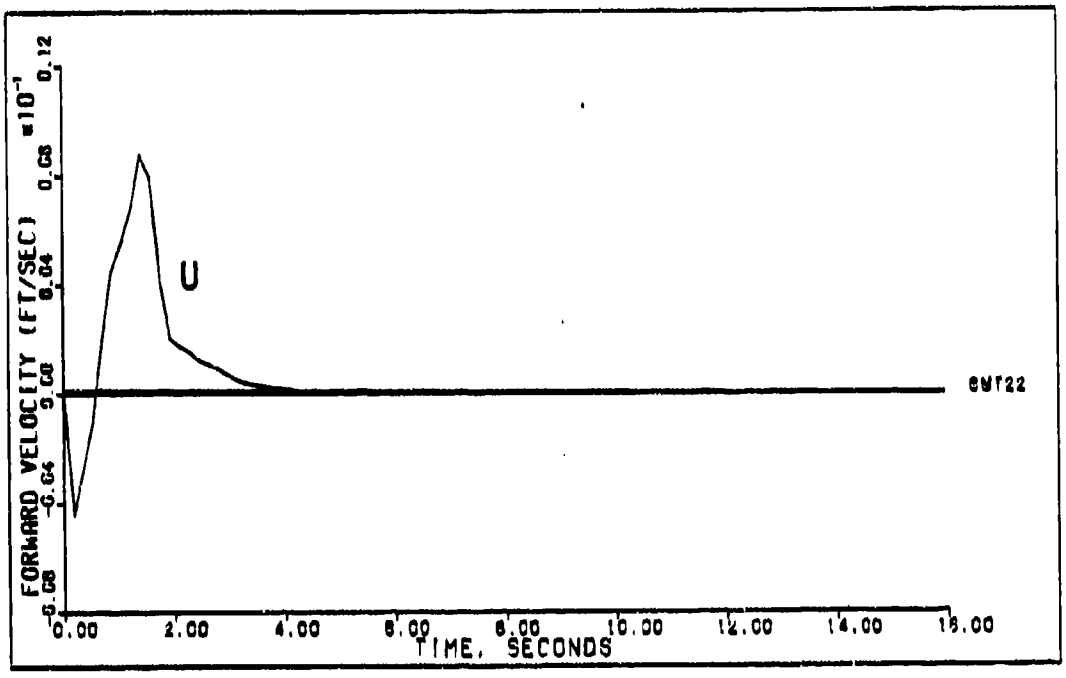

VERTICAL TRANSLATION (1.2M 16K FT) ACTUATORS

Figure F-79

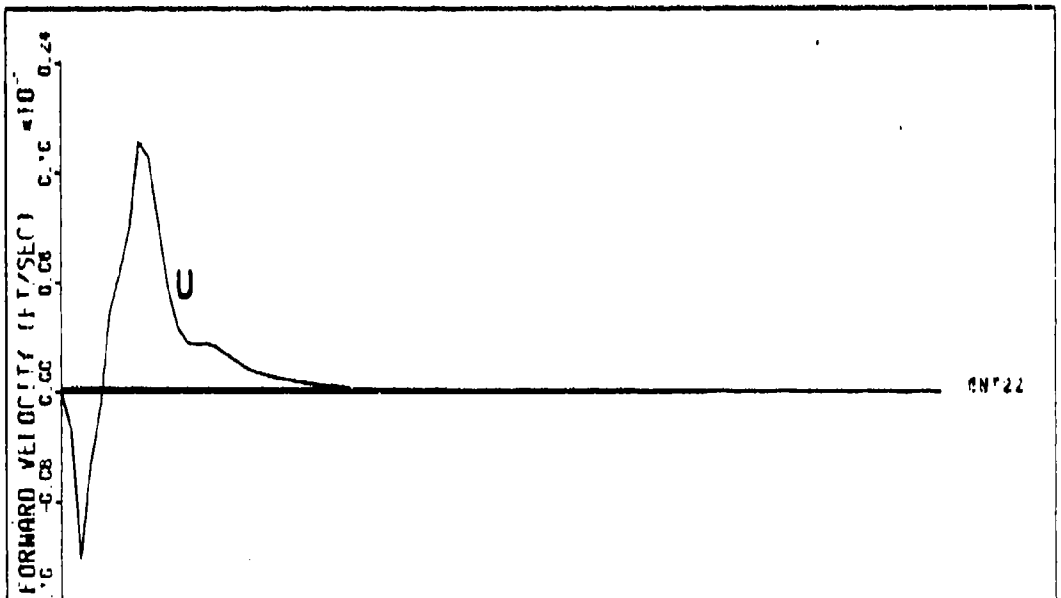

VERTICAL TRANSLATION (1.2M 16K FT) DELAY=0.025 SEC ACTUATORS

Figure F-80

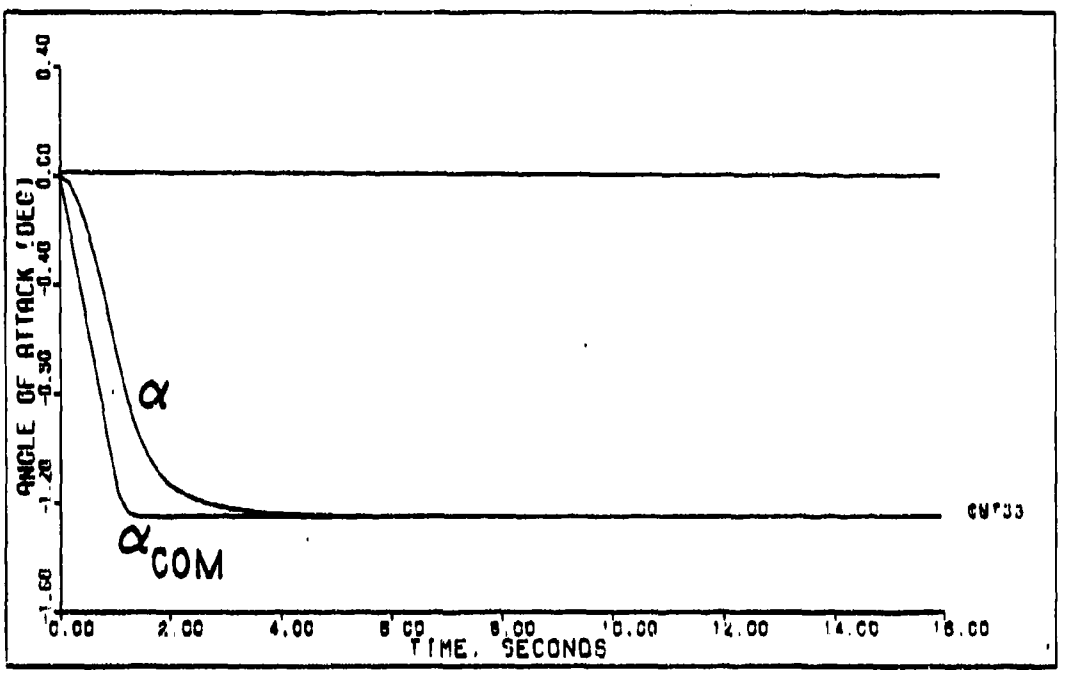

VERTICAL TRANSLATION (1.2M 15K FT)

Figure F-81

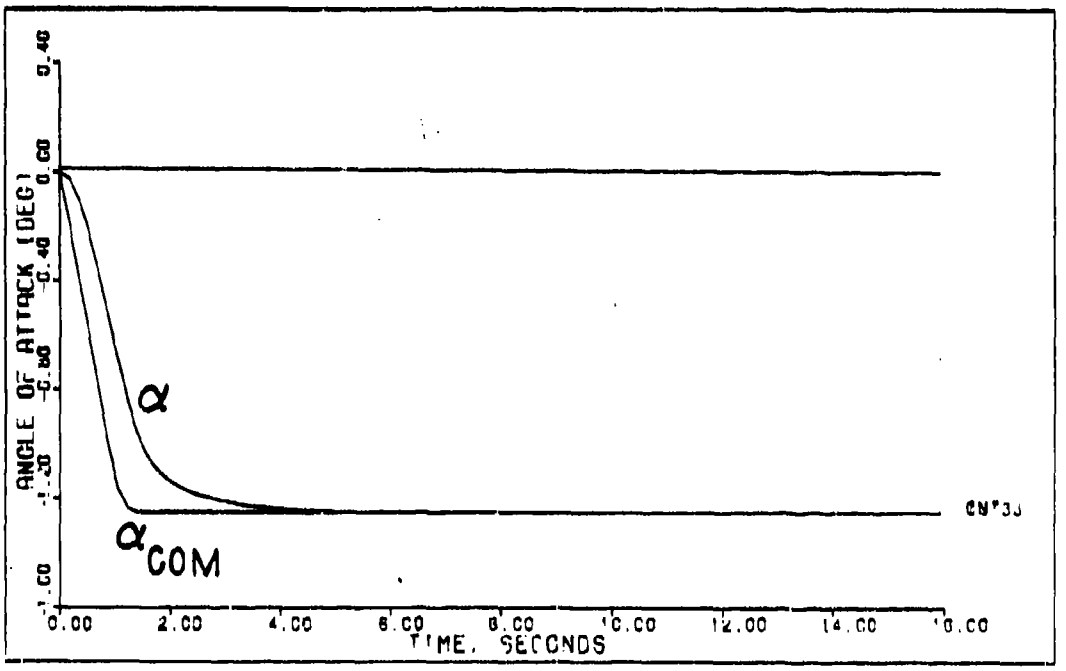

VERTICAL TRANSLATION (1.2M 15K FT) DELAY=0.025 SEC

Figure F-82

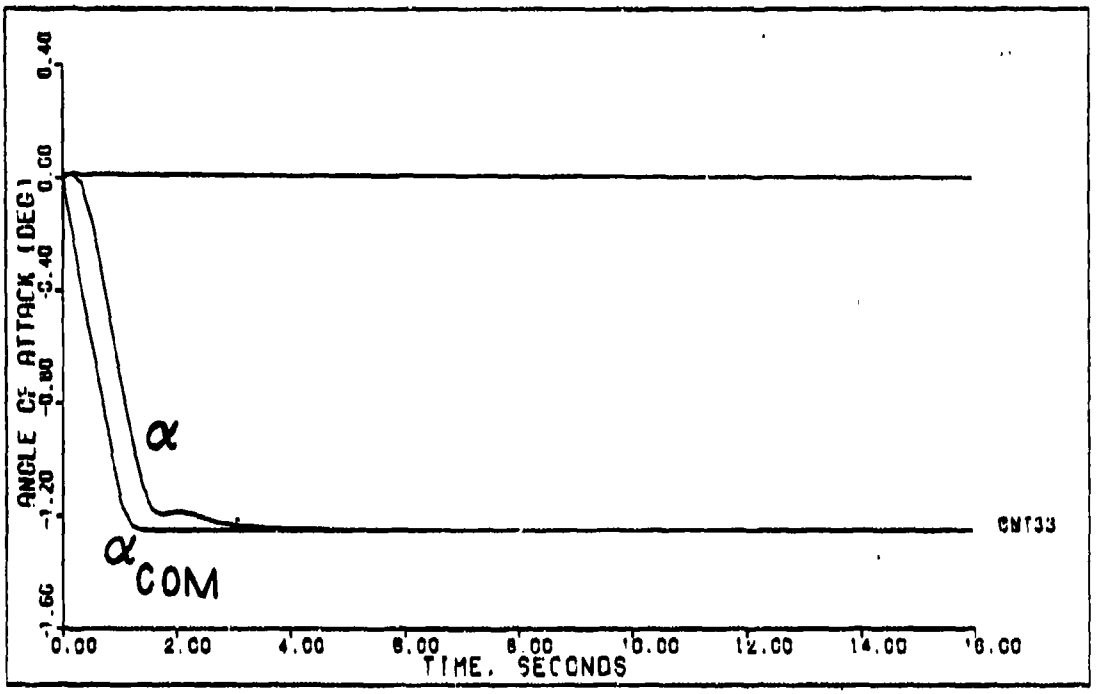

VERTICAL TRANSLATION (1.2M 15K FT) ACTUATORS

Figure F-83

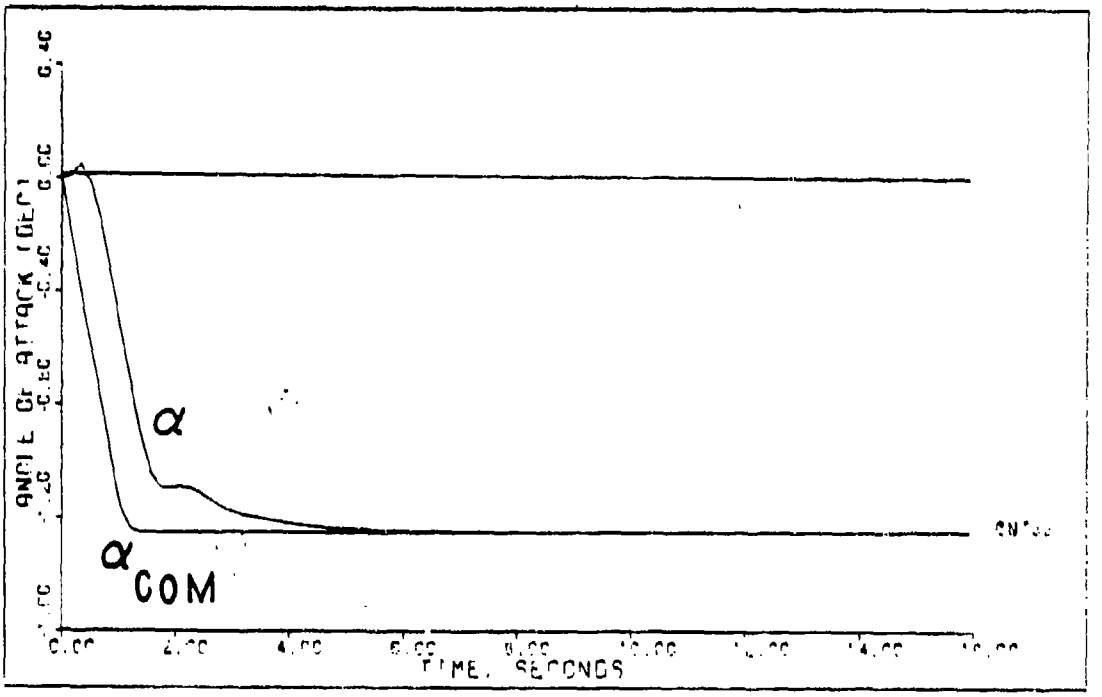

VERTICAL TRANSLATION (1.2M 15K FT) DELAY=0.0 SEC ACTUATORS

Figure F-84

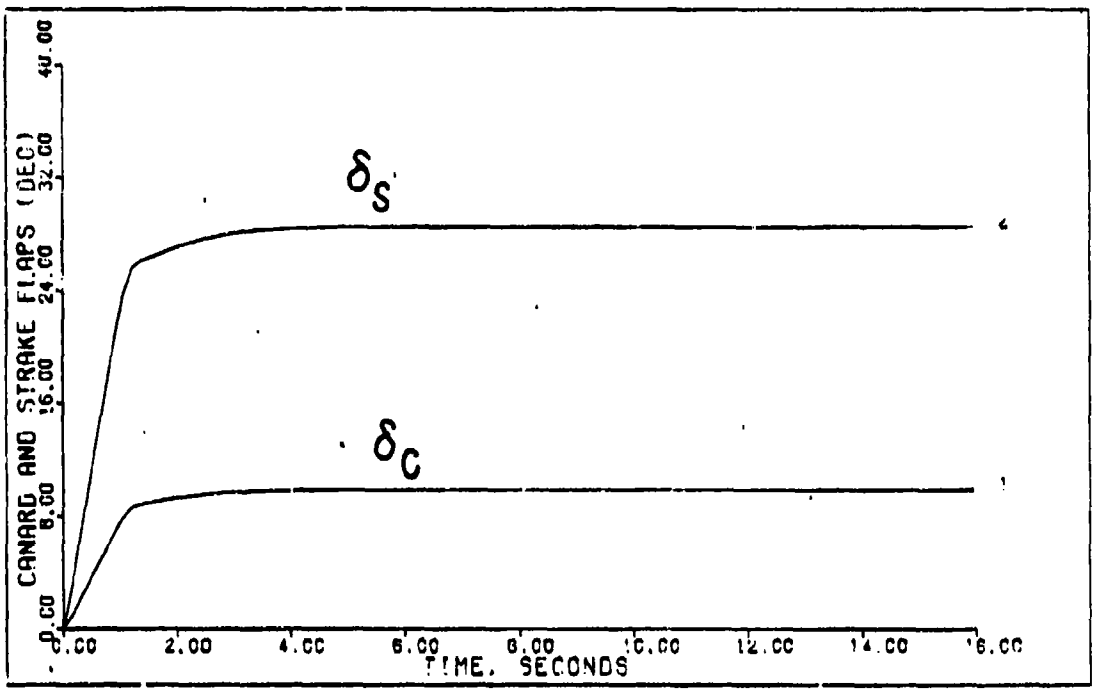

VERTICAL TRANSLATION (1.2M 15K FT)

Figure F-85

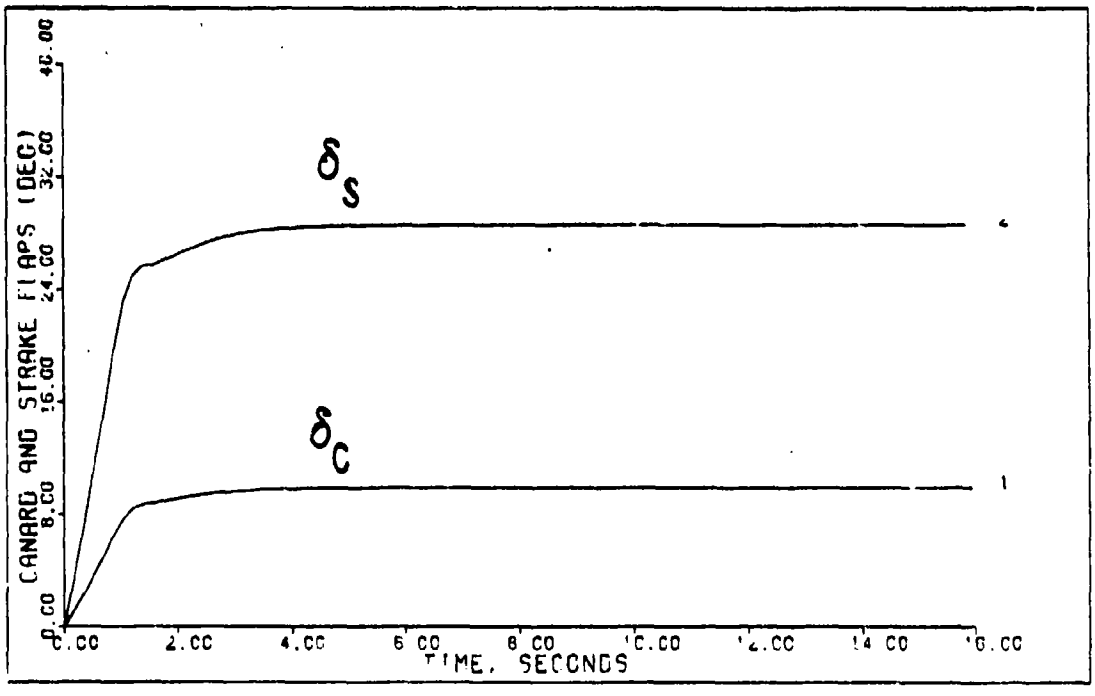

VERTICAL TRANSLATION (1.2M 15K FT) DELAY=0.025 SEC

Figure F-86

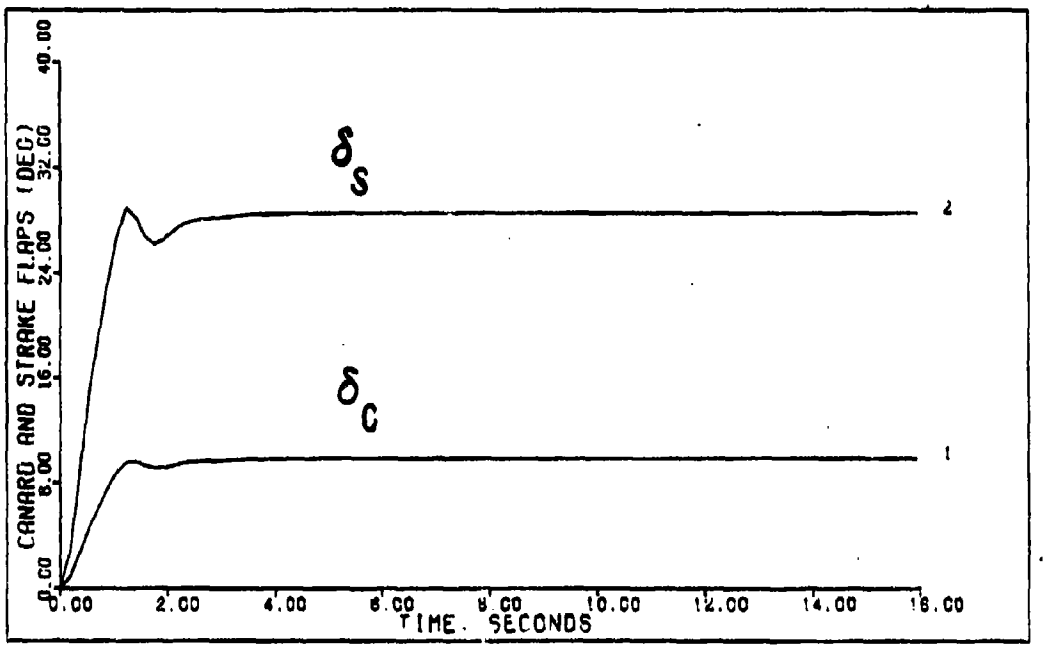

VERTICAL TRANSLATION (1.2M 15K FT) ACTUATORS

Figure F-87

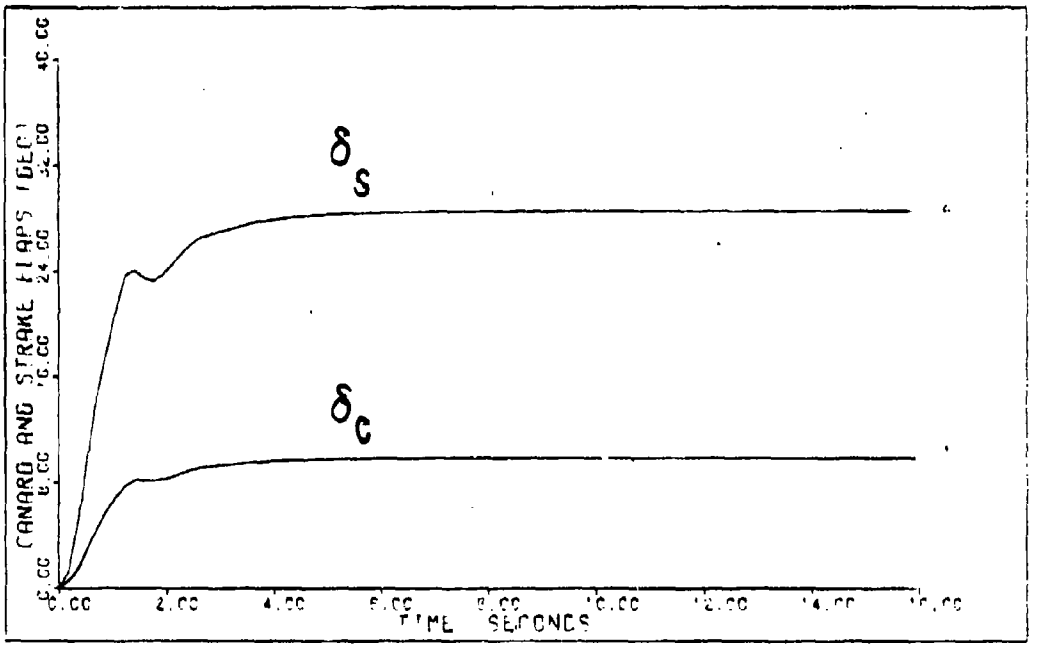

VERTICAL TRANSLATION (1.2M 15K FT) DELAY=0.025 SEC ACTUATORS

Figure F-88

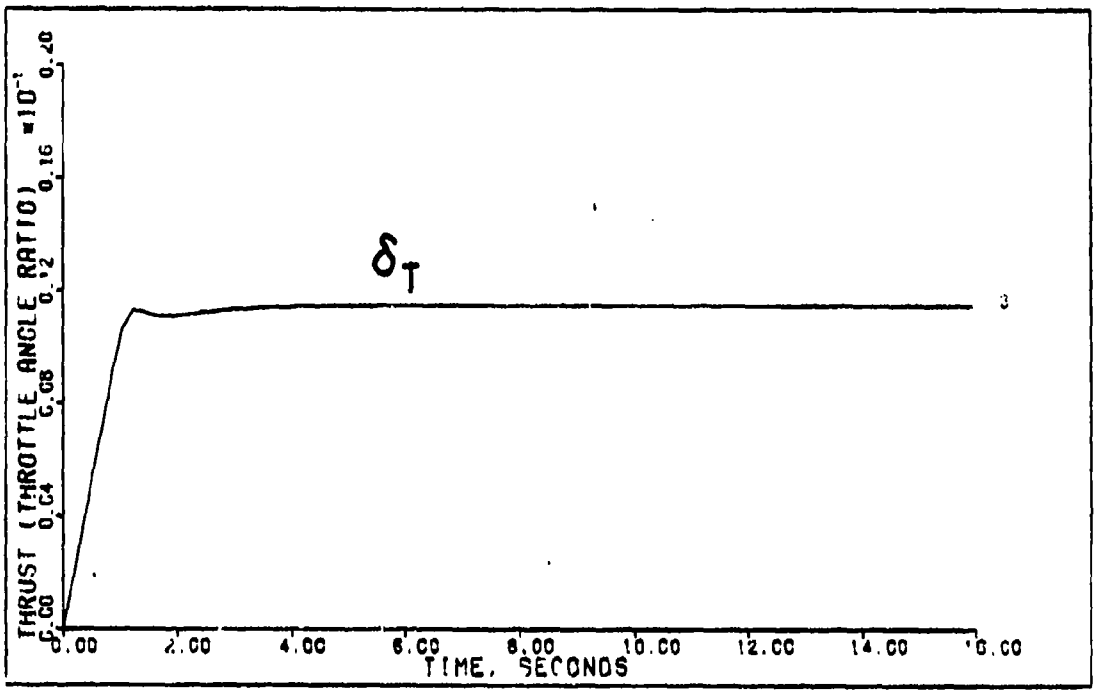

VERTICAL TRANSLATION (1.2M 15K FT)

Figure F-89

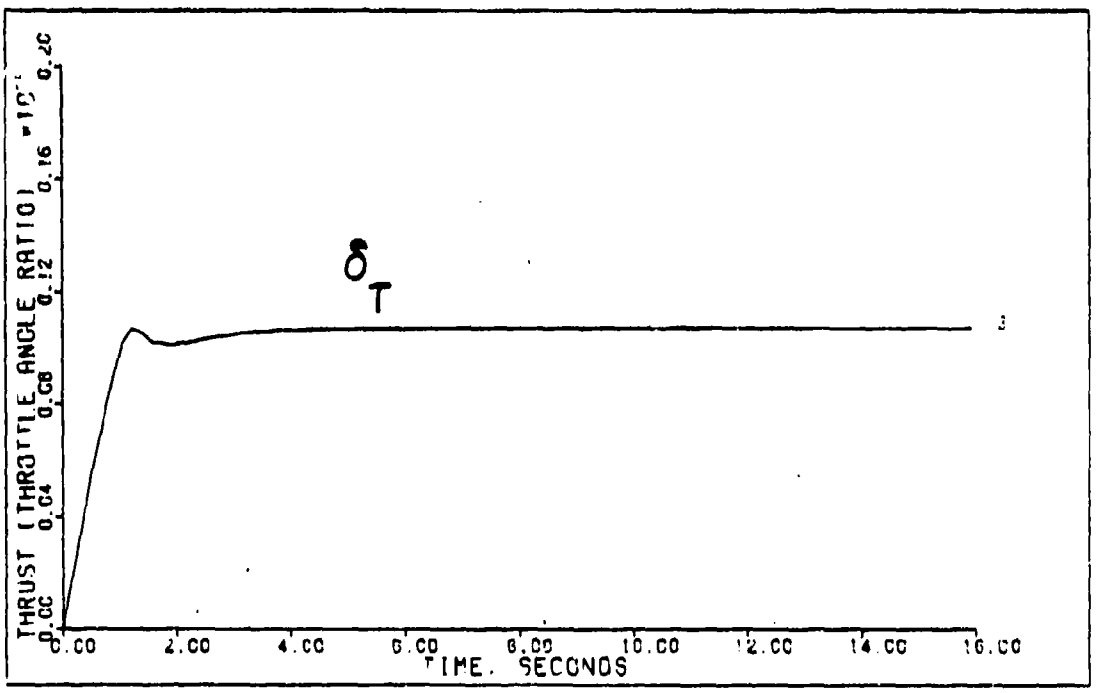

VERTICAL TRANSLATION (1.2M 15K FT) DELAY=0.025 SEC

Figure F-90

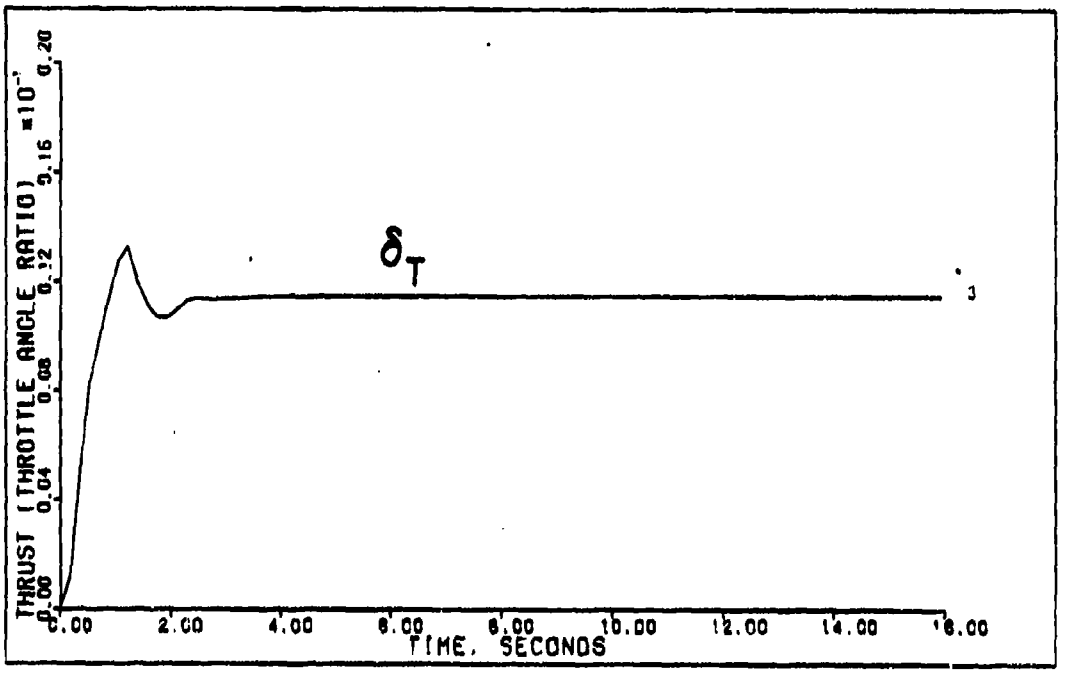

VERTICAL TRANSLATION (1.2M 15K FT) ACTUATORS

Figure F-91

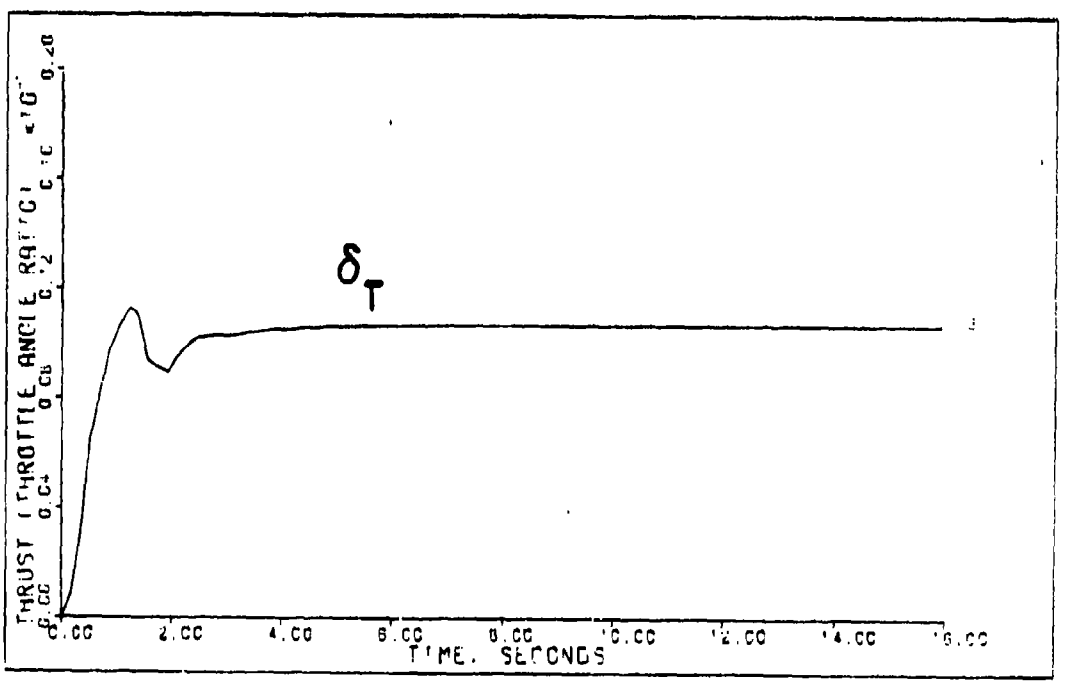

VERTICAL TRANSLATION (1.2M 15K FT) DELAY=0.025 SEC ACTUATORS

Figure F-92

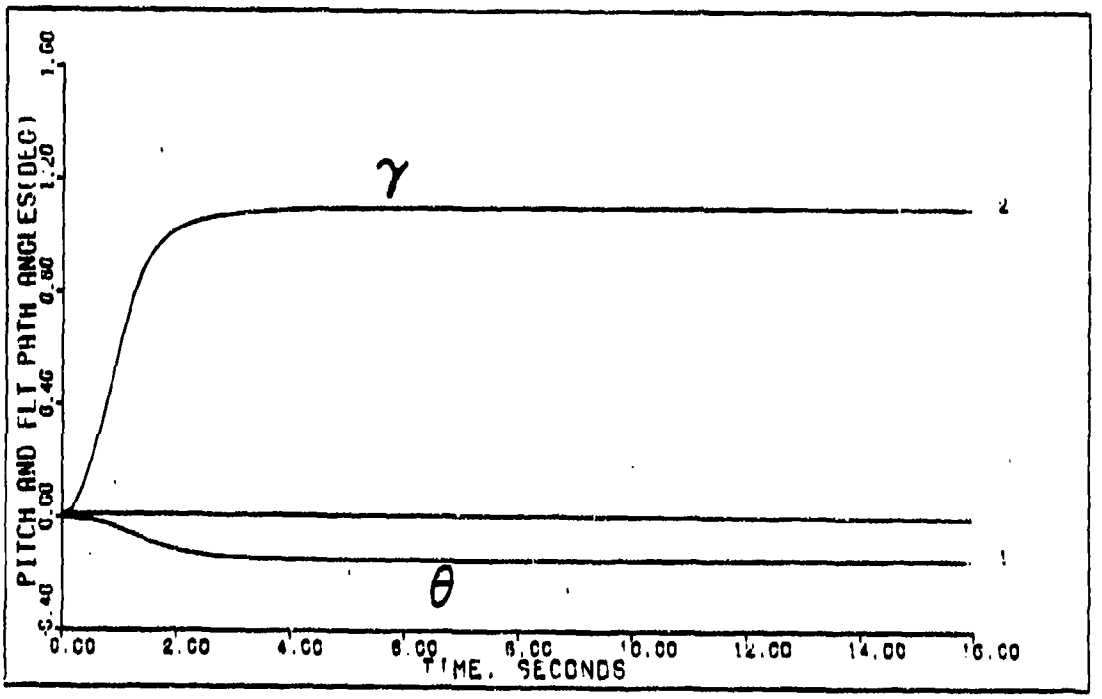

VERTICAL TRANSLATION (1.2M 15K FT)

Figure F-93

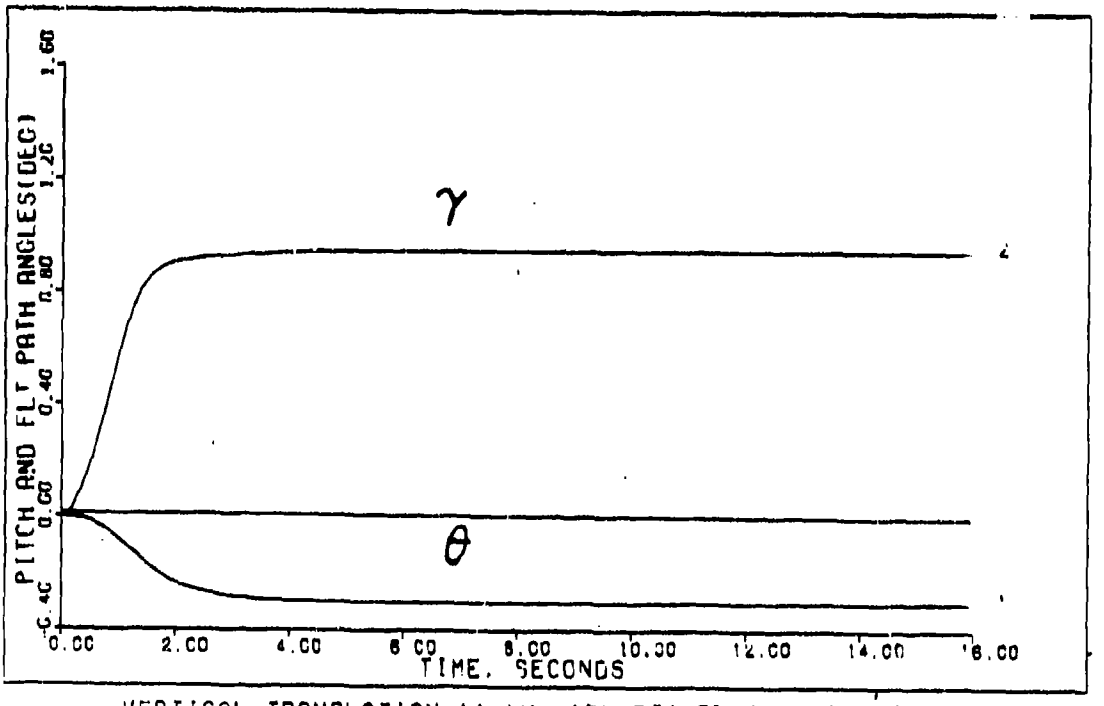

VERTICAL TRANSLATION (1.2M 15K FT) DELAY=0.025 SEC

Figure F-94

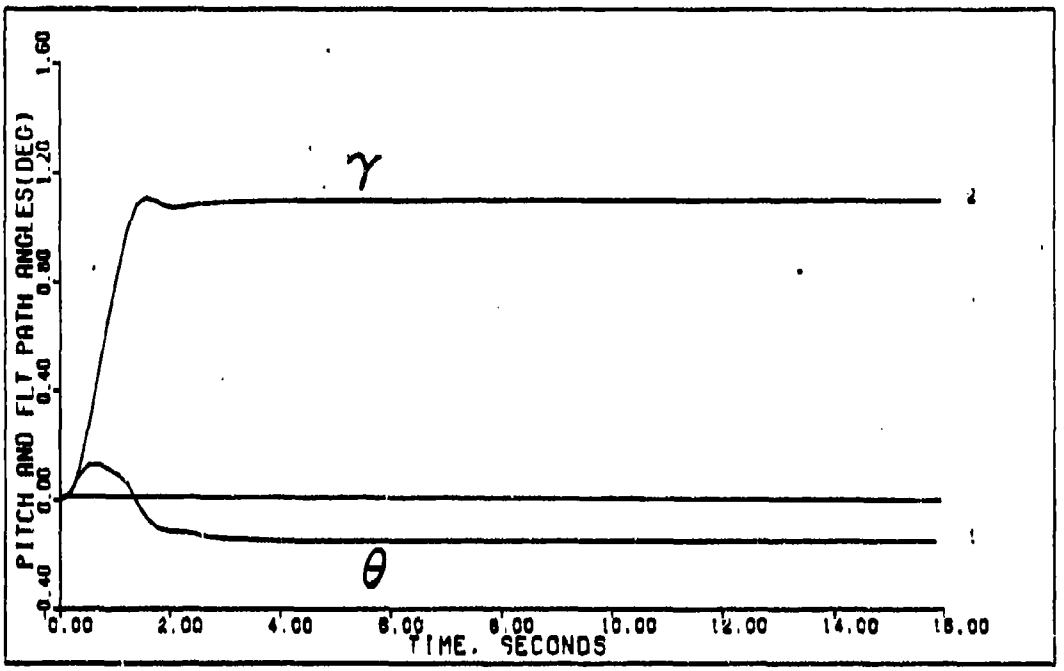

VERTICAL TRANSLATION (1.2M 15K FT) ACTUATORS

Figure F-95

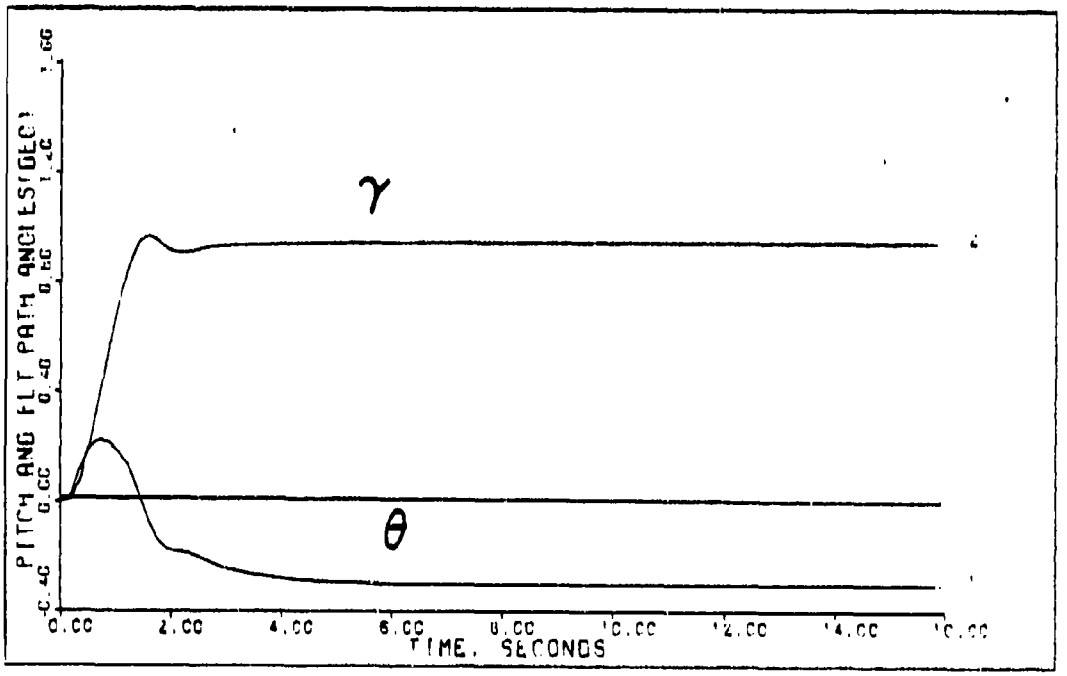

VERTICAL TRANSLATION (1.2M 15K FT) DELAY=0.025 SEC ACTUATORS

Figure F-96

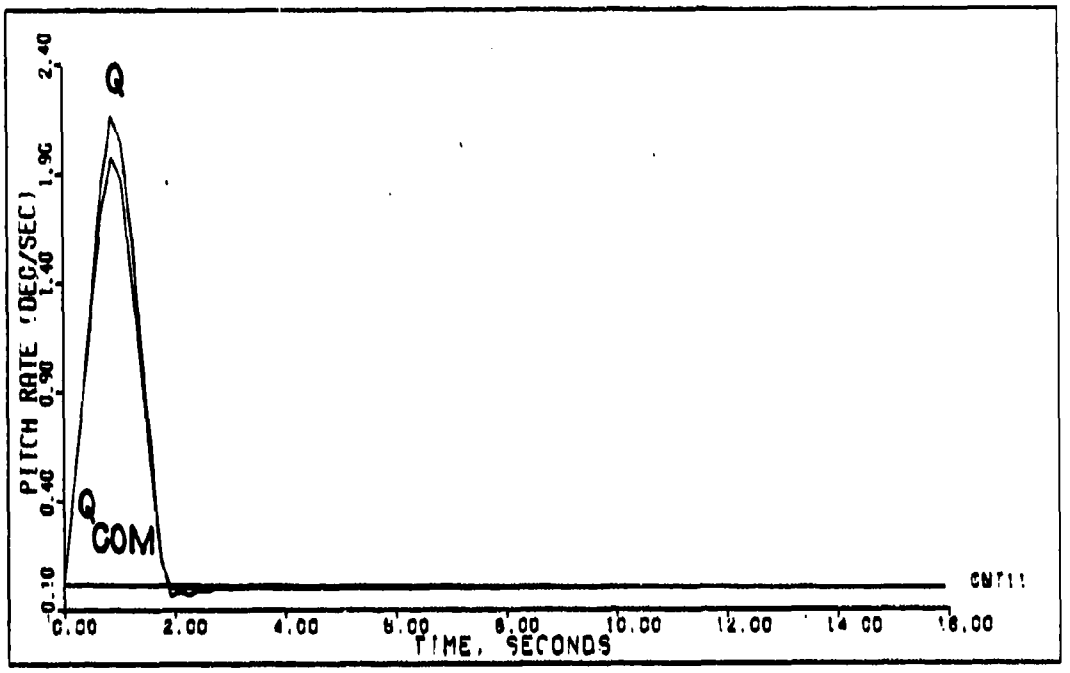

PITCH POINTING (0.7M 15K FT)

Figure F-97

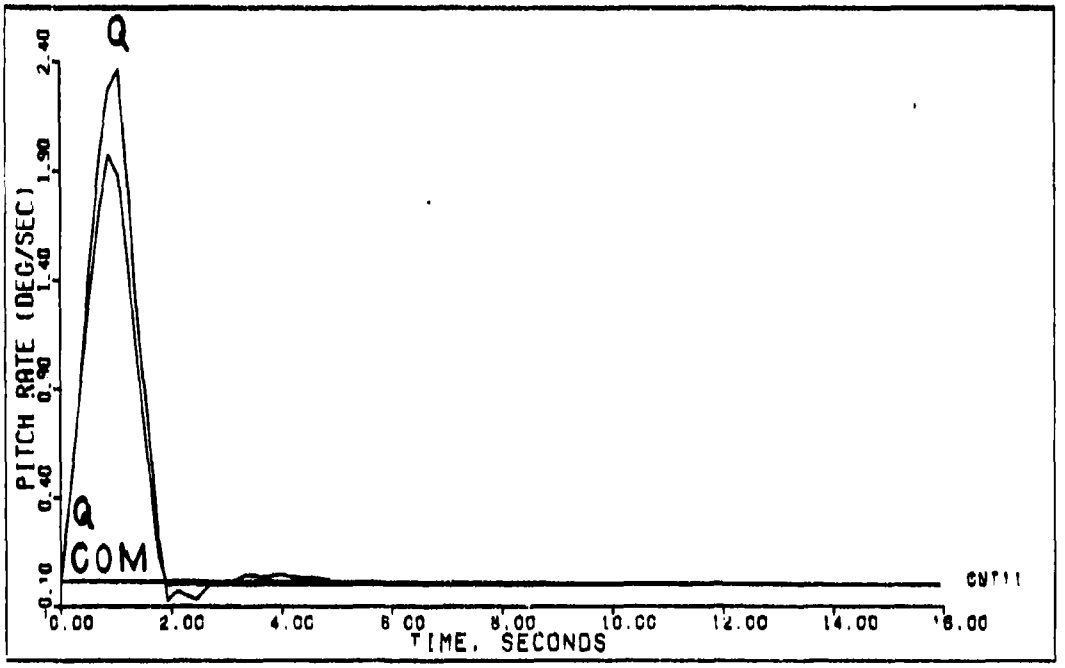

PITCH POINTING (0.7M 15K FT) DELAY=0.025 SEC

Figure F-98

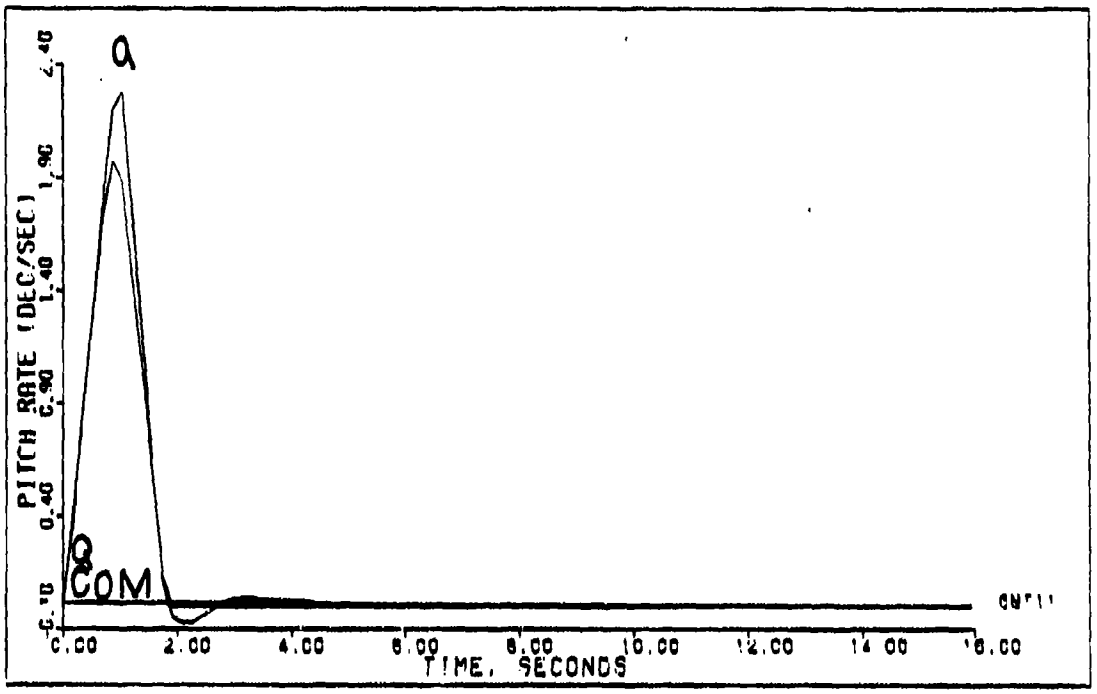

PITCH POINTING (0.7M 15K FT) ACTUATORS

Figure F-99

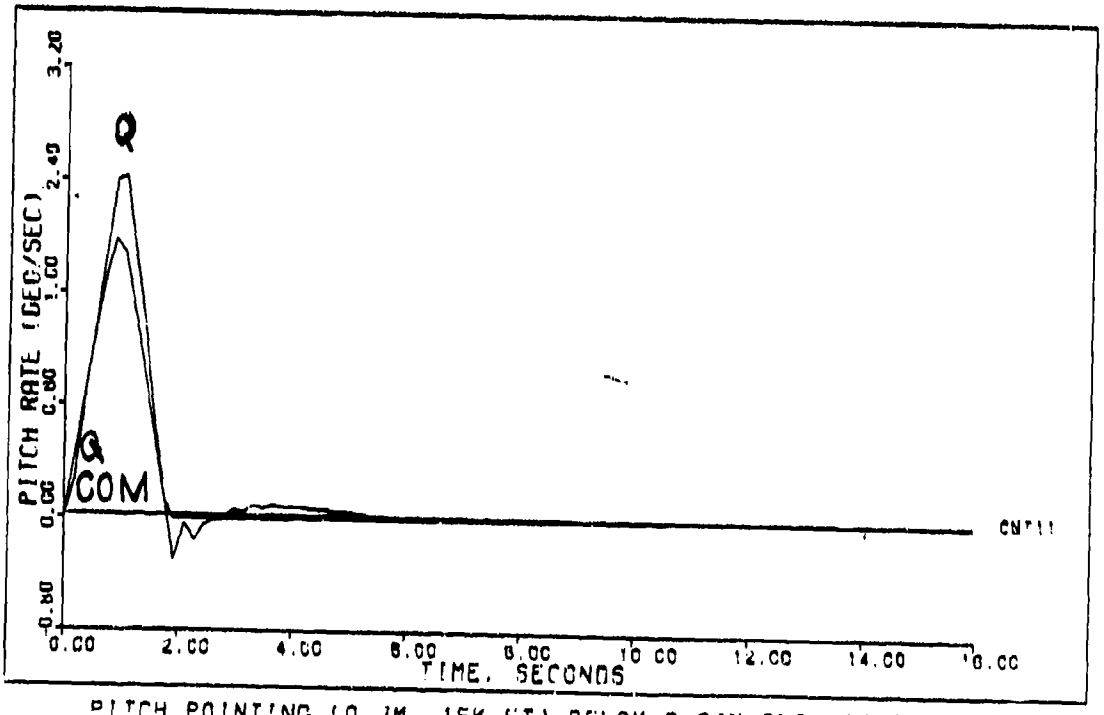

PITCH POINTING (0.7M 15K FT) DELAY=0.025 SEC ACTUATORS

Figure F-100

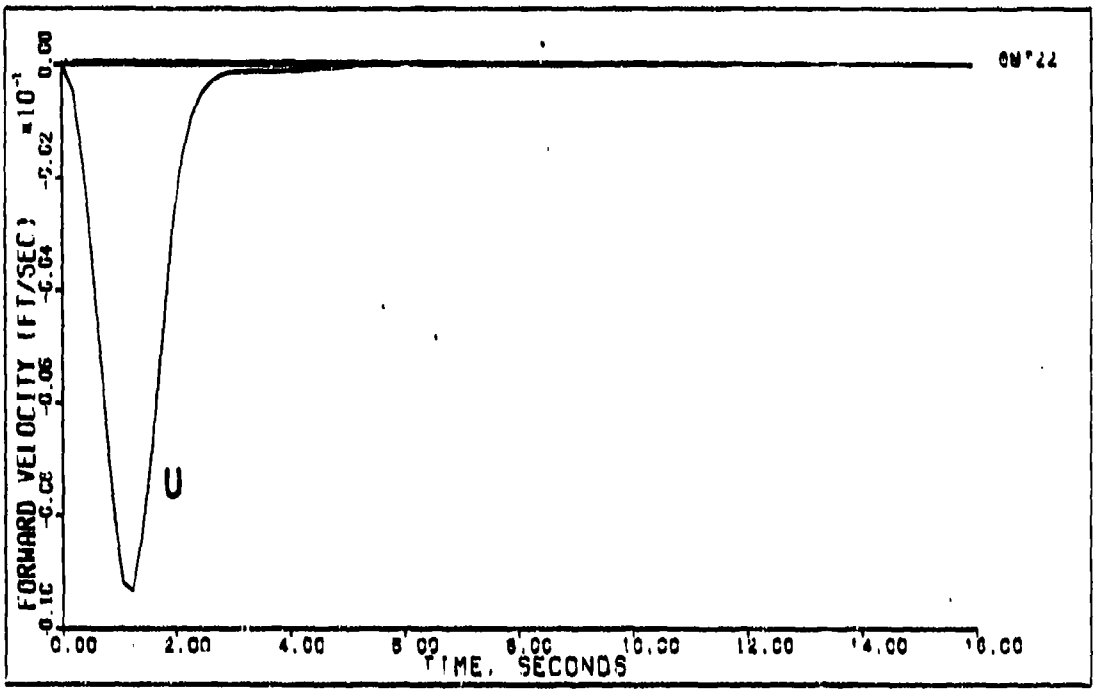

PITCH POINTING (0.7M 15K FT)

Figure F-101

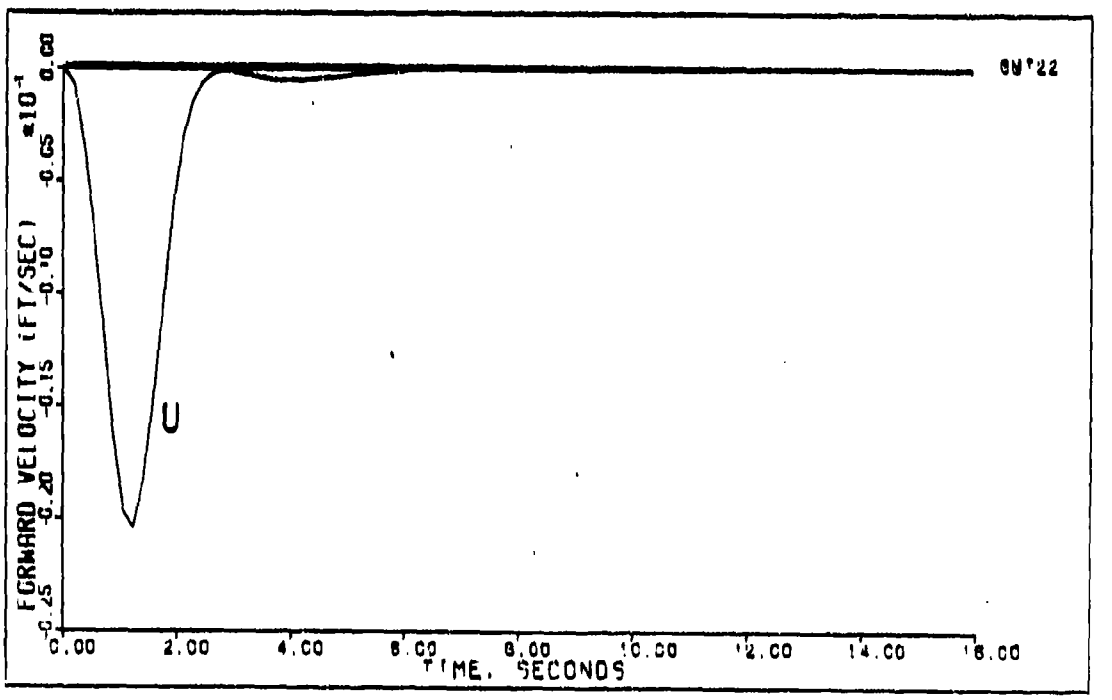

PITCH POINTING (0.7M 15K FT) DELAY=0.025 SEC

Figure F-102

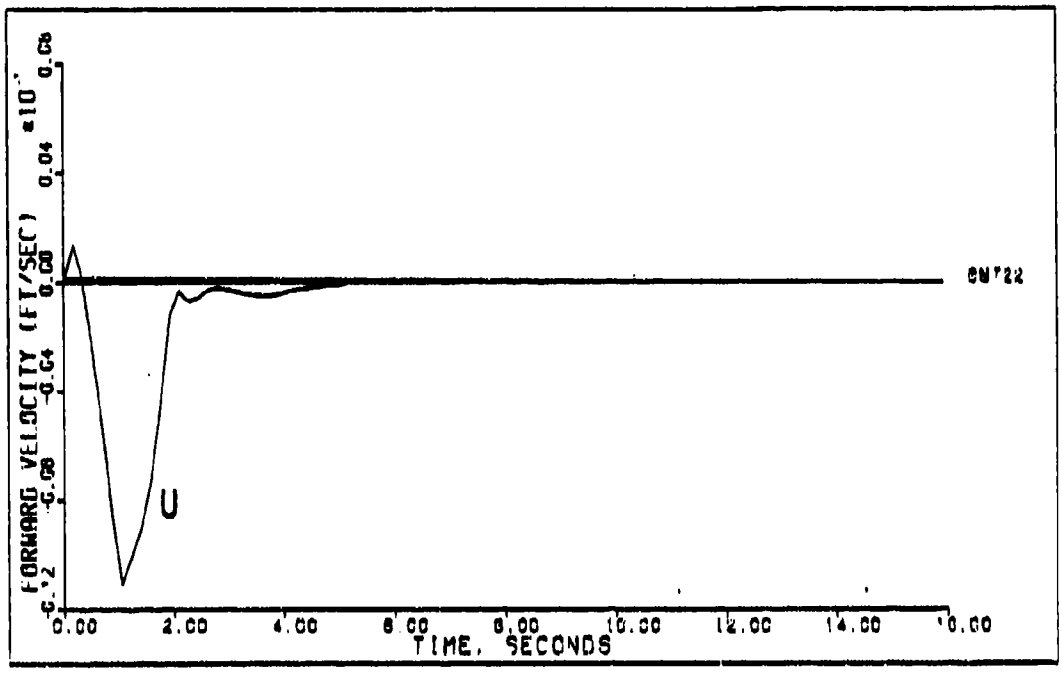

PITCH POINTING (0.7M 15K FT) ACTUATORS

Figure F-103

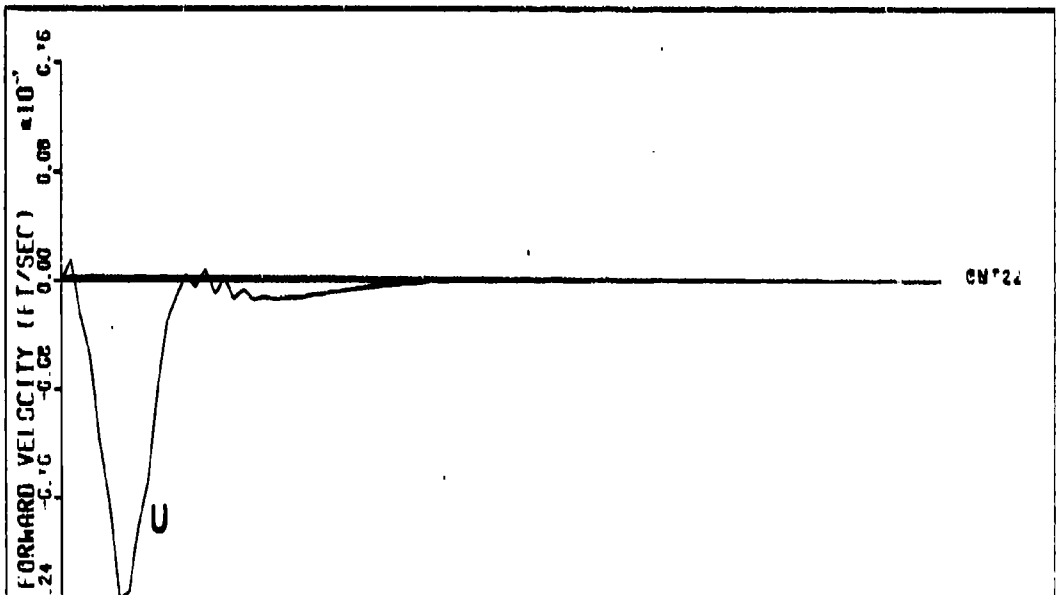

PITCH POINTING (0.7M 15K FT) DELAY=0.025 SEC ACTUATORS

Figure F-104

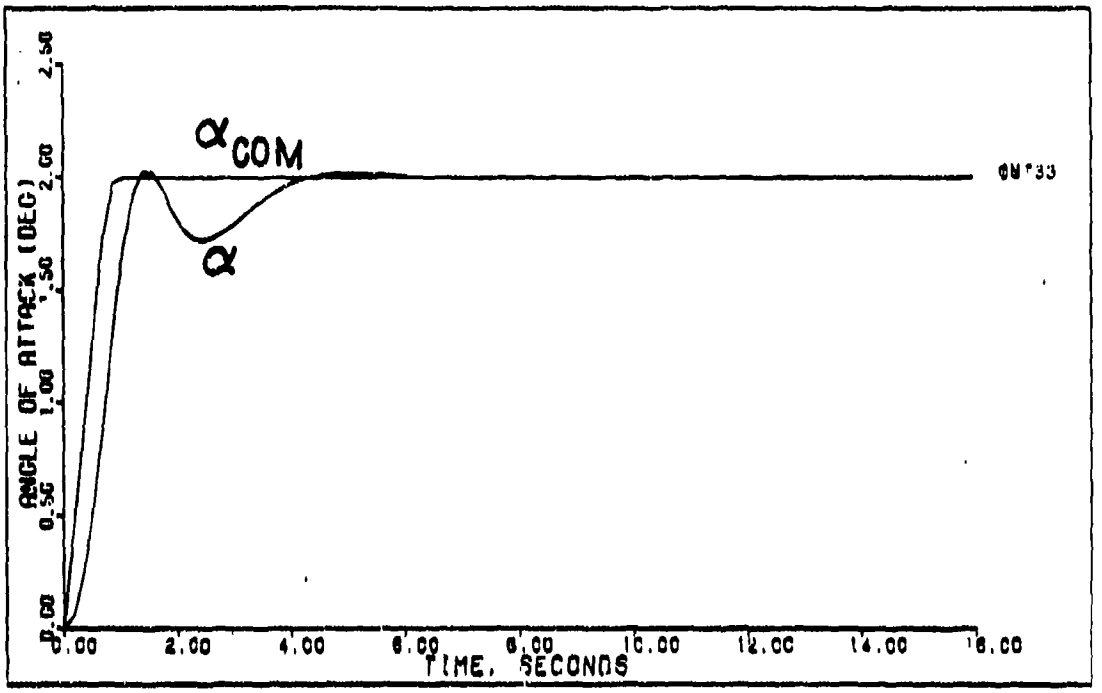

PITCH POINTING (0.7M 15K FT)

Figure F-105

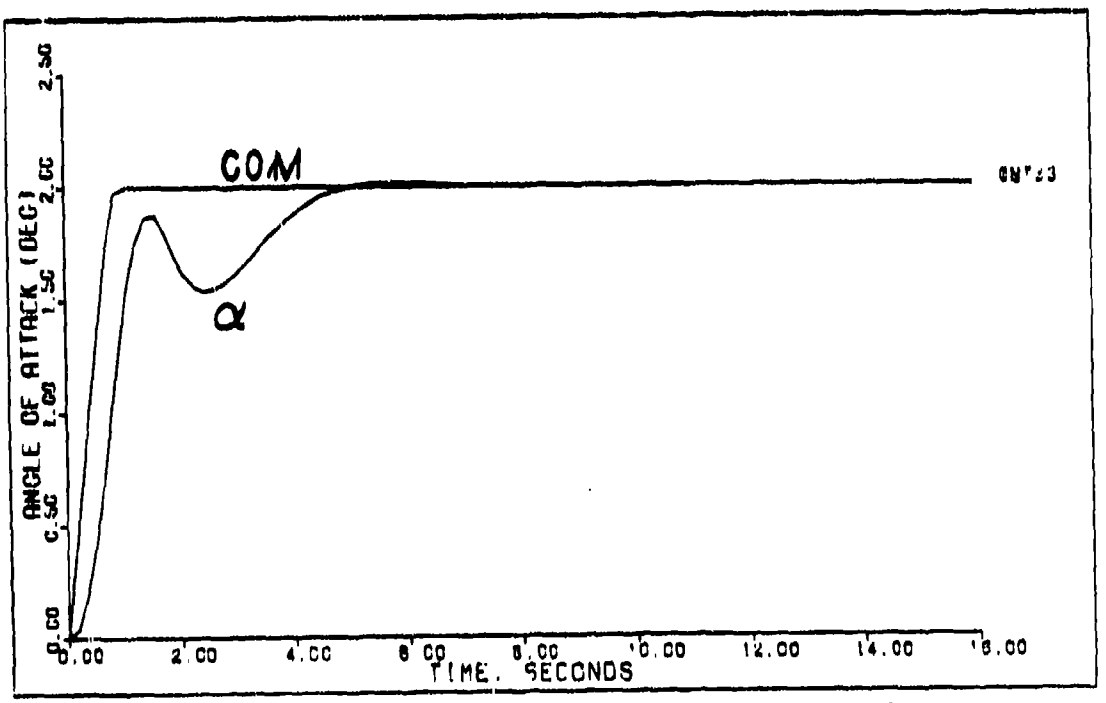

PITCH POINTING (0.7M 15K FT) DELAY=0.025 SEC

Figure F-106

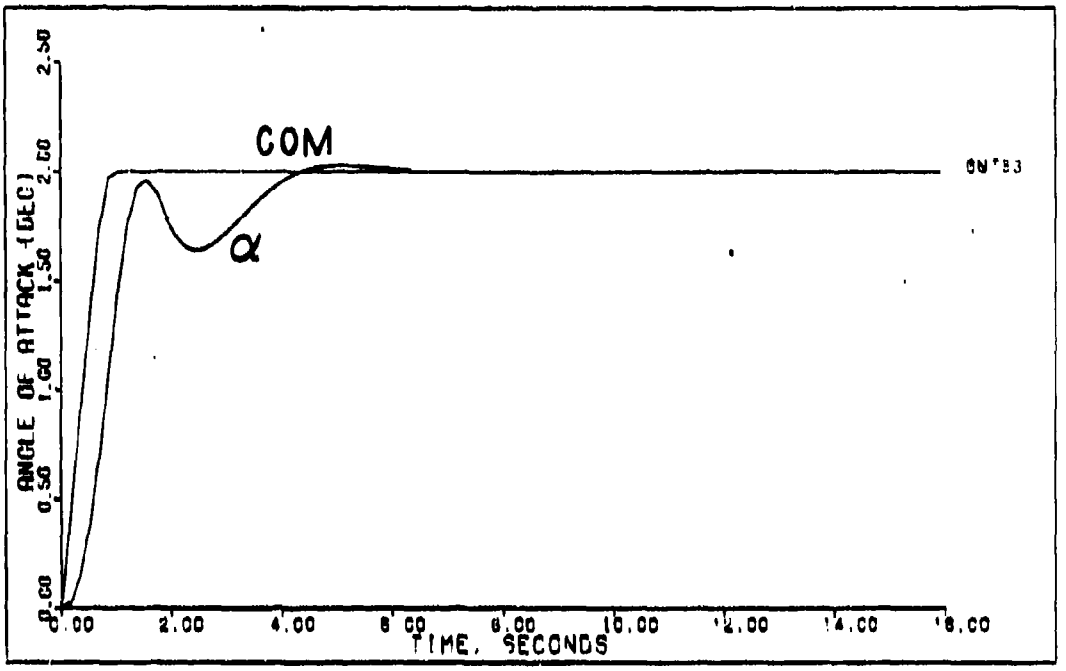

PITCH POINTING (0.7M 15K FT) ACTUATORS

Figure F-107

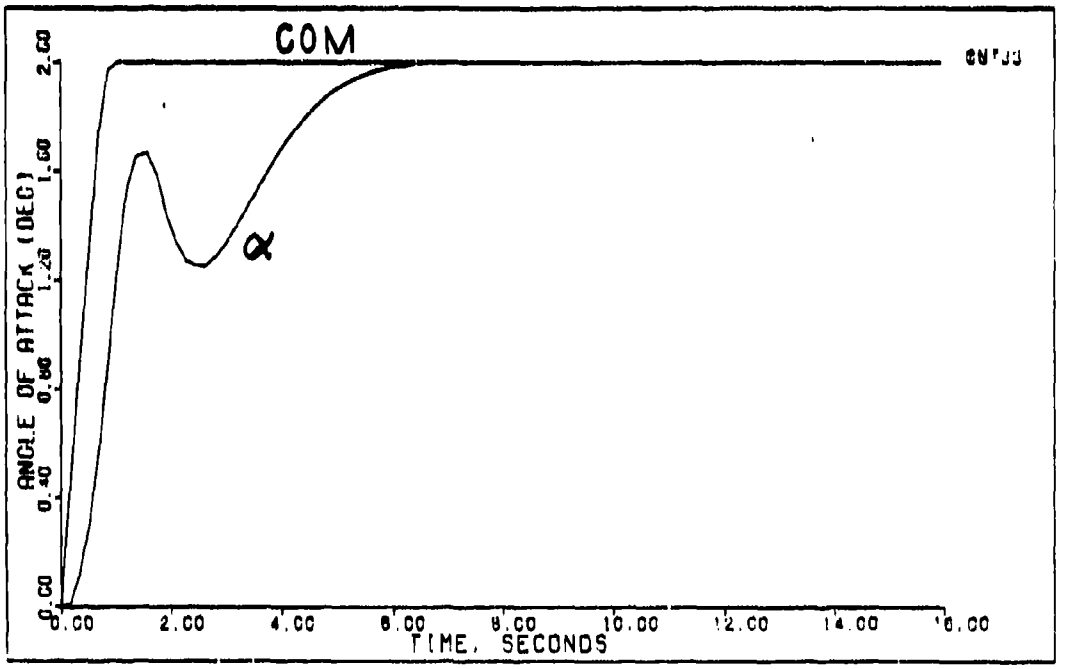

PITCH POINTING (0.7M 15K FT) DELAY=0.025 SEC ACTUATORS

Figure F-108

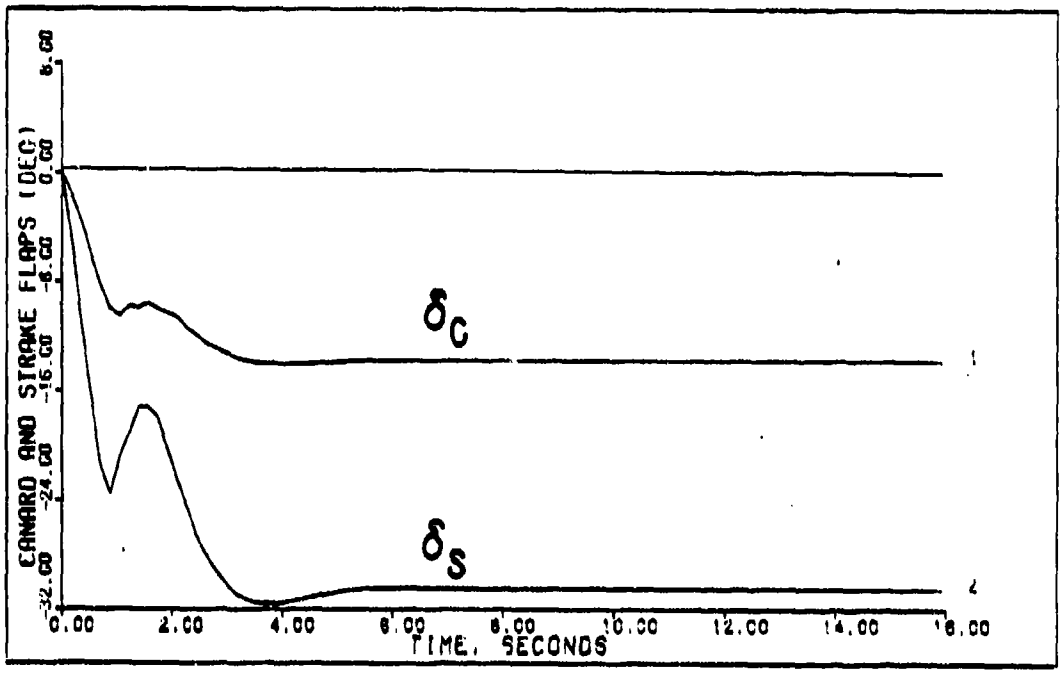

PITCH POINTING (0.7M 15K FT)

Figure F-109

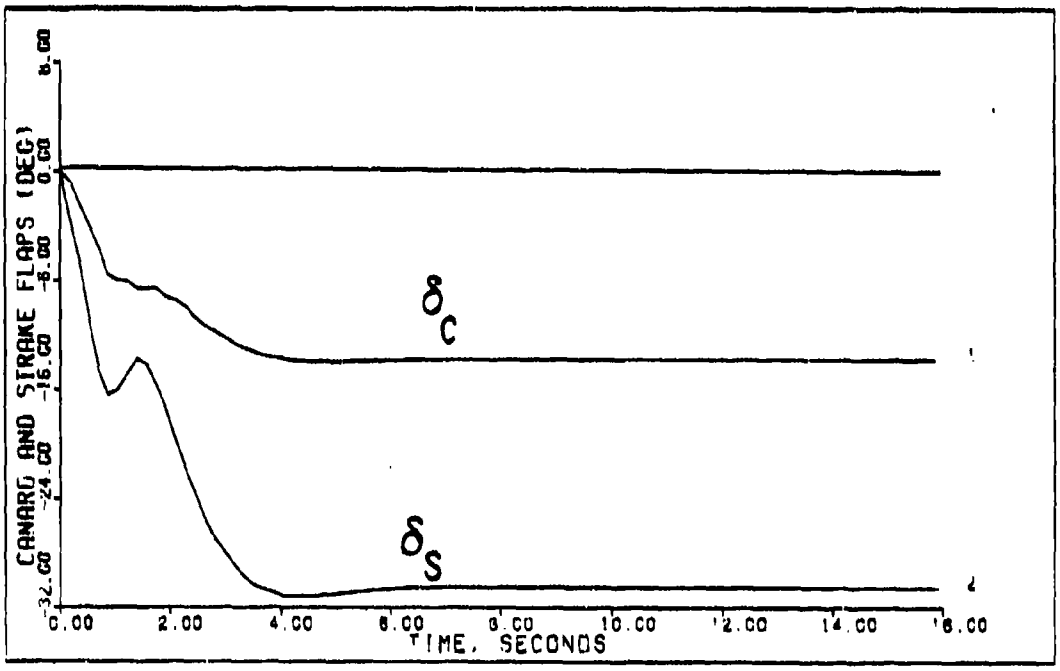

PITCH POINTING (0.7M 15K FT) DELAY=0.025 SEC

Figure F-110

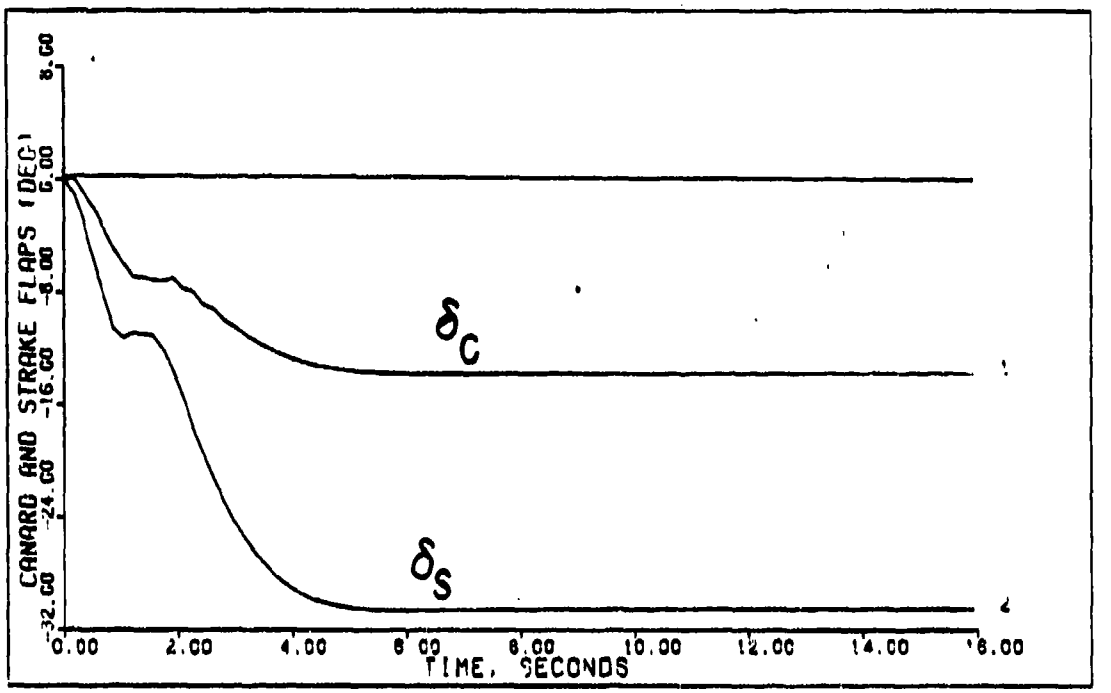

PITCH POINTING (0.7M 15K FT) DELAY=0.025 SEC ACTUATORS

Figure F-111

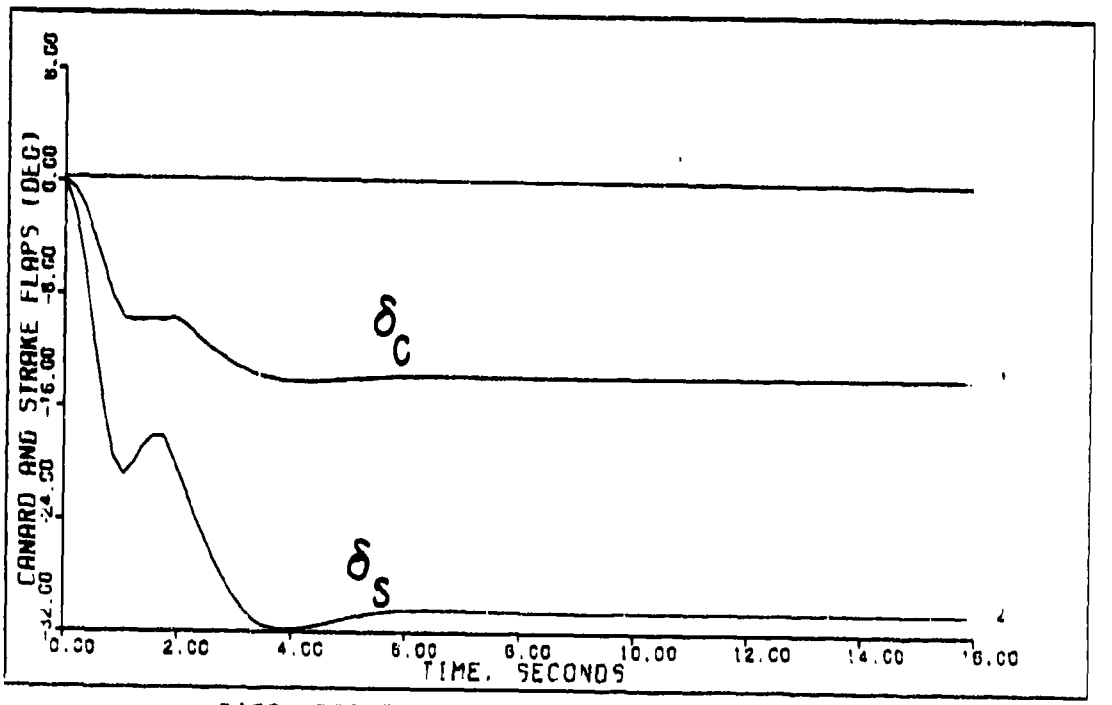

PITCH POINTING (0.7M 15K FT) ACTUATORS

Figure F-112

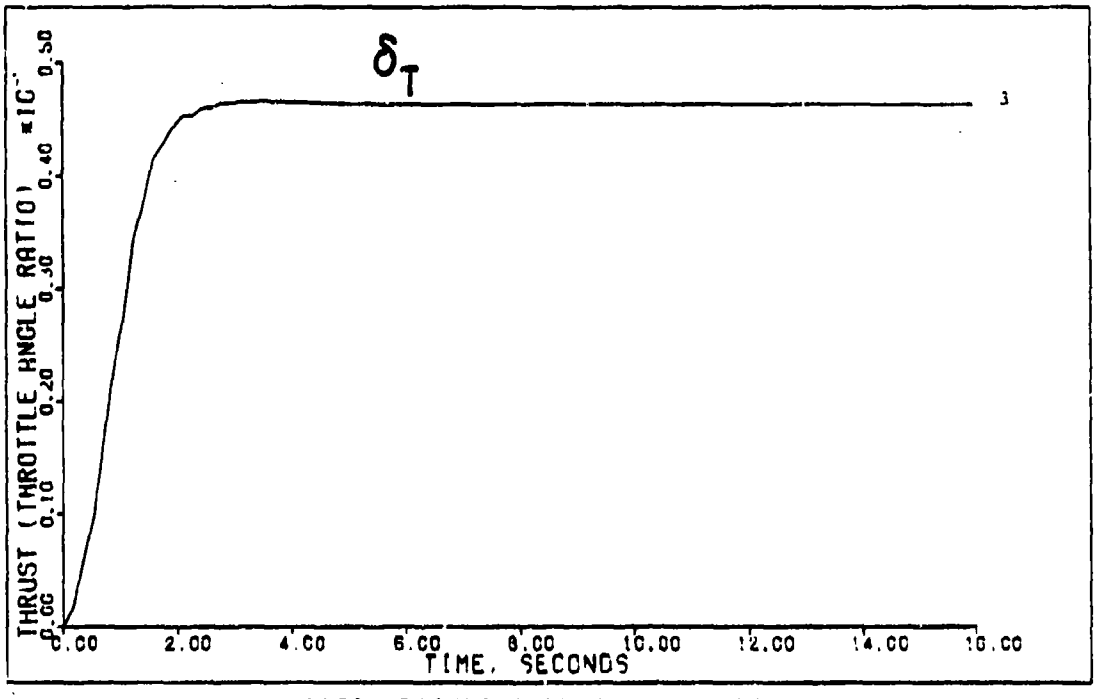

PITCH POINTING (0.7M 15K FT)

Figure F-113

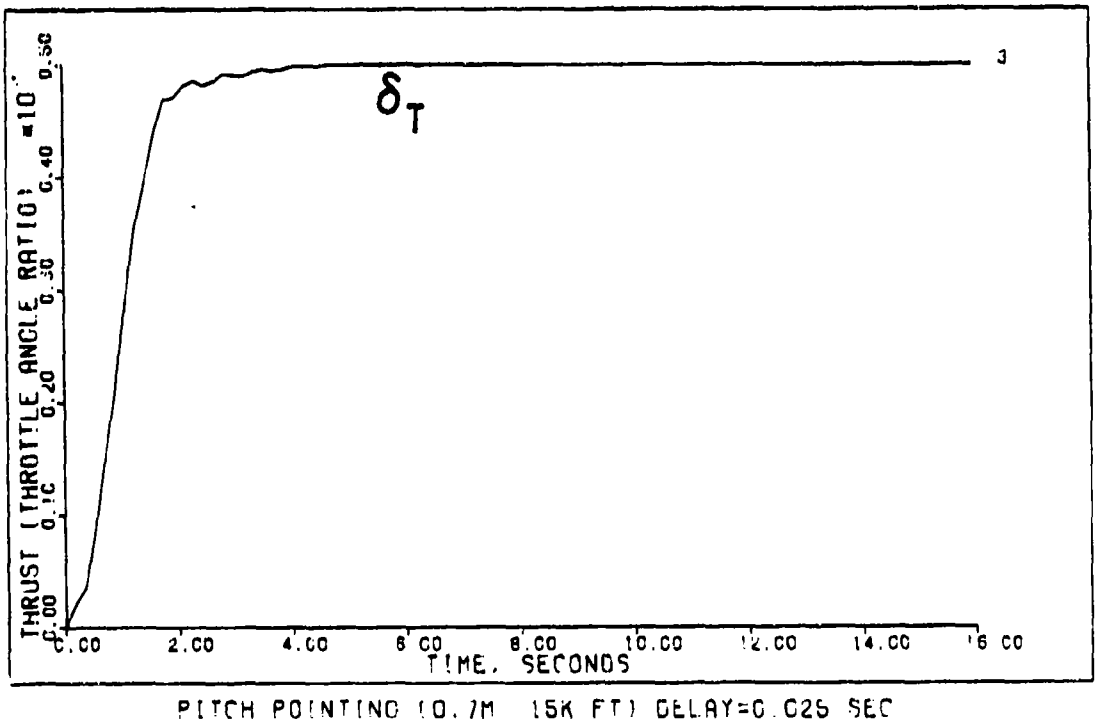

PITCH POINTING (0.7M 15K FT) DELAY=0.025 SEC

Figure F-114

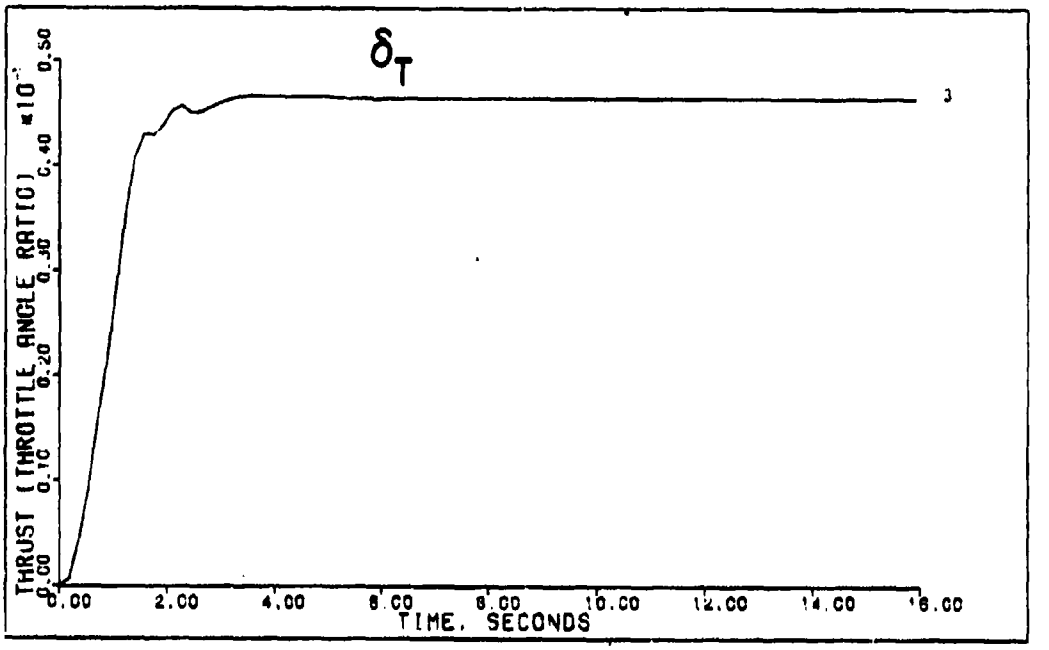

PITCH POINTING (0.7M 15K FT) ACTUATORS

Figure F-115

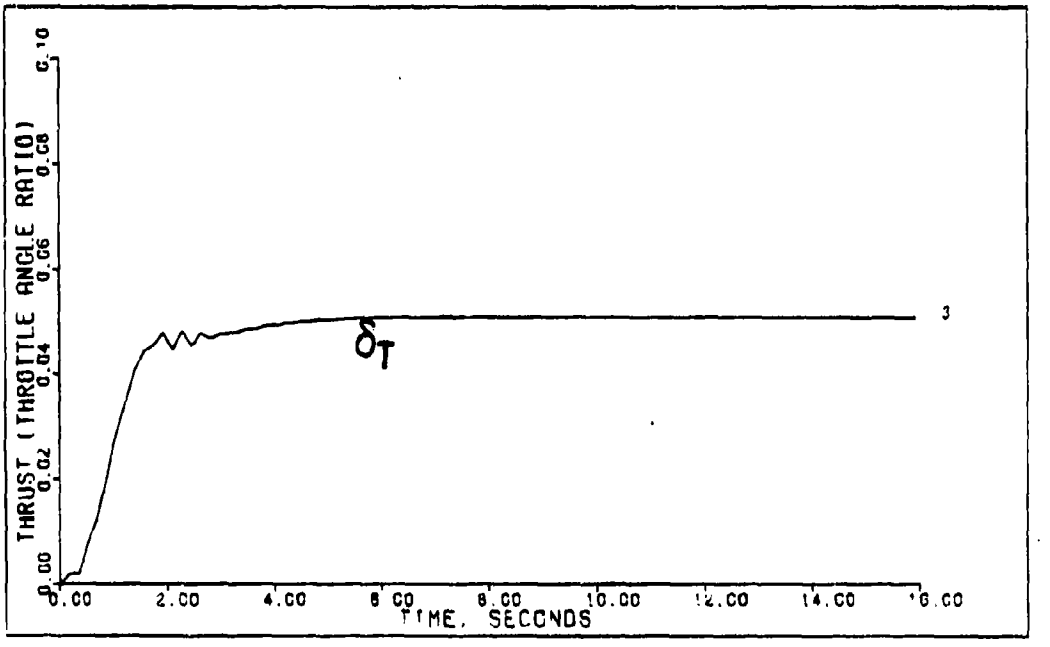

PITCH POINTING (0.7M 15K FT) DELAY=0.025 SEC ACTUATORS

Figure F-116

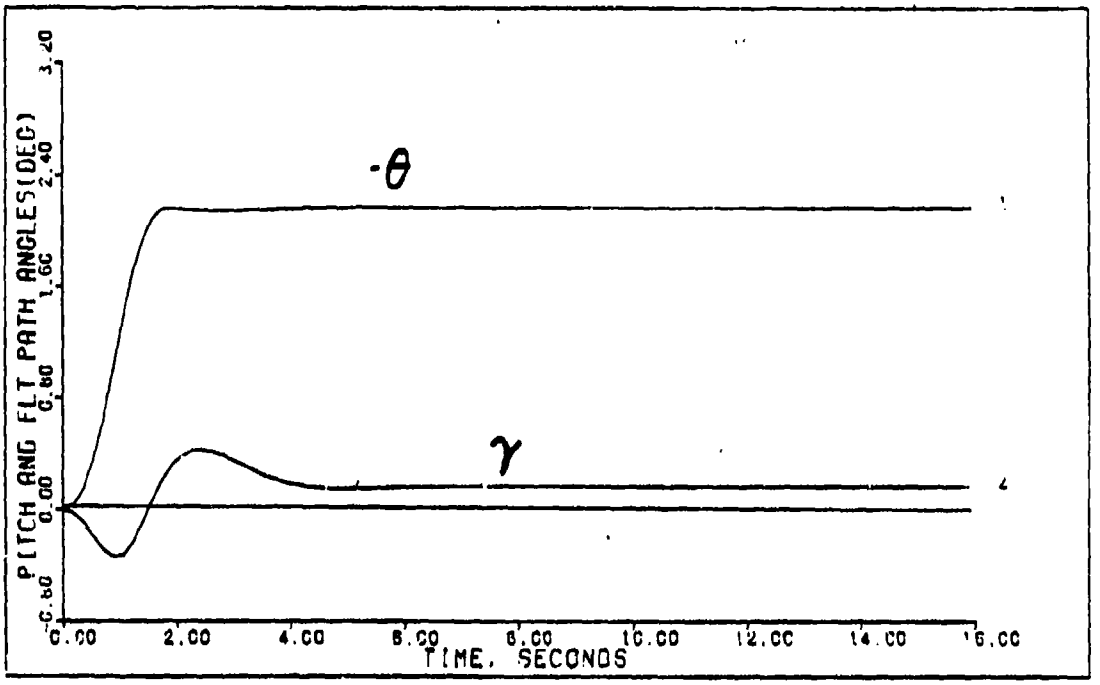

PITCH POINTING (0.7M 15K FT)

Figure F-117

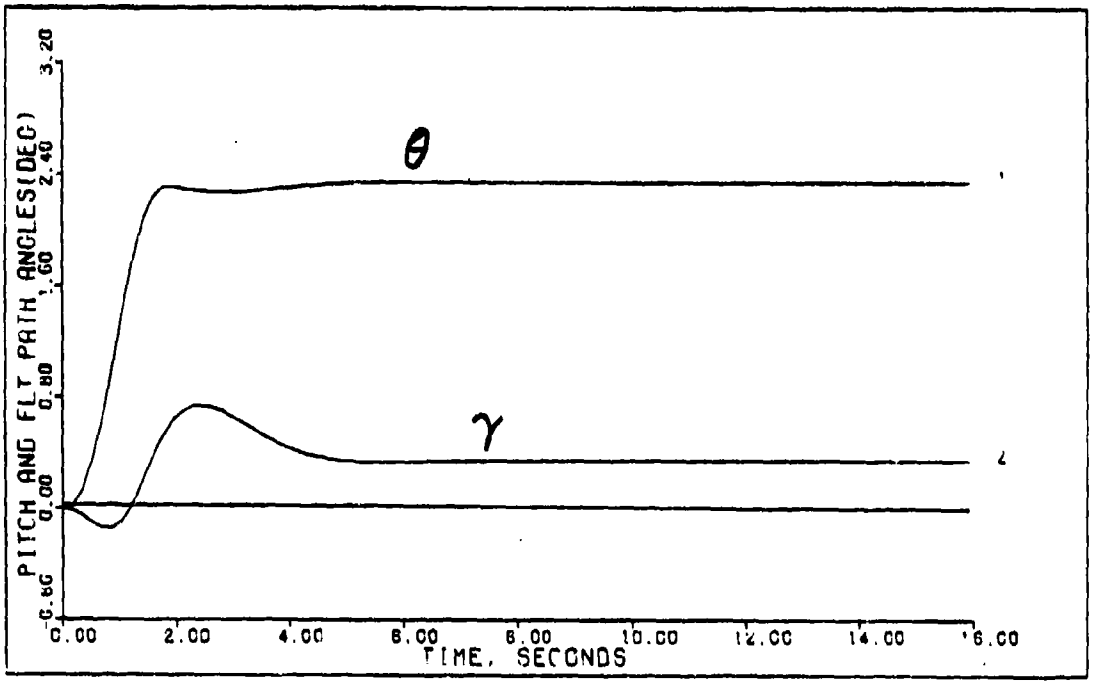

PITCH POINTING (0.7M 15K FT) DELAY=0.025 SEC

Figure F-118

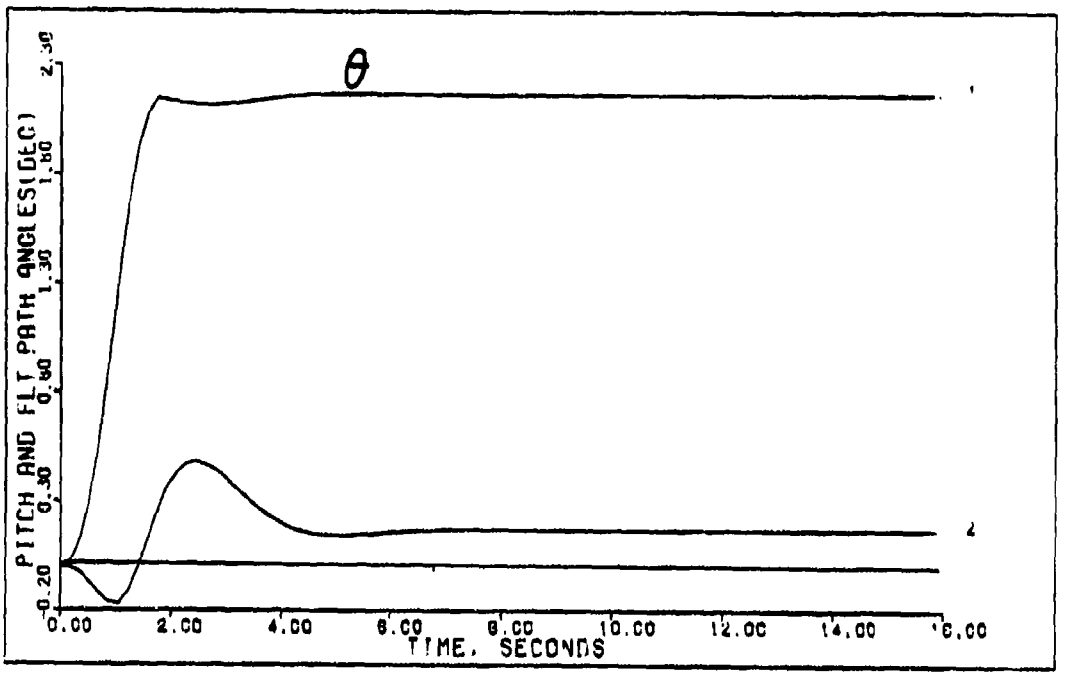

PITCH POINTING (0.7M 15K FT) ACTUATORS

Figure F-119

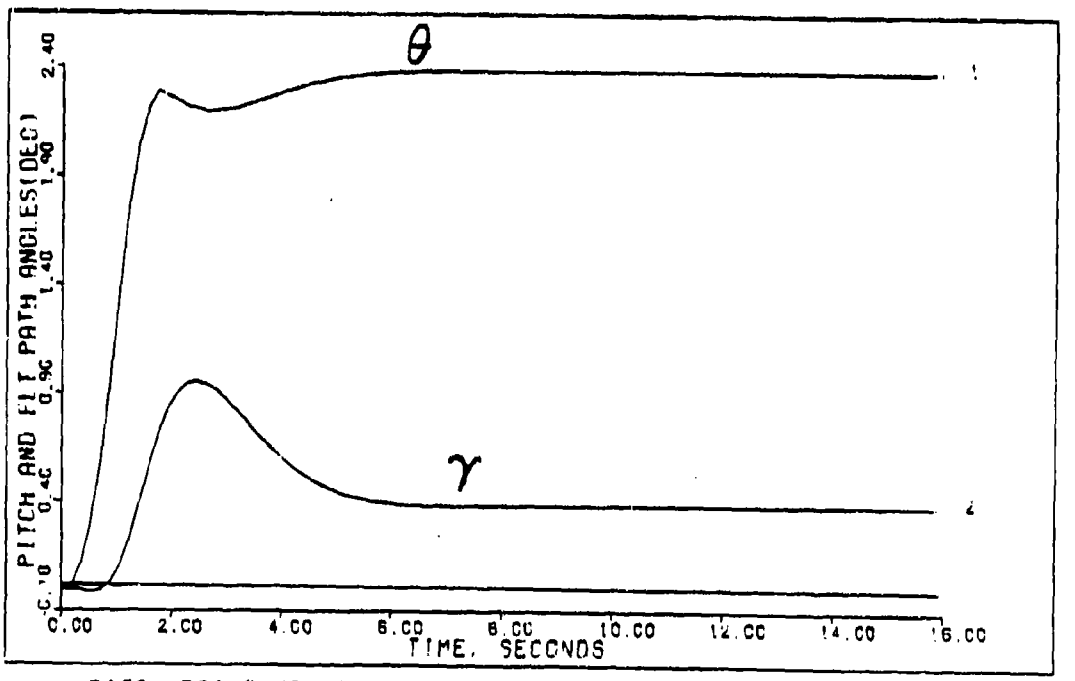

PITCH POINTING (0.7M 15K FT) DELAY=0.025 SEC ACTUATORS

Figure F-120

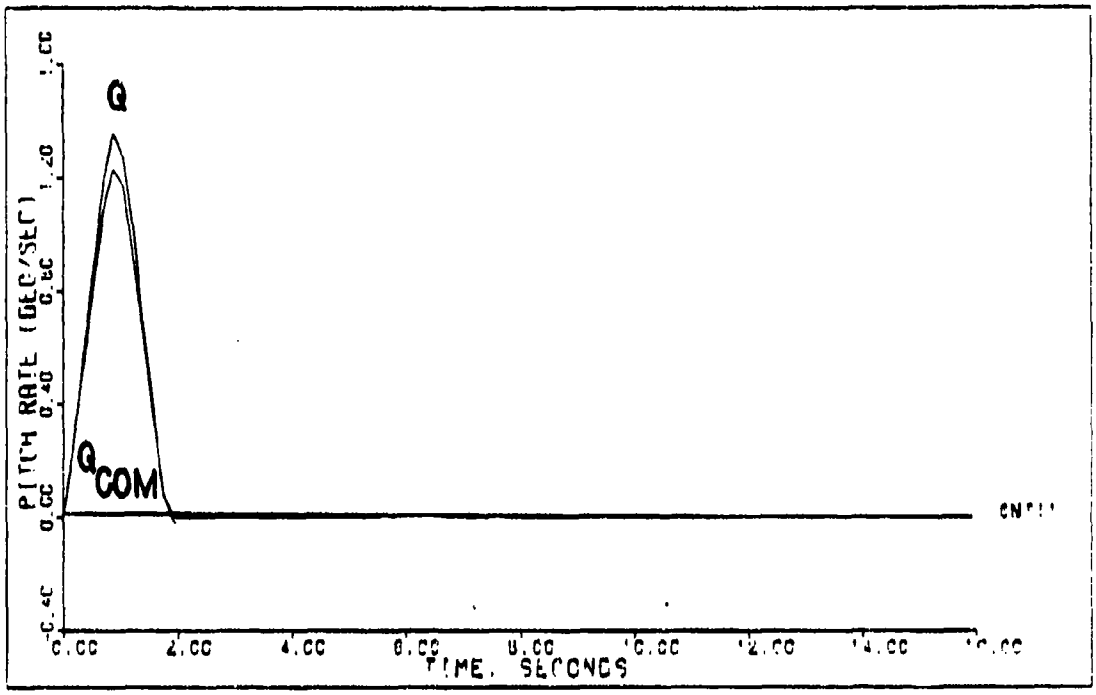

PITCH POINTING (1.2M 15K FT)

Figure F-121

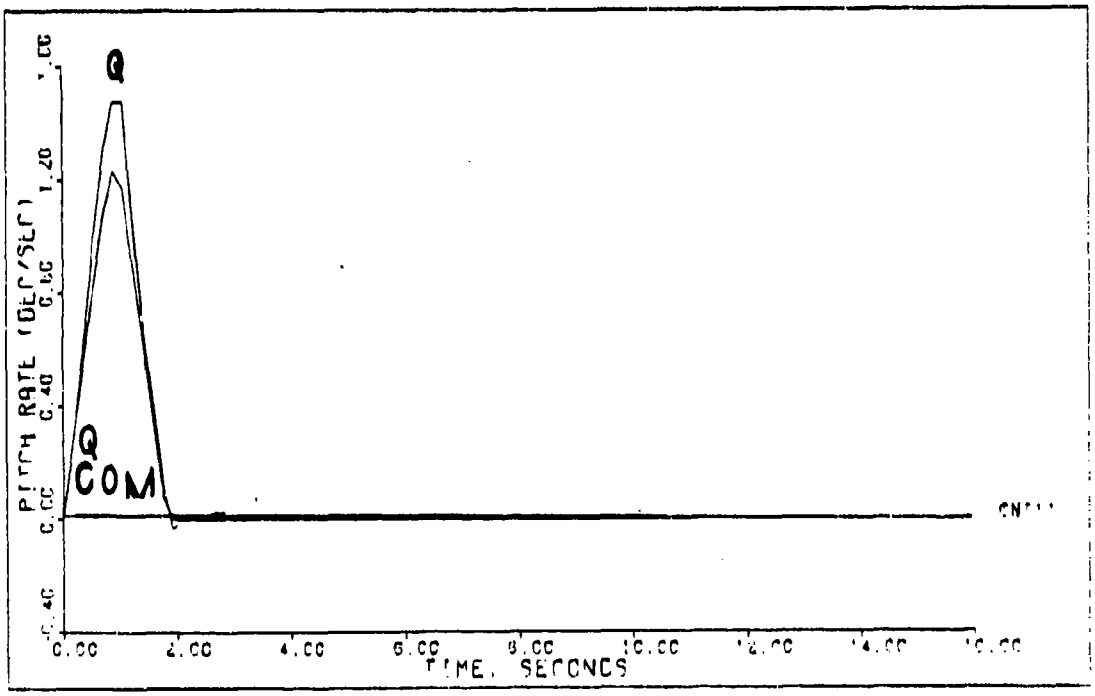

PITCH POINTING (1.2M 15K FT) DELAY=0.025 SEC

Figure F-122

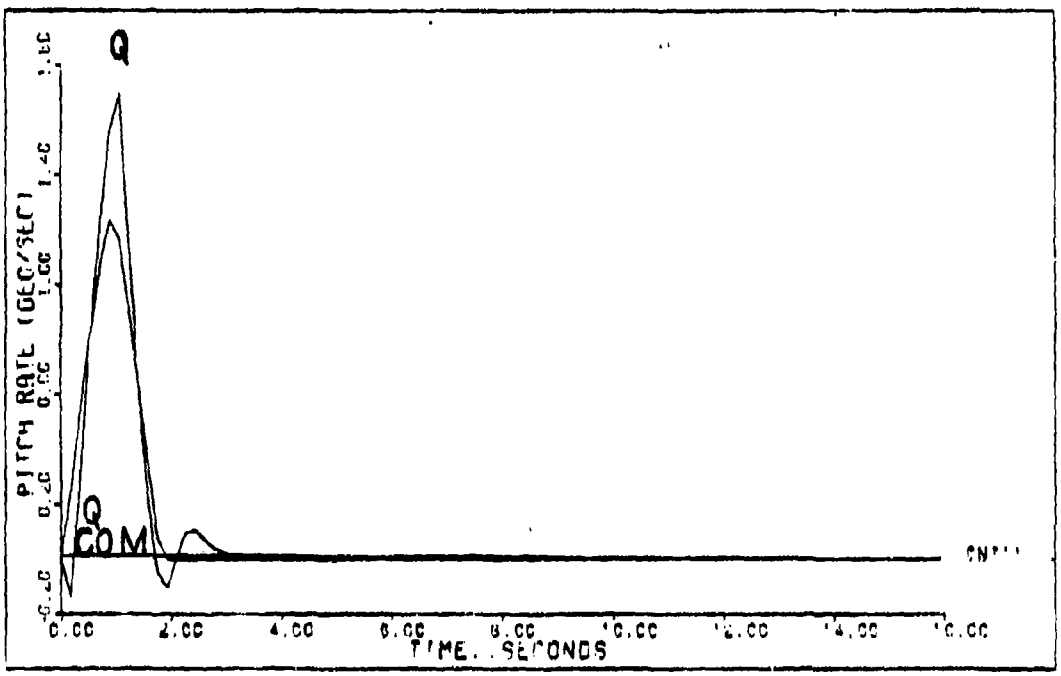

PITCH POINTING 11.2M 15K FT1 ACTUATORS

Figure F-123

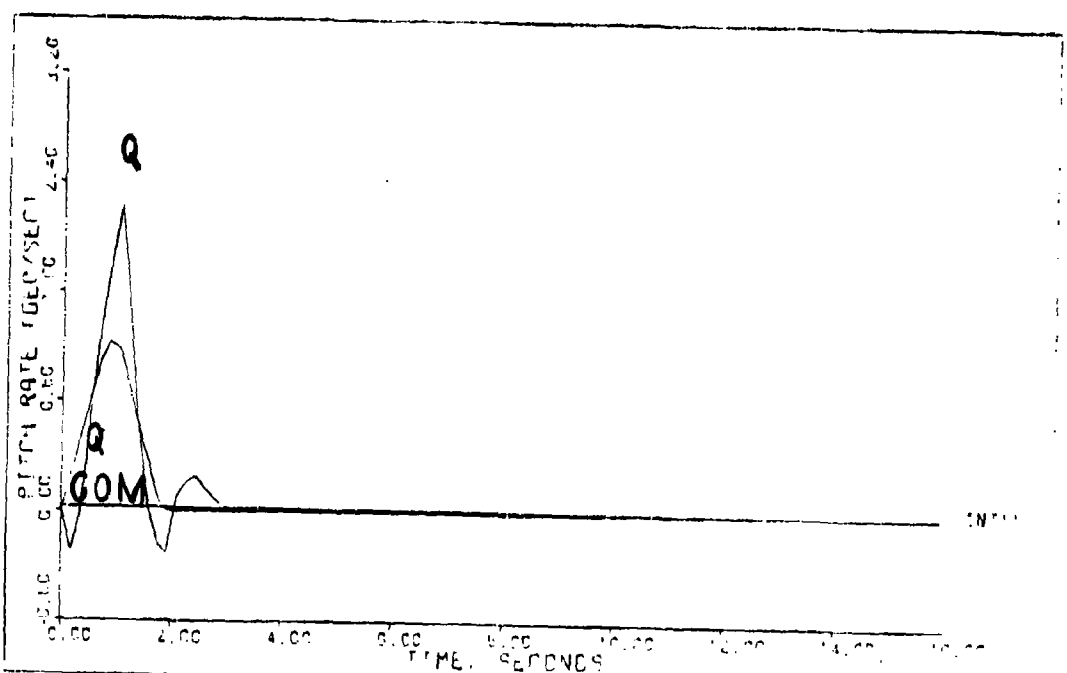

Figure F-124

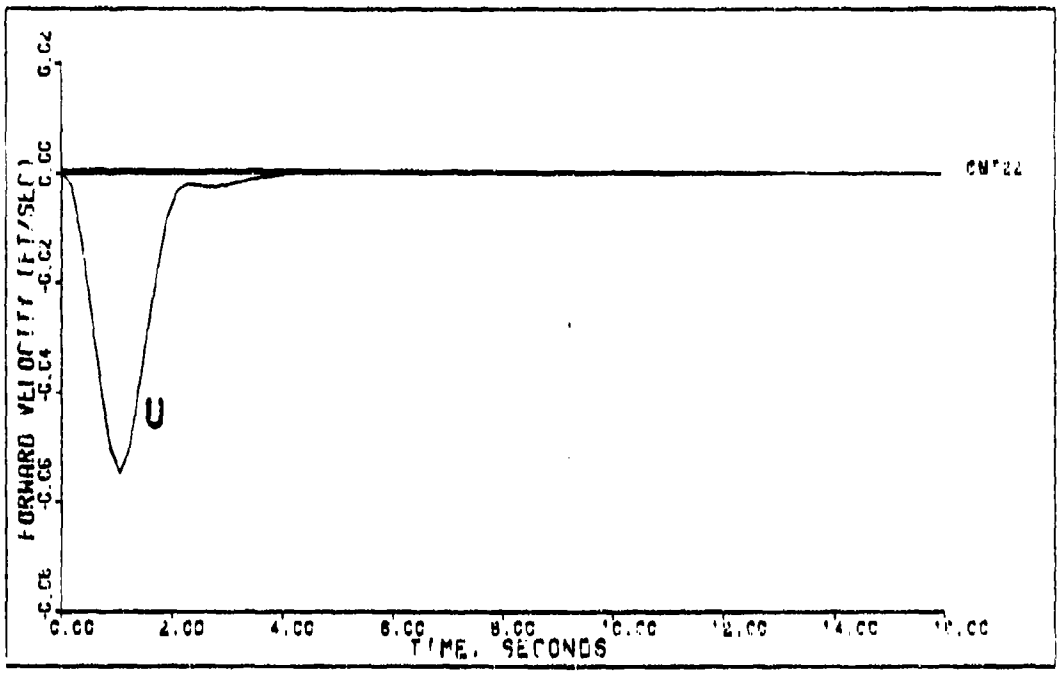

PITCH POINTING (1.2M 15K FT)

Figure F-125

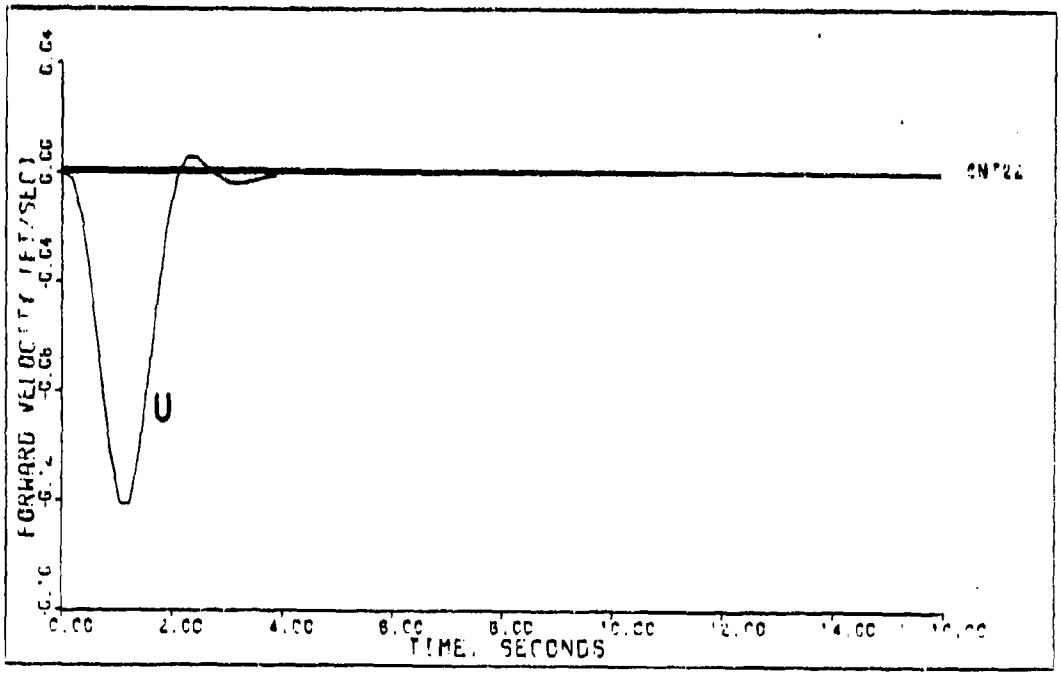

PITCH POINTING (1.2M 15K FT) DELAY=0.025 SEC

Figure F-126

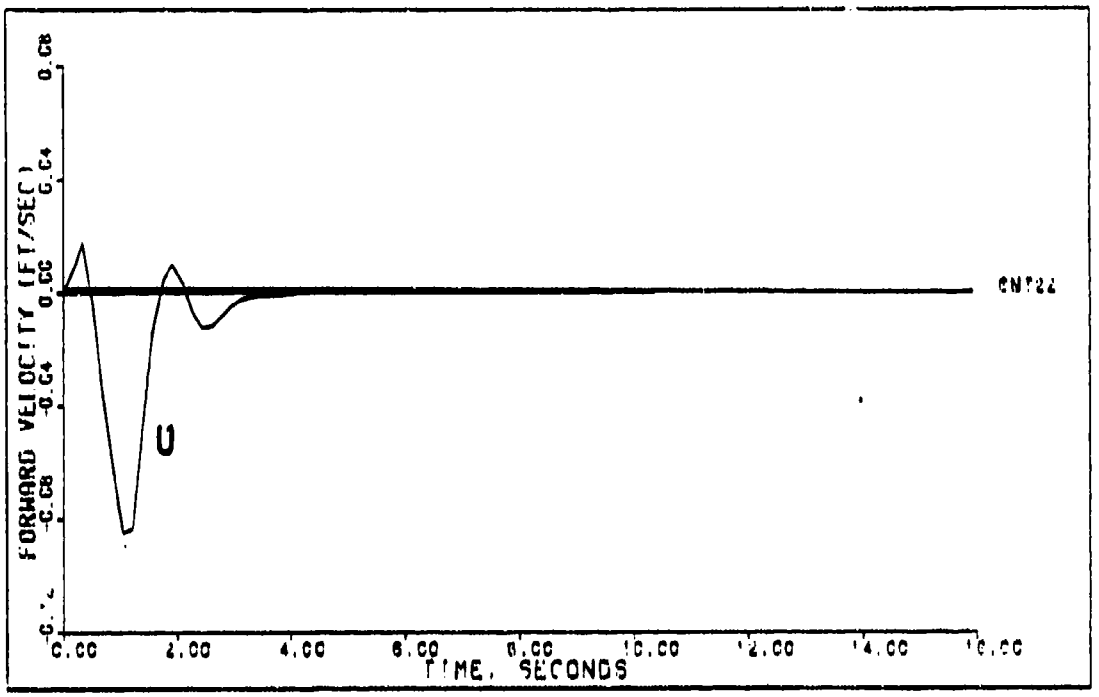

PITCH POINTING (1.2M 15K FT) ACTUATORS

Figure F-127

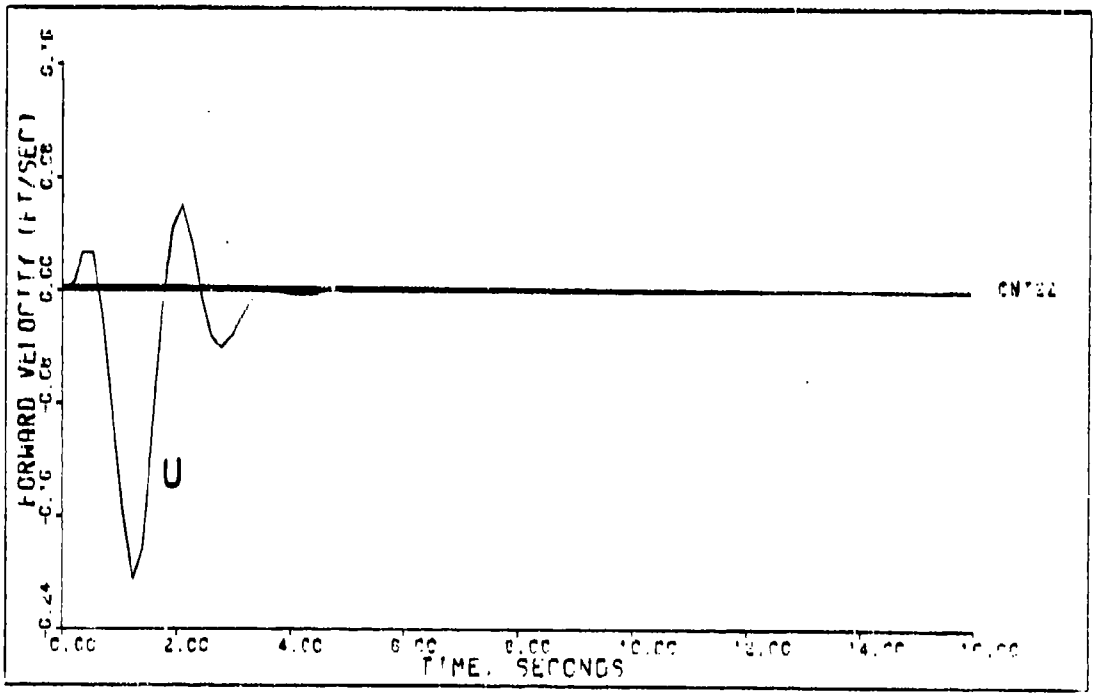

PITCH POINTING (1.2M 15K FT) DELAY=0.025 SEC ACTUATORS

Figure F-128

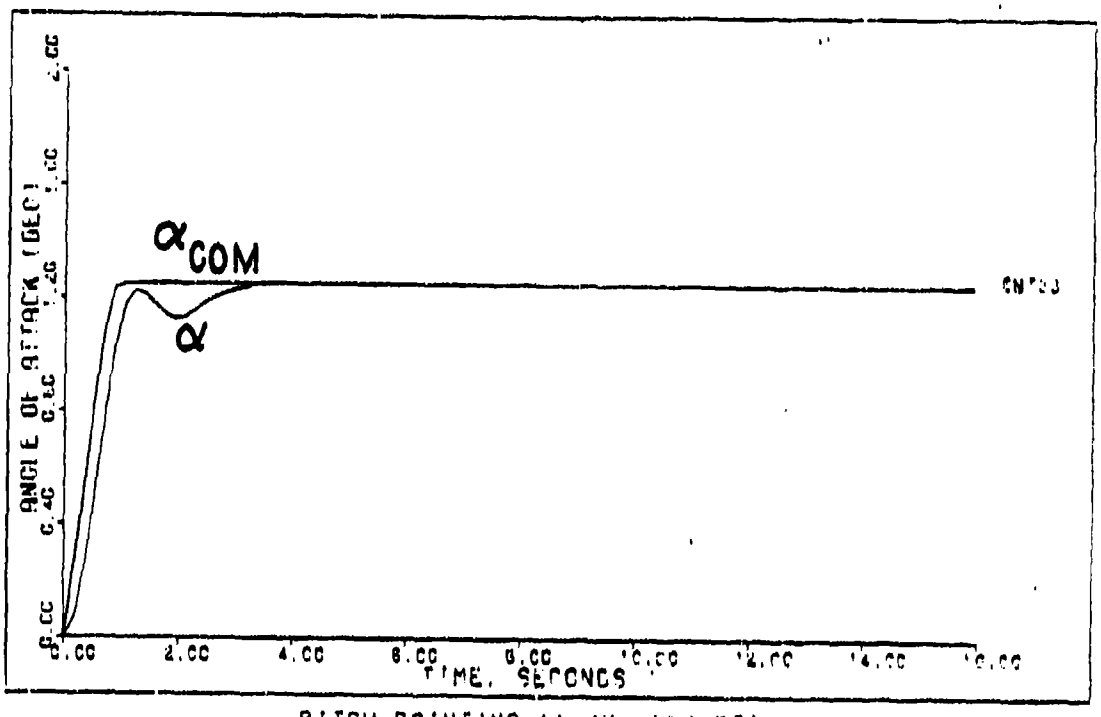

PITCH POINTING (1.2M 15K FT)

Figure F-129

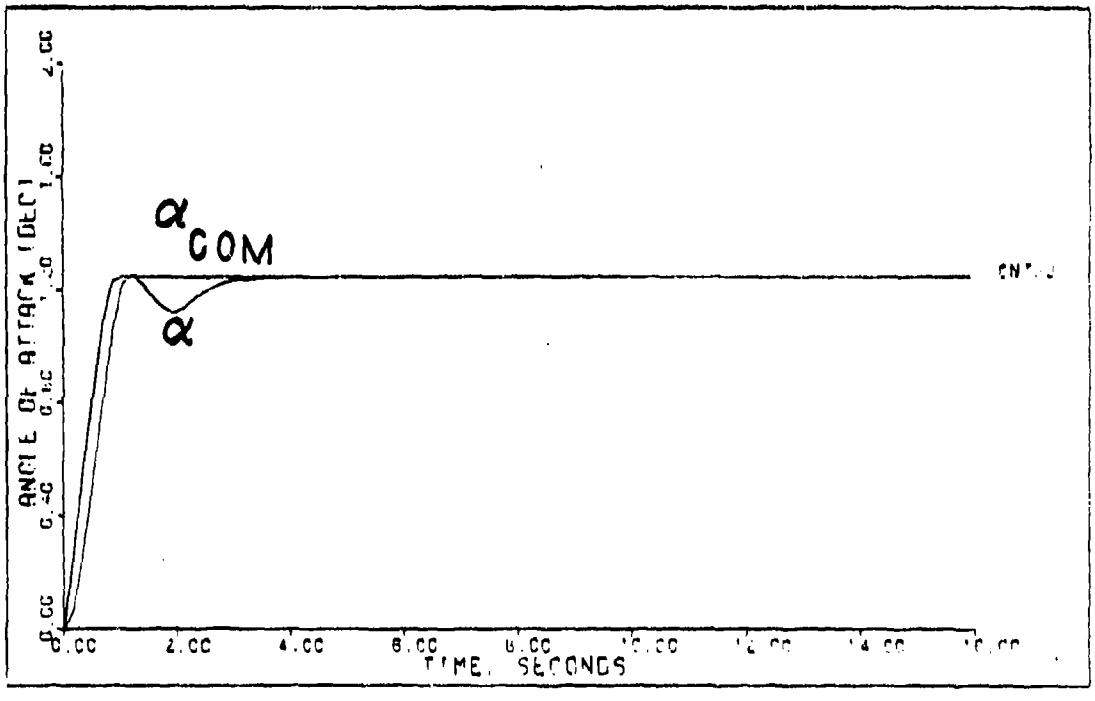

PITCH POINTING (1.2M 15K FT) DELAY=0.026 SEC

Figure F-130

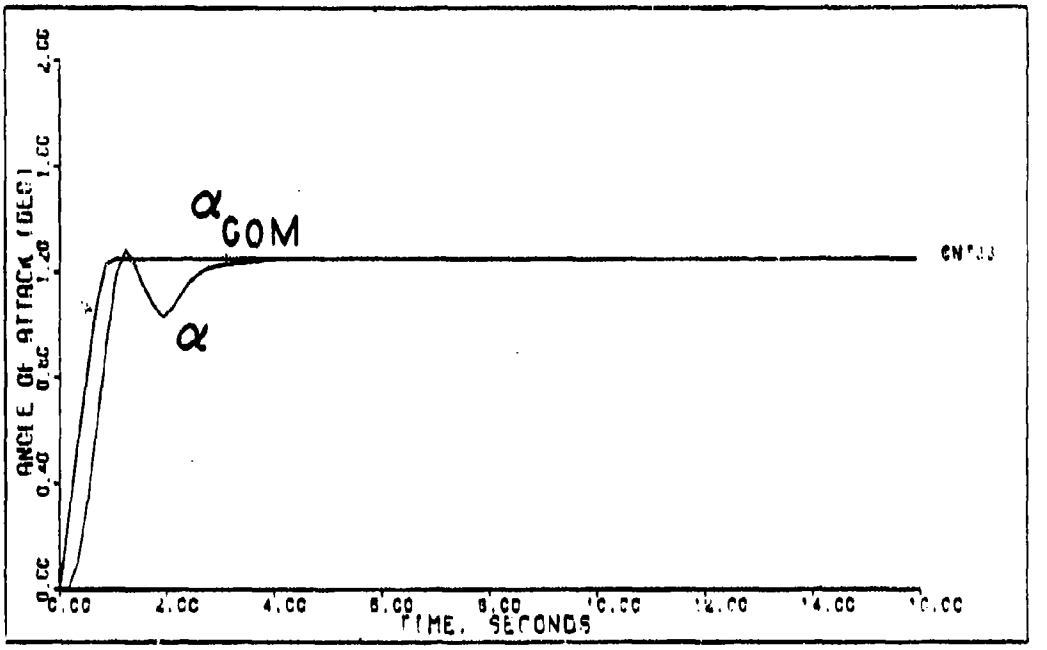

PITCH POINTING (11.2M 15K FT) ACTUATORS

Figure F-131

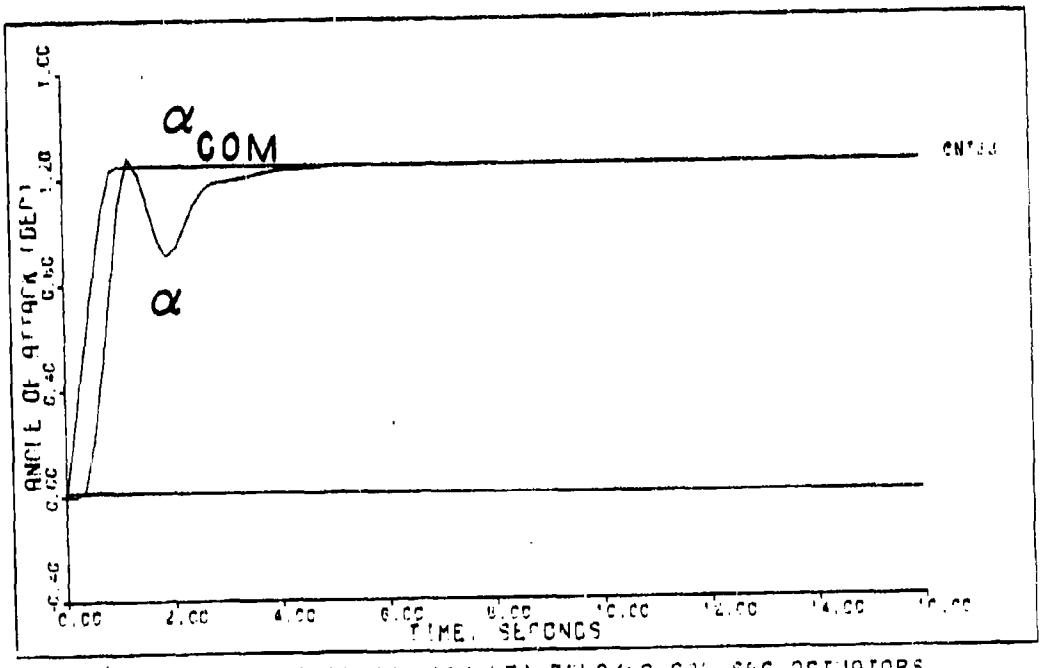

PITCH POINTING (11.2M 15K FT) DELAY=0.025 SEC ACTUATORS

Figure F-132

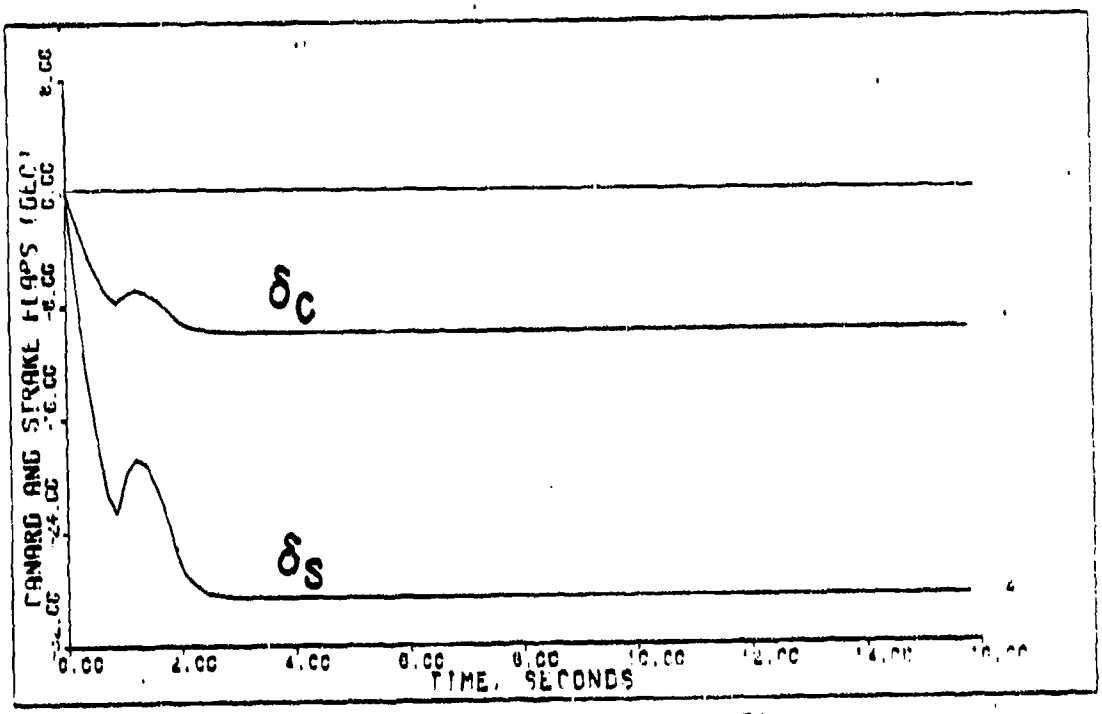

PITCH POINTING (1.2M 15K FT)

Figure F-133

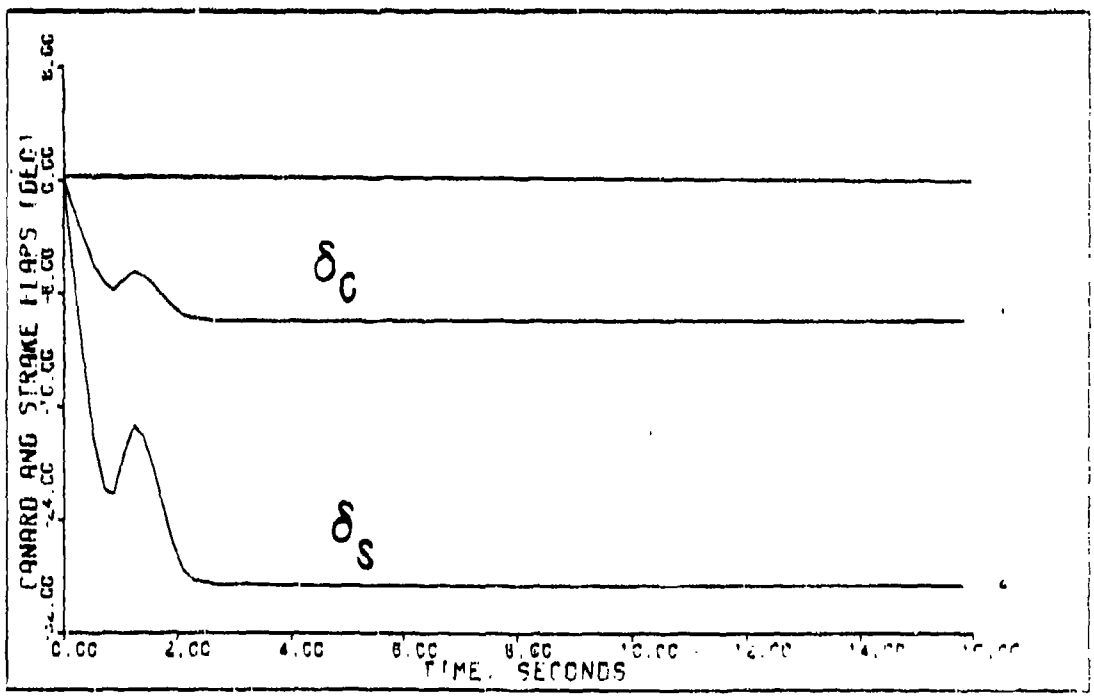

PITCH POINTING (1.2M 15K FT) DELAY=0.025 SEC

Figure F-134

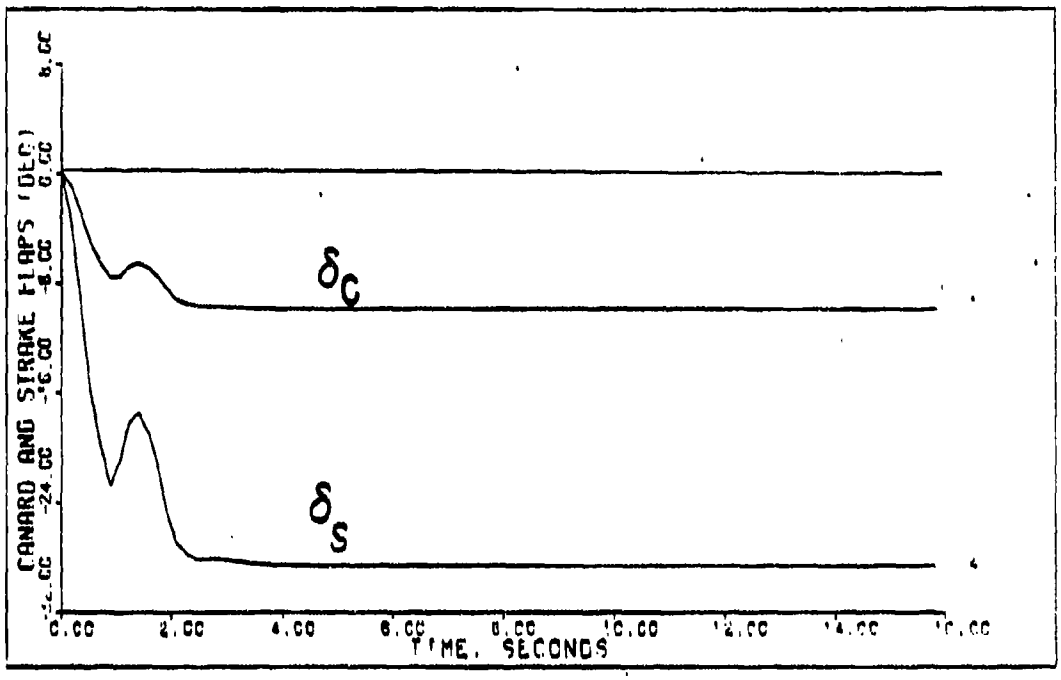

PITCH POINTING (1.2M 15K FT) ACTUATORS

Figure F-145

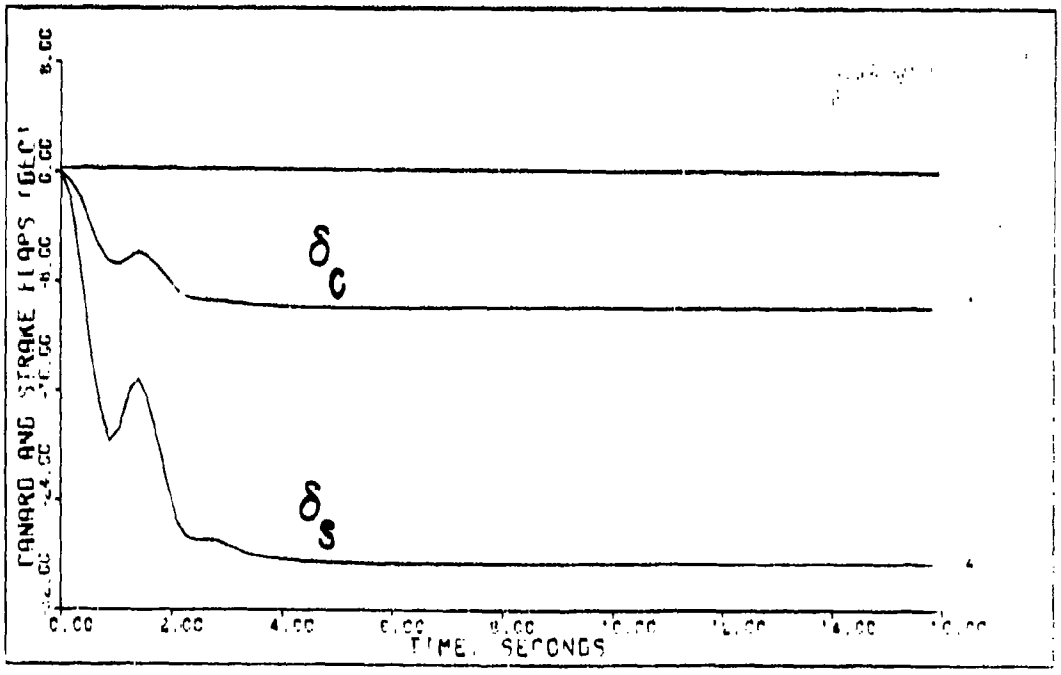

PITCH POINTING (1.2M 15K FT) ω_{BW}=0.02π RAD/SEC ACTUATORS

Figure F-146

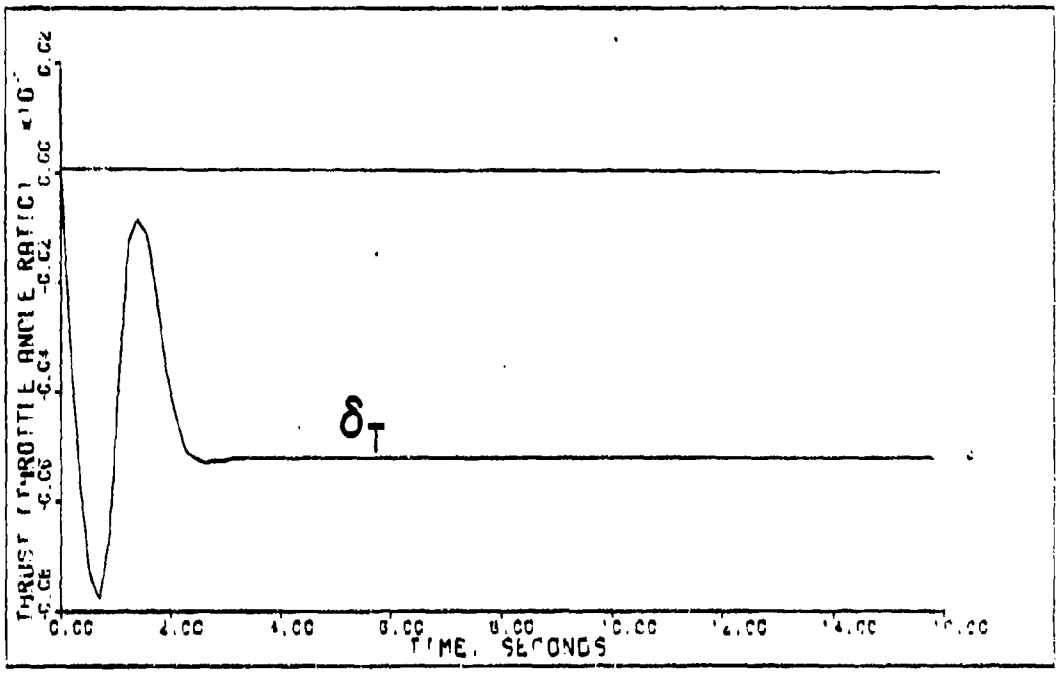

PITCH POINTING (1.2M 15K FT)

Figure F-147

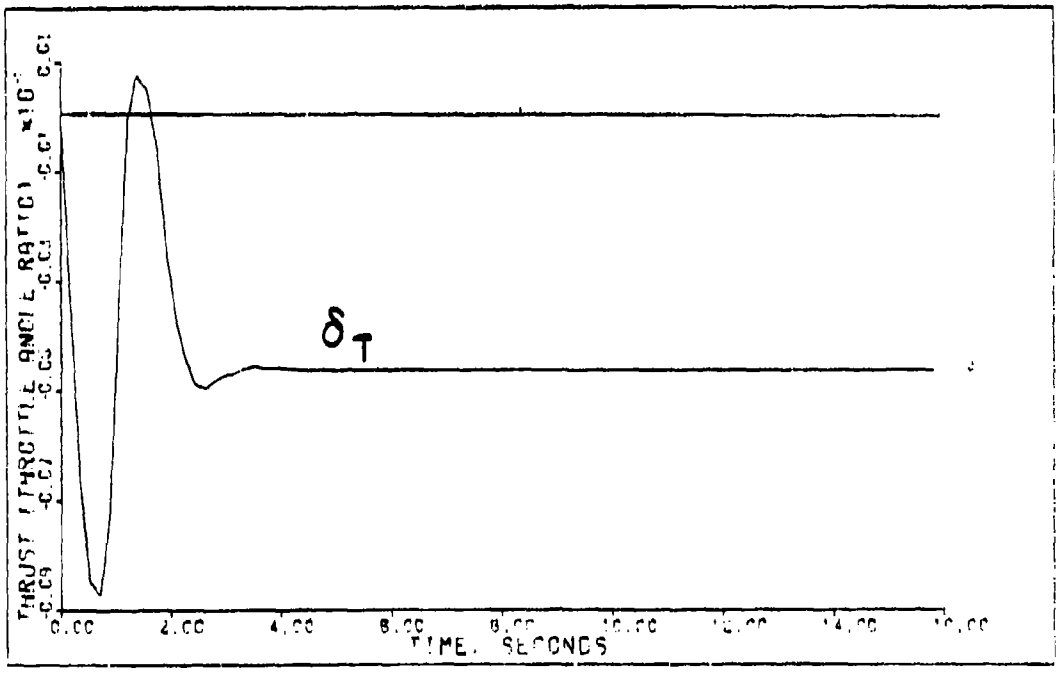

PITCH POINTING (1.2M 15K FT) DELAY=0.020 SEC

Figure F-148

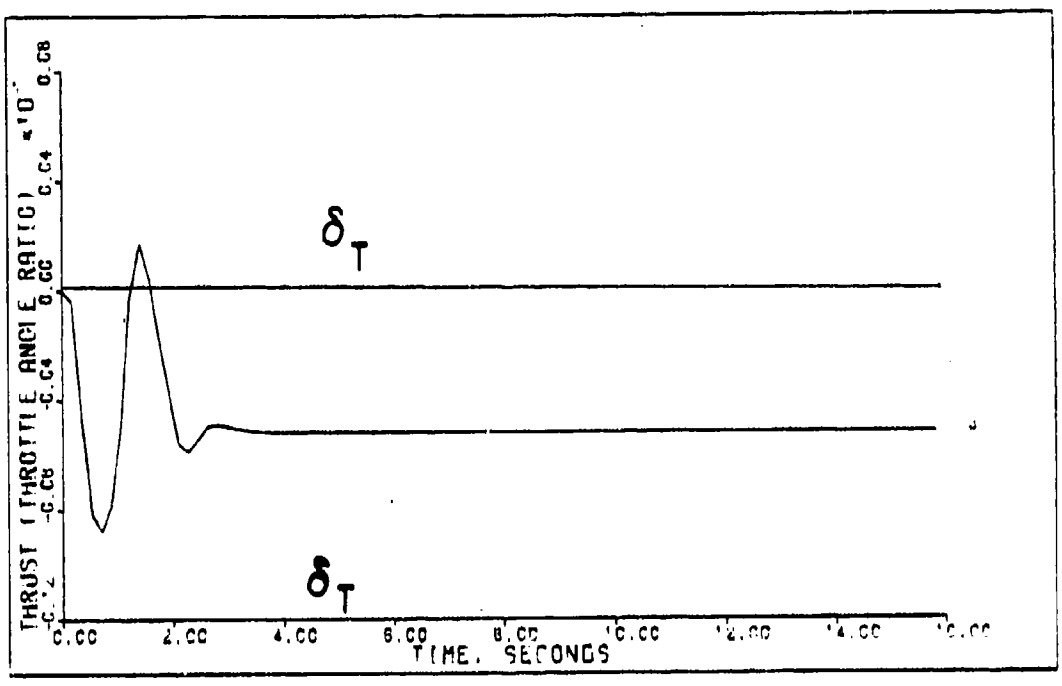

PITCH POINTING (1.2M 15K FT) ACTUATORS

Figure F-149

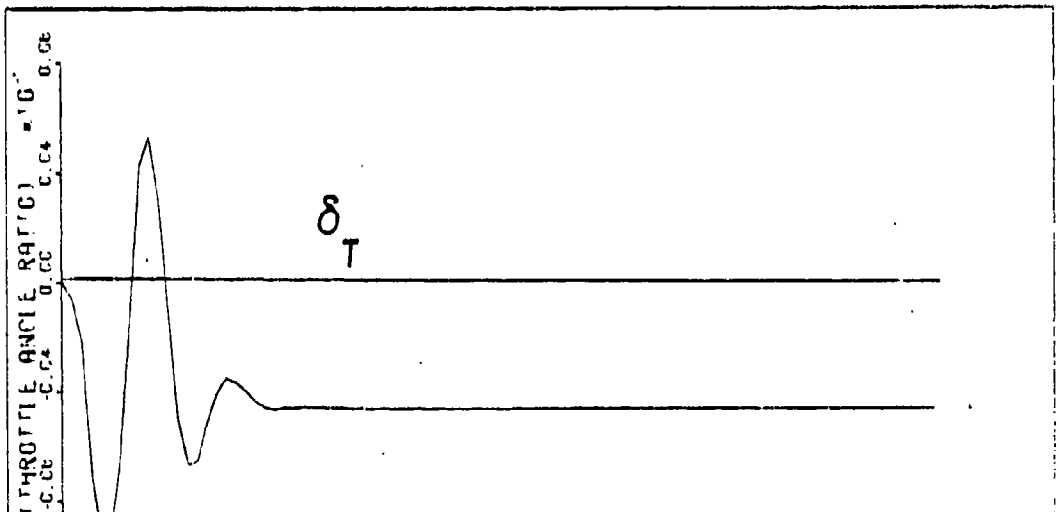

PITCH POINTING (1.2M 15K FT) DELAY=0.025 SEC ACTUATORS

Figure F-150

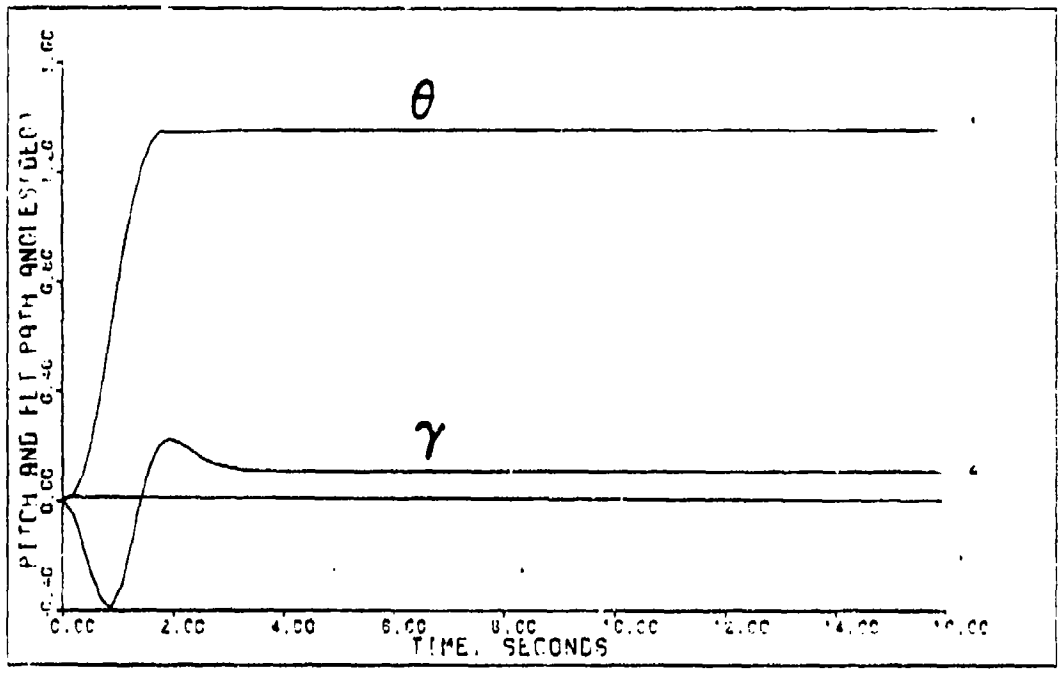

Figure F-151

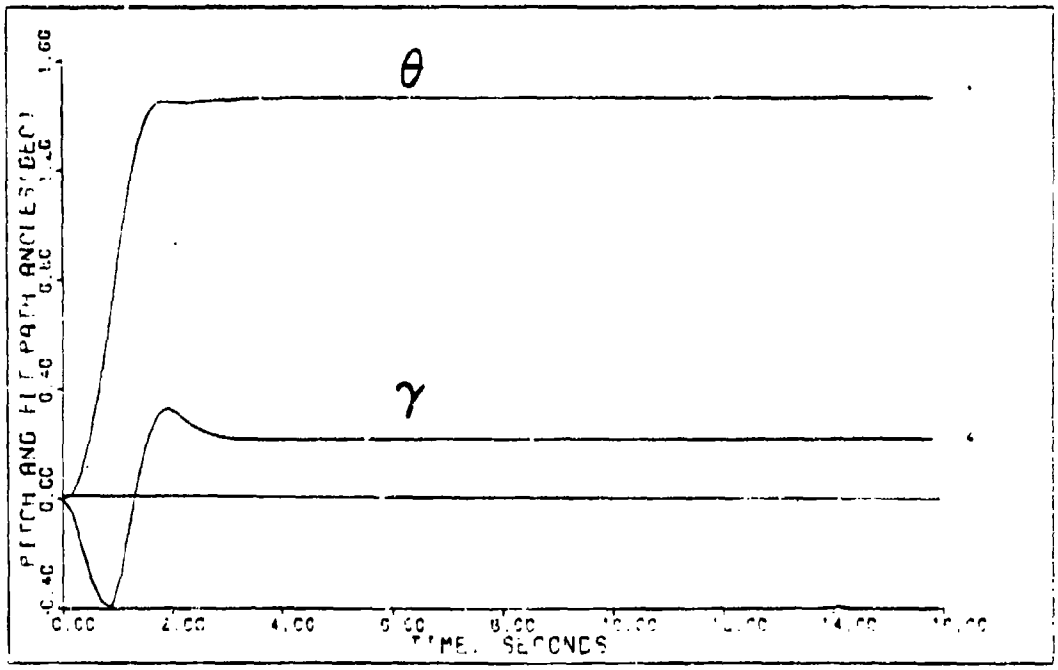

Figure F-152

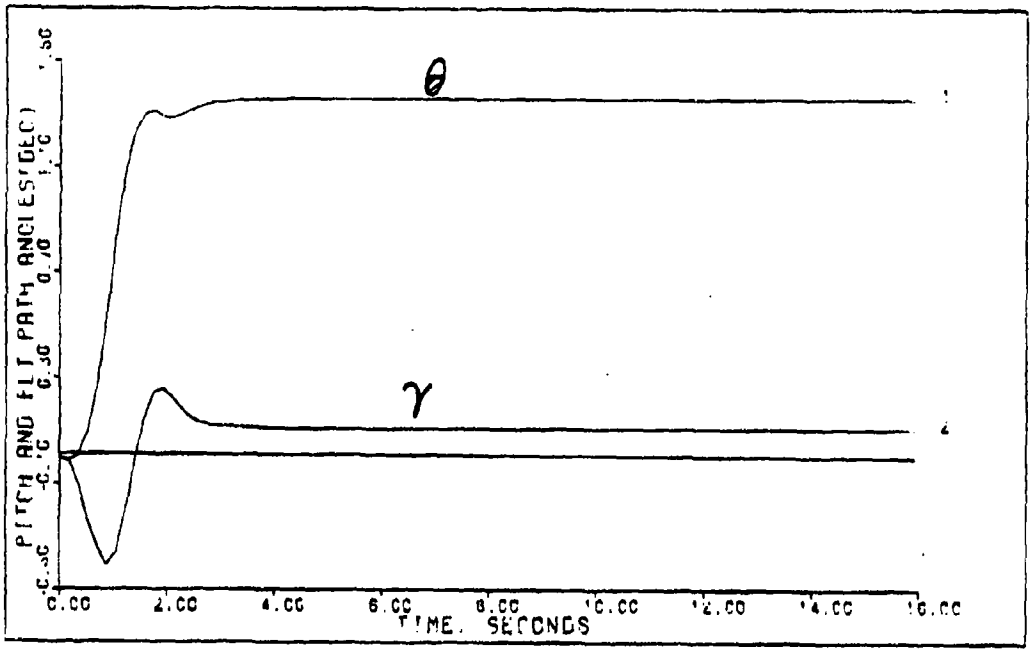

PITCH POINTING (1.2M 15K FT) ACTUATORS

Figure F-153

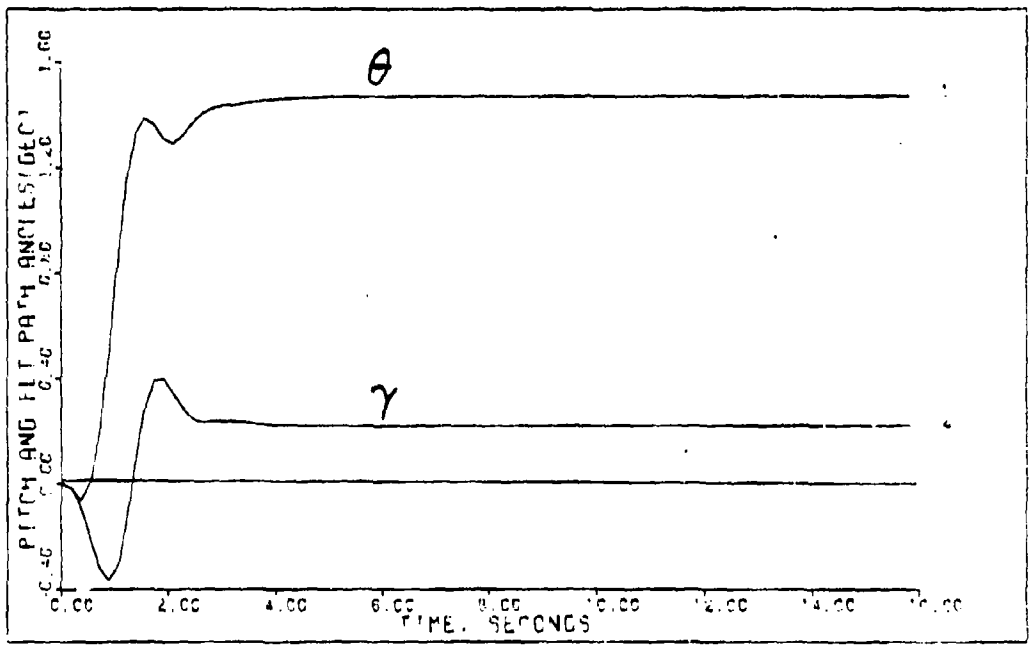

PITCH POINTING (1.2M 15K FT) DELAY=0.025 SEC ACTUATORS

Figure F-154

Appendix G: Lateral State Space Matrices

Tables in this appendix list the linearized lateral state space matrices of the X-29 aircraft for the following flight conditions:

1. 0.4 Mach at Sea Level
2. 0.9 Mach at Sea Level
3. 1.2 Mach at 15,000 Feet
4. 0.9 Mach at 50,000 Feet

TABLE G-1

LATERAL STATE SPACE MATRICES

FLIGHT CONDITION: 0.4 Mach at Sea Level

A (Plant Matrix)

.0000E+00	.0000E+00	.1000E+01	.7996E-01
.7181E-01	-.2052E+00	.7971E-01	-.9968E+00
.0000E+00	-.9003E+01	-.2637E+01	.1124E+01
.0000E+00	.5079E+01	-.8816E-01	-.1061E+00

B (Control Input Matrix)

.0000E+00	.0000E+00
.7953E-03	.8768E-03
.9747E+00	.1503E+00
.6165E-01	-.4984E-01

C (Output Matrix)

.1000E+01	.0000E+00	.0000E+00	.0000E+00
.0000E+00	.1000E+01	.0000E+00	.0000E+00

Notes

1. States (listed in order) are bank angle, sideslip angle, roll rate, and yaw rate.

2. Control inputs (listed in order) are flaperon and rudder.

3. Outputs (listed in order) are bank angle and sideslip angle.

TABLE G-2

LATERAL STATE SPACE MATRICES

FLIGHT CONDITION: 0.9 Mach at Sea Level

A (Plant Matrix)

.0000E+00	.0000E+00	.1000E+01	.4385E-01
.3119E-01	-.4664E+00	.4810E-01	-.9990E+00
.0000E+00	-.6582E+02	-.8976E+01	.2229E+01
.0000E+00	.1864E+02	-.2631E+00	-.1606E+00

B (Control Input Matrix)

.0000E+00	.0000E+00
-.2465E-02	.1395E-02
.2784E+01	.6007E+00
.1805E+00	-.1832E+00

C (Output Matrix)

.1000E+01	.0000E+00	.0000E+00	.0000E+00
.0000E+00	.1000E+01	.0000E+00	.0000E+00

Notes

1. States (listed in order) are bank angle, sideslip angle, roll rate, and yaw rate.

2. Control inputs (listed in order) are flaperon and rudder.

3. Outputs (listed in order) are bank angle and sideslip angle.

TABLE G-3

LATERAL STATE SPACE MATRICES

FLIGHT CONDITION: 1.2 Mach at 15000 Feet

A (Plant Matrix)

.0000E+00	.0000E+00	.1000E+01	.4289E-01
.2530E-01	-.4128E+00	.4285E-01	-.9991E+00
.0000E+00	-.9657E+02	-.7995E+01	.2723E+01
.0000E+00	.1870E+02	-.1485E+00	-.4619E+00

B (Control Input Matrix)

.0000E+00	.0000E+00
-.2226E-02	.4270E-03
.1171E+01	.2431E+00
.2306E+00	-.8425E-01

C (Output Matrix)

.1000E+01	.0000E+00	.0000E+00	.0000E+00
.0000E+00	.1000E+01	.0000E+00	.0000E+00

Notes

1. States (listed in order) are bank angle, sideslip angle, roll rate, and yaw rate.

2. Control inputs (listed in order) are flaperon and rudder.

3. Outputs (listed in order) are bank angle and sideslip angle.

TABLE G-4

LATERAL STATE SPACE MATRICES

FLIGHT CONDITION: 0.9 Mach at 50000 Feet

A (Plant Matrix)

.0000E+00	.0000E+00	.1000E+01	.9501E-01
.3659E-01	-.7060E-01	.9458E-01	-.9955E+00
.0000E+00	-.7951E+01	-.8525E+00	.5087E+00
.0000E+00	.3321E+01	-.3066E-01	-.1703E-01

B (Control Input Matrix)

.0000E+00	.0000E+00
-.3293E-03	.2960E-03
.4336E+00	.1137E+00
.2519E-01	-.3314E-01

C (Output Matrix)

.1000E+01	.0000E+00	.0000E+00	.0000E+00
.0000E+00	.1000E+01	.0000E+00	.0000E+00

Notes

1. States (listed in order) are bank angle, sideslip angle, roll rate, and yaw rate.

2. Control inputs (listed in order) are flaperon and rudder.

3. Outputs (listed in order) are bank angle and sideslip angle.

Appendix H: Lateral Controller Response Plots

This appendix includes lateral time history plots for the X-29 closed-loop flight control system incorporating a controller designed with the Porter method. The response plots are presented for the following maneuvers and flight conditions:

Coordinaced Turn

1. 0.4 Mach at Sea Level
2. 0.9 Mach at Sea Level
3. 1.2 Mach at 15,000 Feet
4. 0.9 Mach at 50,000 Feet

Beta Pointing

1. 0.4 Mach at Sea Level
2. 0.9 Mach at Sea Level
3. 1.2 Mach at 15,000 Feet
4. 0.9 Mach at 50,000 Feet

The lateral design parameters, controller matrices, and figures of merit for these plots are located in Tables 6-2 through 6-5 of Chapter 6.

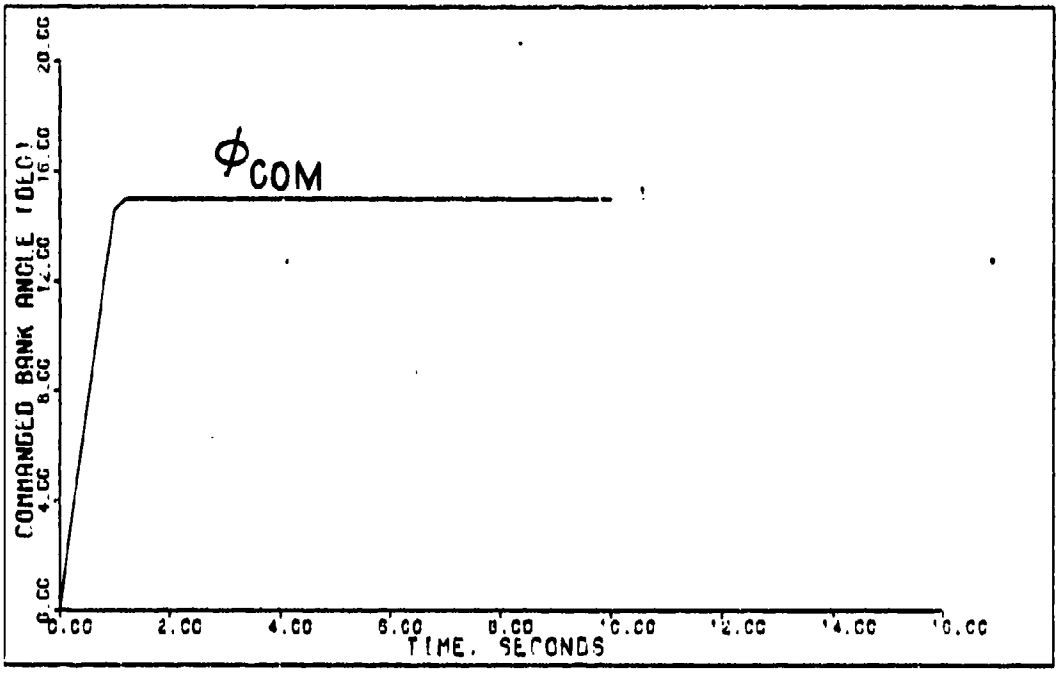

COORDINATED TURN (0.4M OK FT) DELAY=0.025 SEC ACTUATORS

Figure H-1

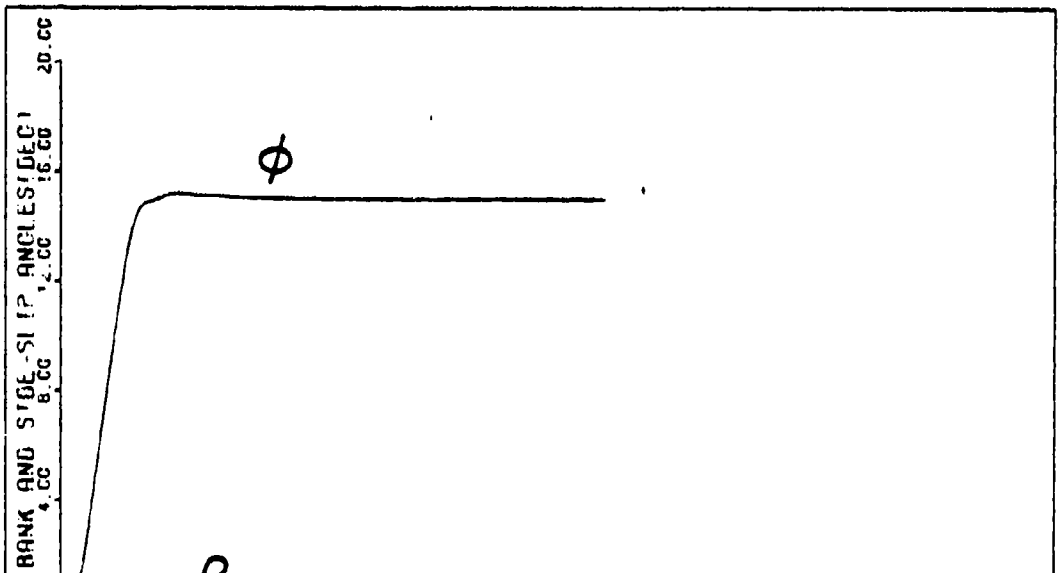

COORDINATED TURN (0.4M OK FT) DELAY=0.025 SEC ACTUATORS

Figure H-2

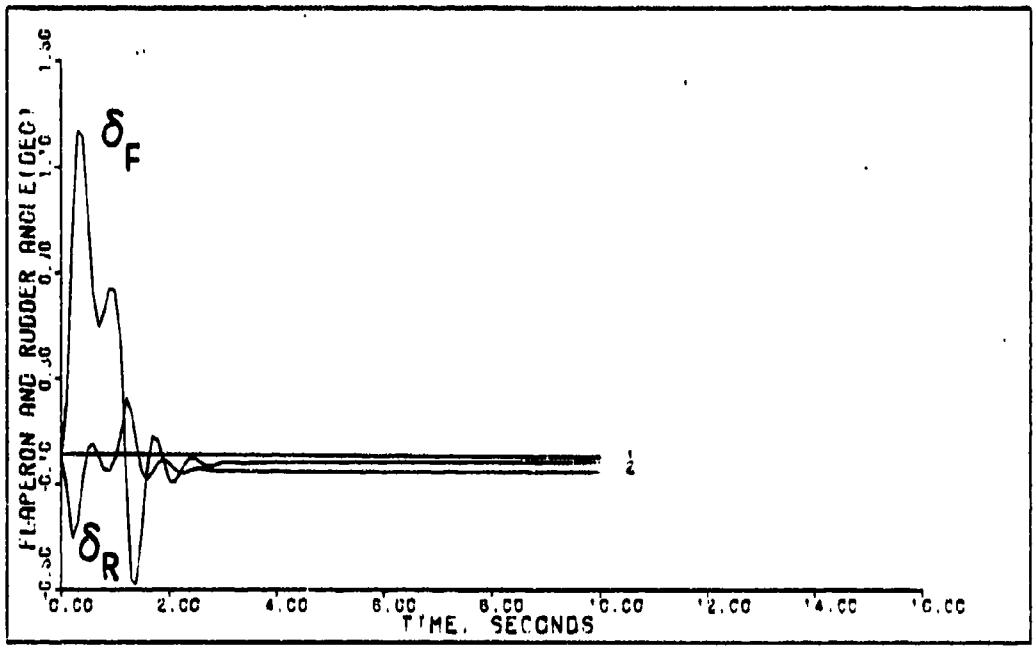

COORDINATED TURN (0.4M OK FT) DELAY=0.025 SEC ACTUATORS

Figure H-3

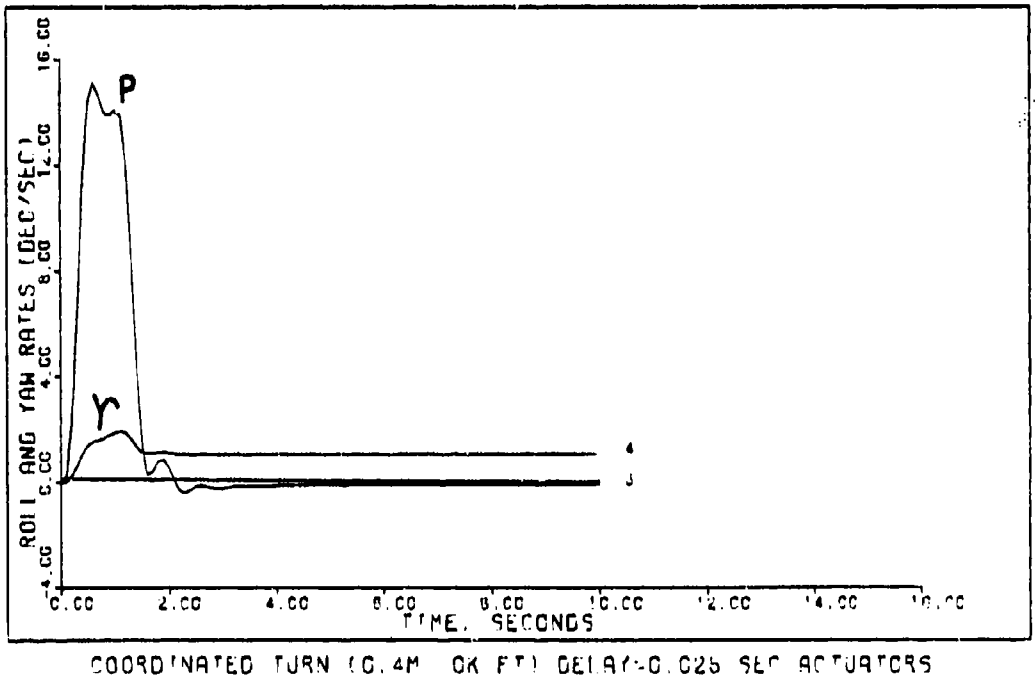

COORDINATED TURN (0.4M OK FT) DELAY=0.025 SEC ACTUATORS

Figure H-4

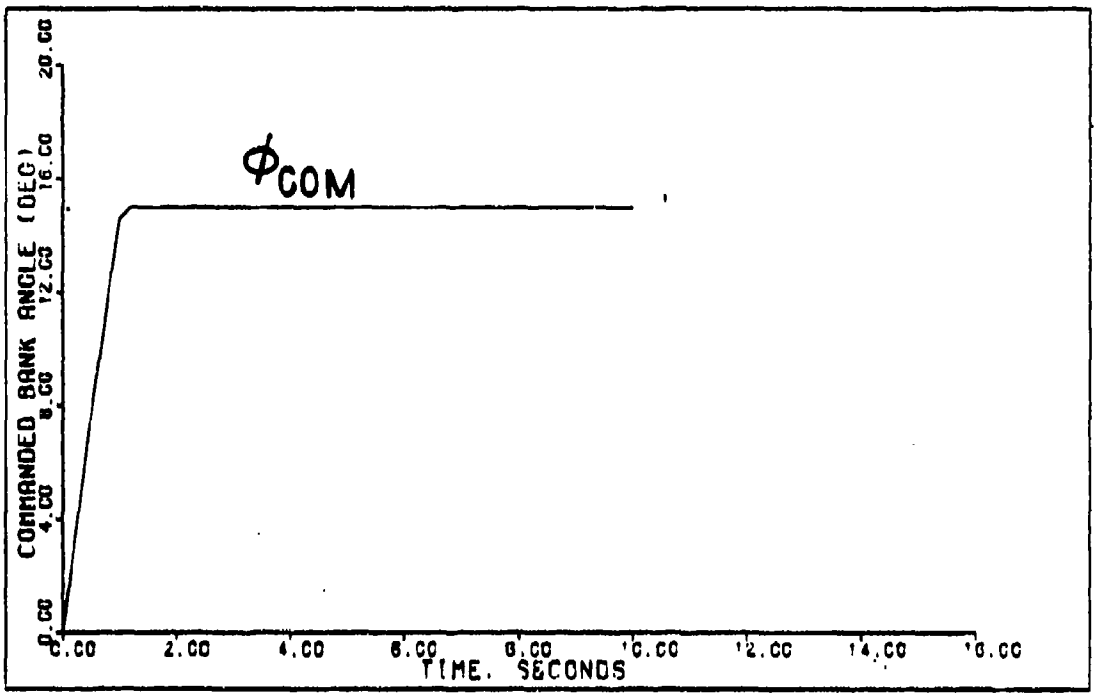

COORDINATED TURN (0.9M OK FT) DELAY=0.025 SEC ACTUATORS .

Figure H-5

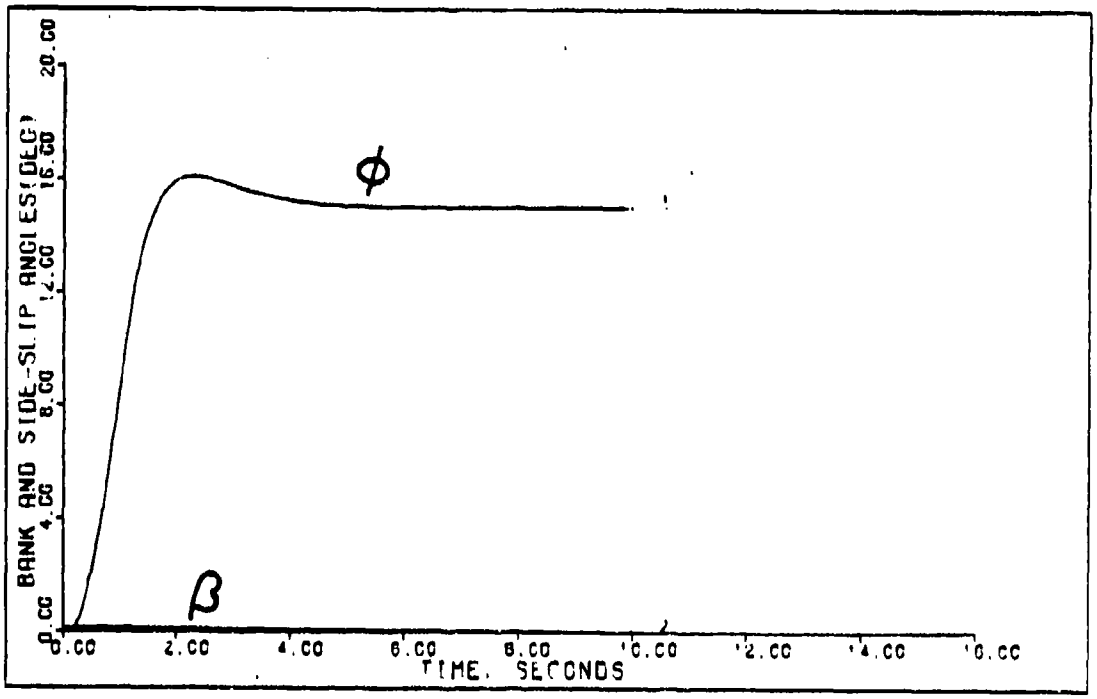

COORDINATED TURN (0.9M OK FT) DELAY=0.025 SEC ACTUATORS

Figure H-6

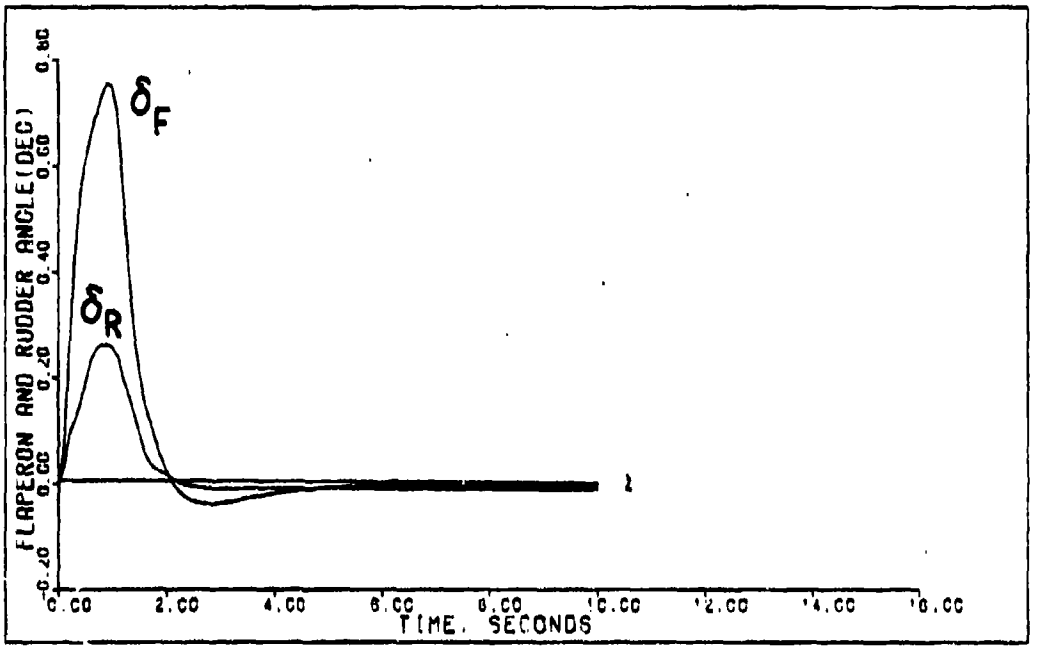

COORDINATED TURN (0.9M OK FT) DELAY=0.025 SEC ACTUATORS

Figure H-7

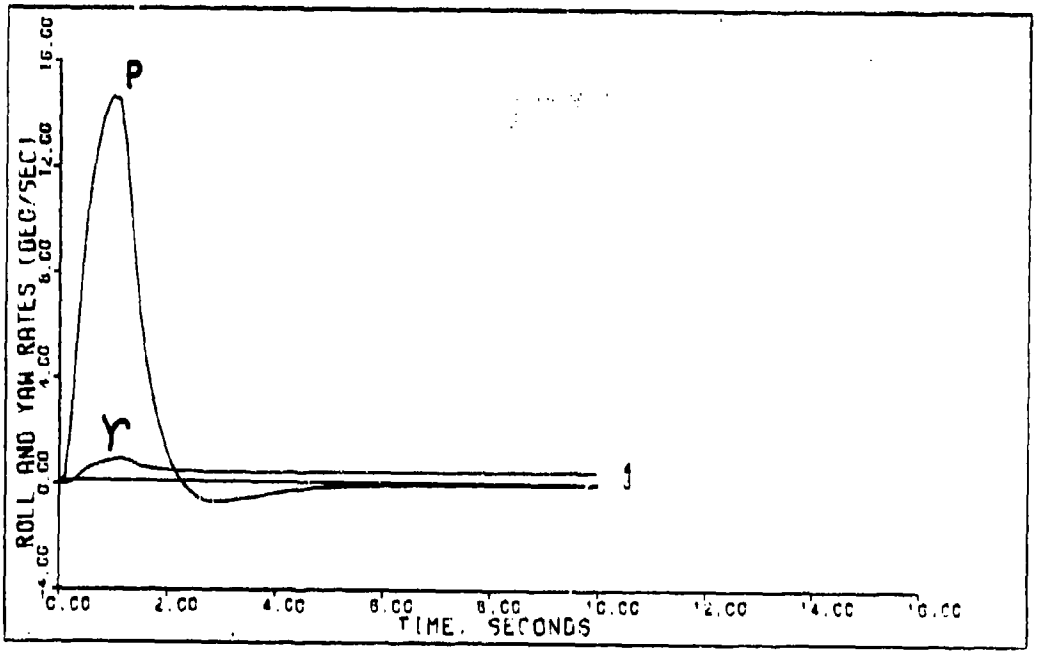

COORDINATED TURN (0.9M OK FT) DELAY=0.025 SEC ACTUATORS

Figure H-8

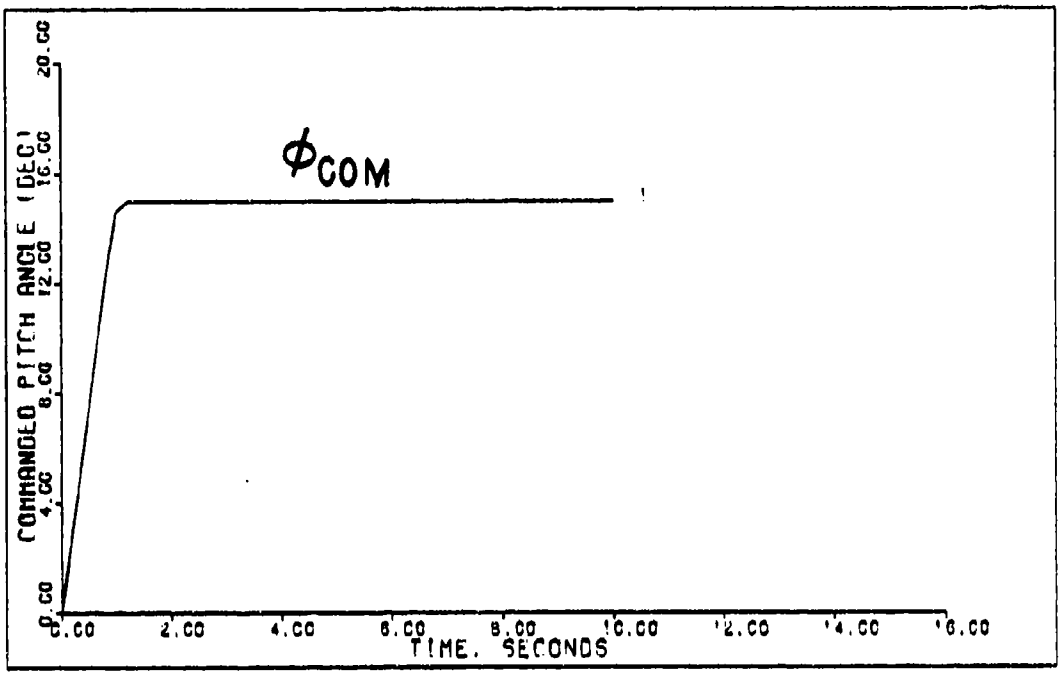

COORDINATED TURN (1.2M 15K FT) DELAY=0.025 SEC ACTUATORS

Figure H-9

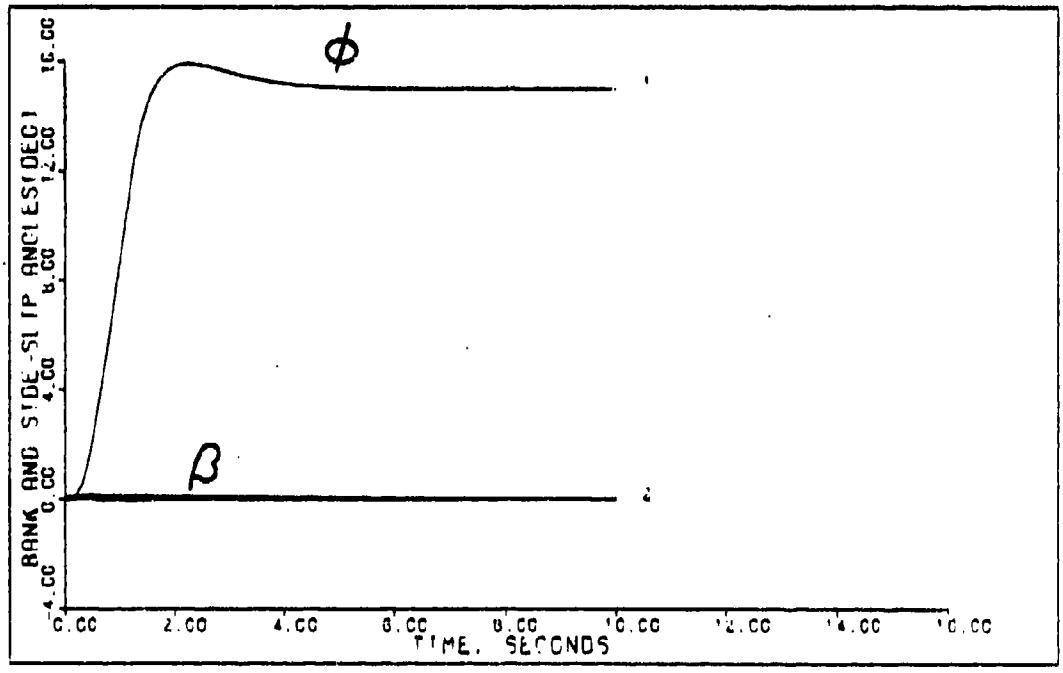

COORDINATED TURN (1.2M 15K FT) DELAY=0.025 SEC ACTUATORS

Figure H-10

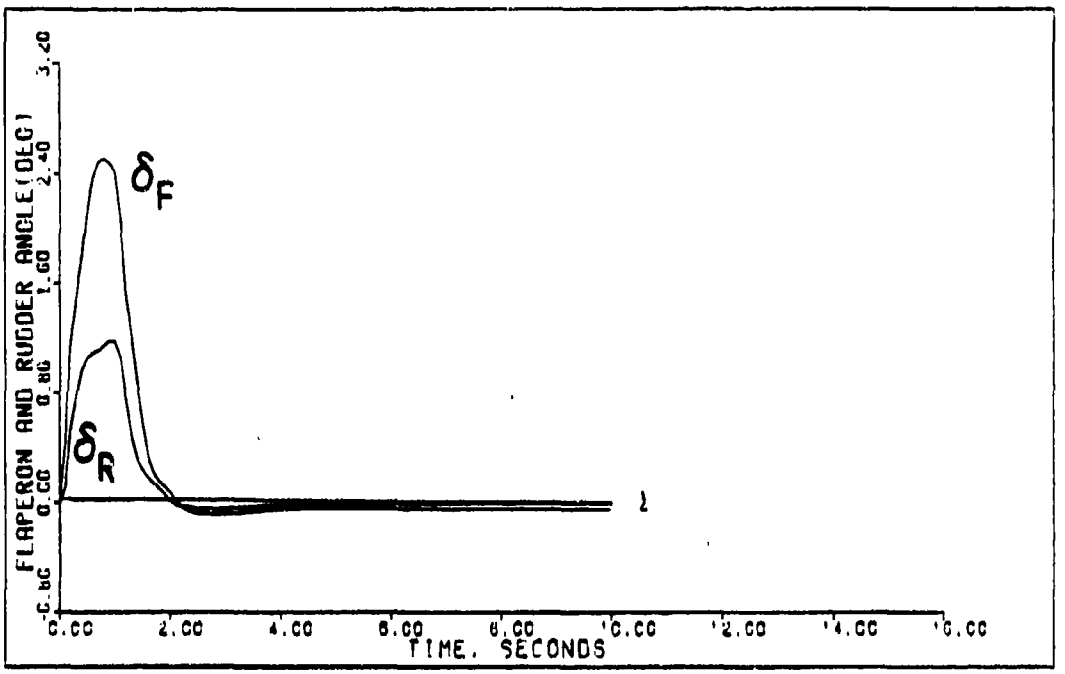

COORDINATED TURN (1.2M 15K FT) DELAY=0.025 SEC ACTUATORS

Figure H-11

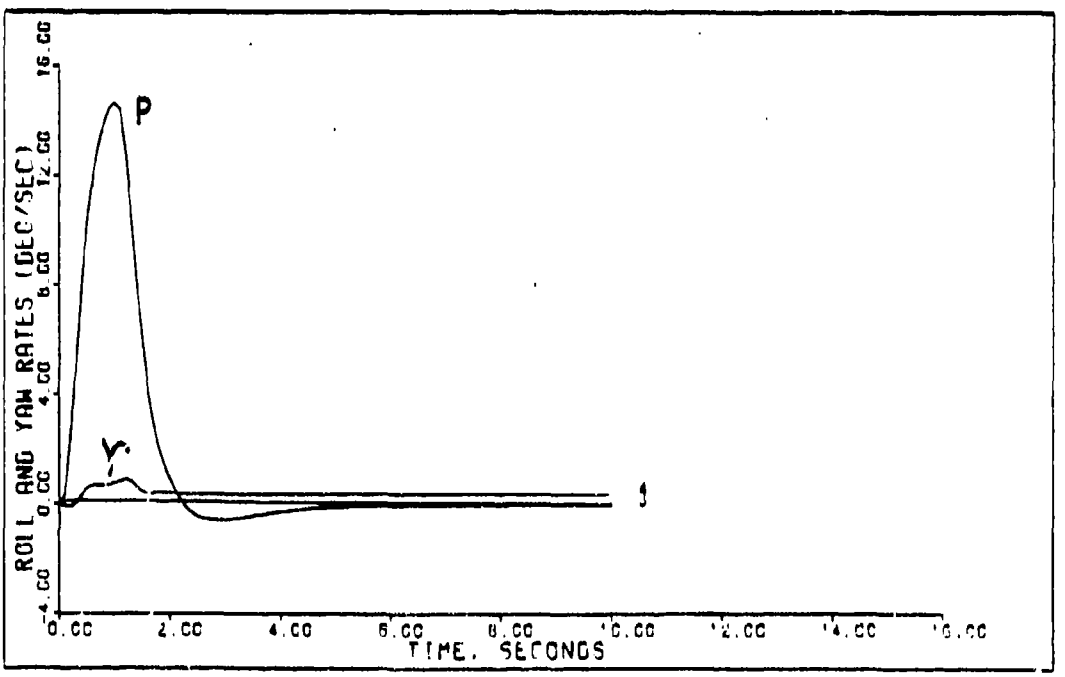

COORDINATED TURN (1.2M 15K FT) DELAY=0.025 SEC

Figure H-12

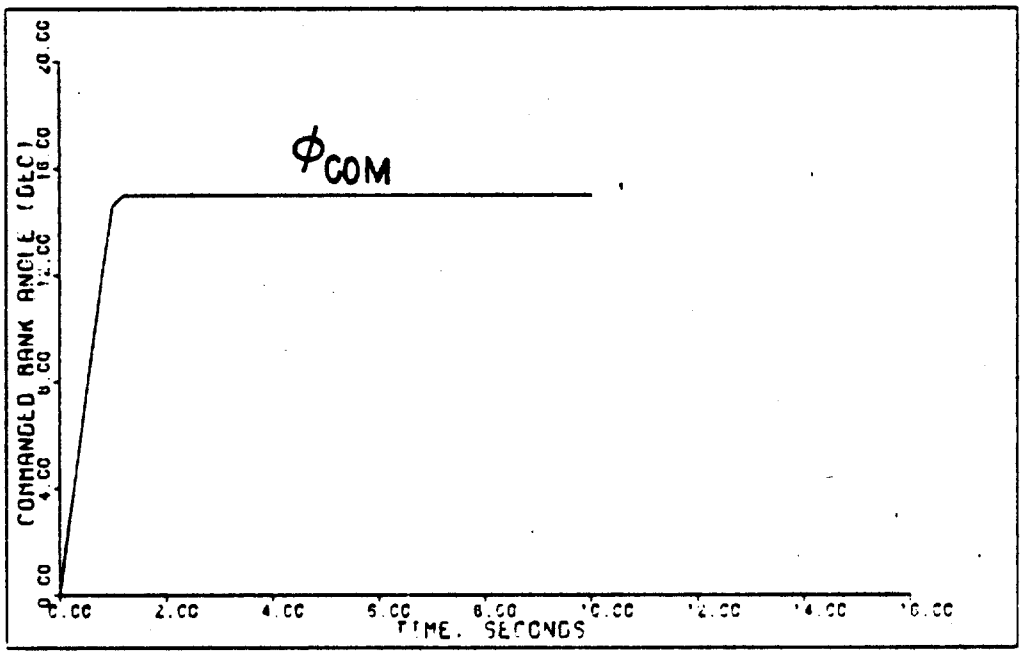

COORDINATED TURN (0.9M 50K FT) DELAY=0.025 SEC ACTUATORS

Figure H-13

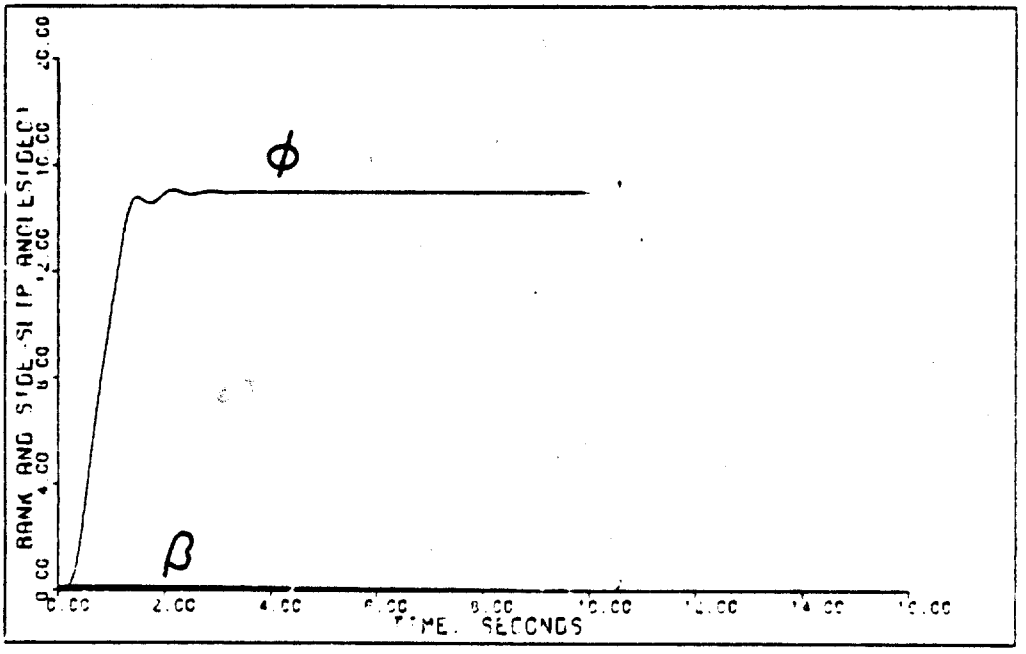

COORDINATED TURN (0.9M 50K FT) DELAY=0.025 SEC ACTUATORS

Figure H-14

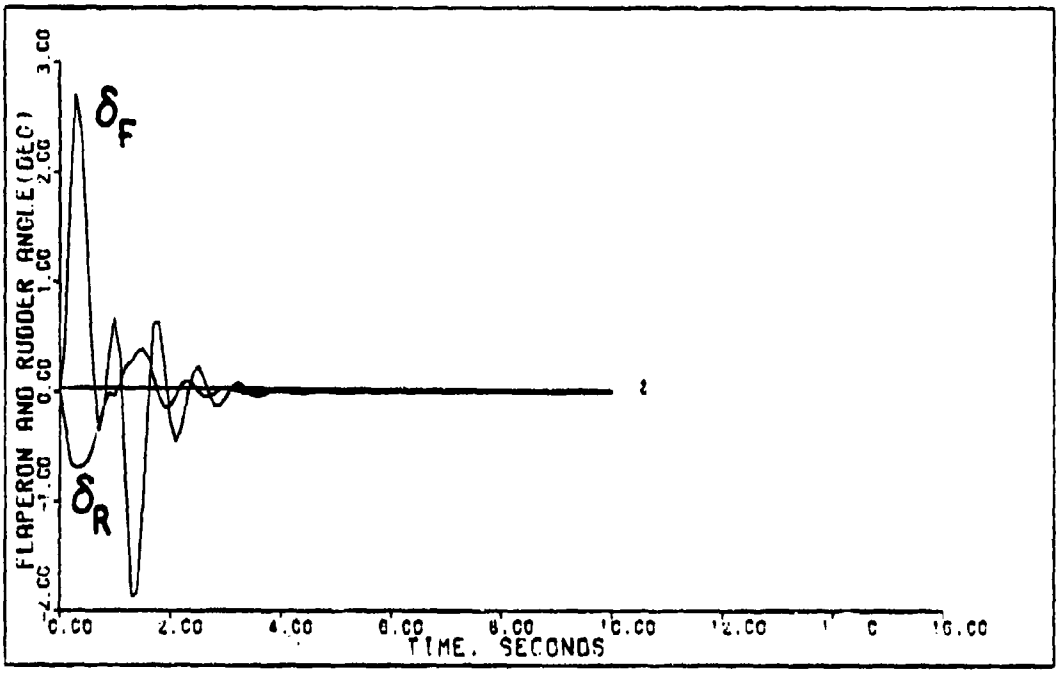

COORDINATED TURN (0.9M .50K FT) DELAY=0.025 SEC ACTUATORS

Figure H-15

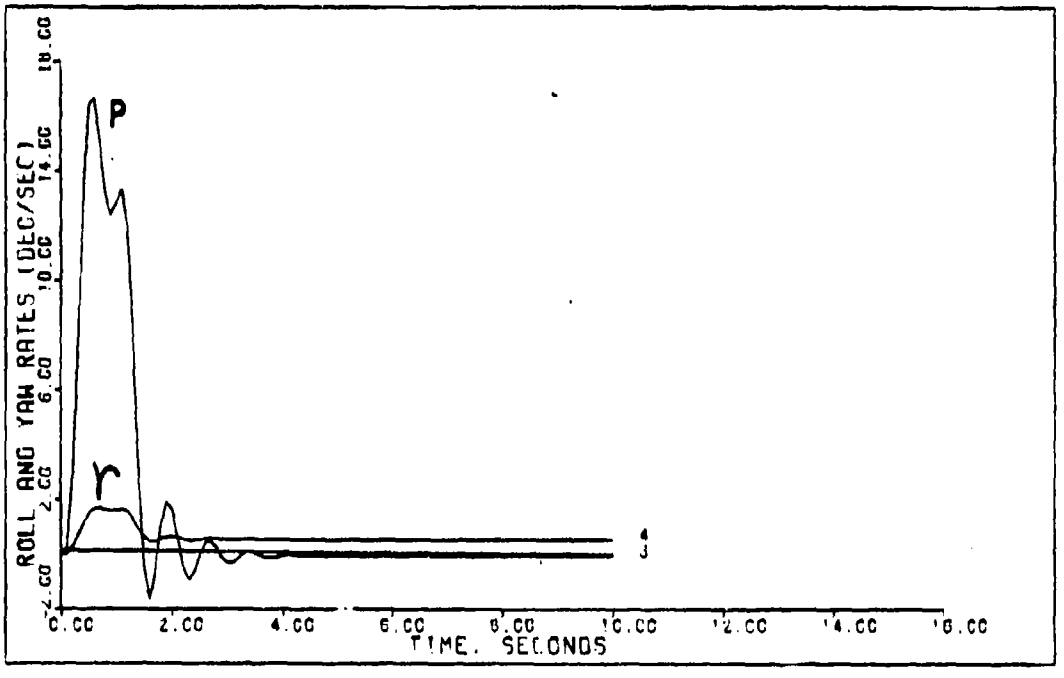

COORDINATED TURN (0.9M 50K FT) DELAY=0.025 SEC ACTUATORS

Figure H-16

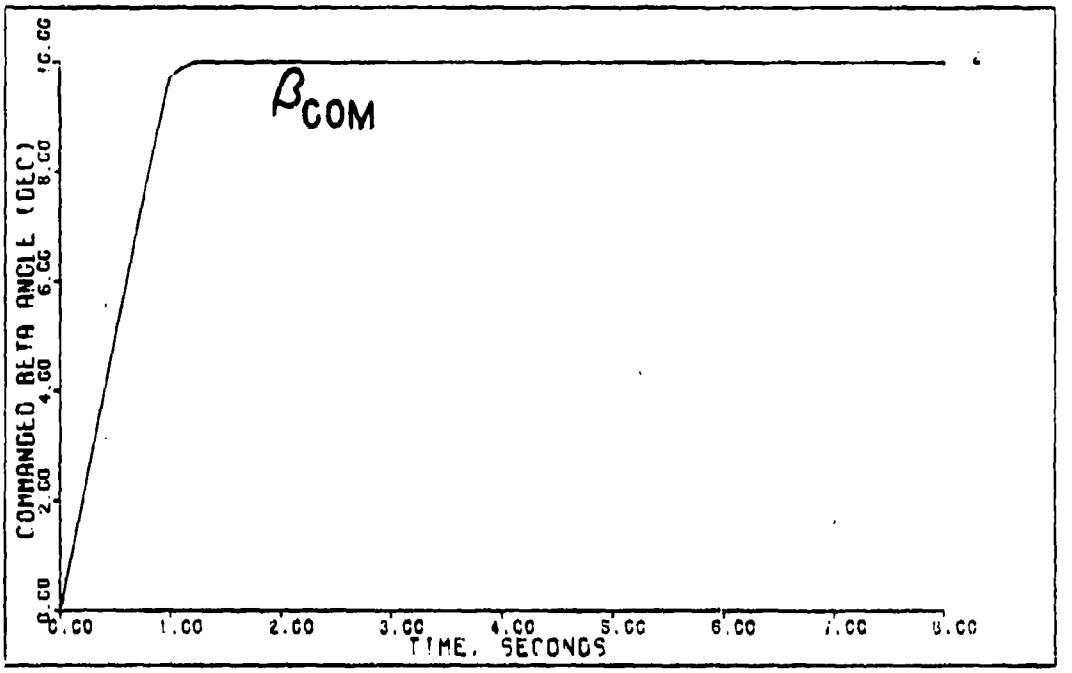

BETA POINTING (0.4M OK FT) DELAY=0.025 SEC ACTUATORS

Figure H-17

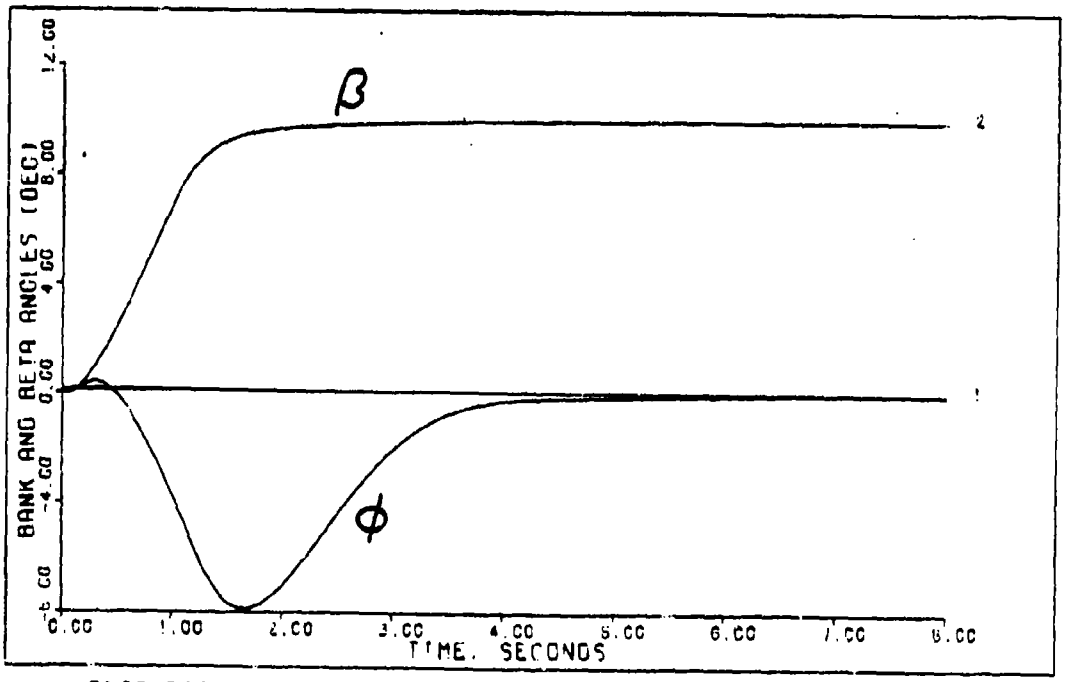

BETA POINTING (0.4M OK FT) DELAY=0.025 SEC ACTUATORS

Figure H-18

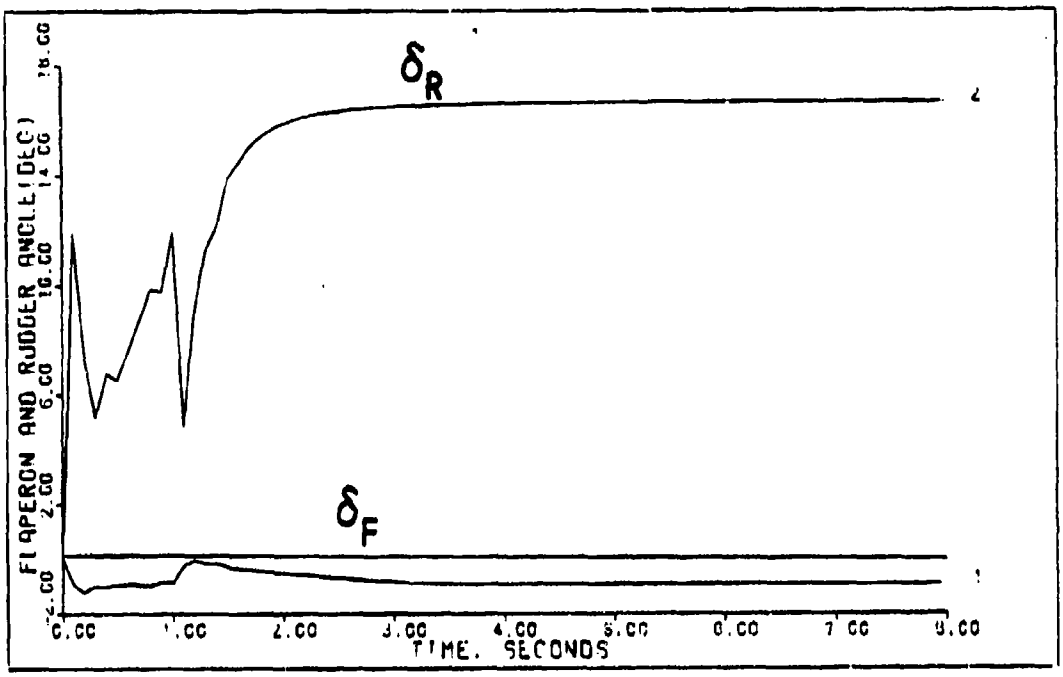

BETA POINTING (0.4M OK FT) DELAY=0.025 SEC ACTUATORS

Figure H-19

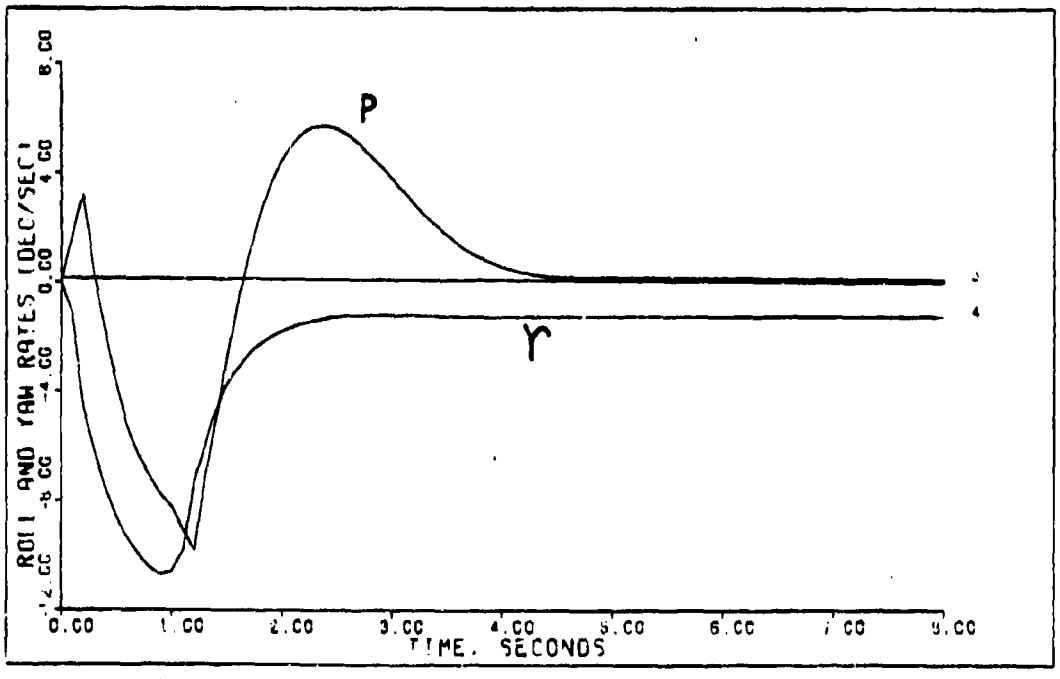

BETA POINTING (0.4M OK FT) DELAY=0.025 SEC ACTUATORS

Figure H-20

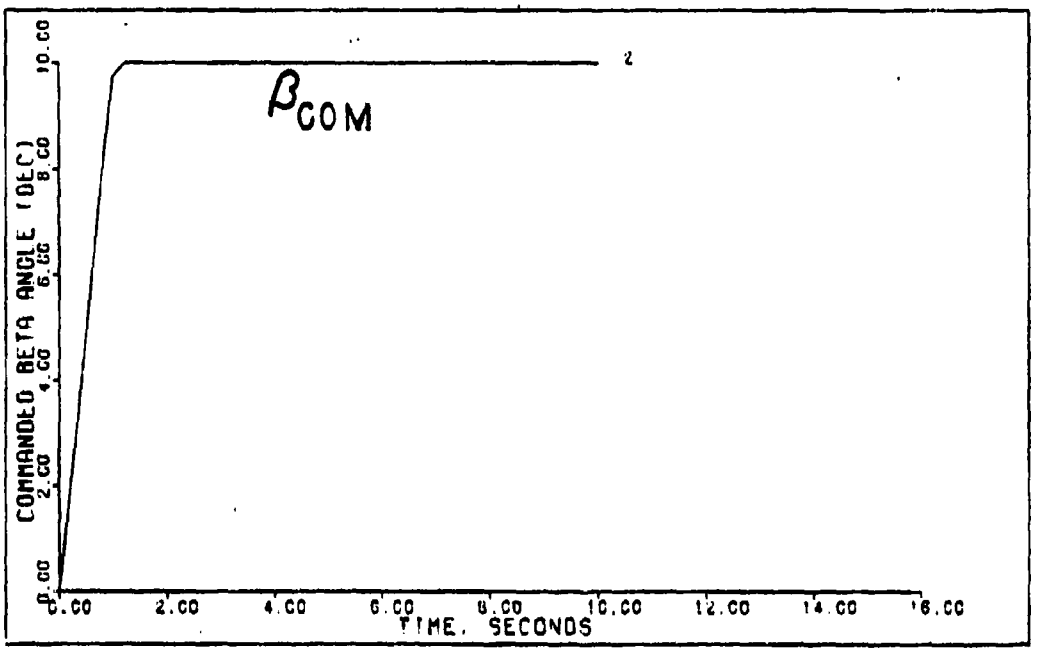

BETA POINTING (0.9M OK FTI DELAY=0.025 SEC ACTUATORS

Figure H-21

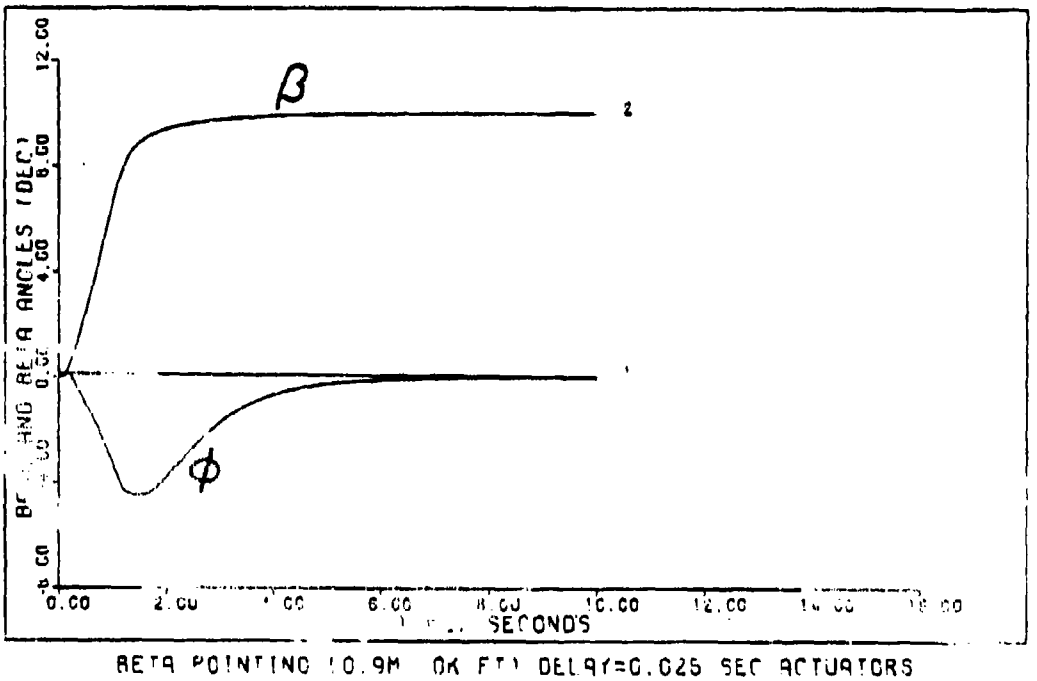

BETA POINTING (0.9M OK FTI DELAY=0.025 SEC ACTUATORS

Figure H-22

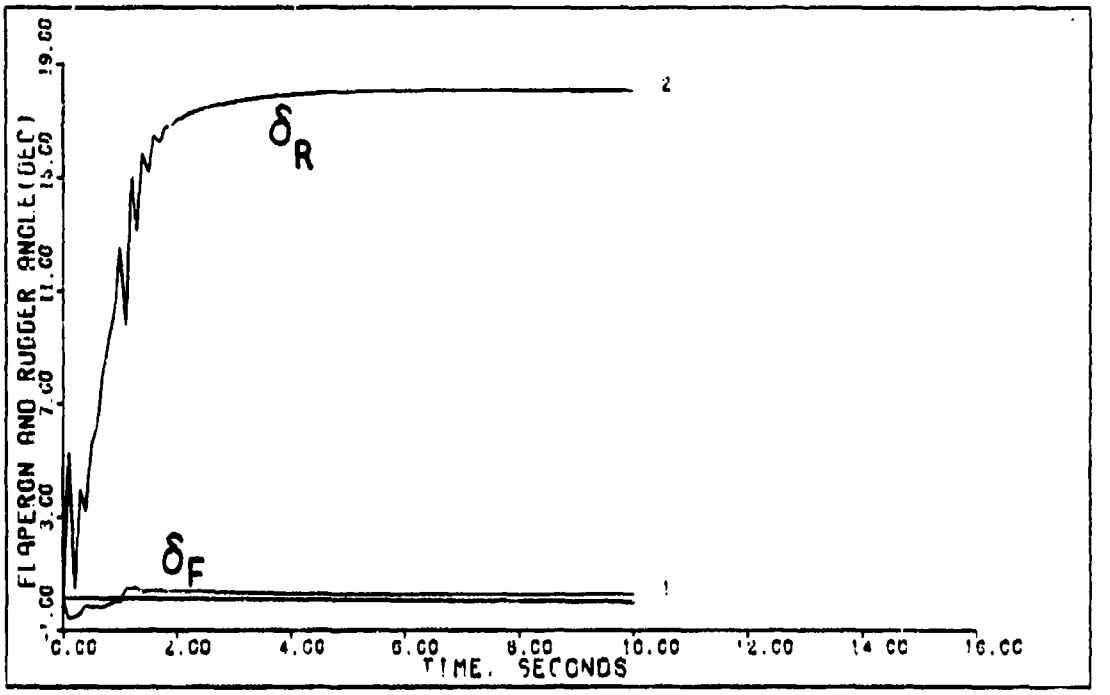

Figure H-23

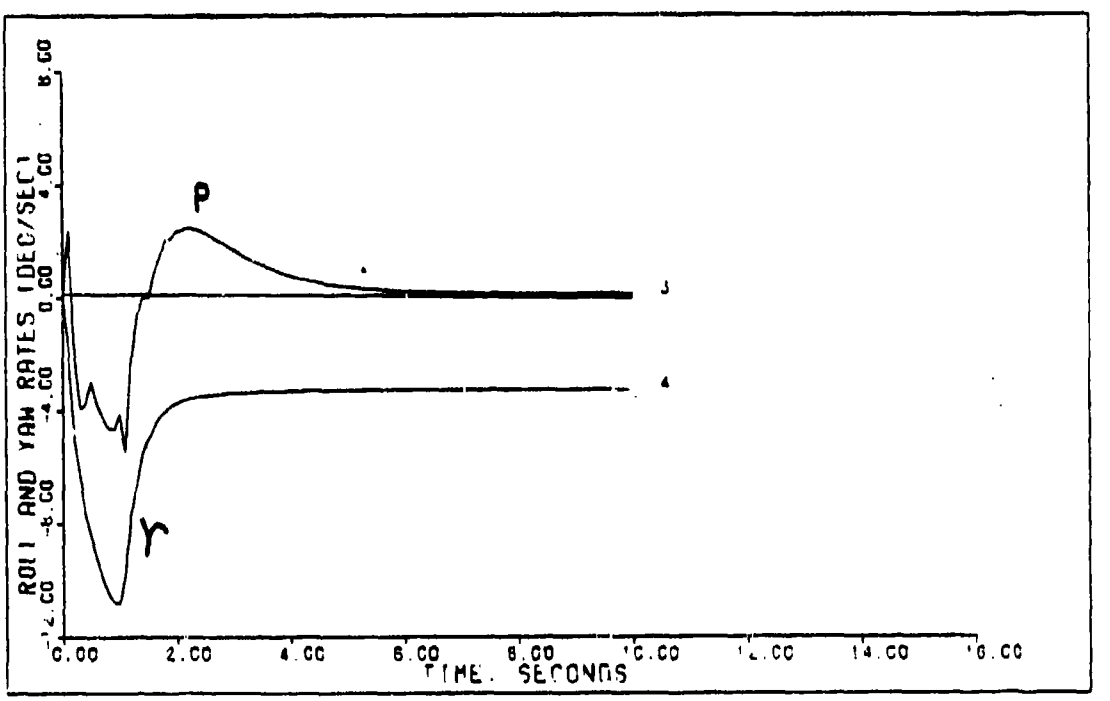

Figure H-24

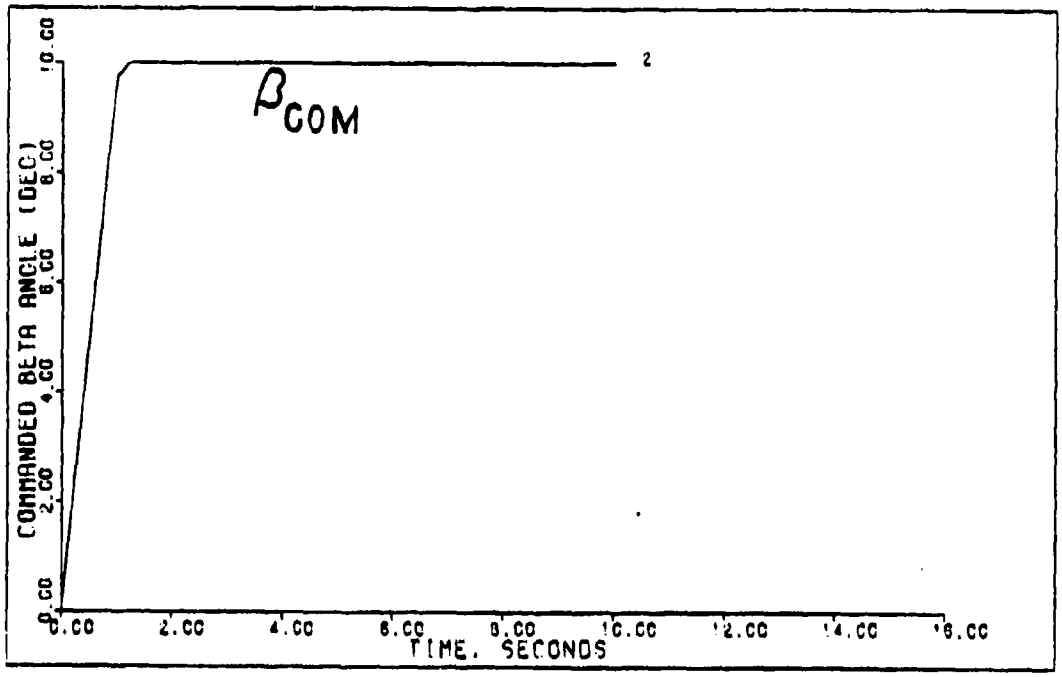

BETA POINTING (1.2M 15K FT) DELAY=0.025 SEC ACTUATORS

Figure H-25

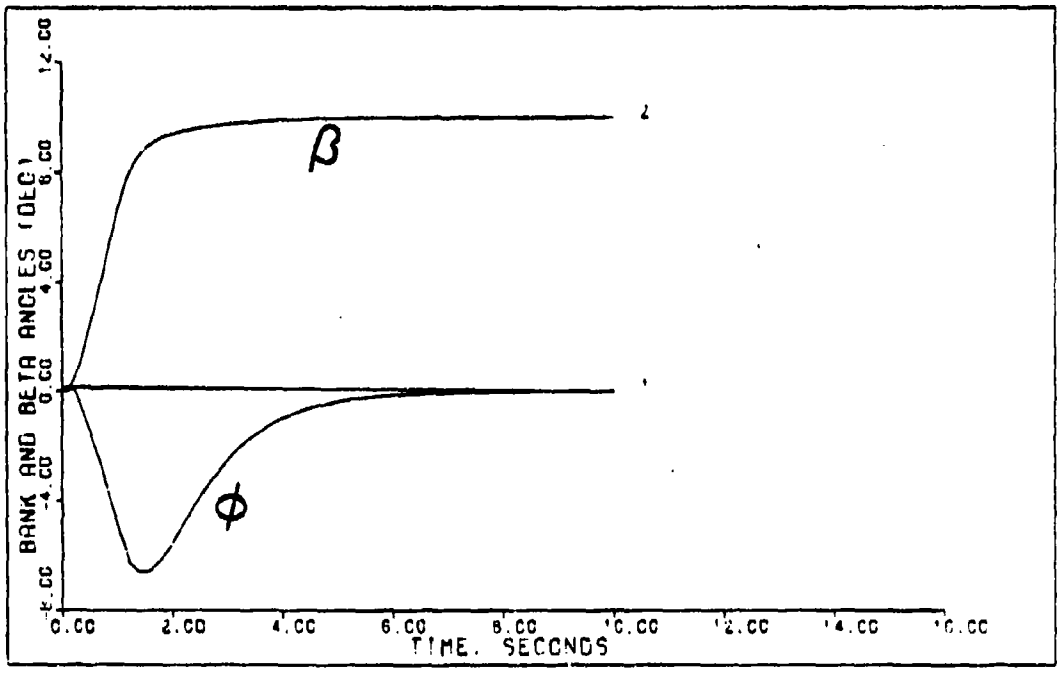

BETA POINTING (1.2M 15K FT) DELAY=0.025 SEC ACTUATORS

Figure H-26

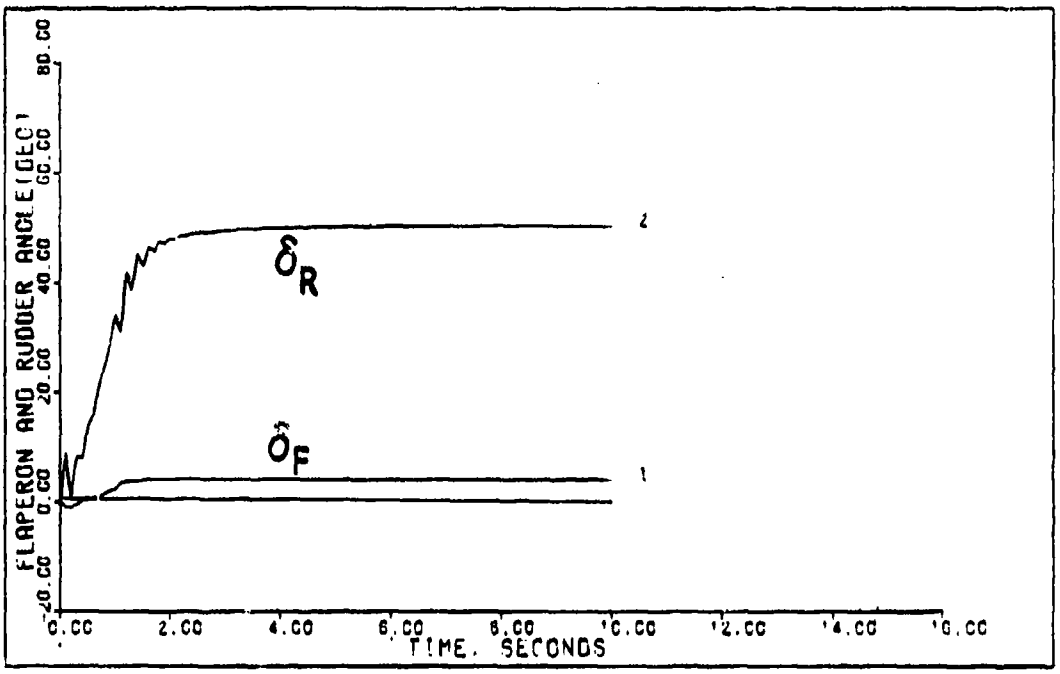

BETA POINTING (1.2M 15K FT) DELAY=0.025 SEC ACTUATORS

Figure H-27

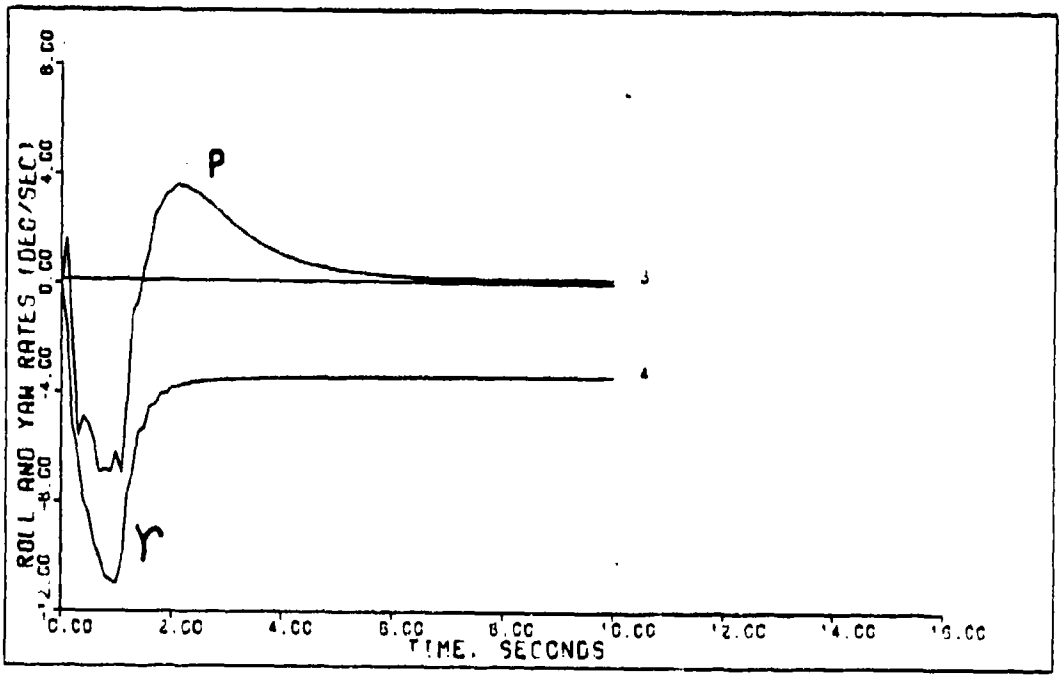

BETA POINTING (1.2M 15K FT) DELAY=0.025 SEC ACTUATORS

Figure H-28

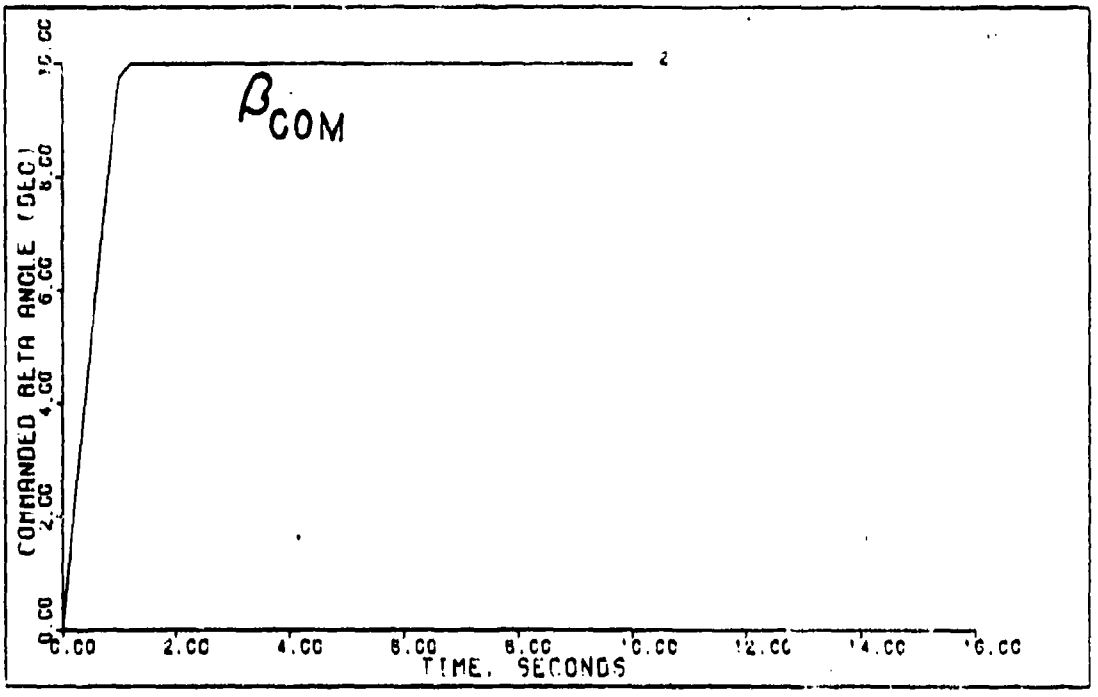

Figure H-29

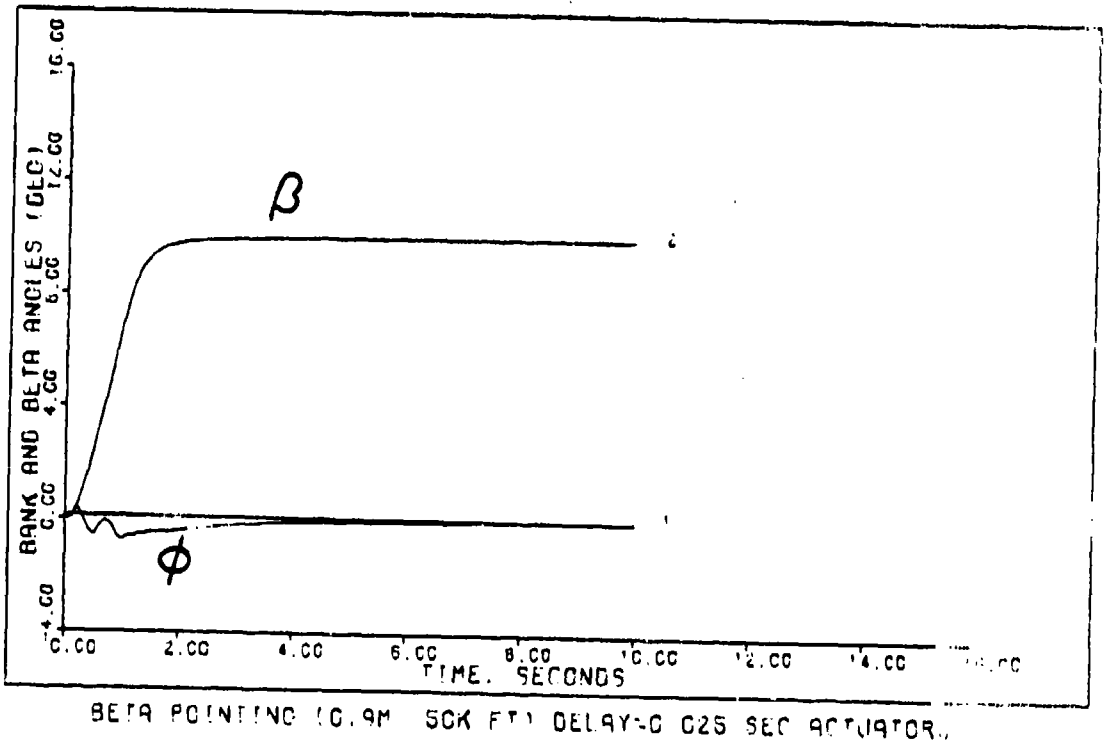

Figure H-30

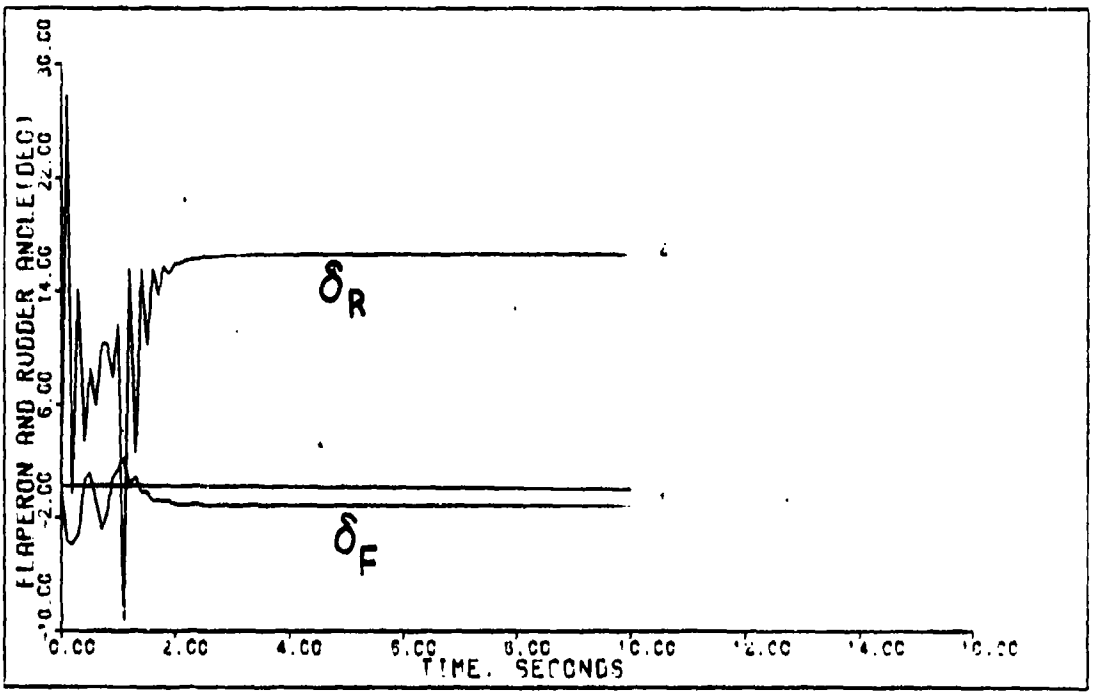

BETA POINTING (0.9M 50K FT) DELAY=0.025 SEC ACTUATORS

Figure H-31

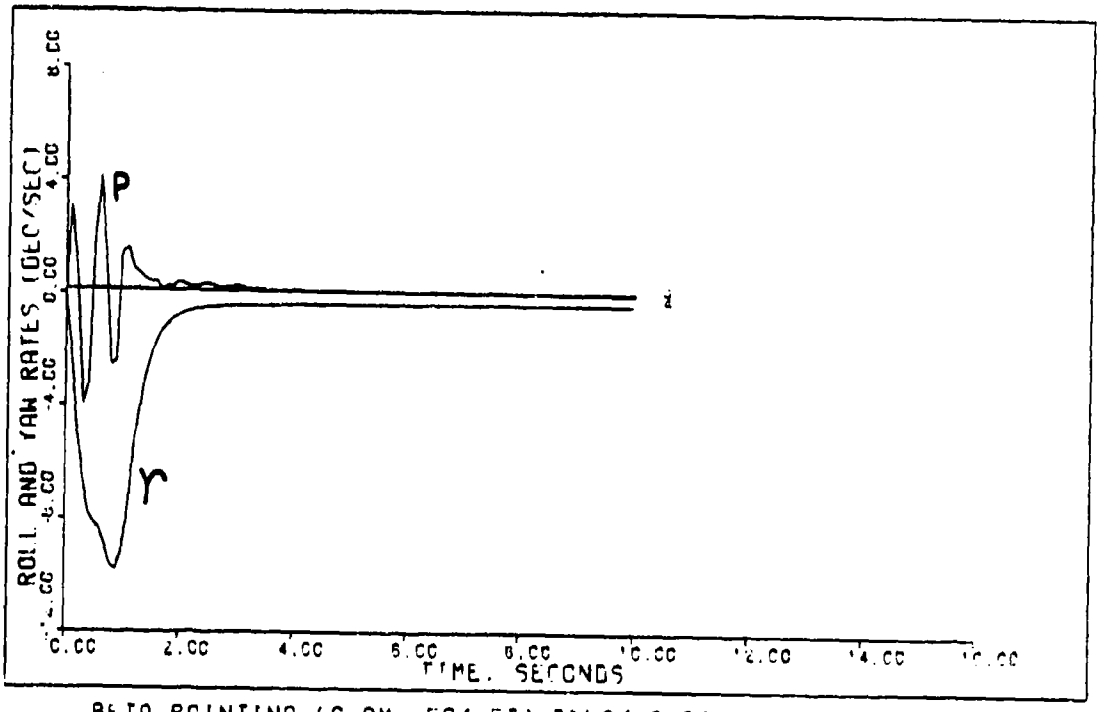

BETA POINTING (0.9M 50K FT) DELAY=0.025 SEC ACTUATORS

Figure H-32

Appendix I: Other Design Approaches

As discussed in Chapter 7, Conclusions and Recommendations, an unsuccessful attempt was made to control acceleration first by implementing the actuator dynamics into the state equations, thus eliminating the necessity for a feedforward D matrix. The result was transmission zeros in the right half s-plane. For the benefit of future work in this area this appendix expands on the results by providing a sample of the actual transmission zeros calculated on TOTAL using the Macro program written by Barfield (1). The same results were confirmed using the ZERO program written by Lewis (7). For the flight condition of 0.7 Mach at 15,000 feet, the following longitudinal equations of motion and resulting transmission zeros are listed as follows:

$$\begin{bmatrix} \dot{\theta} \\ \dot{u} \\ \dot{\alpha} \\ \dot{q} \\ \dot{\delta}_C \\ \dot{\delta}_S \\ \dot{\delta}_T \end{bmatrix}$$

$$= \begin{bmatrix} 0 & 0 & 0 & 1 & 0 & 0 & 0 \\ -32.13 & -.0119 & -1.718 & -.3504 & -.05895 & .02621 & 27.24 \\ -.3243E-06 & -.0001298 & -1.138 & .9917 & -.001161 & -.0007808 & -.002099 \\ 0 & -.0002986 & 18.92 & -.4928 & .1720 & -.05630 & -.1929 \\ 0 & 0 & 0 & 0 & -20.0 & 0 & 0 \\ 0 & 0 & 0 & 0 & 0 & -5.0 & 0 \\ 0 & 0 & 0 & 0 & 0 & 0 & -20 \end{bmatrix} \begin{bmatrix} \theta \\ u \\ \alpha \\ q \\ \delta_C \\ \delta_S \\ \delta_T \end{bmatrix}$$

$$+ \begin{bmatrix} 0 & 0 & 0 \\ 0 & 0 & 0 \\ 0 & 0 & 0 \\ 0 & 0 & 0 \\ 20.0 & 0 & 0 \\ 0 & 5.0 & 0 \\ 0 & 0 & 20.0 \end{bmatrix} \begin{bmatrix} e_C \\ e_S \\ e_T \end{bmatrix}$$

$$\begin{bmatrix} q \\ u \\ A_{ZP} \end{bmatrix} = \begin{bmatrix} 0 & 0 & 0 & 1 & 0 & 0 & 0 \\ 0 & 1 & 0 & 0 & 0 & 0 & 0 \\ -.6659E\text{-}04 & .003022 & 27.72 & .15 & .04111 & .01320 & -.01613 \end{bmatrix} \begin{bmatrix} p \\ \beta \\ \phi \\ R \\ \delta_F \\ \delta_R \end{bmatrix}$$

$$M = \begin{bmatrix} 0 & .25 & 0 & 0 \\ 0 & 0 & .25 & 0 \\ 0 & 0 & 0 & 0 \end{bmatrix}$$

Transmission Zero Locations

-.36E-05

-.16E-03

-290.9

+15.16

For the lateral equations of motion at 0.7 Mach at 15,000 feet, the equations and resulting transmission zeros are listed below:

$$\begin{bmatrix} \dot{P} \\ \dot{\beta} \\ \dot{\phi} \\ \dot{R} \\ \dot{\delta}_F \\ \dot{\delta}_R \end{bmatrix} = \begin{bmatrix} -2.989 & -17.93 & 0 & 1.090 & 1.493 & .2670 \\ .0571 & -.2210 & .04334 & -.9984 & -.0008361 & .0009071 \\ 1 & 0 & 0 & .05710 & 0 & 0 \\ -.09651 & 7.836 & 0 & -.09504 & .09608 & -.08655 \\ 0 & 0 & 0 & 0 & -10.0 & 0 \\ 0 & 0 & 0 & 0 & 0 & -30.0 \end{bmatrix} \begin{bmatrix} P \\ \beta \\ \phi \\ R \\ \delta_F \\ \delta_R \end{bmatrix}$$

$$+ \begin{bmatrix} 0 & 0 \\ 0 & 0 \\ 0 & 0 \\ 0 & 0 \\ 10.0 & 0 \\ 0 & 30.0 \end{bmatrix} \begin{bmatrix} e_F \\ e_R \end{bmatrix} ; \quad \begin{bmatrix} P \\ q \end{bmatrix} = \begin{bmatrix} 1 & 0 & 0 & 0 & 0 \\ 0 & 1 & 0 & 0 & 0 \end{bmatrix} \begin{bmatrix} P \\ \beta \\ \phi \\ R \\ \delta_F \\ \delta_R \end{bmatrix}$$

Transmission Zero Locations

$$\begin{matrix} -0.002476 \\ -2.048 \\ -4.0 \\ +1.952 \end{matrix} \quad \text{for } M = \begin{bmatrix} .25 & 0 & 0 & 0 \\ 0 & 0 & 0 & .25 \end{bmatrix}$$

$$\begin{matrix} -0.002475 \\ -1.0 \\ -1.065 \\ +0.9385 \end{matrix} \quad \text{for } M = \begin{bmatrix} 1 & 0 & 0 & 0 \\ 0 & 0 & 0 & 1 \end{bmatrix}$$

The transmission zeros lie even farther in the right half s-plane if the equations are changed so the output $\underline{y}$ vector is bank angle ϕ and sideslip angle β. For other measurement matrix values and locations, the results are similarly unsatisfactory.

Bibliography

1. Barfield, A. Multivariable Control Law Development for the AFTI/ F-16. MS Thesis, AFIT/GE/EE/84S-4. School of Engineering, Air Force Institute of Technology (AU), Wright-Patterson AFB OH, December 1982.

2. Clark, B. X-29 Trim and Linearized Data Routine Forward Swept Wing Simulation Six Degree of Freedom. NASA Dryden, Edwards AFB CA, May 1984.

3. D'Azzo, J. and C. Houpis. Linear Control Systems Analysis and Design (Second Edition). New York: McGraw-Hill Book Company, 1981.

4. Eslinger, R. Multivariable Control Law Design for the AFTI/F-16 with a Failed Control Surface. MS Thesis, AFIT/GE/ENG/84D-28. School of Engineering, Air Force Institute of Technology (AU), Wright-Patterson AFB OH, December 1984.

5. Feldman, S. Multivariable Control Law Development for the X-29. MS Thesis, AFIT/GE/EE/84M-3. School of Engineering, Air Force Institute of Technology (AU), Wright-Patterson AFB OH, December 1983.

6. Krone, N. "Forward Swept Wing Design," No. 80-3047. American Institute of Aeronautics and Astronautics, 555 West 57th Street, New York NY, 1980.

7. Lewis, T. High Gain Error Actuated Flight Control for Continuous Multivariable Plants. MS Thesis, AFIT/GAE/EE/82D-1. School of Engineering, Air Force Institute of Technology, Wright-Patterson AFB OH, December 1982.

8. Masi, A. and D. Russ. MULTI User's Manual. AFWAL-TM-83-182-FIGL. Air Force Flight Dynamics Laboratory, Wright-Patterson AFB OH, August 1984.

9. Papsco, R. Flight Control System Midterm Technical Review. Grumman Aerospace Corporation, Bethpage NY, June 1983.

10. Porter, B. and A. Bradshaw. "Design of Linear Multivariable Discrete-Time Tracking Systems Incorporating Fast-Sampling Error-Actuated Controllers," International Journal of System Science, 2 (7): 817-826 (1980).

11. -----. "Singular Perturbation Methods in the Design of Tracking Systems Incorporating High-Gain Error Actuated Controllers," International Journal of Systems Science, 12 (10): 1169-1220 (1981).

12. Pugh, A. "Transmission and System Zeros," International Journal of Control, 26 (2): 315-324 (1977).

13. Ridgley, B., S. Banda, and J. D'Azzo. "Decoupling of High-Gain Multivariable Tracking Systems," AIAA 21st Aerospace Sciences Conference, Reno NV, January 1983, AIAA Paper No. 83-0280.

14. Spacht, G. Forward Swept Wing Demonstrator Technology Integration and Evaluation Study. AFWAL-TR-80-3145, Vol. I. Air Force Flight Dynamics Laboratory, Wright-Patterson AFB OH, December 1980.

15. Stiles, H. X-29A FCS Interim Design Report. No. 712/ENG-RPT-83-029. Grumman Aerospace Corporation, Bethpage NY, June 1983.

16. Taylor, J. Jane's All the World Aircraft. New York: Jane's Publishing Incorporated, 1983.

Vita

Terry L. Courtheyn is a native of Augusta, Ohio. He graduated from the University of Cincinnati, Ohio and received a Bachelor of Science in Electrical Engineering in 1970. Upon graduation, he received a commission in the USAF through the ROTC program. He completed pilot training and received his wings in October 1971. Then he served as a RF-4C aircraft commander in the 30th Tactical Reconnaissance Squadron, Royal Air Force Alconbury, England from 1972 to 1976. His next assignment was with the Air Force Weapons Laboratory at Kirtland AFB, New Mexico from 1976 to 1979. There, he served as an electrical engineer responsible for electronic instrumentation of field test programs evaluating simulated nuclear effects on Peace Keeper missile basing concepts. Thereafter, he resumed flying duties as a flight commander and an instructor pilot with the 16th Tactical Reconnaissance Training Squadron (TRTS) at Shaw Air Force Base, South Carolina and the 45th TRTS at Bergstrom AFB, Texas. In 1983 he entered the School of Engineering, Air Force Institute of Technology, Wright-Patterson AFB, Ohio.

UNCLASSIFIED

SECURITY CLASSIFICATION OF THIS PAGE

REPORT DOCUMENTATION PAGE

1a. REPORT SECURITY CLASSIFICATION: UNCLASSIFIED	1b. RESTRICTIVE MARKINGS
2a. SECURITY CLASSIFICATION AUTHORITY	3. DISTRIBUTION/AVAILABILITY OF REPORT: As it appears on the report
2b. DECLASSIFICATION/DOWNGRADING SCHEDULE	
4. PERFORMING ORGANIZATION REPORT NUMBER(S): AFIT/GE/ENG/84D-21	5. MONITORING ORGANIZATION REPORT NUMBER(S)
6a. NAME OF PERFORMING ORGANIZATION: Air Force Institute of Technology; 6b. OFFICE SYMBOL (If applicable): AFIT/EN	7a. NAME OF MONITORING ORGANIZATION
6c. ADDRESS (City, State and ZIP Code): Wright-Patterson AFB, OH 45433	7b. ADDRESS (City, State and ZIP Code)
8a. NAME OF FUNDING/SPONSORING ORGANIZATION: Flight Dynamics Laboratory; 8b. OFFICE SYMBOL (If applicable): AFWAL/FIGL	9. PROCUREMENT INSTRUMENT IDENTIFICATION NUMBER
8c. ADDRESS (City, State and ZIP Code): Wright-Patterson AFB, OH 45433	10. SOURCE OF FUNDING NOS. — PROGRAM ELEMENT NO. / PROJECT NO. / TASK NO. / WORK UNIT NO.
11. TITLE (Include Security Classification): See Block 19	
12. PERSONAL AUTHOR(S): Terry L. Courtheyn, Major, USAF	
13a. TYPE OF REPORT: MS Thesis; 13b. TIME COVERED: FROM _____ TO _____; 14. DATE OF REPORT (Yr., Mo., Day): 84 December; 15. PAGE COUNT: 306	
16. SUPPLEMENTARY NOTATION: Approved for public release; IAW AFR 190-17 (Fr. 1473B)	
17. COSATI CODES — FIELD / GROUP / SUB. GR.	18. SUBJECT TERMS (Continue on reverse if necessary and identify by block number): Wings; Swept Wings; Supercritical Wings; Swept Forward Wings; Flight Control Systems; Fly-by-Wire Control; Airfoils. (Thesis). End

19. ABSTRACT (Continue on reverse if necessary and identify by block number) And

Title: Multivariable Control Law Design for the X-29 Aircraft

Thesis Chairman: John J. D'Azzo

Approved for public release: IAW AFR 190-17.
LYNN E. WOLAVER 28 Feb 85
Dean for Research and Professional Development
Air Force Institute of Technology (AIG)
Wright-Patterson AFB OH 45433

20. DISTRIBUTION/AVAILABILITY OF ABSTRACT: UNCLASSIFIED/UNLIMITED ☒ SAME AS RPT. ☒ DTIC USERS ☐	21. ABSTRACT SECURITY CLASSIFICATION: UNCLASSIFIED
22a. NAME OF RESPONSIBLE INDIVIDUAL	22b. TELEPHONE NUMBER (Include Area Code) / 22c. OFFICE SYMBOL

DD FORM 1473, 83 APR EDITION OF 1 JAN 73 IS OBSOLETE.

SECURITY CLASSIFICATION OF THIS PAGE

Flight control laws are designed for the X-29 forward swept wing demonstrator aircraft using a design technique based on multivariable control law theory developed by Professor Brian Porter of the University of Salford, England. The computer-aided design program called MULTI is used to develop and refine the control laws. MULTI also simulates the complete closed-loop control system and generates appropriate time response plots for analysis.

Aircraft dynamics for several points in the flight envelope are represented by linearized state space equations obtained from NASA Dryden, an agency responsible for the development and testing of the X-29. Decoupled longitudinal and lateral equations are used to design separate longitudinal and lateral controllers.

Control laws are developed to stabilize the aircraft and perform longitudinal maneuvers (direct climb, vertical translation, and beta pointing) at three different flight conditions, with and without first order-actuator dynamics and computational time delay added to the simulation. The responses are compared. Although some degradation of performance is observed when the actuator dynamics and time delay are added, the results show fast and well-behaved control of the aircraft motion parameters with quick and smooth tracking of pilot input commands. Similarly, lateral control laws are developed for the coordinated turn and beta pointing maneuvers at five different flight conditions with comparable results.

Finally, future areas of research are recommended which also include proposed modifications and additions to MULTI.

Originator-supplied Keywords included

(40 1473A)